NATIONAL COOPERATIVE HIGHWAY RESEARCH PROGRAM
REPORT 125

OPTIMIZATION OF DENSITY AND MOISTURE CONTENT MEASUREMENTS BY NUCLEAR METHODS

HIGHWAY RESEARCH BOARD
NATIONAL RESEARCH COUNCIL
NATIONAL ACADEMY OF SCIENCES—NATIONAL ACADEMY OF ENGINEERING

NATIONAL COOPERATIVE HIGHWAY RESEARCH PROGRAM
REPORT 125

OPTIMIZATION OF DENSITY AND MOISTURE CONTENT MEASUREMENTS BY NUCLEAR METHODS

R. P. GARDNER, W. L. DUNN,
F. H. McDOUGALL, AND W. J. LIPPOLD
NORTH CAROLINA STATE UNIVERSITY
RALEIGH, NORTH CAROLINA

RESEARCH SPONSORED BY THE AMERICAN ASSOCIATION
OF STATE HIGHWAY OFFICIALS IN COOPERATION
WITH THE FEDERAL HIGHWAY ADMINISTRATION

AREAS OF INTEREST:
CONSTRUCTION
GENERAL MATERIALS
FOUNDATIONS (SOILS)

HIGHWAY RESEARCH BOARD
DIVISION OF ENGINEERING NATIONAL RESEARCH COUNCIL
NATIONAL ACADEMY OF SCIENCES—NATIONAL ACADEMY OF ENGINEERING 1971

NATIONAL COOPERATIVE HIGHWAY RESEARCH PROGRAM

Systematic, well-designed research provides the most effective approach to the solution of many problems facing highway administrators and engineers. Often, highway problems are of local interest and can best be studied by highway departments individually or in cooperation with their state universities and others. However, the accelerating growth of highway transportation develops increasingly complex problems of wide interest to highway authorities. These problems are best studied through a coordinated program of cooperative research.

In recognition of these needs, the highway administrators of the American Association of State Highway Officials initiated in 1962 an objective national highway research program employing modern scientific techniques. This program is supported on a continuing basis by funds from participating member states of the Association and it receives the full cooperation and support of the Federal Highway Administration, United States Department of Transportation.

The Highway Research Board of the National Academy of Sciences-National Research Council was requested by the Association to administer the research program because of the Board's recognized objectivity and understanding of modern research practices. The Board is uniquely suited for this purpose as: it maintains an extensive committee structure from which authorities on any highway transportation subject may be drawn; it possesses avenues of communications and cooperation with federal, state, and local governmental agencies, universities, and industry; its relationship to its parent organization, the National Academy of Sciences, a private, nonprofit institution, is an insurance of objectivity; it maintains a full-time research correlation staff of specialists in highway transportation matters to bring the findings of research directly to those who are in a position to use them.

The program is developed on the basis of research needs identified by chief administrators of the highway departments and by committees of AASHO. Each year, specific areas of research needs to be included in the program are proposed to the Academy and the Board by the American Association of State Highway Officials. Research projects to fulfill these needs are defined by the Board, and qualified research agencies are selected from those that have submitted proposals. Administration and surveillance of research contracts are responsibilities of the Academy and its Highway Research Board.

The needs for highway research are many, and the National Cooperative Highway Research Program can make significant contributions to the solution of highway transportation problems of mutual concern to many responsible groups. The program, however, is intended to complement rather than to substitute for or duplicate other highway research programs.

NCHRP Report 125

Project 10-5A FY '68
ISBN 0-309-02005-0
L. C. Catalog Card No. 75-180699

Price $4.40

Published reports of the

NATIONAL COOPERATIVE HIGHWAY RESEARCH PROGRAM

are available from:

Highway Research Board
National Academy of Sciences
2101 Constitution Avenue
Washington, D.C. 20418

(See last pages for list of published titles and prices)

FOREWORD

By Staff
Highway Research Board

The results of this study have been evaluated sufficiently to permit immediate application. Combination with previous research and experience such as that contained in *NCHRP Report 43* provides a valid basis for adequate calibration and practical field use of commercially available nuclear density and moisture content gauges for the control of compaction during highway construction. The report also describes the development and use of the Quality Factor concept for combining all identified errors of a nuclear density gauge into one parameter that can be used as an indication of the over-all performance of the gauge. The report should be of particular interest and value to highway department materials and testing engineers and others concerned with the quality assurance of embankment and base course construction. In addition, the report contains considerable technical and investigative background information on nuclear measurement principles which should prove useful to researchers and nuclear equipment manufacturers.

The majority of acceptance specifications or quality assurance procedures for controlling the compaction of highway embankments, subgrades, and base courses involve the determination of densities and moisture contents of soil and aggregate materials during the construction process. Nuclear gauges for making these measurements first became available in the late 1950's. However, although the gauges seemed to answer a need for rapid and nondestructive testing, growth in their acceptance and use has been rather slow until the past few years, due largely to questions concerning measurement accuracy. Early experiences with regard to field reliability, economics, radiation, and licensing of operators also tended to discourage the use of nuclear equipment by highway departments, but these problems appear to have been overcome in recent years.

The accompanying sketch shows the operational principles of gamma-ray nuclear density gauges. When gamma rays are emitted from a radiosotope source in proximity to a surface they interact with the material and are scattered or absorbed. The count of the gamma rays emerging from the surface at some point is influenced by the density and the composition of the material. A typical gauge consists of a gamma-ray source, a detector with associated counting electronics, and shielding between the two to prevent direct transmission of the gamma rays from the source to the detector. A wide variety of gauge configurations is possible, involving source energy and intensity, type and efficiency of detector, and source-detector separation. The most universally employed method of determining density with a gamma-ray gauge is by use of a calibration curve prepared from the empirically determined relationships between density and response for each individual instrument. The calibration curve for a particular instrument is originally obtained by plotting the response measured by the gauge for a set of calibration standards of known density.

NCHRP Report 43 describes the factors that influence the accuracy of nuclear density gauge measurements and methods that can be used for their reduction. The primary sources of error were identified as (1) inaccurate calibration techniques, (2) sensitivity to soil composition, and (3) sensitivity to surface roughness. The first two sources of error apply about equally to both direct-transmission and backscatter-type gauges. The surface roughness problem is considerable for backscatter-type gauges and almost negligible for the transmission type. The report describes a mathematical model technique for preparation of calibration curves of suitable accuracy for highway construction control for identifiable soil types, thus making it possible to practically eliminate the first two sources of error. However, it was also found that a dual-gauge technique was equally effective and did not require knowledge of the soil composition. This dual-gauge technique consists of using two gauges, each with a different relative sensitivity to soil density and composition, and solving the calibrations models of each simultaneously. A nomograph solution of the air-gap calibration method, which employs the dual-gauge principle, is included in Appendix A of *NCHRP Report 43*. It is recommended as the most practical method for using existing nuclear density gauges.

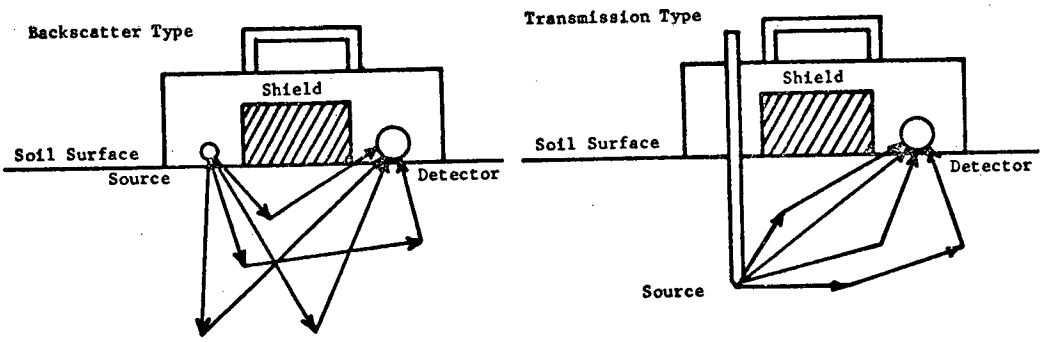

*Representative gamma-ray paths for density gauges.**

Determination of the dry density of the soil or aggregate materials being placed, which is necessary for computing percent compaction, depends on a reasonably accurate method for measurement of moisture content. When nuclear equipment is used to determine total density, the same equipment is normally used to measure the moisture content of the soil. A neutron moisture gauge essentially consists of a fast-neutron source and a slow-neutron detector with associated counting electronics. When the gauge is exposed to a surface the number of slow neutrons in the vicinity of the detector is determined mainly by the hydrogen content of the surface material. If most of the hydrogen is present in the form of water, the gauge, with proper calibration, can be used to measure the moisture content.

According to *NCHRP Report 43*, nuclear moisture content gauges are sensitive to variations in soil density and to soil composition. However, the accuracy of these gauges has not been questioned to the same extent as that of density gauges, probably for the reason that a greater percent error of moisture content can be tolerated. When the moisture content of the soil is about 10 percent, 10 percent deviation from the mean will result in a possible error of only 1 pcf.

The objective of the study reported herein was to minimize the errors identified with measurement of density and moisture content of soils using nuclear gauges. In approaching the problem of optimization of density gauges the North Carolina State University researchers recognized the need to consider the interaction of all possible errors. For example, the best gauge configuration or technique for minimizing surface roughness errors might result in an increase in errors influenced by composition. To provide a reasonable basis for optimization, the errors were combined to yield a single criterion, the Quality Factor, which can be used to evaluate the over-all performance of a nuclear density gauge. Research aimed at minimizing moisture content measurement errors involved using the Monte Carlo or random walk method to simulate gauge response, checking the results of the simulation against experimental studies, and attempting to generalize the Monte Carlo results.

The over-all project objectives were accomplished by several somewhat independent research efforts under the supervision of Dr. R. P. Gardner, who then prepared the main body of this report. The independent efforts culminated in three graduate theses, which are included as appendices.

The study has verified that, with proper calibration, currently available nuclear equipment for measurement of density and moisture content provides satisfactory accuracy for the control of compaction of highway embankments and base courses when used within the concept of random sampling and statistically based quality assurance programs. It has also provided the Quality Factor as a means for evaluating the performance of existing nuclear gauges and methods to refine the calibration of gauges when improved accuracy is desired. In addition, the research provides the necessary technical and investigative background for the production of the next generation of nuclear density and moisture content measurement equipment, which should be even more accurate and require less surface preparation than current models. Thus, the results will provide highway agencies with both immediate and long-range benefits.

* Gardner, R. P., and Roberts, K. F., "Density and Moisture Content Measurements by Nuclear Methods." *NCHRP Report 43* (1967).

CONTENTS

ACKNOWLEDGMENTS

The research reported herein was performed under NCHRP Project 10-5A by the Department of Nuclear Engineering, North Carolina State University, with Dr. R. P. Gardner, Professor of Nuclear and Chemical Engineering, as principal investigator. He was assisted in both the research work and in writing the report by Research Assistants W. L. Dunn, F. H. McDougall, and W. J. Lippold.

OPTIMIZATION OF DENSITY AND MOISTURE CONTENT MEASUREMENTS BY NUCLEAR METHODS

Section I

GAMMA-RAY GAUGES FOR MEASURING SOIL DENSITY

CHAPTER ONE

INTRODUCTION AND RESEARCH APPROACH

In previous work (*1, 2*) on the gamma-ray soil density gauges three sources of error were identified: (1) sensitivity to surface roughness, (2) sensitivity to soil composition, and (3) inaccurate calibration techniques. The last two of these errors were minimized to the point of being negligible by the calibration model method (*2*), which essentially consists of devising a mathematical model that relates the gauge response to both the density and the composition of a soil. Then a calibration is performed to determine the model constants by taking the responses for a given gauge on a series of laboratory standards of known densities and compositions. With these specific values of the constants the model can be used to calculate the calibration curve for that gauge for soil of any arbitrary composition.

A major disadvantage of the calibration model method was having to determine the composition of the soil being measured by some independent means. Subsequent to the development of the calibration model method, the dual-gauge principle, which eliminates this disadvantage, was discovered (*2*). This principle essentially consists of using two gauges that have different relative sensitivities to density and composition. The calibration models for these two gauges are solved simultaneously for density while eliminating composition. Kuhn (*3*) had previously discovered the air gap method, which is based on the same underlying principle but uses the same gauge at two heights above the soil surface. Subsequent testing of these methods has shown that they can be used to eliminate the effect of soil composition (*4, 5, 6, 7, 8, 9*). However, both methods are still significantly affected by sensitivity to surface roughness, as are all commercial surface-type nuclear density gauges.

It appeared that the further development and complete optimization of the dual-gauge principle should be based on the minimum combination of all the important errors, such as those due to surface roughness and soil composition. These errors have been combined in the present work to yield a single criterion, the Quality Factor, that can be used to judge gauge quality.

The work presented here is directed solely toward the improvement of the backscatter-type density gauges. Transmission-type gauges have significantly lower errors than the simple backscatter-type gauges, but suffer from the disadvantage that they require the punching or drilling of a hole in the soil sample. This means that these gauges do not give a truly nondestructive measurement and are, therefore, somewhat limited in application. If the measurement interferences pertinent to the backscatter-type density gauge can be made comparable to those pertinent to the transmission-type gauge, the backscatter-type gauge would be preferred. This objective was accomplished in the present work.

CHAPTER TWO

FINDINGS

The results of the current study of gamma-ray soil density gauges are divided into five parts. The first part identifies and defines the errors that are considered to be important in gamma-ray soil density gauges. The second part delineates the Quality Factor concept, which attempts to approximately weight and combine all the errors into a single parameter that will serve as the criterion for evaluating these gauges. The third part contains the results of the studies on optimization of the air-gap method used with existing commercial gauges utilizing the Quality Factor concept. The fourth and fifth parts give the results of the studies on optimization of simple-detector dual gauges and more sophisticated configurations utilizing the Quality Factor concept.

IDENTIFICATION AND DEFINITION OF ERRORS

The errors considered to be important in the use of gamma-ray soil density gauges are: (1) those due to variations in soil composition, (2) those due to variations in the surface roughness of samples, (3) that due to uncertainty in the detection of radiation, and (4) that due to sample heterogeneities other than that attributed to surface roughness. The first of these can be determined by comparing the measured densities with the known densities of a set of soil samples that have a representative range of densities and compositions. It is impractical, however, to obtain such a set of soil samples. Therefore, a particular set of standard materials has been chosen. These consist of magnesium, aluminum, chalk, and limestone, representing a range of densities from 110 to 168 pcf and compositions ranging from sand plus 3.6 percent iron to sand plus 11.8 percent iron. The soil composition standard error is then defined as

$$\sigma_c(\rho) = \left[\sum_{i=1}^{4} \frac{(\bar{\rho}i - \rho i)^2}{4}\right]^{\frac{1}{2}} \qquad (1)$$

in which $\sigma_c(\rho)$ is the standard error due to composition variations, $\bar{\rho}i$ is the known density of the ith one of the four standard materials, and ρi is the measured density of the ith one of the four standard materials.

The second error (surface roughness) is similar to the first in that it can be determined by comparing the measured densities with the known densities of a set of samples that have representative densities and surface roughnesses. However, because it would be impossible even to ascertain what surfaces are representative, a somewhat arbitrary definition of surface roughness must be used. The proposed definition of error due to surface roughness is that error introduced by comparing the density measured 1/16 in. above a smooth surface with the density measured flush on the same surface. This error is denoted E_{se}. Accurate methods of measuring this error are described in Appendices A and B. It should be noted that this error, unlike the composition error, is not normally distributed.

The third error, that due to uncertainty in the detection of radiation, can be determined from the slope of the calibration curve and the standard deviation of the counting rate measurement; that is,

$$\sigma_s(\rho) = \frac{\partial \rho}{\partial R}\,\sigma(R) \qquad (2)$$

in which $\sigma_s(\rho)$ is the standard error of the measured value of density, $\partial\rho/\partial R$ is the slope of the calibration curve, and $\sigma(R)$ is the standard deviation of the counting rate measurement. The standard deviation of the counting rate depends on the statistical nature of counting rate measurements and the instability of the associated electronics. If at least 10,000 counts are accumulated to ascertain the counting rate, and if the ratio of the sample counting rate to the counting rate of a standard is taken as the gauge response, R, a good rule of thumb is to take $\sigma(R)$ as 1 percent of the gauge response, R.

The fourth error, that due to sample heterogeneities other than surface roughness, is again like the first two. It could be obtained if measurements could be made on a set of samples of known densities with representative density heterogeneities. Again, it would be impossible to ascertain what heterogeneities are representative. This source of error is further complicated by the fact that no one sample depth or size can be established as the optimum because this varies from one application and one user to another. However, as a general rule, sample heterogeneities are minimized if the effective sample volume being measured is increased. Therefore, a volume factor is defined and taken as a measure of the error due to sample heterogeneity. This volume factor is taken as

$$\mathrm{VF} = 0.1\ x\ w\ d/288 + 0.9 \qquad (3)$$

in which VF is the volume factor; x is the effective sample depth, in inches; w is the sample width, in inches; and d is the source-to-detector distance, in inches. The effective sample depth is taken as the first moment of the response with respect to sample depth and is determined as described in the report by Gardner and Roberts (*2*). The sample width is taken as 4 in. and the source-to-detector distance can be measured directly. For a transmission-type gauge the sample width, w, would be one-half the detector width and the effective sample depth, x, would be the depth that the source (or detector) had been inserted into the sample. The factors 0.1, 288, and 0.9 are used to force the volume factor to vary from a minimum of 0.9 to a maximum of 1.0 so that this factor is not given much weight in comparison to the other errors. (If one does not wish to take the trouble to measure the volume factor

of a given gauge, a value of 1.0 can be assumed for the calculation of the Quality Factor if the gauge design is similar to that of existing commercial gauges.)

Table 1 gives some representative values of these errors for commercial backscatter-type and transmission-type surface gauges. These results were obtained on four representative backscatter-type and two representative transmission-type commercial gauges at the Nuclear Soil Gauge Calibration Workshop-Symposium (*5*).

TABLE 1

TYPICAL ERRORS FOR REPRESENTATIVE COMMERCIAL NUCLEAR SOIL DENSITY GAUGES

GAUGE TYPE	ERROR (PCF)		
	$\sigma_c(\rho)$	E_{se}	$\sigma_s(\rho)$
Backscatter	2.0–5.0	6.7–13.0	0.7–1.2
Transmission	1.7–4.0	1.4– 2.1	0.5–0.8

QUALITY FACTOR CONCEPT

The Quality Factor concept as developed by Dunn and McDougall (*9*) is an attempt to combine all of the errors identified and defined in the previous section to form one parameter that can be used as an indication of the quality of a nuclear soil density gauge. (Large values of the Quality Factor indicate higher-quality gauges.) Because the composition and counting-rate measurement errors, $\sigma_c(\rho)$ and $\sigma_s(\rho)$, are normally distributed, they may be combined in the usual way to obtain a total normal error, $\sigma_n(\rho)$; that is,

$$\sigma_n(\rho) = \sqrt{\sigma_c^2(\rho) + \sigma_s^2(\rho)} \tag{4}$$

This normal error may either add to or subtract from the surface roughness error, E_{se}. If the lowest most probable error is defined as that obtained when the normal error is subtracted from the surface roughness error, and the highest most probable error as that obtained when the two are added,

$$L = E_{se} - \sigma_n(\rho) \tag{5}$$

$$H = E_{se} + \sigma_n(\rho) \tag{6}$$

in which L and H are the lowest and highest most probable errors. Inasmuch as the value of $\sigma_n(\rho)$ is always positive, the lowest most probable error is representative of the error level. The range of the error is obtained by taking the difference between the highest and lowest most probable errors, or

$$D = H - L = 2\,\sigma_n(\rho) \tag{7}$$

in which D is the error range. A good indication of the total of the three errors is obtained by taking the square root of the sum of the squares of the level and range of the errors. However, when the error level is negative ($\sigma_n(\rho) > E_{se}$), one would like to take the difference in the sum of the squares. Therefore,

$$E_t = \sqrt{D^2 \pm L^2} \tag{8}$$

in which E_t is the total error and the plus sign in the square root term is used when L is positive and the minus sign when L is negative. If it is desired to make the Quality Factor large for better gauges, one could combine E_t and VF in the following way to obtain the Quality Factor:

$$\mathrm{QF} = \frac{2\,\mathrm{VF}}{\sqrt{D^2 \pm L^2}}$$

The factor of 2 is used to normalize the Quality Factor to 1 when VF = 1.0, $E_{se} = 1$ pcf, and $\sigma_n(\rho) = 1$ pcf. One would strive for a Quality Factor of 1 as representative of a high-quality gauge.

To illustrate the dependence of the Quality Factor on the individual errors, Figure 1 shows the Quality Factor for various values of the normal error and the surface roughness errors when each is held alternately constant at 1.0 pcf. Note that the Quality Factor decreases monotonically when either the normal error or the surface roughness error increases while holding the other error constant.

Some typical Quality Factor values for backscatter-type and transmission-type commercial nuclear density gauges are given in Table 2. The data used in obtaining these values were collected during the Nuclear Soil Gauge Calibration Workshop-Symposium (*5*).

OPTIMIZATION OF THE AIR-GAP METHOD

The air-gap method is an important method for applying the dual-gauge principle, because it can be used with existing commercial backscatter-type nuclear density gauges. The method essentially consists of taking the normal gauge response flush on the surface of a sample and another at a predetermined height above the surface. The ratio of the two is then used to determine the density. This ratio is found to be less sensitive to variations in composition than the normal response. The air-gap height was originally obtained by determining the height at which the gauge response was a maximum.

A more refined technique for eliminating soil composition dependence by the air-gap method is illustrated by Gardner, et al. (*4*) using the solution to an accurate mathematical model of each gauge response. The optimum air-gap height in this case was determined as the height that would give the minimum composition error. It appeared that an even better optimization of this principle could be obtained by maximizing the Quality Factor as a function of air-gap height. This was done for the data presented by Gardner, et al. (*4*), the maximum Quality Factor so obtained being 0.36 at an air-gap height of 2 in. The previous technique had yielded an optimum air-gap height of 2¾ in. However, the Quality Factor did not exhibit a sharp maximum, varying only from 0.344 to 0.359 over the range of air-gap heights from 1¾ in. to 2¾ in. Nevertheless, the Quality Factors so obtained were considerably better than the best (0.183) found by the original air-gap ratio method, which did not incorporate the mathematical model approach.

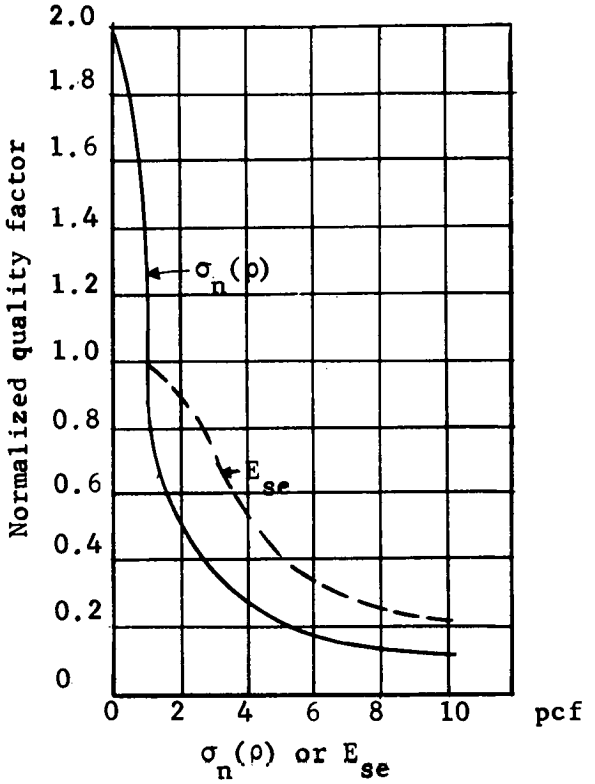

Figure 1. Quality Factor as a function of normal error and surface-effect error.

TABLE 2

TYPICAL QUALITY FACTORS FOR REPRESENTATIVE COMMERCIAL NUCLEAR SOIL DENSITY GAUGES

GAUGE TYPE	QUALITY FACTOR RANGE
Backscatter	0.17–0.33
Transmission	0.36–0.56

TABLE 3

SURFACE-EFFECT ERRORS AND QUALITY FACTORS FOR TYPICAL COMMERICAL BACKSCATTER-TYPE GAUGES WITH AND WITHOUT AIR-GAP METHOD [a]

	SURFACE-EFFECT ERROR		QUALITY FACTOR	
GAUGE	WITHOUT AIR-GAP (PCF)	WITH AIR-GAP	WITHOUT AIR-GAP	WITH AIR-GAP
A	12.2	8.5	0.180	0.239
B	13.0	12.5	0.171	0.179
C	6.7	6.1	0.329	0.359
D	12.3	11.7	0.180	0.188

[a] Data collected during the Nuclear Soil Gauge Calibration Workshop-Symposium (*5*).

A significant finding of this study is that the surface roughness error cannot be minimized to any significant extent by the air-gap method, so that the air-gap method is limited in the amount of improvement that it can make over the use of conventional gauges. This is illustrated by Table 3, which gives the values for four typical commercial gauges.

OPTIMIZATION OF SIMPLE-DETECTOR, DUAL GAUGES

A program was undertaken to optimize the dual-gauge principle for gauges with simple, Geiger-Mueller-type detectors. Such detectors are eminently suited for routine field application because they are rugged, stable, and inexpensive. To obtain the optimum dual gauge for this case, the Quality Factor previously described was maximized with respect to the four variables: source energy, source-detector distance, Geiger-Mueller counter type, and source collimation. This study is described in detail in Appendix A.

The optimization program was carried out by first developing the calibration model for 46 individual gauges with various values of the four variables previously mentioned. The calibration model relates the gauge response to the density and composition of the soil sample. It is described in *NCHRP Report 43* (*2*) and in Appendices A and B. The source energies used consisted of ^{133}Ba with gamma-ray energies up to 0.38 MeV, ^{137}Cs with a gamma-ray energy of 0.66 MeV, and ^{60}Co with gamma-ray energies up to 1.33 MeV. The source-detector distances were varied from 4 to 12 in. Geiger-Mueller types included a simple stainless steel thin-wall type with relatively small low-energy efficiency, and, at the other extreme, the same counter with 10 mg/cm^2 of platinum plated on the inner wall to obtain relatively large low-energy efficiency. Source collimation was varied by placing the source from ⅛ in. from the bottom of a 3/16-in.-diameter hole to 2 in. from the bottom.

The optimum dual-gauge design with a Quality Factor of 1.34 was obtained by searching through 826 possible dual-gauge combinations. The optimum two single-gauge configurations combined to form the best possible dual gauge had the design parameters given in Table 4. It should be noted that the design parameters are not particularly critical except that the source-detector separation of one configuration should be small whereas the other should be large, and one Geiger-Mueller counter should have a relatively low efficiency whereas the other should have a relatively high efficiency for low-energy gamma rays. A total of 19 dual-gauge configurations were identified with Quality Factors greater than 1.

Perhaps the most significant result of this study was to show that the surface roughness error could be reduced by proper dual-gauge design to essentially negligible values. Twelve of the best 25 dual-gauge designs had surface roughness errors of less than 0.35 pcf compared to the lowest value of 6.1 pcf for the existing commercial backscatter-type density gauges.

OPTIMIZATION OF ENERGY-DISCRIMINATION, STRINGENTLY COLLIMATED GAUGES

The possibility exists that backscatter-type gauges with energy-discrimination and stringent collimation of source and detector capabilities can be designed to eliminate or minimize the effect of soil composition and surface roughness, respectively. The work of Preiss (*10*) is representative of this approach to density gauge design studies. The principle behind this energy-discrimination approach is essentially that the gauge response due to high-energy gamma rays is almost entirely independent of the normal fluctuations in soil composition. Therefore, if low-energy gamma rays are excluded from the gauge response by discrimination with a detector system capable of gamma-ray spectrometry, the resulting gauge will be free of the soil composition measurement interference.

The energy-discrimination principle appears to be a promising concept for the elimination of the soil composition measurement interference in nuclear density gauges. However, this relatively simple principle has several disadvantages that have not been fully recognized by many workers in this field. The first of these disadvantages is that the necessary detection systems capable of gamma-ray spectrometry are less stable, less rugged, and more expensive than the simple Geiger-Mueller counters that can be used in other gauges. The second is that only a very small percentage of the gamma rays scattered back from the soil are energetic enough to be free from the soil composition measurement interference. This means that more intense sources have to be used with this principle. A third disadvantage is that the response of backscatter-type density gauges depends on density and composition in a more complex way than that of transmission-type gauges and this means that a simple comparison of individual gamma-ray sensitivities to soil density and soil composition is not legitimate. An analysis described under "Sensitivity Analysis for Application to Gauge Response" in Appendix B indicates that a comparison of these sensitivities should never be made directly on a one-to-one basis. The actual sensitivity to soil composition is always higher than the simple one-to-one comparison would indicate. The fourth and final disadvantage is the fact that the total gauge error is not necessarily reduced when the composition error is reduced by this technique. In fact, the present studies indicate that the surface roughness error is increased for a given gauge configuration when low-energy gamma rays are excluded from the gauge response. This can be explained on the basis that the surface roughness error is accentuated when the depth response of a gauge is reduced. As might be expected, backscattered gamma rays of low energy have undergone more interactions on the average and, therefore, have come from greater depths within the sample.

To eliminate the last of these disadvantages of the energy-discrimination principle it has been suggested that the source and detector be stringently collimated to force the backscattered gamma rays to have a deeper sample penetration. In conjunction with gamma-ray energy discrimination the stringent-collimation principle might accomplish the desired objective of reducing the soil composition and surface roughness errors simultaneously. The reasoning behind this is that high gamma-ray energies detected under a stringent collimation of source and detector would be those that travel in a path indicated by the intersection of the lines drawn along the directions of the source and detector collimations. For example, suppose both the source and the detector were collimated at 45° angles to the sample surface and were directed toward each other as shown in Figure 2. If the source and detector collimators are 6 in. apart at the sample surface, the gamma ray would first travel 4.25 in. into the soil then would be scattered at a 90° angle toward the detector, and, finally, would travel 4.25 in. back through the sample to the detector. The energy of such a gamma ray can be calculated by application of a simple formula relating the scattered energy of a gamma ray to the original gamma-ray energy and scattering angle,

$$E_s = \frac{E_o}{1 + (1 - \cos\theta)\, E_o / 0.51} \qquad (10)$$

in which E_s is the scattered gamma-ray energy, E_o is the original gamma-ray energy, and θ is the angle of scatter.

For example, the scattered energy of a 1.33-MeV gamma ray emitted by ^{60}Co and scattered through an angle of 90° would be 0.368 MeV. It was assumed by some researchers that gamma rays undergoing more than one scatter, and therefore traveling a more tortuous and possibly shorter path within the sample, would have lower energies by virtue of the fact that they would be scattered more than once. This assumption is easily proved wrong by simply applying Eq. 10 twice. If instead of a single 90° scatter two 45° scatters are hypothesized, the resulting doubly scattered gamma ray with original energy of 1.33 MeV has an energy of 0.525 MeV, which is considerably higher than the 0.368 MeV calculated for a single 90° scatter.

In spite of these misconceptions and overlooked disadvantages, the principles of energy discrimination and stringent collimation still appeared to offer some possible improvement in gauge design. However, it appeared that studies of these principles should also be based on the

TABLE 4

DESIGN PARAMETERS FOR THE INDIVIDUAL GAUGE CONFIGURATION GIVING THE OPTIMUM SIMPLE-DETECTOR DUAL GAUGE

GAUGE CONFIGURATION	SOURCE	SOURCE-DETECTOR SEPARATION (IN.)	COLLIMATION LENGTH (IN.)	GEIGER-MUELLER COUNTER TYPE
1	^{60}Co	4.5	10/16	Standard [a]
2	^{60}Co	10.0	10/16	Special [b]

[a] Harshaw model G17-6 with a 0.020-in.-thick stainless steel wall, 13/32-in. outer diameter, 7/8 in. long, filled with halogen gas. It has a relatively low efficiency for low-energy gamma rays.

[b] Harshaw model G17-6P; identical to Harshaw model G17-6 except that it has a 10-mg/cm^2 coating of platinum on the inside of the tube wall. It has a relatively high efficiency for low-energy gamma rays.

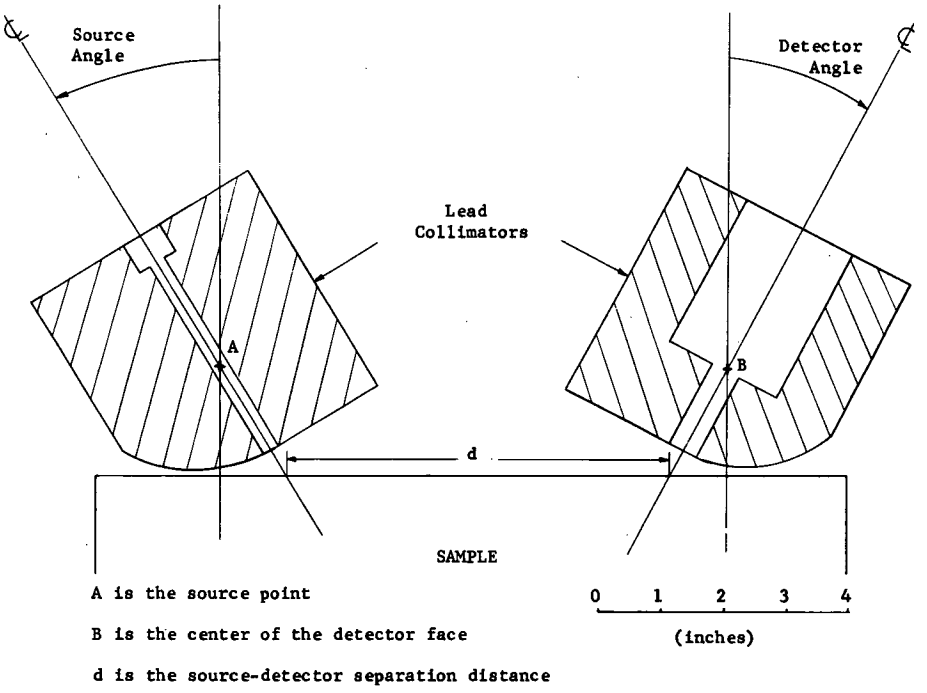

Figure 2. Final prototype gauge design.

concept of maximizing the Quality Factor, inasmuch as this concept is based on total gauge error.

A study was made of these energy-discrimination and stringent-collimation principles by designing a prototype gauge that incorporated gamma-ray spectrometer capability with stringent, variable collimation of source and detector. This prototype gauge is described in detail in Appendix B. A complete gamma-ray, pulse-height spectrum could be taken with this gauge for any of the three gamma-ray sources, ^{60}Co, ^{137}Cs, and ^{133}Ba, representing a range of gamma-ray energies from 0.38 to 1.33 MeV. The source and detector collimators were adjusted to allow sample surface entrance angles from 15° to 45° and the source-detector separation was adjusted from 4 to 6 in. This study indicated that an optimum gauge was obtained with a ^{137}Cs gamma-ray source (gamma-ray energy of 0.662 MeV), source and detector collimation entrance angles of 15°, a source-detector separation of 4.75 in., and a gamma-ray, pulse-height energy range from 0 to 0.110 MeV. The maximum Quality Factor for this case was found to be 0.664. However, this value is somewhat misleading because it is based on a composition error calculated from composition-corrected calibration curves. This implies that such a Quality Factor is possible only if the soil composition is known. It is likely that the best Quality Factor obtainable when an average soil calibration curve is used would be around 0.3.

This disappointingly low Quality Factor is caused primarily by the fact that the surface roughness error was never reduced to less than 2.5 pcf and the lower values of this error were paired with relatively high soil composition and counting-rate measurement errors. Because of this it was decided to apply the dual-gauge principle to this type of gauge. This effort was also somewhat disappointing because the highest Quality Factor obtained for any dual-gauge combination was only 0.46.

One encouraging result of these studies was that effective sample depths approaching 6 in. were obtained with the optimum single gauge using the energy-discrimination and stringent-collimation prototype gauge. This is about 2.3 times as large as any of the commercial gauges reported previously by Gardner and Roberts (*2*).

These results led to a preliminary study of a triple-gauge principle. One cannot expect that a combination of two gauges (the dual-gauge principle) can eliminate the two measurement interferences of soil composition and surface roughness. To accomplish this without relying on encountering fortuitous compensating phenomena, one must use gauge responses from three separate gauge configurations. This leads to a rather complex mathematical problem involving the solution of a cubic equation. The preliminary study is described in detail in Appendix B. It essentially consists of modifying the previous gauge response model to include density, soil composition, and air-gap height. It is reasoned that the surface roughness error can be simulated by some equivalent air-gap height. The responses to three separate gauge configurations are then solved simultaneously for density independent of the soil composition and surface roughness (simulated by an arbitrary air-gap height) measurement interferences. This triple-gauge principle looks promising, but no conclusive results were obtained in this preliminary feasibility study.

CHAPTER THREE

INTERPRETATION, APPRAISAL, AND APPLICATION

The Quality Factor concept developed in this study appears to be an excellent method for comparing the over-all quality of all types of nuclear density gauges. Because it is based on combining all the significant gauge errors, it would seem to be an ideal method for evaluating the performance of existing and future gauge designs. On the basis of this Quality Factor it is found that the existing commercial transmission-type density gauge is significantly better than the existing commercial backscatter-type density gauge. However, the transmission-type gauges require that a hole be punched or drilled in the sample.

The performance of existing commercial backscatter-type density gauges can be significantly improved by using the air-gap dual-gauge approach suggested by Gardner, et al. (*4*). However, the Quality Factors obtained by this method are still not as large (not as good) as are those for the existing commercial transmission-type density gauges. In deciding whether to use the transmission type or the backscatter type with the air-gap dual-gauge method, the potential user must judge whether or not the increased accuracy of the former offsets the disadvantage of having to punch or drill a hole in the sample. His choice will be governed by the availability of one type or the other to him.

It has been shown possible to design a backscatter-type dual gauge on the basis of the maximum Quality Factor that will show significant improvement over either the transmission-type gauge or the backscatter-type gauge used with the air-gap dual-gauge method. In fact, the surface roughness error has been reduced so significantly in these new dual-gauge designs that most of the surface preparation time required could be essentially eliminated, thereby allowing many more measurements to be made in a given workday.

This brings up an important point on the use of these new gauges. Inasmuch as many more density data can be taken when these gauges become commercially available, the concepts of statistical sampling and acceptance specifications should be reexamined in this light when they are introduced.

At present, nuclear gauge users may wish to apply the Quality Factor concept in the evaluation of different types of gauges they have on hand, or in deciding on which new gauges to purchase. The Quality Factor can be measured for a given gauge by performing the following steps:

1. Make a gauge calibration using measurements on the four standards specified in *NCHRP Report 43*(*2*). The user should calibrate according to the method of use envisioned. The options available include a single calibration curve to be used for all soil types, multiple calibration curves to be used for identified soil types, or the air-gap dual-gauge method outlined in *NCHRP Report 43*.
2. Calculate the soil composition standard error, $\sigma_c(\rho)$, as given by Eq. 1.
3. Calculate the standard error due to uncertainty in the detection of radiation, $\sigma_s(\rho)$, as given by Eq. 2.
4. Calculate the total normal error, $\sigma_n(\rho)$, from Eq. 4.
5. Measure the surface roughness error E_{se} by determining the average error obtained on the four standards specified in *NCHRP Report 43*. This can be done simply by determining the difference in measured density between flush measurements and measurements made at 1/16 in. above the sample surface. More accurate measurements of this error can be made by the techniques outlined in Appendices A and B.
6. Assume a volume factor, VF, of 1.0. This is valid for existing commercial gauges or if other similar gauge designs are to be compared. More accurate and refined techniques for evaluations of this factor are given in Appendices A and B.
7. Calculate the Quality Factor as outlined by Eqs. 5 through 9.

CHAPTER FOUR

CONCLUSIONS AND SUGGESTED RESEARCH

The following conclusions can be made as a result of this study:

1. The Quality Factor concept, which combines all the pertinent nuclear density gauge errors, is an excellent measure of gauge quality.
2. Either the existing transmission-type or backscatter-type commercial density gauges used with the air-gap dual-gauge method can be used at present with relatively high Quality Factors and corresponding low total errors.
3. New backscatter-type dual-gauge designs of significantly higher Quality Factors and correspondingly low total gauge errors can now be constructed. These new gauges will also allow many more measurements to be taken per unit of time, due to the reduction of surface preparation time.

The new three-gauge principle incorporating energy discrimination and stringent source and detector collimation may offer a future further improvement in gauge design. This principle should be studied and developed in more detail.

Section II

NEUTRON GAUGES FOR MEASURING SOIL MOISTURE CONTENT

CHAPTER FIVE

INTRODUCTION AND RESEARCH APPROACH

In previous work (*1, 2*) on nuclear soil moisture content gauges three practical sources of error were identified: (1) sensitivity to soil density, (2) sensitivity to soil composition, and (3) inaccurate calibration techniques. The approach pursued here to minimize these errors is the calibration model method. This method, as with the nuclear density gauges, consists of developing a calibration model that relates gauge response to soil moisture content, density, and composition. The responses to homogeneous, stable laboratory samples can then be used with a least-squares method to determine the model constants. Calibration curves for every nuclear soil moisture content gauge can then be prepared for every soil density and composition that is likely to be encountered in the field. The density as measured by a nuclear soil density gauge can be used to establish the proper density calibration. Another independent measurement of the soil composition must be made to establish the proper composition calibration.

In the present work an attempt has been made to use the Monte Carlo or random walk method to simulate nuclear soil moisture content gauge response. The results of this simulation have been checked against experimental studies and a tentative empirical generalization of the verified results has been developed. Results of the application of this model for the North Carolina State University Nuclear Soil Gauge Calibration Workshop-Symposium (*5*) are reported.

CHAPTER SIX

FINDINGS

The results of this study of neutron soil moisture content gauges are divided into four parts. The first describes the Monte Carlo or random walk simulation of the gauge response; the second, the experimental studies carried out to verify the Monte Carlo results and an attempt to develop homogeneous, stable laboratory standards. The third part describes an attempt to completely generalize the Monte Carlo results, which failed, and a less ambitious attempt to generalize these results for a more limited range of soil and gauge variables, which appears promising. The fourth describes the suggested method of use for the tentative calibration model that has been developed.

MONTE CARLO SIMULATION

Previous attempts to develop a suitable calibration model (*1, 2, 11, 12, 13, 14*) for the surface-type nuclear soil moisture content gauges by the neutron diffusion treatment have met with difficulty. This treatment is particularly difficult to use under neutron source and boundary conditions that represent an adequate approximation to the surface-type gauge. Because of this difficulty a Monte Carlo simulation has been attempted. The conditions chosen for this simulation are (a) a point source of neutrons with energies distributed from 0 to 11 MeV, as in a Ra-Be isotopic source, (b) situated on the surface of a homogeneous, infinite half-space medium, with (c) compositions and densities representative of soil. The details of this simulation are given in Appendix C. Much of the development given here is adapted from Lippold, Carnesale, and Gardner (*15*).

A very general and detailed Monte Carlo neutron transport computer code, "05R," available from the Radiation Shielding Information Center (*16*) at Oak Ridge National Laboratory, was used in this study. The code was modified to permit simulation of a point source of neutrons on the surface of a homogeneous, infinite half-space medium.

The neutron source had the distribution of energies from 0 to 11 MeV reported by DePaugher (*17*) for the isotopic neutron source ^{226}Ra-Be, and the infinite half-space was approximated by a right circular cylinder with radius and length of 25 cm. The neutron point source was placed at the center of the top (ground-surface) circular face of the cylinder. This modified version of the 05R program is written in FORTRAN IV and assembly language and is compatible with the IBM 360/75 computer. Neutron cross sections required in the simulation were also obtained from the Radiation Shielding Information Center (*16*). Cross sections for all the elements used in the present study were available in the energy range from 0.025 eV to 12 MeV. Each Monte Carlo simulation was performed in two parts. Part I consisted of generating a large number of neutron histories (i.e., random walks) and, for each neutron emerging from the upper surface of the medium, recording the distance, r, from the source to the point of emergence; the neutron energy, E, at emergence; and the three direction cosines characteristic of the emergent direction of motion. These data were obtained for 9,000 histories for each of 19 simulated construction soil media (requiring several hours on the IBM 360/75), and were permanently stored on magnetic tape for future use. Part II of the simulation involved determination of the expected fraction of the emergent neutrons that would be detected by a right circular cylindrical detector lying on the surface of the medium, with the line of contact between medium and surface being perpendicular to a line drawn from its midpoint to the source.

Because the yield (number detected per total number of neutrons emitted) of the surface-type neutron gauges is quite low, several variance reduction techniques were incorporated into the simulation to reduce the number of random walks required for a given accuracy. Firstly, only those neutrons from the isotropic neutron source directed into the cylindrical medium were considered. This effectively reduces by a factor of two the number of random walks required. Secondly, no neutron absorption events were allowed; instead, a weighting factor equal to the nonabsorption probability was applied after each scattering event. Finally, because the number of neutrons emerging per unit area of surface should depend only on the distance from the source (i.e., radial symmetry should exist), the emergent neutrons recorded in Part I of the simulation were assumed to be emergent from each of 40 sectors of equal size encompassing the entire circular top of the cylindrical medium. The probability, p, of detection of each emergent neutron was determined by

$$p = 1 - e^{m} \tag{11}$$

in which $m = -\Sigma_a l$, Σ_a is the macroscopic absorption cross section for the detector, and l is the neutron path length through the detector.

Due to the several variance reduction techniques used, the variance of the Monte Carlo results could not be obtained from simple binomial probability distributions. However, an estimate of the variance of these results was obtained for several runs known to be representative of the range of variances to be encountered. This was accomplished by splitting each run into 9 parts of 1,000 random walks each so that the final detected number of neutrons, n_i, for each 1,000-random-walk run could be used in the general experimental estimator to predict the variancy for any single 1,000-history run. Thus,

$$\sigma^2(n) = \sum_{i=1}^{N} (n_i - \bar{n})^2/(N-1) \tag{12}$$

in which $\sigma^2(n)$ is the variance of the predicted yield of any 1,000-random-walk run, n_i is the yield of the ith 1,000-random-walk run, $\bar{n}$ is the average yield of all runs, and N is the total number of 1,000-random-walk runs ($N = 9$ in this case). The predicted variance of the average value obtained from all runs is obtained from

$$\sigma^2(\bar{n}) = \sigma^2(n)/N \tag{13}$$

The relative standard deviations, $\sigma(\bar{n})/\bar{n}$, obtained by this method varied from 6 to 10 percent over the range of media considered. The media with higher hydrogen content corresponded to the lower relative standard deviations.

Monte Carlo simulation results were obtained for 19 different media. First, results for 10 media were obtained for a particular detector, detector position, and neutron source. These media were reproduced in the laboratory, and experiments were performed to determine if the Monte Carlo simulation correctly reproduced experimental results. Mixtures of pure silica sand, iron powder, and polyethylene powder to simulate water were used as the media in these 10 runs. The next 8 runs corresponded to simulated media containing a range of water contents in two typical soils; one composed of pure silica sand, and the other containing pure silica sand and 15 percent (by weight) iron. All of these 8 soil media had a constant wet density of 2.082 g/cm^3. The final (19th) result was obtained for conditions identical to Sample 5 except that water replaced the polyethylene powder. This run was used to accurately simulate water. The important characteristics of the media for the 19 samples are given in Table 5.

The predicted counting yields for the first 10 samples for two BF_3 proportional counter detectors are given in Table 6. Corresponding experimental results for these samples are also listed here for comparison. The BF_3 detectors used have a filling pressure of 25 cm of Hg, inside diameters of 3.5 cm, lengths of 16.9 cm; were 96 percent enriched in ^{10}B; and were placed on the surface of the medium with their centers 2.5 cm away from the center of the neutron source.

As mentioned previously, the neutron yield at the medium surface as a function of distance from the source, neutron energy, and the three direction cosines was generated for the 19 media and has been permanently stored on magnetic tape. It is possible to use Part II of the Monte Carlo simulation program with these data to predict the counting yield of any type and size of neutron detector for any of the solid media. However, Part II of the program takes a considerable amount of computer time per calculation. Therefore, cumulative thermal and epithermal neutron yields as a function of distance from the source have been calculated from the detailed Part I data and

TABLE 5

CHARACTERISTICS OF THE MEDIA FOR ALL SAMPLES

SAMPLE NO.	WET DENSITY (G/CM³)	WEIGHT FRACTIONS				HYDROGEN DENSITY (G/CM³)
		CH_2	H_2O	SiO_2	Fe	
1[a]	1.335	0.080	0.000	0.920	0.000	0.01535
2	1.078	0.160	0.000	0.840	0.000	0.02479
3	0.912	0.240	0.000	0.760	0.000	0.03147
4[a]	0.821	0.320	0.000	0.680	0.000	0.03789
5[a]	0.863	0.320	0.000	0.530	0.150	0.03970
6	0.987	0.240	0.000	0.510	0.150	0.03406
7	1.206	0.160	0.000	0.690	0.150	0.02773
8[a]	1.466	0.080	0.000	0.770	0.150	0.01685
9	1.590	0.000	0.000	1.000	0.000	0.00000
10	0.999	0.000	1.000	0.000	0.000	0.11177
11	2.082	0.000	0.066	0.934	0.000	0.01535
12	2.082	0.000	0.107	0.893	0.000	0.02479
13	2.082	0.000	0.136	0.864	0.000	0.03147
14	2.082	0.000	0.164	0.836	0.000	0.03789
15	2.082	0.000	0.172	0.678	0.150	0.03970
16	2.082	0.000	0.147	0.703	0.150	0.03406
17	2.082	0.000	0.120	0.730	0.150	0.02773
18	2.082	0.000	0.073	0.777	0.150	0.01685
19	0.863	0.000	0.414	0.436	0.150	0.03970

[a] These samples have been retained for further use.

are also permanently stored. Epithermal neutrons are taken here as those with energies between 1 eV and 100 KeV. Efforts are now being made to fit these data to empirical expressions. Sample thermal and epithermal cumulative neutron yields as a function of distance from the source for Sample 4 are given in Figure 3.

The neutron yield data generated in Part I of the Monte Carlo analysis are of a more general nature than is immediately apparent. Indeed, proper normalization permits extension of the results for each of the 19 simulated soils to soils of the same relative composition but differing in density. This normalization is accomplished by expressing the distance from the source to the point of emergence in terms of the product ρr, where ρ is the density of the simulated soil. Then, if the cumulative neutron yield is described as a function of ρr (rather than r), the resultant function is applicable without reference to the soil density. (The validity of this assertion may be established by noting that all neutron cross sections are linearly proportional to material density; hence, all mean free paths are inversely proportional to material density.) Care must be taken not to extend this generalization to soil densities far below the density employed in the corresponding Monte Carlo calculation, for then the finite medium (a cylinder of 25-cm radius and 25-cm length) employed in the simulation may not reasonably represent an infinite half-space. It is expected that extension to densities as low as one-half of the computational density is always permissible, because this corresponds to an improvement in the simulation of the infinite half-space. Figure 3 shows the cumulative neutron yields for Sample 4 as a function of the product ρr as well as for r.

TABLE 6

MONTE CARLO PREDICTIONS AND EXPERIMENTAL COUNTING YIELDS FOR BF_3 PROPORTIONAL COUNTERS

SAMPLE NO.	MONTE CARLO COUNTING YIELD AT 2.5 CM ($\times 10^{-4}$)	EXPERIMENTAL COUNTING YIELD ($\times 10^{-4}$)		
		AT 2.5 CM	AT 6 CM	AT 10 CM
1	0.674	0.830	0.775	0.617
2	1.467	1.765	1.565	1.285
3	2.034	2.284	1.995	1.572
4	2.550	2.903	2.399	1.943
5	2.360	2.620	2.235	1.867
6	2.028	2.233	1.926	1.719
7	1.611	1.701	1.515	1.158
8	0.840	0.792	0.650	0.612
9	0.017	0.006	0.028	0.008
10	9.904	9.482	6.008	3.020
11	1.167	—	—	—
12	2.268	—	—	—
13	2.990	—	—	—
14	3.657	—	—	—
15	2.985	—	—	—
16	2.514	—	—	—
17	1.802	—	—	—
18	0.820	—	—	—
19	2.553	—	—	—

The Monte Carlo detector yield results given in Table 6 illustrate the effect of sample density and sample composition. These effects are shown in Figure 4. The samples of curves 1 and 2 have a constant wet density of 2.082 g/cm³ and compositions that are representative of low- and high-

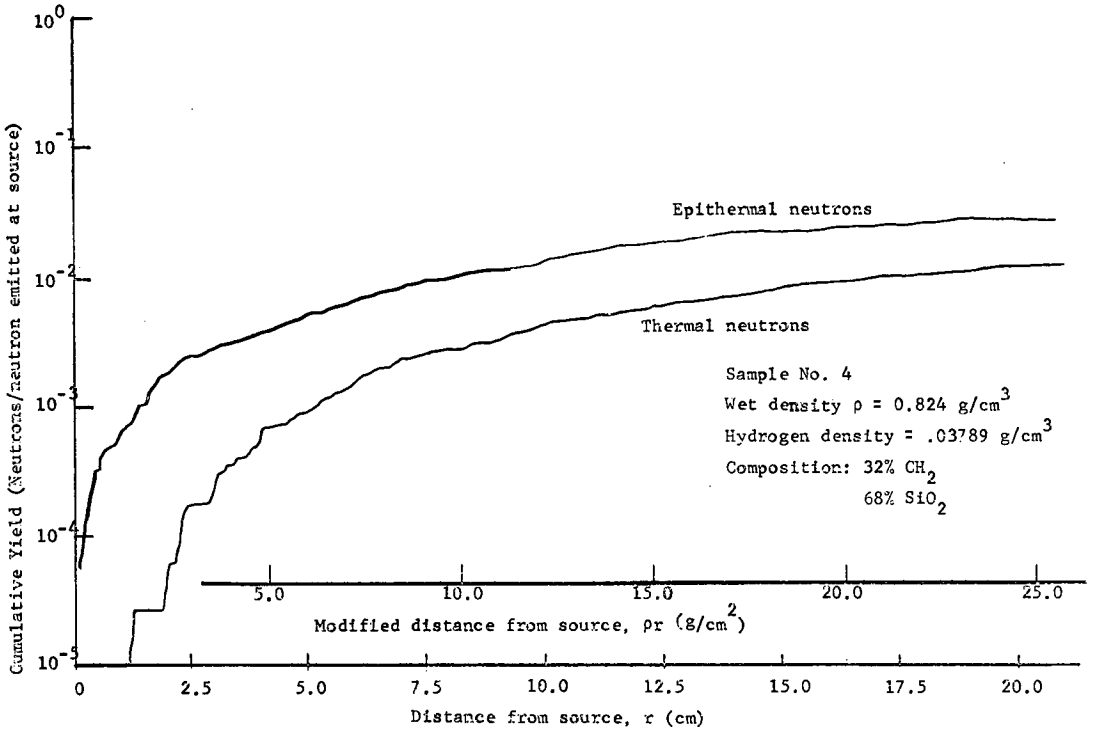

Figure 3. Cumulative neutron yields as a function of distance from source.

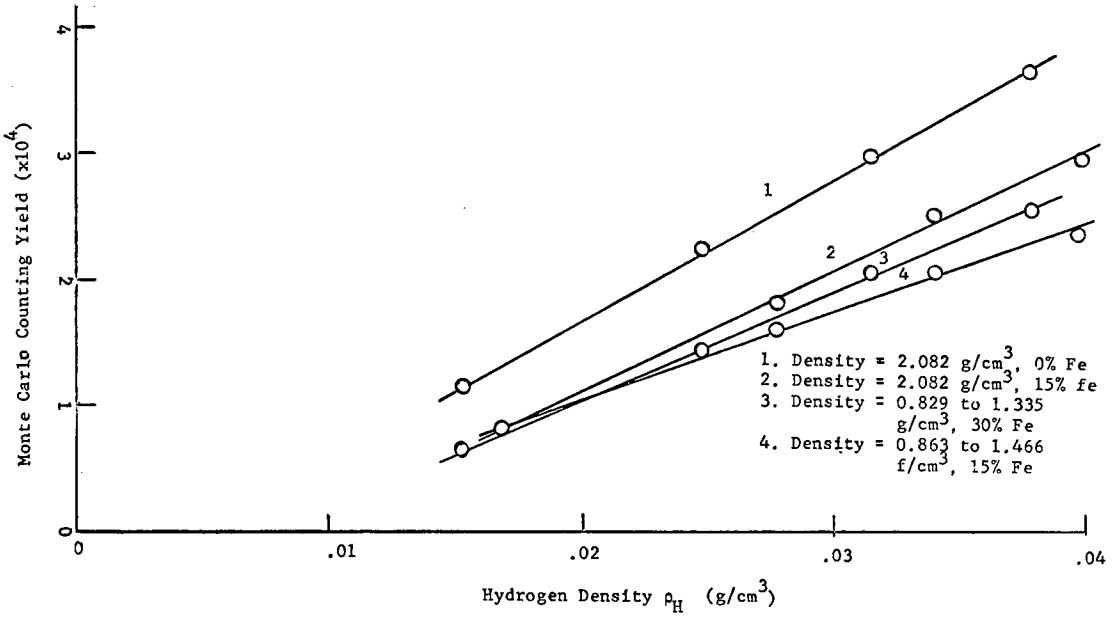

Figure 4. Effect of sample composition and density on detector yield predicted by Monte Carlo.

absorbing media, respectively. Although the samples of curves 3 and 4 have variable wet densities, their densities average about one-half of those in curves 1 and 2 and the compositions of the curve 3 and 4 samples are also representative of low- and high-absorbing media, respectively. Therefore, the effect of sample density on detector response can be observed by comparing curves 1 with 3 and 2 with 4, while the effect of sample composition (low- or high-absorbing media) can be observed by comparing curves 1 with 2 and 3 with 4. It can be seen that a change in sample density by a factor of about 2 affects the detector yield slightly more than a relative change in iron content from 0 to 15 percent. These results are indications of the effects that can be studied with the Monte Carlo simulation.

EXPERIMENTAL STUDIES AND LABORATORY STANDARDS

To check the Monte Carlo predictions, experimental detector yields were taken under conditions that duplicated the Monte Carlo calculations for Samples 1 through 10. Sample containers were made by cutting in half steel drums having radii of 29 cm, slightly larger than the 25 cm used in the Monte Carlo simulations. The samples of sand, iron powder, and polyethylene powder were mixed in a small portable concrete mixer, then placed in the drum and shaken for 16 to 20 min at 17 cycles per second with a lateral amplitude of 1.2 mm. Sufficient sample was prepared to ensure a sample depth of 25 cm. The major deficiency of these samples is that they are not representative of actual construction soil densities. The wet densities of these samples range from 0.824 to 1.590 g/cm^3, considerably lower than the average value of about 2 g/cm^3 for construction soils.

Two BF_3 detectors as described in the previous section were used with a 1.1-millicurie ^{226}Ra-Be isotopic neutron source to experimentally determine the counting yields. The neutron source was calibrated against a standard ^{226}Ra-Be source and found to have a total neutron emission rate of 3.295×10^4 neutrons per second. In addition to determining experimental counting yields at source-to-detector distances of 2.5 cm, results were also taken at 6 and 10 cm distances (Table 6).

The correlation between the results predicted by the Monte Carlo simulation and the experimental results is shown in Figure 5 for the first 8 samples at a source-detector separation of 2.5 cm. The straight line through the 8 samples determined by a least-squares analysis of the data has a slope of 0.870 and an intercept of only 0.050. The standard deviation of the Monte Carlo yields from this least-squares straight line is $\pm 0.079 \times 10^{-4}$, which represents a maximum deviation of about 12 percent when referred to the smallest Monte Carlo yield of Sample 1. Inasmuch as the relative standard deviation of the Monte Carlo yields is estimated to vary from 6 to 10 percent, the straight-line correlation appears to be at least as good as the individual results can be interpreted. The very small intercept of the least-squares straight line indicates that the Monte Carlo results deviate from the experimental results by a simple, constant bias. This could easily be caused by obtaining the wrong value for the source emission rate or the wrong value for the macroscopic absorption cross section of the BF_3 detectors, or any similar simulation discrepancy. Considering the accuracies with which these factors can be obtained, the correlation between the Monte Carlo simulation and the experimental results is considered to be good.

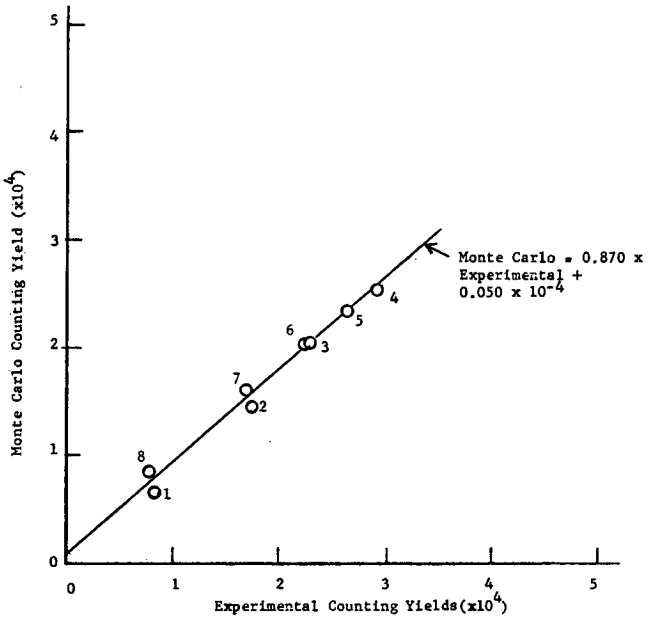

Figure 5. Correlation between Monte Carlo and experimental counting yields.

GENERALIZATION OF MONTE CARLO RESULTS

An effort was made to generalize the Part I results of the Monte Carlo simulation for subsequent use in a numerical integration of all emergent neutrons that would be detected by a detector of any type, size, and location. To reduce this problem somewhat, only emergent thermal neutrons (energy less than 1 eV) and epithermal neutrons (energy from 1 eV to 100 KeV) were treated. The cumulative number of emergent neutrons in each of these energy groups was tabulated as a function of distance from the source for each of the 19 Monte Carlo runs. These data have been stored on computer cards for future use.

Several semiempirical forms derived from two-group diffusion theory treatments were tried for fitting the cumulative number of emerging neutrons versus distance of emergence from the source. Only the forms found most successful are reported here. For the thermal group of neutrons the cumulative number of emerging neutrons could be fit by

$$C_t(r\rho) = A_1\left[1 - \left(1 + \frac{r\rho}{A_2}\right)e^{-r\rho/A_2}\right] \qquad (14)$$

in which $C(r\rho)$ is the cumulative number of neutrons emerging at the distance, r, from the source when the total soil density is ρ and A_1 and A_2 are constants determined by a least-squares analysis of the data for each sample. For the epithermal group of neutrons the expression was

$$C_\epsilon(r\rho) = B_1\left[B_2\left(1 - e^{-r\rho/B_2}\right) - B_2\left(1 - e^{-r\rho/B_3}\right)\right] \qquad (15)$$

in which B_1, B_2, and B_3 are constants determined by a least-squares analysis of the data for each sample. The corresponding differential number of neutrons per unit area can be obtained from

$$\phi(r, \rho) = \frac{1}{2\pi r}\frac{\overline{dC}(rp)}{dr} \qquad (16)$$

in which $\phi(r, \rho)$ is the differential number of neutrons per unit area at distance r and density ρ. It should be noted that $\phi(r, \rho)$ depends on both r and ρ and not solely on the product $r\rho$. The thermal differential number of neutrons per unit area becomes

$$\phi_t(r, \rho) = \frac{A_1 \rho^2 e^{-r\rho/A_2}}{2\pi A_2^2} \tag{17}$$

and the epithermal differential number of neutrons per unit area becomes

$$\phi_e(r, \rho) = \frac{B_1 \rho}{2\pi r}[e^{-r\rho/B_2} - e^{-r\rho/B_3}] \tag{18}$$

The constants for these expressions were obtained for the 19 Monte Carlo results. Assuming that the emerging neutrons were equally distributed in all directions out of the surface, the differential number of neutrons per unit area per total number of neutron histories was multiplied times the macroscopic detector absorption cross section times the effective detector dimension in the direction of the emergent neutron times the fractional solid angle subtended by the detector. This product was integrated over the entire sample surface. The results of this integration did not match the specific Part II Monte Carlo predictions of gauge response previously given, indicating that the assumption that the neutrons emerging at all points were emitted in equal numbers in all directions out of the surface is not correct. Attempts at this complete generalization have been abandoned at present.

A more limited generalization attempt has met with better success. The Monte Carlo Part II results for gauge response previously reported for a BF_3 detector placed 2.5 cm from the source have been fit to the expression:

$$R_m = 0.00636\ (6.05\ w_{\mathrm{Fe}} + 1)\ \rho^2 \left(\frac{2.082\rho_{\mathrm{H}}}{\rho}\right)^{1.31+1.87\ w_{\mathrm{Fe}}} \tag{19}$$

in which R_m is the Monte Carlo predicted gauge response per unit source intensity, w_{Fe} is the weight fraction of iron contained in the sample, and ρ_{H} is the hydrogen density in grams per cubic centimeter of hydrogen. In the more usual engineering units this expression becomes

$$R_m = 1.633 \times 10^{-6}\ (6.05\ w_{\mathrm{Fe}} + 1)\ \rho^2 \left(\frac{0.2327\rho_w}{\rho}\right)^{1.31+1.87\ w_{\mathrm{Fe}}} \tag{20}$$

in which the density, ρ, and the moisture content, ρ_w, are in pounds per cubic foot. This empirical formula fits the 8 Monte Carlo runs (11 through 18) to within a relative standard deviation of 2 percent. It will adequately serve as a tentative calibration model for neutron gauges of the general type that use a BF_3 proportional counter, any alpha-particle-emitting radioisotope with beryllium neutron source, and an approximate source-to-detector center distance of 1 in. It probably should not be used with neutron gauges that contain neutron moderators such as polyethylene and have a large background response when no moisture is present in the sample.

USE OF THE TENTATIVE CALIBRATION MODEL

The proposed use of the tentative calibration model first involves determining if the nuclear moisture gauge to be calibrated is adequately described by the tentative calibration model. The previous section showed that the gauge should have the following design characteristics: (1) a BF_3 proportional counter as the detector, (2) an alpha-particle-emitting radioisotope mixed with beryllium isotopic source (^{226}Ra-Be and ^{241}Am-Be are proper), (3) an approximate source-to-center-of-detector distance of 1 in., and (4) no moderator material incorporated in the gauge that would give a high background or zero moisture gauge response. If there is some doubt about these characteristics the manufacturer should be consulted. Second, one must construct four to six laboratory standard samples such as the ones described under "Experimental Studies and Laboratory Standards." If desired, one could also construct samples consisting of iron powder, sand, and water. However, such samples would not be stable and may not have a homogeneous distribution of water. At any rate, the samples should have a representative range of moisture content (say from 5 to 30 pcf), a representative range of total density (say from 110 to 140 pcf), and a representative range of composition (say from 0 to 10 percent by weight of iron). Third, one should obtain gauge responses on all the prepared samples. Fourth, one should determine the best least-squares analysis of the data to obtain the constant in the calibration model:

$$R_G = k\, R_m \tag{21}$$

in which R_G is the gauge response and k is the constant to be determined by a least-squares analysis of the response data. The pertinent values of the Monte Carlo predicted gauge response, R_m, can be obtained by substituting the appropriate values of weight fraction of iron, total sample density, and moisture content for each sample in Eq. 20.

Once k in Eq. 21 has been determined by this method, it is suggested that a family of calibration curves for various values of iron content and total sample density be prepared by use of Eq. 21. A typical family of such curves is shown in Figure 6. In the field one would use the particular calibration curve having the value of density and iron content closest to that encountered.

One point should be made about the sample composition. Iron content has been taken here as being completely representative of the effect of soil composition. Although it is probable that iron is the major component of interest in most soils, other elements have a similar effect. The "iron equivalent" should be used for other elements that exhibit this effect. It can be obtained from

$$w_{\mathrm{ei}} = w_i \left(\frac{A_{\mathrm{Fe}}}{A_i}\right)\left(\frac{\sigma_i}{\sigma_{\mathrm{Fe}}}\right) \tag{22}$$

in which w_{ei} is the equivalent weight fraction of iron, w_i is the weight fraction of the element of interest, A_{Fe} and A_i are the atomic masses of iron and the element of interest, and σ_{Fe} and σ_i are the effective absorption cross sections of iron and the element of interest. Table 7 gives some conversion factors for typical elements likely to be encountered. Of the elements listed, potassium has about 0.6, sodium about 0.25, and calcium about 0.15 the importance of iron due to their relative abundance in soils. These conversion factors can be used in

$$w_{ei} = C\, w_i \tag{23}$$

The tentative calibration model has been checked for

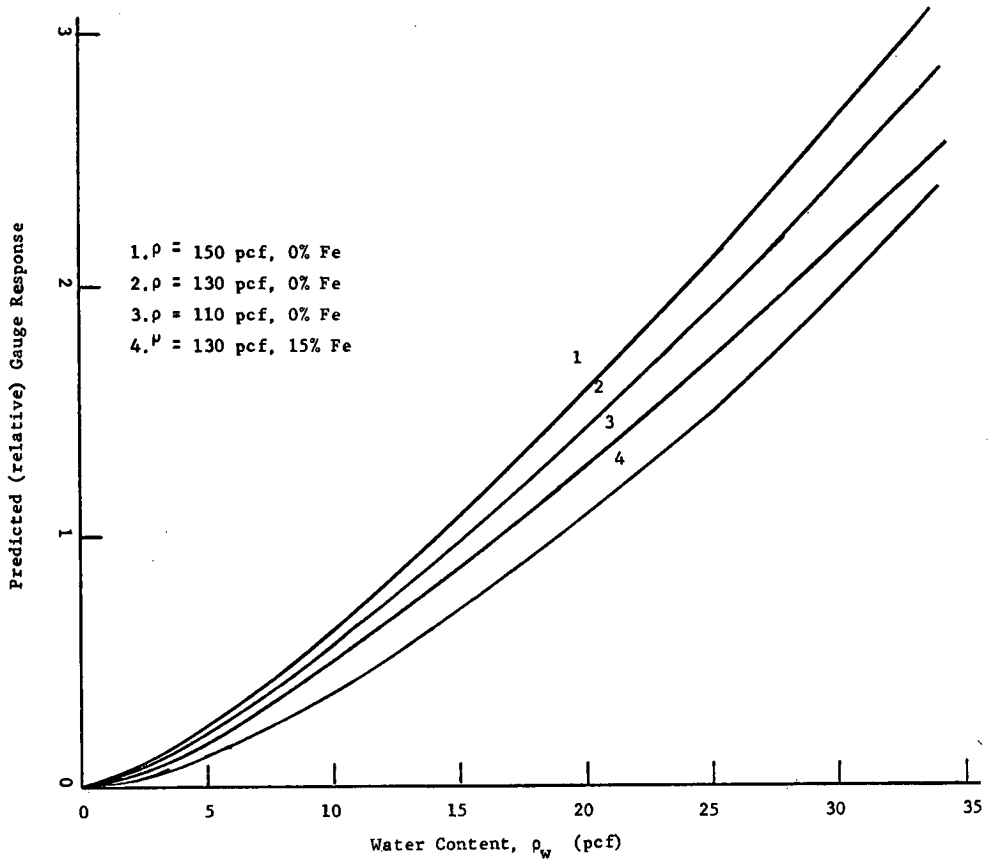

Figure 6. Calibration curves predicted by the tentative calibration model.

four commercial gauges on 15 prepared soil samples at the North Carolina State University Nuclear Soil Gauge Calibration Workshop-Symposium (*5*). No attempt was made to obtain the proper composition calibration curve, but density corrections by the use of Eq. 21 did reduce the standard deviation of all gauges from the average to 1.2 pcf from a value of 2.2 pcf when the single calibration curves of the manufacturers were used. It is probable that if the proper composition calibration curves were established the standard deviation would be reduced further by about one-half.

TABLE 7

CONVERSION FACTORS FOR GENERAL ELEMENTS OF INTEREST FOR OBTAINING EQUIVALENT IRON WEIGHT FRACTIONS

ELEMENT	CONVERSION FACTOR, C	ABUNDANCE (%)
Sodium	0.465	2.8
Potassium	1.150	2.6
Calcium	0.229	3.6
Iron	1.000	5.0

CHAPTER SEVEN

INTERPRETATION, APPRAISAL, AND APPLICATION

Several important future uses for the Monte Carlo simulation results and program are worth describing here. The program can be used directly in design studies for minimizing density and composition effects by calculating optimum source-detector separations and investigating different types of detectors. Unfortunately, the present code cannot be used to study the effects of reflectors or moderators incorporated in the gauge design.

Part II of the program can also be used with experimental responses on several of the samples described in Table 1 to calibrate neutron moisture gauges. This would be accomplished by calculating detector yields for all of the 19 samples listed in Table 1 for the particular detector type and size employed in the gauge of interest. Then experimental detector yields would be obtained by taking responses on several of the samples. A comparison of the Monte Carlo detector yields with the experimental yields would hopefully give a constant factor, as it did in the results of this study. This constant factor would then be applied to the Monte Carlo results for typical soils (Samples 11 through 18) to give calibrations for two representative soil compositions—one a low-absorbing, the other a high-absorbing soil. With minor modifications the program could be used to calculate detector yields for these samples at various densities by taking advantage of the normalized form of the results previously discussed. Samples 1, 4, 5, and 8 have been retained for this purpose. A preliminary investigation of this technique gave promising results.

The calibration technique just mentioned would be relatively expensive, due to the large amount of computer time required. As an alternative to this technique, one could develop a simple integration approach similar to that of Olgaard and Haahr (*12*). This would first require that the thermal neutron flux as a function of position be available for the various samples. The most convenient method of accomplishing this would be to obtain empirical relationships for the flux for each sample; however, these fluxes could be used directly in a numerical integration as derived from the Part I data stored on magnetic tape.

Probably the most important use of the Monte Carlo results generated here would be in their use for substantiating any analytical model that might be developed for the surface-type neutron gauges. Such a model would be much more convenient to use for either calibrations or design studies.

The tentative calibration model should prove useful for the more limited case when a gauge is used that incorporates a BF_3 proportional counter at a source-to-detector center distance of about 1 in. It should be pointed out that this method has not been extensively tested.

CHAPTER EIGHT

CONCLUSIONS AND SUGGESTED RESEARCH

The conclusions that can be drawn from this study of nuclear moisture content gauges are that: (1) the Monte Carlo simulation of these gauges is accurate, but requires a large amount of computer time; (2) attempts at a complete generalization of the Monte Carlo simulation results have not been successful to date; and (3) a less complete and empirical generalization of the Monte Carlo results appears promising as tested at the North Carolina State University Nuclear Soil Gauge Calibration Workshop-Symposium.

A numerical solution of the neutron transport equation as a possible more general calibration model for the neutron soil moisture content gauges should be investigated. If this model is successful, a dual-gauge principle for eliminating the effect of soil composition should also be investigated. The researchers plan to use the Monte Carlo results in the near future in other projects to determine the effect of various kinds of detectors on the neutron gauge sensitivity to soil composition and density. In addition to the BF_3 proportional counter detectors studied in the present work, lithium-loaded crystal detectors and ^3He-filled proportional counter detectors are to be investigated.

REFERENCES

1. BALLARD, L. F., and GARDNER, R. P., "Density and Moisture Content Measurements by Nuclear Methods—Interim Report." *NCHRP Rep. 14* (1965) 32 pp.
2. GARDNER, R. P., and ROBERTS, K. F., "Density and Moisture Content Measurements by Nuclear Methods—Final Report." *NCHRP Rep. 43* (1967) 38 pp.
3. KUHN, S. H., "The Effects of Type of Material on Nuclear Density Measurements." *Hwy. Res. Record No. 66* (1965) pp. 1-14.
4. GARDNER, R. P., ROBERTS, K. F., HUGHES, C. S., and ANDAY, M. C., "A Calibration Model for Optimizing the Air-Gap Method of Compensating Nuclear Density Gauges for Soil Composition Variations." *Jour. of Materials,* Vol. 2, No. 1, p. 3 (1967).
5. MCDOUGALL, F. H., DUNN, W. L., and GARDNER, R. P., "Report on Nuclear Soil Gauge Calibration Workshop-Symposium." Unpublished report from North Carolina State Univ. (Apr. 1969).
6. GARDNER, R. P., "Minimizing Nuclear Soil Density and Moisture Content Gauge Errors." *Hwy. Res. Record No. 290* (1969) pp. 1-8.
7. GARDNER, R. P., "Elimination of Measurement Interferences from Surface-Type Nuclear Soil Density and Moisture Gauges." *Trans. American Nuclear Society Topical Meeting on Radiation and Isotope Technology in Latin American Development.* San Juan, P. R. (May 1969).
8. GARDNER, R. P., "Gamma-Ray Gauges for Measuring the Density of Building Materials." *Proc. of International Symposium on Radiometric Methods and Instruments for the Determination of Soil and Building Materials Density and Moisture.* Brno, Czechoslovakia (Oct. 1969).
9. DUNN, W. L., and MCDOUGALL, F. H., "Minimizing Errors in Gamma-Ray Surface-Type Density Gauges: Existing Gauges and New Design Concepts." *Hwy. Res. Record No. 301* (1970) pp. 40-52.
10. PREISS, K., "Analysis and Improved Design of Gamma-Ray Backscattering Density Gauges." *Hwy. Res. Record No. 107* (1966) pp. 1-12.
11. SEMMLER, R. A., "Neutron-Moderation Moisture Meters: Analysis of Application to Coal and Soil." Final Report from Laboratories for Applied Sciences, Univ. of Chicago, Div. of Isotopes Development, USAEC, C00-712-73 (1963).
12. OLGAARD, P. L., and HAAHR, V., "Comparative Experimental and Theoretical Investigations of the DM Neutron Moisture Probe," *Nuc. Eng. and Design,* Vol. 5 (1967) p. 311.
13. COUCHAT, P. J., "La Methode Neutronique de Mesure de l'Humidité des Sols." *Rapport CEA-R3298,* Centre d'Etudes Nucléaires de Cadaraches (1967).
14. KASI, S., and KOSKINEN, H., "Analysis, Calculations and Measurements Concerning the Moisture Measuring by the Neutron Method." *Nuc. Eng. and Design,* Vol. 3, p. 74 (1966).
15. LIPPOLD, W. J., CARNESALE, A., and GARDNER, R. P., "A Monte Carlo Simulation of the Surface-Type Neutron Moisture Gauge." *Nuc. Eng. and Design,* Vol. 10, p. 373 (1969).
16. IRVING, D. C., FREESTONE, R. M., and KANN, F. B. K., "05R Code Users Manual." ORNL-3622, UC-32, TID-4500, USAEC, Oak Ridge, Tenn. (1965).
17. DEPAUGHER, J., "Double Moderation Neutron Dosimeter." USAEC HW-57293 (July 1958).

APPENDIX A

OPTIMIZATION OF A DUAL-GAUGE PRINCIPLE FOR GAMMA-RAY BACKSCATTER DENSITY GAUGES *

By WILLIAM L. DUNN

One specific problem to which radioisotope applications have been addressed is that of measuring certain soil parameters for highway construction purposes. Nuclear gauges for determining weight density and moisture content of soils have been developed and have attracted considerable attention because they offer some obvious advantages over their nonnuclear counterparts, including speed and ease of measurement, reproducibility, and, in the case of surface-type backscatter gauges, nondestructiveness of the measured sample. This appendix considers one type of nuclear gauge, the gamma-ray backscatter gauge for measuring density.

The type of gauge is based on the principle that a flux of gamma radiation incident on a soil surface is attenuated due to scattering and absorption within the soil, and that the scattered gamma flux reemerging from the soil surface carries information about the density and chemical composition of the soil. The absorption is due to the photoelectric absorption process, which is dependent on soil composition and density, whereas the scattering is due mainly to the Compton scattering process, which is dependent essentially only on density. Density is the parameter to be measured; thus, soil composition represents a measurement interference.

A typical gauge consists of a sealed isotopic gamma-ray source, a detector with associated counting electronics, and shielding between the two, as in Figure A-1. The gauge can be used flush on the sample or raised, leaving an air gap between the sample surface and the bottom of the gauge. Until more completely defined under "Experimental Apparatus," a gauge configuration as used here refers to any single combination of a source fixed in location, a detector and its shielding, a fixed source-detector separation, and a fixed air-gap height.

The type of detector most often used is the Geiger-Mueller (G-M) tube because of its ruggedness, stability, and low cost. The backscattered gamma rays detected by the G-M tube are counted by a scaler, and the response in number of counts per unit time is used to find density. The method employed almost universally at present for determining density from response involves use of a calibration curve; i.e., a graph of response, R, in counts per minute (cpm), or the ratio of a test count to a standard count, versus density, ρ, in pounds per cubic foot (pcf). The graph is originally obtained by fitting a curve to the responses taken on a set of calibration standards (samples of known density, and sometimes of known composition).

Since the advent of nuclear gauges in about 1950 there has been some question as to their accuracy. It has long been maintained that nuclear techniques were potentially as accurate as others for measuring soil density; however, widespread acceptance of nuclear gauges has been delayed because their measurements have not always agreed well with those obtained by conventional gravimetric techniques. Methods to improve their accuracy have been sought and their sources of error have been identified as (a) sensitivity to variations in sample composition, (b) poor calibration technique, and (c) sensitivity to surface heterogeneities. Three gauge errors are defined in a later section, together with a means of combining them into a quality factor by which gauges can be compared.

Use of a particular mathematical model for gauge response (calibration model), also considered in a later section, forms the basis for much of the study of gauge performance and gauge errors. This model is used to obtain the dual-gauge principle, which, briefly, involves simultaneous solution of calibration models for two gauges to eliminate the measurement interference of chemical composition while solving for density. It is now suggested that the dual-gauge principle can be used to reduce the composition error and optimum use of this principle can minimize the combined error to acceptable values.

The section on "Experimental Apparatus" discusses the gauge parameters studied in order to optimize the dual-gauge principle and describes the prototype gauge used. It should be understood that a dual gauge consists either of two separate gauges with different calibration models or of a single gauge used in two configurations that have different calibration models. One of the parameters studied, air-gap height, can be varied on existing commercial

* This appendix comprises the essential portions of a thesis bearing the same title prepared under the NCHRP Project 10-5A contract and submitted to the North Carolina State University (1970) in partial fulfillment of the requirements for the degree of Master of Science.

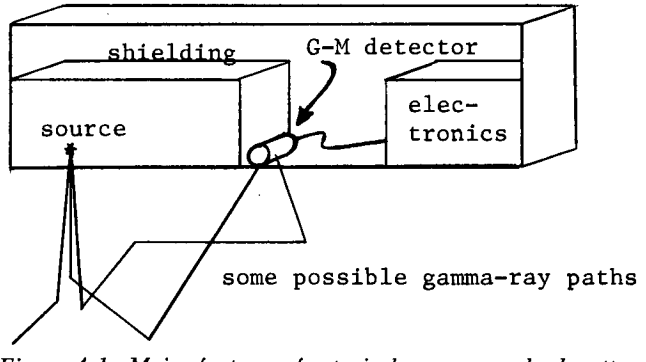

Figure A-1. Major features of a typical gamma-ray backscatter density gauge.

gauges, thereby affording them the capability of acting as dual gauges. There is an optimum value of this parameter such that the dual-gauge solution is characterized by the largest quality factor (quality factor, defined under "Gauge Errors," increases for decreasing combined error and increasing measurement volume).

LITERATURE REVIEW

According to Gunderman (*15*, p. 1), Pieper (*14*) reported in 1949 the results of his experimental study of soil moisture content measurements by neutron thermalization. This subject gains relevance to the subject of gamma-ray backscatter density gauges when it is realized that the two have since developed very closely: nuclear methods for the measurement of moisture content and density have often been studied simultaneously, and a large percentage of commercial nuclear density gauges are also moisture-measuring devices. Thus, the plausibility of using nuclear techniques to measure soil properties had begun to be investigated.

In 1950 Belcher, et al. (*2*) presented results of their studies using subsurface nuclear probes, including a radium source and G-M tube detector for density measurements; and in February 1952, Belcher, et al. (*3*) described surface-type nuclear instruments for measuring soil moisture content and density, concluding that further development was required to obtain instruments for field use.

In 1953 Horonjeff and Goldberg (*10*) stated that subsurface nuclear probe measurements were reproducible but varied as much as 25 percent from measurements by conventional means.

During the mid-1950's most publications were concerned with moisture gauges and transmission-type density gauges. Then, in October 1958, Hoffmeyer (*9*) reported that an average accuracy of ± 2 pcf was obtained by use of a preliminary engineering model of a surface density gauge manufactured by Nuclear-Chicago. Portable nuclear moisture and density gauges became commercially available in about 1959 (*11*). In 1960, Carlton (*4*) described the use of surface-type nuclear soil meters for compaction control testing during actual construction and concluded that the reliability of nuclear methods for compaction control was comparable with that of nonnuclear methods.

Kuhn (*13*) in 1963 proposed an air-gap ratio method for using backscatter density gauges. This first dual-gauge density measurement method has been used to some extent in recent field work.

The question of nuclear gauge accuracy drew increased attention when, at the 1964 Highway Engineering Course at Oak Ridge, the gauge manufacturers present tested several sites (under poorly controlled conditions) and variations as large as 20 pcf were reported (*15*, p. 7). This caused enough concern that in July 1965 the Virginia Council of Highway Investigation and Research conducted a correlation conference so that comparative tests could be run among nuclear gauges under well-controlled conditions. Results of this conference (*11*) showed standard errors of 11.0 pcf for backscatter gauges using normal calibration techniques and 2.6 pcf for backscatter gauges using the Kuhn air-gap calibration technique.

In 1964, NCHRP Project 10-5, "Density and Moisture Content Measurements by Nuclear Methods," was begun with Dr. R. P. Gardner, of Research Triangle Institute, as principal investigator. Gardner and associates proposed a mathematical model for density gauge response (presented later herein) and used it to study some of the data from the Virginia correlation conference. The result was that "when the Gardner model was used to calculate the calibration curves, 26 of the 42 results had standard errors of less than 2.4 pcf" (*15*, p. 9), a considerable improvement over most results presented earlier.

In 1965 Ballard and Gardner (*1*) summarized their work to date on Project 10-5 in an interim report that concluded that composition dependence of density gauges was the most significant source of error and stressed that nuclear backscatter density gauge results were more reproducible and potentially as accurate as results from nonnuclear techniques while offering the additional advantage of nondestructiveness. In 1967 Gardner and Roberts (*6*) issued a final report on Project 10-5 containing a complete analysis of their mathematical model for density gauges and a thorough summary of their dual-gauge studies.

In March 1967, Gardner, et al. (*7*) published a work that used the Gardner model to demonstrate the optimization of the air-gap method of using nuclear density gauges.

In July 1969, McDougall, et al. (*16*) reported a method of calibrating gauges according to a dual-gauge nomograph, as well as definitions of various gauge errors and results of laboratory and field testing of four commercial gauges.

Finally, in 1969, Gardner (*8*) described the development of the calibration model approach, the dual-gauge principle, and the identification of errors for nuclear density and moisture gauges.

THEORY OF THE DUAL-GAUGE PRINCIPLE

Calibration Model

The calibration model alluded to previously and reported by Gardner and Roberts (*6*) is presented here as

$$R = C \exp_{10} (a + bC + cP) \qquad \text{(A-1)}$$

in which R is the gauge response; C and P are the normalized * Compton scattering and photoelectric absorption probabilities, respectively; a, b, and c are model constants;

$$C = \frac{\rho}{10} \sum_{i=1}^{m} \frac{w_i Z_i}{A_i} \qquad \text{(A-2)}$$

$$P = \frac{\rho}{10^6} \sum_{i=1}^{m} \frac{w_i Z_i^5}{A_i} \qquad \text{(A-3)}$$

ρ is sample density in pcf; w_i, Z_i, and A_i are the weight fraction, atomic number, and atomic weight, respectively, of element i; and m is the number of elements in the sample. It is important to note that the Compton scattering probability, C, is approximately equal to $\rho/20$, because

* C and P are normalized to values near 1 as required for the best least-squares fit; hence, the factors 10 and 10^6 in the denominators of Eqs. A-2 and A-3, respectively.

for most elements contained in soils the ratio Z/A is very nearly 0.5 (a notable exception is hydrogen, for which $Z/A \simeq 1$). On the other hand, the photoelectric absorption probability, P, is strongly dependent on elemental composition, since it varies as Z^5/A. The dependence of gauge response on composition can now be recognized as due primarily to photoelectric absorption. A simple argument verifies this. Consider two soil samples of equal density but different composition. A flux of gamma rays incident on one sample would experience scattering and absorption in the soil and would produce at the soil surface a backscattered flux that could be detected. If an identical flux was incident similarly on the second sample, the scattering would be much the same (because the scattering probability, C, is much the same) but the flux degradation would be different (because of the difference in the absorption probability, P) and so the response at the soil surface would be different. Hence, the dependence on composition.

A more detailed description of the response term, R, in the calibration model now seems appropriate. Generally, the response will be considered to be

$$R = (r - B)/(\hat{r} - B) \qquad \text{(A-4)}$$

in which r is the total number of counts registered by the gauge on the test sample, $\hat{r}$ is a reference count equal to the total number of counts registered on a reference sample, and B is the background (which might be thought of physically as the total number of counts registered on a sample of zero density, $r\,(0)$).

The a, b, and c parameters of Eq. A-1 have previously been identified as model constants. Because the background, B, is difficult to measure accurately, it is considered as a fourth model constant and must be found by fitting data to the calibration model. Each gauge configuration has a unique set of model constants. They are determined by first choosing an interval for B (for instance, $0 \leq B \leq R_s - 10{,}000$, in which R_s is the smallest of the four calibration sample responses) and using a Fibonacci search routine to locate a minimum composition error, $\sigma_{c1}(\rho)$, in that range (the Fibonacci search routine does not guarantee that the absolute minimum in that range will be located; if there are relative minima, one of these may be located). For each value of B chosen, a least-squares analysis of data taken on a set of m calibration standards is performed, as explained by Gardner and Roberts (*1*), to obtain the a, b, and c model constants; then the density, $\hat{\rho}$, of each standard is backcalculated using a Newton-Raphson iteration technique and compared with the actual density, ρ, as follows:

$$\sigma_{c1}(\rho) = \left[\sum_{i=1}^{m} \frac{(\rho_i - \hat{\rho}_i)^2}{m}\right]^{\frac{1}{2}} \qquad \text{(A-5)}$$

By searching on B until a minimum $\sigma_{c1}(\rho)$ is found, an "optimum background" and the corresponding a, b, and c constants are obtained.

Use of the ratio of net count to net reference count in Eq. A-4 is considered good engineering practice, as it minimizes the effects of drifts in counting rates between separate uses of a gauge.

If some average values of C and P are used, the calibration model can be graphed as in Figure A-2. The points refer to data for each of four hypothetical calibration standards. They are displaced from the "average curve" because in general the standards will have Compton and photoelectric probabilities different from the "average" values. The least-squares equations are used to find the model constants a, b, and c, which best fit the calibration model to these points. For calibration purposes, standards that represent the extreme high and low values of ρ, C, and P expected in soils to be tested should be used.

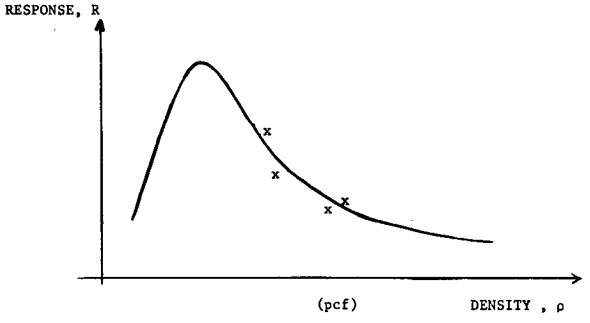

Figure A-2. A graph of the calibration model, $R = C10^{a+bC+cP}$, *versus density,* ρ, *for "average" values of* C *and* P.

Dual-Gauge Solution

The dual-gauge solution for density was an outgrowth of the attempt by Gardner and associates to devise a mathematical model for gauge response. The fact that the density dependence and the composition dependence were located in separate terms in the calibration model led to the idea that two models could be solved simultaneously for density independently of the composition parameter, P. Several methods of applying this principle have been developed, and the mathematics behind these have been published (*6, 7*). A skeletal presentation of some of the major methods and arguments is given here for convenience.

Consider the calibration models of two gauges and denote them by subscripts 1 and 2. Thus,

$$R_i = C \exp_{10}(a_i + b_i C + c_i P) \quad i = 1, 2 \qquad \text{(A-1)}$$

Solve each for P, obtaining

$$P = [\log(R_1/C) - a_1 - b_1 C]/c_1 \qquad \text{(A-6}a\text{)}$$

and

$$P = [\log(R_2/C) - a_2 - b_2 C]/c_2 \qquad \text{(A-6}b\text{)}$$

Use the relation $C' = C/\rho$ and let T be the difference between the two solutions for P, above. Then

$$T(\rho) = \frac{\log(R_1/C'\rho) - a_1 - b_1 C'\rho}{c_1} - \frac{\log(R_2/C'\rho) - a_2 - b_2 C'\rho}{c_2} \qquad \text{(A-7)}$$

Differentiating T with respect to density gives

$$T'(\rho) = \frac{dT(\rho)}{d\rho} = \frac{0.434294 + b_2 C'}{c_2} - \frac{0.434294 + b_1 C'}{c_1} \quad \text{(A-8)}$$

The Newton-Raphson iteration technique for solving nonlinear equations can be used to find the zeros of T; i.e., the values of density for which $T(\rho) = 0$. First a value of density is assumed and labeled ρ_1. Then other values of density, ρ_i, are calculated from

$$\rho_i + 1 = \rho_i - T(\rho_i)/T'(\rho_i) \quad \text{(A-9)}$$

The process is continued until $|\rho_{i+1} - \rho_i|/\rho_i < E$, where E is arbitrarily chosen (as 10^{-6} for calculations reported herein), in which case $\rho = \rho_{i+1}$.

Other possible dual-gauge solutions include an exact solution of the equation $T(\rho) = 0$ after substitution of the series approximation (*7*)

$$\log \rho \simeq \log 130 + 0.86859\left[\frac{\rho - 130}{\rho + 130}\right] \quad \text{(A-10)}$$

and a nomograph solution (*7*).

Thus, using the calibration model presented as Eq. A-1, methods are available for finding approximations to density, ρ, independent of the composition variable, P.

GAUGE ERRORS

Development of the calibration model has afforded the opportunity of an entirely new approach to the study of gauge errors. Whereas previously sources of error could be hypothesized, now errors can be defined, calculated, and at least partially explained. Past work has mentioned as sources of error such things as variations in elemental composition, poor calibration technique, and surface roughness. Recent work on NCHRP Project 10-5A has led to a formulation of gauge errors as follows:

1. Composition error, due to the range of chemical compositions found in soils.
2. Surface-effect error, due generally to rough and irregular soil surfaces.
3. Counting rate measurement error, stemming from the inherent uncertainties in counting rate measurements.

These errors are discussed and defined individually in the following in terms of the calibration model and the dual-gauge principle, and a method is given of combining them and forming a quality factor by which gauges can be compared.

Counting Rate Measurement Error

As noted in the previous section Gardner, et al. (*7*) have published a method for using two calibration models simultaneously and making the series approximation

$$\log \rho \simeq 2.11394 + 0.86859\left[\frac{\rho - 130}{\rho + 130}\right] \quad \text{(A-11)}$$

to obtain the quadratic equation

$$X\rho^2 + Y\rho + Z = 0 \quad \text{(A-12)}$$

in which X, a constant for any particular dual-gauge combination, is given by

$$X = 0.05\ (c_1\ b_2 - c_2\ b_1) \quad \text{(A-13)}$$

and Y and Z, functions of the two gauge responses, R_1 and R_2, are given by

$$Y = c_2 \log R_1 - c_1 \log R_2 - 1.6815\ (c_2 - c_1) + c_1 a_2 - c_2 a_1 + 6.5\ (c_1 b_2 - c_2 b_1) \quad \text{(A-14)}$$

and

$$Z = 130\ c_2 \log R_1 - 130\ c_1 \log R_2 + 7.2384\ (c_2 - c_1) + 130\ (c_1 a_2 - c_2 a_1) \quad \text{(A-15)}$$

The solution for density is, then,

$$\rho = \frac{-Y \pm (Y^2 - 4XZ)}{2X} \quad \text{(A-16)}$$

The statistical nature of radiation counting places uncertainties on the gauge responses, denoted by $\sigma(R_1)$ and $\sigma(R_2)$. The propagation of these uncertainties results in an uncertainty in the value of density obtained from the responses. According to the study of statistics, propagation of error follows the rule

$$\sigma^2(x_o) \simeq \sum_{i=1}^{m}\left[\frac{\partial M_o}{\partial M_i}\right]\sigma^2(x_i) \quad \text{(A-17)}$$

in which x_i is the ith measured quantity; $x_o = f(x_1, x_2, \ldots, x_m)$; M_i is the mean of the distribution function, $P(x_i)$, for x_i; M_o is the mean of the distribution function, $P(x_o)$, for x_o; $\sigma^2(x_i)$ is the variance of the ith measured quantity; $\sigma^2(x_o)$ is the variance of M_o; all the M_i are independent; and m is the number of measured quantities. Thus, a measure of the uncertainty in the value of density due to the uncertainties in the measured counting rates is given by the counting rate measurement error, $\sigma_s(\rho)$, defined as

$$\sigma_s(\rho) = \left[\left(\frac{\partial \rho}{\partial R_1}\right)\sigma^2(R_1) + \left(\frac{\partial \rho}{\partial R_2}\right)^2 \sigma^2(R_2)\right]^{\frac{1}{2}} \quad \text{(A-18)}$$

in which $\sigma(R_i)$ is the uncertainty in the measured value of R_i and $\frac{\partial \rho}{\partial R_i}$ is calculated from Eqs. A-13 through A-16; i.e.,

$$\frac{\partial \rho}{\sigma R_i} = \frac{-1}{2X}\left[\frac{\partial Y}{\partial R_i} \mp \frac{Y\frac{\partial Y}{\partial R_i} - 2X\frac{\partial Z}{\partial R_i}}{(Y^2 - 4XZ)^{\frac{1}{2}}}\right], \quad i = 1, 2 \quad \text{(A-19)}$$

$$\frac{\partial Y}{\partial R_1} = \frac{c_2}{R_1 \ln 10} \quad \text{(A-20)}$$

$$\frac{\partial Y}{\partial R_2} = \frac{-c_1}{R_2 \ln 10} \quad \text{(A-21)}$$

and

$$\frac{\partial Z}{\partial R_i} = 130\frac{\partial Y}{\partial R_i}, \quad i = 1, 2 \quad \text{(A-22)}$$

Two solutions for $\partial\rho/\partial R_i$ are available from Eq. A-19 (notice the $\mp$ symbol). The one is chosen which corresponds to the solution for density from Eq. A-16, which is nearer

the actual (known) value of density on which the measurements were taken (i.e., the + sign is chosen in Eq. A-19 if $|\rho - \rho_1|$, $\rho_1 = \frac{-Y - (Y^2 - 4XZ)^{\frac{1}{2}}}{2X}$, is smaller than $|\rho - \rho_2|$, $\rho_2 = \frac{-Y + (Y^2 - 4XZ)^{\frac{1}{2}}}{2X}$, and vice versa).

As a rule-of-thumb approximation, any measured counting rate, r, such that $r \geq 10{,}000$ cpm, will be within about 1 percent of the true mean 68 percent of the time for measurements from ordinary counting systems; that is,

$$\sigma(r) \simeq 0.01\, r, \quad r \geqq 10{,}000 \text{ cpm} \qquad \text{(A-23)}$$

Actually, because the constant, B (obtained through the Fibonacci search), is subtracted from r to obtain the best model fit, the "net" counting rate, $n = r - B$, should be in excess of 10,000 cpm in order that $\sigma(n)$ be $0.01n$ and counting rate measurement error be minimized. Hence,

$$\sigma(n)/n = \sqrt{n}/n + \hat{\sigma}(n)/n = 0.01, \quad n \geqq 10{,}000 \text{ cpm} \qquad \text{(A-24)}$$

in which $\hat{\sigma}(n)$ is the uncertainty due to system instabilities and $\sigma(n)$ is the over-all uncertainty in the "net" counting rate, n.

The uncertainty in ratio response, R, is ordinarily obtained from

$$R = n/\hat{n} \qquad \text{(A-25)}$$

in which $\hat{n}$ is a net reference count. Then,

$$\begin{aligned}\sigma(R) &= \left[\left(\frac{\partial R}{\partial n}\right)^2 \sigma^2(n) + \left(\frac{\partial R}{\partial \hat{n}}\right)^2 \sigma^2(\hat{n})\right]^{\frac{1}{2}} \\ &= [(0.01\, R) + (0.01)R]^{\frac{1}{2}} \\ &= \sqrt{2}\,(0.01\, R) \end{aligned} \qquad \text{(A-26)}$$

However, in the region of interest ($n \geq 10{,}000$ cpm) uncertainties due to system instabilities ($\hat{\sigma}(n)$) begin to dominate the uncertainties due to normal fluctuations in counting rate measurements ($\sqrt{n}$) and n and $\hat{n}$ are no longer truly independent, so the foregoing derivation of $\sigma(R)$ does not apply. Instead, the uncertainties due to system instabilities (dead time, electronic drift, decay of source with time, etc.) are minimized by use of the ratio technique. Evaluation of the actual uncertainty in ratio response, $\sigma(R)$, would be determined only by extensive experimentation with each system and cannot be specified in general in a manner that can be easily calculated. Hence, it is considered a good approximation that the uncertainty in ratio response is given by

$$\sigma(R) = 0.01\, R \qquad \text{(A-27)}$$

Finally, it should be noted that the magnitude of $\sigma_s(\rho)$ depends somewhat on the density of the sample measured, since it depends on the $\partial\rho/\partial R_i$, $i = 1, 2$, which are certainly not constant over the entire density range of soils encountered in routine field work. The sample used by the author to determine $\sigma_s(\rho)$ was Pyrex, with a density of 135.4 pcf.

Composition Error

If the model constants have been determined, the calibration model can be used to back-calculate the density of a test sample. Consider a gauge that is calibrated on a set of m samples (a response is determined on each sample and these responses are fit to the calibration model). If ρ_i is used to denote the actual density of sample i, and ρ_i' the dual-gauge back-calculated density,* then a composition error, $\sigma_c(\rho)$, can be defined as

$$\sigma_c(\rho) = \left[\sum_{i=1}^{m} \frac{(\rho_i' - \rho_i)^2}{m}\right]^{\frac{1}{2}}, \quad m \geq 4 \qquad \text{(A-28)}$$

Because the back-calculated densities will sometimes be larger and sometimes smaller than the actual densities, any one back-calculated density is liable to be accurate only within $\pm\sigma_c(\rho)$. Actually, this will be a standard error if the m samples used to calculate $\sigma_c(\rho)$ have standard deviations of density and composition representative of those of soils encountered in field work and if density and composition vary approximately linearly with gauge response.

Thus, this error gives an indication of how much, on the average, a gauge is likely to miscalculate density due to variations in composition among soils and inaccuracies in the model fit. The magnitude of this error will, of course, depend on the calibration standards used; those used in this study are described under "Laboratory Standards."

Surface-Effect Error

Rough, warped, or irregular soil surfaces provide poor seating for a gauge and this introduces another error, called the surface-effect error. It is impractical to attempt to reproduce every type of surface condition likely to be encountered in field work, to somehow measure errors due to each of these, and to find a probable surface-effect error from these. It is possible, however, to simulate a surface-effect error by calculating the difference between a density measurement, ρ', taken flush on a smooth sample surface and a measurement, ρ'', taken with the gauge raised a small distance, Δ, above the sample surface. Thus, a surface-effect error, E_{se}, is defined as

$$E_{se} = |\rho' - \rho''| \qquad \text{(A-29)}$$

in which ρ'' is a function of Δ. It seems helpful, and realistic, to assume that this error can be represented by this change in density; for one could argue that a gauge for which $|\rho' - \rho''|$ is small should be less sensitive to surface heterogeneities than a gauge for which $|\rho' - \rho''|$ is large. Thus, the surface-effect error gives a measure of how sensitive a gauge is to the irregularities of soil surfaces.

Several things should be noted concerning this definition. First, E_{se} may be either a single- or a dual-gauge error, depending on whether ρ' and ρ'' are back-calculated from the single-gauge calibration model or by a dual-gauge method. Second, E_{se} is a function of the air gap, Δ, chosen to determine ρ'', and is thus a relative error. The value of Δ has arbitrarily been chosen to be $\frac{1}{16}$ in. for all calculations reported in this study. Third, generally ρ'' will be greater than ρ'. For a single gauge this is obvious, because,

* Unless otherwise stated, a dual-gauge back-calculated density always refers to a density obtained by use of the Newton-Raphson iteration technique previously outlined.

generally, $R(\Delta = 1/16 \text{ in.}) > R(\Delta = 0)$ and a look at the calibration curve (Fig. A-2) reveals that the larger the response, the smaller the density, on the right-hand portion of the curve, which is usually the region of interest. Fourth, it is observed that generally the response, $R(\Delta)$, increases with increasing Δ to some maximum and then begins a slow descent. Fifth, the value of this error depends, to some extent, on the sample tested, inasmuch as the response-versus-air-gap curve depends, to some extent, on the sample tested.

To evaluate surface-effect error, the responses at $\Delta = 0$ and $\Delta = 1/16$ in. must be evaluated. Responses are determined on Pyrex flush and at three or four air-gap heights, Δ. A cubic equation of the form

$$R(\Delta) = \gamma\ \Delta^3 + \zeta\ \Delta^2 + \xi\ \Delta + \eta$$

is fit to the data by a Fibonacci search on η, $R(0) - 0.01R(0) \leqq \eta \leqq R(0) + 0.01R(0)$, and a least-squares analysis for the remaining three constants, γ, ζ, and ξ. Of course, the fit is exact for data taken at only three air-gap heights (any four points can be fit exactly to some cubic), but it is also noted that the fit is well within statistics in every case for which data were taken at four air-gap heights. The equations for γ, ζ, and ξ obtained from the least-squares analysis are

$$\gamma = \frac{S1 - \dfrac{S2 - \dfrac{S7\ S3}{S8}}{D}\, S5 - \dfrac{S6\ S7}{S8} - \dfrac{S6\ S3}{S8}}{S4 + \dfrac{\dfrac{2\ S5\ S6\ S7}{S8} - S5^2 - \dfrac{S6^2\ S7^2}{S8^2}}{S6 - \dfrac{S7^2}{S8}} - \dfrac{S6^2}{S8}} \tag{A-31}$$

$$\zeta = \frac{S2 - \gamma\ S5 - \dfrac{S7\ S3 - S7\ \gamma\ S6}{S8}}{S6 - \dfrac{S7^2}{S8}} \tag{A-32}$$

and

$$\xi = \frac{S3 - \gamma\ S6 - \zeta\ S7}{S8} \tag{A-33}$$

in which

$$S1 = \Sigma\ \Delta_i^3\ (R_i - \eta) \tag{A-34}$$

$$S2 = \Sigma\ \Delta_i^2\ (R_i - \eta) \tag{A-35}$$

$$S3 = \Sigma\ \Delta_i\ (R_i - \eta) \tag{A-36}$$

$$S4 = \Sigma\ \Delta_i^6 \tag{A-37}$$

$$S5 = \Sigma\ \Delta_i^5 \tag{A-38}$$

$$S6 = \Sigma\ \Delta_i^4 \tag{A-39}$$

$$S7 = \Sigma\ \Delta_i^3 \tag{A-40}$$

$$S8 = \Sigma\ \Delta_i^2 \tag{A-41}$$

Minimum Combined Error Criterion

Having noted that $\sigma_s(\rho)$ and $\sigma_c(\rho)$, the counting rate measurement and the composition errors, respectively, are normally distributed, it is logical to define a combined normal error, $\sigma_n(\rho)$, as

$$\sigma_n(\rho) = [\sigma_s^2(\rho) + \sigma_c^2(\rho)]^{1/2} \tag{A-42}$$

In order to combine this with the nonnormally distributed surface effect error, E_{se}, the following quantities are formed:

$$L = E_{se} - |\sigma_n(\rho)| \tag{A-43}$$

and

$$W = 2\ |\sigma_n(\rho)| \tag{A-44}$$

The combined error, E_c, is defined to be

$$E_c = [W^2 \pm L^2]^{1/2} \tag{A-45}$$

in which the + sign is used if $L > 0$ and the − sign is used if $L < 0$. This combined error can be used with information concerning the effective sample volume measured by a gauge to form a quality factor by which gauges can be compared.

Gardner and Roberts (*6*) defined an effective sample depth for a single gauge as

$$\hat{x} = 1/k \tag{A-46}$$

in which k is a constant found by a least-squares fit of experimentally determined x and $R(x)$ to the model

$$R(x) = [R(\infty) - R(0)]\ (1 - e^{-kx}) + R(0) \tag{A-47}$$

in which $R(x)$ is the response of a gauge taken on a sample of thickness x. The effective sample depth, $\hat{x}$, is a cut-off depth such that 68 percent of the response is due to gamma rays that penetrate no farther than x. Multiplication of $\hat{x}$ by d, the source detector separation, and $\hat{\omega}$, the effective sample width (assumed to be 4 in.) gives the effective sample volume, $\hat{V}$, measured by the gauge; that is,

$$\hat{V} = \hat{x}\ d\ \hat{\omega} \tag{A-48}$$

For a dual gauge an average effective sample volume, $\hat{V}'$, is defined as

$$\hat{V}' = \frac{\hat{V}_1 + \hat{V}_2}{2} \tag{A-49}$$

in which the subscripts refer to the two configurations in a dual gauge.

A volume factor, V, obtained as a mapping of $\hat{V}'$ onto the interval $0.9 \leq V \leq 1.0$ is defined by the transformation

$$V = 0.9 + 0.1\frac{\hat{V}'}{288} \tag{A-50}$$

in which 288 is an arbitrarily selected maximum effective sample volume, in cubic inches. Then the quality factor, Q, for a dual gauge is defined as

$$Q = 2V/E_c \tag{A-51}$$

The factor of 2 is used merely to normalize the quality factor to unity for a gauge having $E_{se} = 1.0$ pcf, $\sigma_n(\rho) = 1.0$ pcf, $V = 1.0$.

This quality factor is defined whenever $0 \leqq E_{se} \leqq \infty$, $0 \leqq \sigma_n(\rho) \leqq \infty$, and $0.9 \leqq V \leqq 1.0$. It is infinite only

when $E_c = 0$ (a dual gauge is "infinitely good" when its combined error is zero). To investigate when $E_c = 0$, consider two cases:

(a) $L \geqq 0$ or $E_{se} \geqq \sigma_n(\rho)$. Then,
$W + L = 0 \Rightarrow W = L = 0 \Rightarrow E_{se} = \sigma_n(\rho) = 0.$

(b) $L < 0$ or $E_{se} < \sigma_n(\rho)$. Then,
$W - L = 0 \Rightarrow W = L \Rightarrow 2\,\sigma_n(\rho) = E_{se} - \sigma_n(\rho)$
$\Rightarrow \sigma_n(\rho) = E_{se}$,
which is impossible because $\sigma_n(\rho) > E_{se}$.

Hence, combined error, E_c, is zero only when $E_{se} = \sigma_n(\rho) = 0$. Quality factor is plotted versus surface-effect and counting rate measurement errors in Figure A-3.

EXPERIMENTAL APPARATUS

Development of an optimum dual-gauge combination involves the design of two gauge configurations, which, when used as a dual gauge, are characterized by the largest quality factor. In this study, three major design parameters were studied: source energy, source-detector separation, and shape of the detector efficiency spectrum. In addition, some study of source collimation was included. A prototype gauge was constructed which affords variation of the mentioned parameters.

Prototype Gauge

A schematic representation of the prototype gauge is shown in Figure A-4. The main components are the source holder and collimator (A), the shadow shield (B), the gauge housing (C), the source (D), and the detector (E). The associated electronics are considered exterior to the gauge proper and are discussed in a later section.

The gauge housing is a $17 \times 10 \times 4$-in. aluminum chassis with holes 6×9 in. and ½ in. in diameter cut out of the bottom (see Fig. A-5). The source holder consists of two $4 \times 4 \times 2$-in. lead bricks placed one on top of the other so as to form a cube 4 in. on a side (see Fig. A-5) with an approximately $\frac{5}{8} \times \frac{5}{8} \times 2$-in. hole followed by a cylindrical hole of $\frac{3}{16}$-in. diameter and 2-in. length cut in the center (see Fig. A-6). The shadow shield is a $1 \times 2 \times 8$-in. lead brick that is mounted in the chassis so as to be moveable over a 9½-in. interval (see Fig. A-5). The source is one of three capsules consisting of an approximately $\frac{1}{2} \times \frac{1}{2} \times \frac{1}{2}$-in. cube centered above a 2-in. by $\frac{3}{16}$-in.-diameter cylindrical shaft enclosing an isotopic source of gamma rays near the end away from the tube (see Fig. A-7). It is assumed that the source is located ⅛ in. from the tip of the cylindrical shaft. The detector is any one of three G-M tubes (see Fig. A-5). The assembled prototype gauge is also shown in Figure A-5.

The prototype gauge, as described, permits study of four design parameters: gamma-ray source energy, E; detector efficiency spectrum, $\epsilon(E)$; source-detector separation, d; and source collimation length, s. Three different gamma-ray sources are available for study, ^{133}Ba, ^{137}Cs, and ^{60}Co, with low, medium, and high gamma-ray energies, respectively. The ^{133}Ba source, of strength 5.0 millicuries (6/1/68), was obtained from New England Nuclear Corporation, and has a gamma-ray spectrum as follows (*17*): (lower isomeric state, 7.2 years) 0.081 MeV (delayed), 0.36 MeV, 0.30 MeV, 0.08 — 0.38 MeV (several energies included). The ^{137}Cs and ^{60}Co sources, Tracerlab models R-59 and R31-10, respectively, have source strengths of 5.55 millicuries (8/64) and 10.4 millicuries (5/19/65), respectively, and have predominant gamma-ray energies of (*17*): (^{137}Cs, 30 years) 0.662 MeV; (^{60}Co, 5.26 years) 1.33 MeV, 1.17 MeV. Source-detector separation, d, refers to the distance between the source and the G-M tube, as shown in Figure A-4, and is adjustable from 4 in. to more than 12 in. Source collimation is provided by the $\frac{3}{16}$-in.-diameter by 2-in.-long hole in the source holder and is characterized by source collimation length, which refers to the distance denoted by s in Figures A-4 and A-8, and which is adjustable from ⅛-in. to 2 in. G-M tube efficiency as a function of energy, $\epsilon(E)$, depends on the tube dimensions and material and is in general a complicated function of the energy of the gamma ray to be detected. This parameter is more complex than the others because it requires consideration of the entire efficiency spectrum. By using G-M tubes of different wall materials and/or thickness one can vary the detector efficiency spectrum. Four G-M tubes were used in this study, denoted by the

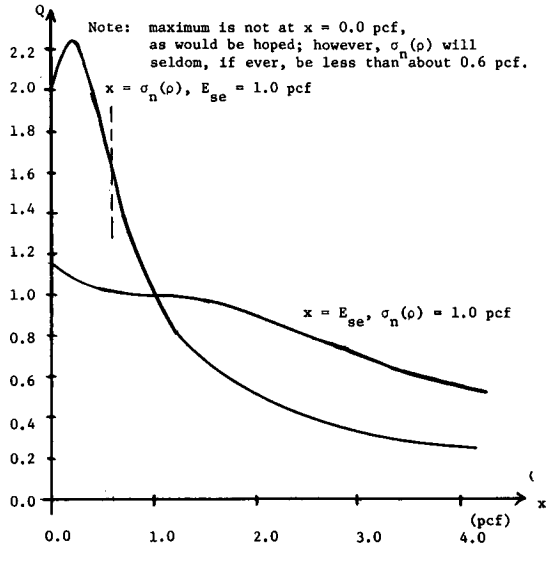

Figure A-3. Quality factor plotted versus each of surface-effect and counting rate measurement errors with the other error held constant and V=*1.0.*

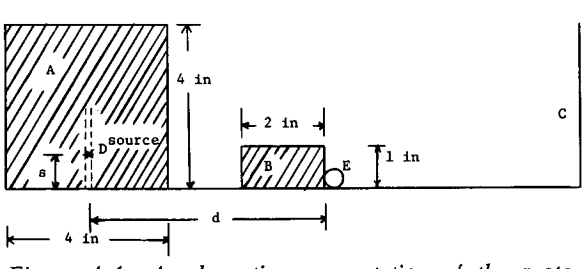

Figure A-4. A schematic representation of the prototype gauge.

numbers 1, 3, 4, and 5. Tube 1 is a Baird Atomic Model 908-690 thin-wall stainless-steel tube, cathode diameter 5/8 in., over-all length 5 5/8 in., three-pin base, wall thickness 30-40 mg/cm², halogen quenched. Tubes 3 and 4 are Harshaw Model G17-6 and Model G17-6P tubes, respectively. Tube 5 is also a Harshaw Model G17-6P and was used in place of Tube 4 after the latter was damaged. The G17-6 has the following characteristics: 13/32-in. outer diameter by 6-in. active length (7 7/8-in. over-all length), halogen quenched, stainless-steel 446 wall material and

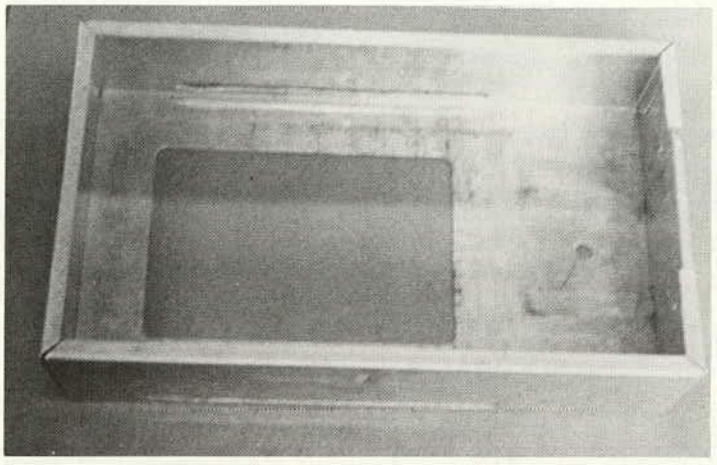

Gauge housing

Shadow shield

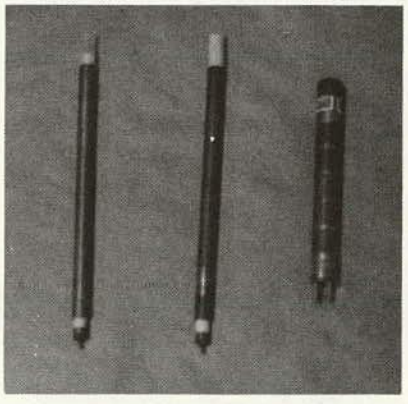

G-M detectors

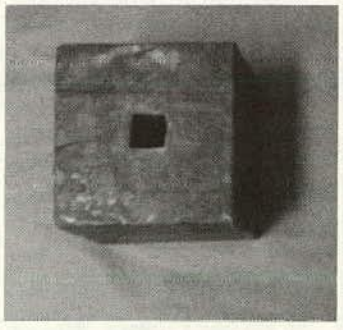

Source holder

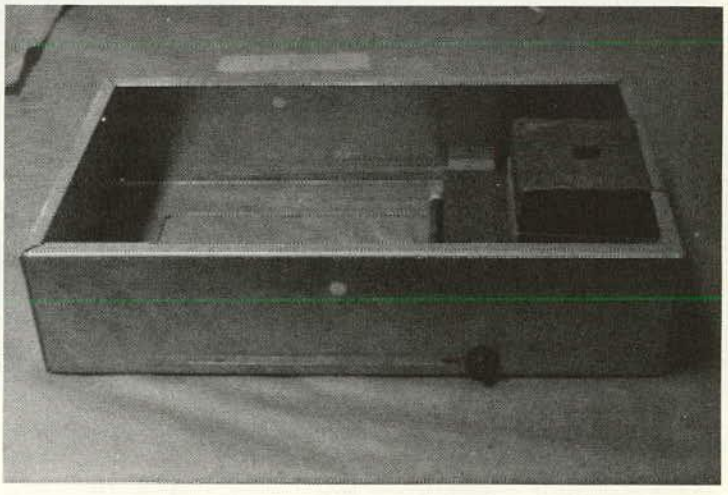

Assembled gauge

Figure A-5. The major components, individually and assembled, of the prototype gauge.

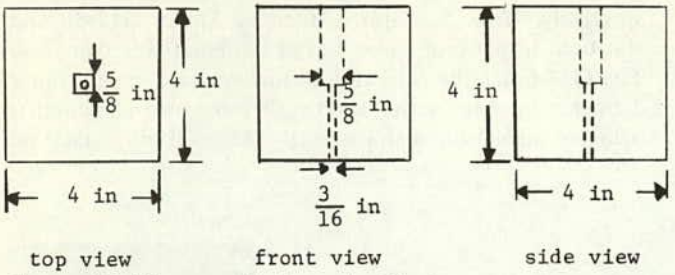

Figure A-6. The source holder and collimator.

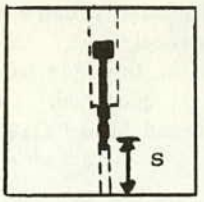

source holder with source capsule inserted.

1 in collimation length.

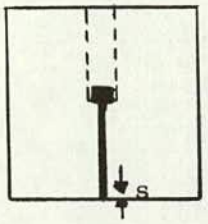

source holder with source capsule inserted.

1/8 in collimation length.

Figure A-8. Source collimation.

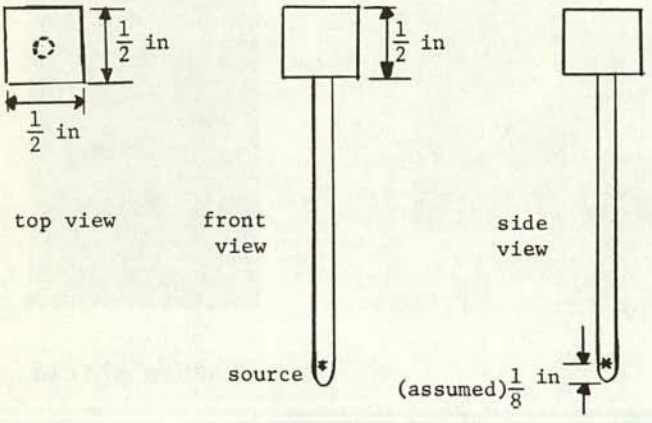

Figure A-7. Any one of the source capsules.

0.020-in. wall thickness. The G17-6P's are identical to the G17-6 except that they have platinum coatings of approximately 10-mg/cm² thickness on their inner walls to increase their low-energy efficiencies. The effect of placing thin sheets of lead (one 8 1/16 × 15/16 × 1/16 in. and one 6 13/16 × 15/16 × 1/8 in., see Fig. A-9) under the G-M tubes to decrease low-energy efficiency was also investigated.

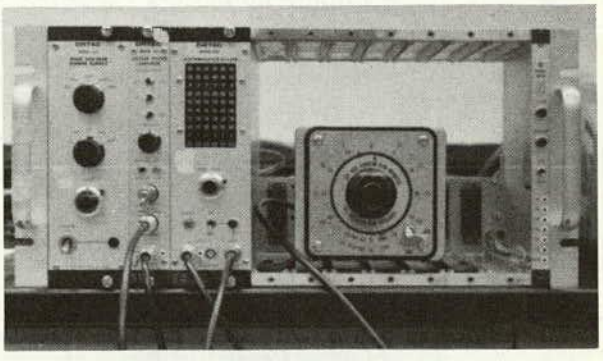

The Ortec electronic equipment

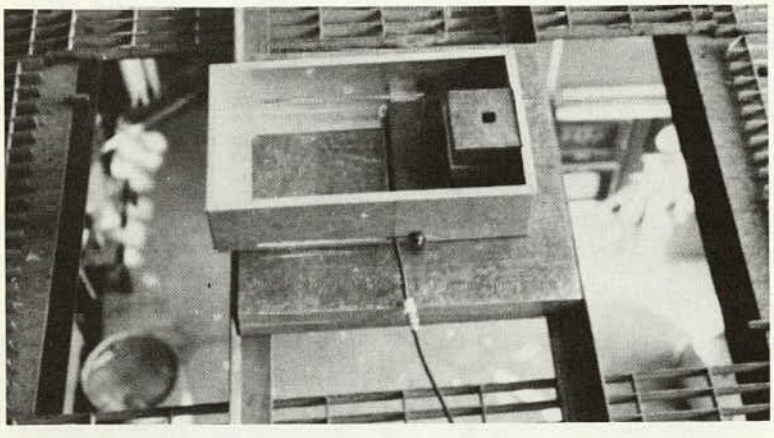

The gauge taking depth data

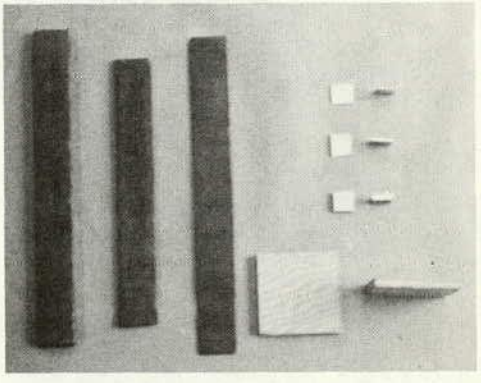

Lead energy filters (left); the blocks used to raise the gauge for taking air-gap data

Figure A-9. Some of the related laboratory equipment.

A gauge configuration consists of any single combination of the four gauge parameters, and a dual gauge refers to a combination of any two gauge configurations. A shorthand notation used to describe a configuration consists of the following: four characters to specify the source (i.e., Co60, C137, or B133), a comma, the source-detector separation expressed in inches, a comma, the number of the G-M tube used (i.e., 1, 3, 4, or 5), another comma, and the collimation length expressed in 1/16ths of an inch. Thus, Co60, 6, 4, 12 describes the configuration consisting of the ^{60}Co source and tube 4, separated from each other by 6 in., and employing a 3/4-in. source collimation length. If one of the lead sheets is placed under the G-M tube to act as an energy filter, the notation will be extended to include another comma, the thickness of the lead sheet used, and an F (for filter). Thus, C137, 6.25, 5, 10, 1/8F refers to the configuration with the ^{137}Cs source, a source-detector separation of 6 1/4 in., tube 5, 5/8-in. collimation length, and the 1/8-in.-thick lead sheet placed under the G-M tube.

Related Laboratory Equipment

To determine surface effect error, responses were taken at various heights, Δ, above a Pyrex sample. To raise the gauge, small metal blocks in thicknesses of 0.050, 0.065, and 0.130 in. and 1/4-in. plywood blocks were used (see Fig. A-9). Some of the electronic equipment and the laboratory standards are also shown in Figure A-9.

Electronics System

A schematic diagram of the electronics system used is shown in Figure A-10. Figure A-9 shows the ORTEC equipment in an ORTEC Model 401A bin and the power supply.

Laboratory Standards

Seven standards were available for use with the prototype gauge: magnesium, two slightly different chalk samples, Pyrex, limestone, glass, and aluminum. Four were chosen for calibration purposes, representing the extremes of density and composition variables that might normally be encountered in field work. These closely approximate the "optimum box shape" described by Gardner and Roberts (*6*, p. 5). Table A-1 gives the density and composition characteristics of these four calibration standards, together with those of the Pyrex sample, which was used to take data to determine counting rate measurement error, surface effect error, and effective sample volume measured. These five samples are homogeneous and stable, and measure 18 × 18 × 6 in., except for the limestone, which is 14 × 17 × 9 in. In addition, the magnesium, aluminum, and pyrex samples are cut into 1-in.-thick slabs. Detailed elemental composition of all standards is given in Table A-2.

Three of the standards (magnesium, chalk, and aluminum) were mounted on a steel frame so that they were about 22 in. above the floor and about 8 to 10 in. apart. The limestone was mounted on concrete blocks and placed about 11 in. from the chalk so that its top was at approximately the same height as those of the other three standards. The Pyrex sample was placed on a 28-in. tall stool several feet from the other samples (Fig. A-9).

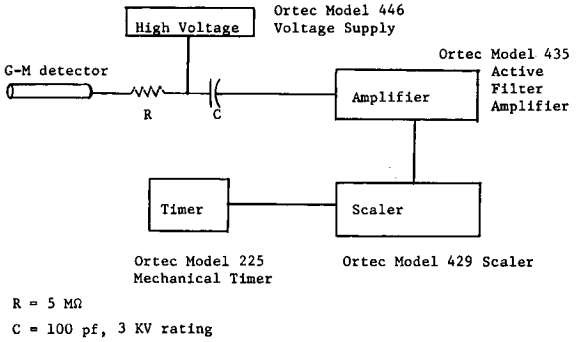

Figure A-10. A block diagram of the electronics system.

TABLE A-1

DENSITY AND COMPOSITION CHARACTERISTICS OF THE SELECTED CALIBRATION STANDARDS

STANDARD SAMPLE	DENSITY		COMPOSITION	
	DESCR.	ρ (PCF)	DESCR.	P
Magnesium	Low	110	Low	1.7635
Chalk	Low	121.7	High	4.0371
Limestone	High	144.9	High	4.7687
Aluminum	High	167.8	Low	2.9648
Pyrex	—	135.4	—	1.1769

TABLE A-2

COMPOSITIONS OF THE LABORATORY STANDARDS [a]

ELEMENT	WEIGHT FRACTION				
	MAGNESIUM	CHALK	PYREX	LIMESTONE	ALUMINUM
Boron			0.03946		
Carbon		0.11943		0.12089	
Oxygen		0.47757	0.54719	0.48169	
Sodium			0.02388		
Magnesium	0.94600			0.00060	0.01000
Aluminum	0.03500	0.00060	0.01217		0.96795
Silicon	0.00050	0.00149	0.37730		0.00400
Sulfur		0.00073			
Calcium	0.00040	0.39938		0.39879	
Titanium					0.00150
Chromium					0.00250
Maganese	0.00450				0.00180
Iron	0.00010	0.00080			0.00700
Copper	0.00050				0.00275
Zinc	0.01300				0.00250

[a] From Gardner and Roberts (*6*), except chalk, obtained from Texas Quarries, Austin, Tex.

SEARCH ROUTINE FOR OPTIMUM DUAL-GAUGE DESIGN

The dual-gauge principle was designed to minimize composition error. There is no immediate reason, then, to assume that use of the dual-gauge principle would significantly reduce the surface-effect error. Consider the over-all problem of measuring the density of a sample with a dual-gauge system. The measured density, ρ', is subject to four measurement interferences: soil composition (reflected in the photoelectric absorption probability, P), surface roughness (reflected in the air gap, Δ, used to calculate surface-effect error), and the uncertainties in the two gauge responses, $\sigma(R_1)$, and $\sigma(R_2)$. The last two measurement interferences give rise to the counting rate measurement error, an inherent error that can never be eliminated but that can be minimized by minimizing $\sigma(R_1)$, $\sigma(R_2)$, $\frac{\partial \rho}{\partial R_1}$, and $\frac{\partial \rho}{\partial R_2}$ (see Eq. A-18). Thus, $\rho' = f(\rho, P, \Delta, \sigma(R_1), \sigma(R_2))$, where ρ is the actual sample density, and it is desired to eliminate the measurement interferences, P and Δ. Theoretically, this would require three independent responses, R_1, R_2, and R_3. But only two responses are available from the dual-gauge system and these are used to minimize the effects of composition variations. Thus, there is no obvious justification for assuming that the dual-gauge principle should also eliminate the effects of the remaining measurement interference, Δ, or surface roughness. However, there is ample experimental evidence to show that indeed the surface-effect error of a dual gauge is often reduced by a factor of 2 or 3 or more as against the surface-effect errors of either of the two single-gauge configurations that comprise the dual gauge. For example, Table A-3 gives the surface-effect errors of four commercial single gauges, the corresponding surface-effect errors of these same gauges used in combinations as dual gauges, and reduction factors that represent the ratio of dual-gauge surface-effect error to the smallest of the two corresponding single-gauge surface-effect errors.

That use of the dual-gauge principle can result in significant reduction of both composition and surface-effect errors is a rather fortuitous characteristic of this principle. At the outset of this investigation of dual-gauge systems it was hoped, but not assured, that the dual-gauge principle could be used to simultaneously reduce composition and surface-effect errors substantially while also keeping the counting rate measurement error small. At any rate, the purpose of the program was to design an optimum dual-gauge system on the basis, mainly, of finding the minimum combination of the gauge errors.

TABLE A-3

SURFACE-EFFECT ERRORS FOR COMMERCIAL SINGLE AND DUAL GAUGES

GAUGE	E_{se} (PCF)	REDUCTION FACTOR
A	12.2	—
B	13.0	—
C	6.7	—
D	12.3	—
A and B	3.6	0.295
A and C	1.1	0.164
A and D	3.1	0.254
B and C	10.8	1.61
B and D	2.5	0.203
C and D	4.5	0.672

Actually, in order to evaluate the performance of a dual gauge the quality factor, Q, as defined previously, is calculated for that dual gauge. The data necessary to make that calculation consist of the following for each configuration of the dual gauge: a response on each of the four calibration standards; air-gap responses on Pyrex (i.e., a flush response and responses for at least three different air-gap heights greater than zero); and, if possible, responses on 1-, 2-, 3-, 4-, 5-, and 6-in. depths of Pyrex (the 6-in. depth response is the same as the flush air-gap response).

To search for an optimum dual gauge, data for N different configurations are taken, each configuration is calibrated, and finally dual-gauge combinations are formed and the respective quality factors are computed. The gauge with the largest quality factor is the best dual gauge, and further study is dependent on the trends noticed.

To analyze the data, a computer program was written in the FORTRAN IV language for use on an IBM model 360/75 digital computer. A complete listing of the program is not given here, but is available to qualified researchers on request to: Program Director, NCHRP, Highway Research Board, 2101 Constitution Avenue, Washington, D.C. 20418. A description of the program, accompanied by mathematical or other explanations, follows.

The following data are read in (not all at the beginning of the program):

KMAX	The total number of gauge configurations.
DEN(J), CC(J), PC(J)	The density, Compton and photoelectric interaction probabilities, respectively, of laboratory standard J, $J = 1, 4$.
GR(J), S(KK), SD(KK), ITU(KK), ICOL(KK), NGAP	The gross responses taken on laboratory standard J, $J = 1, 4$; the source, source-detector separation, G-M tube number, and collimation length of the KKth configuration, $1 \leqq KK \leqq KMAX$ and the number of different air-gap responses taken on Pyrex.
DEL(I)	The air-gap heights at which air-gap responses were taken on Pyrex, $1 \leqq I \leqq NGAP$.
RD(I)	The air-gap responses taken on Pyrex.
RDEP(L)*	The Pyrex depth responses, $L = 1, 2, \ldots, 5$.
C, P RHO	The Compton and photoelectric interaction probabilities, and the density of Pyrex, respectively.

The model constants, B, a b, and c, are determined for each configuration using a Fibonacci search on B and a

least-squares fit of the calibration model (Eq. A-1) to the ratio responses, $R(J)$, $J = 1, 4$, for the four laboratory standards. The ratio responses are obtained from the gross responses as

$$R(J) = \frac{GR(J) - B}{GR(1) - B}, \quad J = 1, 2, 3, 4, \qquad \text{(A-52)}$$

in which the gross response of laboratory standard 1 (magnesium) is used as the gross reference response and B is varied according to the Fibonacci search. In the case that a ratio response is larger than the corresponding maximum response of the calibration model, the ratio response is set equal to the maximum response so that a back-calculation for density using that response will exist. The maximum response, R_{max}, is calculated as follows:

Let $C' = C/\rho$ and $P' = P/\rho$. Then,

$$R = C' \exp_{10} (a + bC'\rho + cP'\rho) \qquad \text{(A-53)}$$

and

$$\frac{\partial R}{\partial \rho} = C' \exp_{10} (a + bC'\rho + cP'\rho) \, |1 + \rho \log_{10} (bC' + cP')| \qquad \text{(A-54)}$$

Then, if $\left.\frac{\partial R}{\partial \rho}\right|_{\rho = \rho'} = 0$, ρ' can be found as

$$\rho' = \frac{-1}{\log_{10} (bC' + cP')} \qquad \text{(A-55)}$$

Finally,

$$R_{max} = C'\rho' \exp_{10} (a + bC'\rho' + cP'\rho') \qquad \text{(A-56)}$$

The Newton-Raphson interation technique is used to back-calculate the density of each laboratory standard and a standard deviation, STD, is formed,

$$\text{STD} = \left[\sum_{i=1}^{4} \frac{(\rho_i - \rho_i')^2}{4} \right]^{\frac{1}{2}} \qquad \text{(A-57)}$$

in which ρ_i is the actual density of standard i and ρ_i' is the back-calculated density of standard i.

The air-gap data are fit to a cubic (see Eq. A-30) and the flush and 1/16-in. air-gap responses, PYR and PYRP, respectively, are determined from the cubic.

If data to determine effective sample depth, $\hat{x}$, have been taken, an effective measurement volume is calculated.

The different configurations are combined into pairs (dual gauges) as desired and the following dual-gauge error analysis is performed for each dual gauge. If effective measurement volumes have been calculated, the volume factor (see Eq. A-50) is formed. A check is made to ensure that both flush responses, PYR(KK), KK = 1, 2, on Pyrex are greater than their corresponding maximum responses. If $R_{max_1} > \text{PYR(I)}$, $I = 1, 2$, the Newton-Raphson iteration technique is used to find the dual-gauge back-calculated densities of the laboratory standards and of Pyrex, and the composition error, $\sigma_c(\rho)$, is calculated as in the earlier section on "Gauge Errors."

If $\text{PYR}(1) \geqq R_{max_1}$, the flush and air-gap responses on Pyrex are adjusted as follows:

$$\text{PYR}(1) = R_{max_1} - (\text{PYRP}(1) - \text{PYR}(1)), \qquad \text{(A-58)}$$

$$\text{PYRP}(1) = R_{max_1} \qquad \text{(A-59)}$$

and similarly for PYR(2), and execution continues as in the foregoing case where $R_{max_1} > \text{PYR(I)}$, $I = 1, 2$. Next, the 1/16-in. air-gap responses on Pyrex, PYRP(I) = 1, 2, are tested to see if they are greater than the corresponding maximum responses. If one is, a linear relationship between response and air-gap height, Δ, is assumed for $0 \leqq \Delta \leqq 1/16$ in., Δ is halved and $\Delta' = \Delta/2$, and the response at Δ' is checked against its maximum response. The halving process is repeated, if necessary, until the response is less than or equal to the maximum response. (If both air-gap responses are greater than their corresponding maximum responses, the foregoing halving procedure is applied to both air-gap responses.) Then, the dual-gauge, air-gap back-calculated density, $\rho_s(\Delta')$, of Pyrex is determined and the surface-effect error, E_{se}, is calculated by

$$E_{se} = 2^n \, | \, \rho_s(o) - \rho_s(\Delta') \, | \qquad \text{(A-60)}$$

in which $\rho_s(o)$ is the dual-gauge back-calculated density of Pyrex using the flush responses, $\rho_s(\Delta')$ is as described previously, and n is the number of times Δ was halved (see Fig. A-11).

The counting rate measurement error, $\sigma_s(\rho)$, is then determined using the flush responses on Pyrex, PYR(K), $K = 1, 2$, and finally the quality factor, Q, is calculated. This completes the dual-gauge error analysis.

After all desired dual-gauge combinations have undergone the dual-gauge error analysis, the program is terminated. Figure A-12 is a flow diagram of the computer program.

EXPERIMENTAL RESULTS

Results of two experimental programs, denoted initial and secondary, as well as results of final testing of the optimum

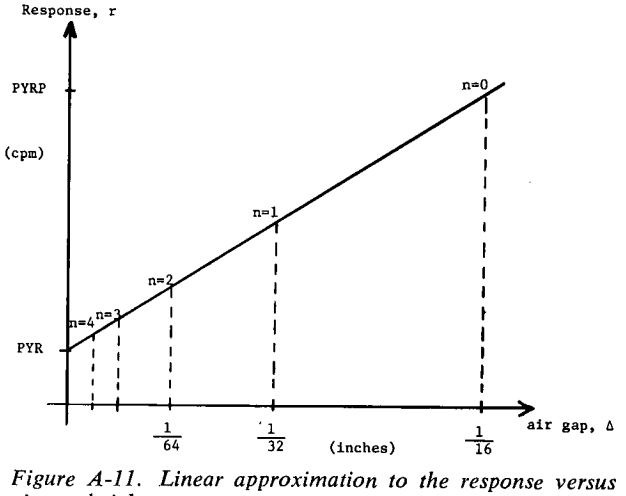

Figure A-11. Linear approximation to the response versus air-gap height curve.

* Omitted if Pyrex depth data are not available

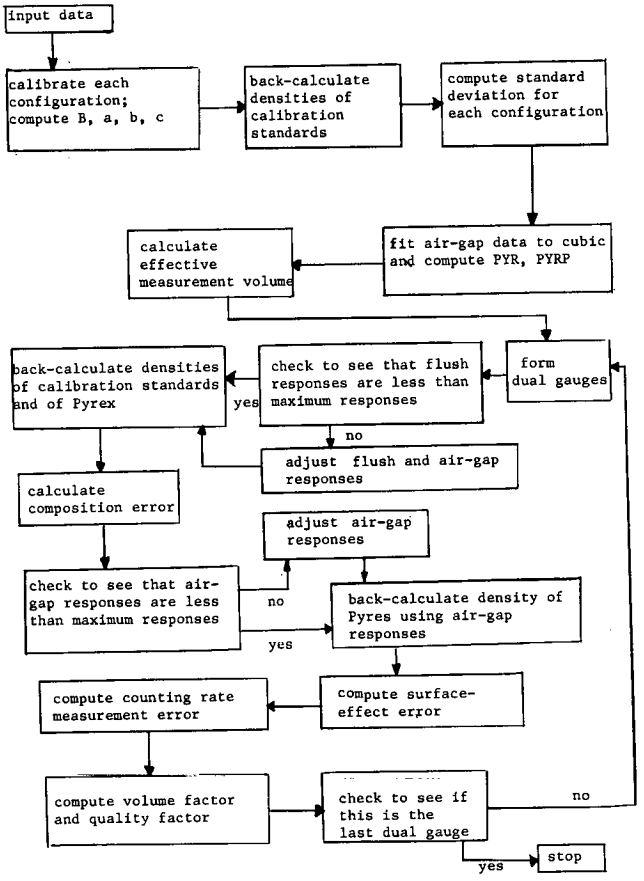

Figure A-12. Flow diagram of the calibration and error program.

TABLE A-4

THE CONFIGURATIONS STUDIED IN THE INITIAL AND SECONDARY EXPERIMENTAL PROGRAMS

NO.	CONFIGURATION	NO.	CONFIGURATION
I-1	Co60,4,1,10	I-24	Co60,4,3,10(2)[a]
I-2	Co60,6,1,10	I-25	Co60,4,3,10,1/16F
I-3	Co60,8,1,10	I 26	Co60,4,3,10,1/8F
I-4	C137,4,1,10	I-27	Co60,4,3,18
I-5	C137,6,1,10	I-28	Co60,5,3,10
I-6	Co60,4,4,10	S-1	Co60,4,3,11
I-7	Co60,5,4,10	S-2	Co60,4.5,3,11
I-8	Co60,6,4,10	S-3	Co60,4.75,3,11
I-9	Co60,7,4,10	S-4	Co60,5,3,11
I-10	Co60,8,4,10	S-5	Co60,4.75,3,14
I-11	Co60,9,4,10	S-6	Co60,4.75,3,17
I-12	Co60,10,4,10	S-7	Co60,4.25,3,8
I-13	C137,4,4,10	S-8	Co60,4.25,3,10
I-14	C137,6,4,10	S-9	Co60,4.5,3,10
I-15	C137,8,4,10	S-10	Co60,4.5,3,8
I-16	B133,4,4,10	S-11	C137,4,3,14
I-17	B133,5,4,10	S-12	Co60,10,5,4
I-18	B133,6,4,10	S-13	Co60,10,5,8
I-19	C137,4,3,10	S-14	Co60,10,5,9
I-20	C137,6,3,10	S-15	Co60,10,5,10
I-21	Co60,4,3,10	S-16	Co60,10,5,6
I-22	Co60,6,3,10	S-17	Co60,10,5,2
I-23	Co60,8,3,10	S-18	Co60,11,5,4

[a] The (2) in this notation indicates that this is the second time this configuration appears in the table.

dual gauge, are discussed. The results were obtained, for the most part, from three separate runs of the calibration and error program, referred to as Runs 1, 2, and 3 for convenience in identification. The experimental programs consisted of data accumulation for individual configurations and a search via the calibration and error program for an optimum dual-gauge combination of two configurations. The initial criterion for judging dual gauges is the quality factor. Among those dual gauges with the largest quality factors other considerations (such as feasibility of commercial production and cost to manufacture) may be used to determine the "optimum" dual gauge.

Selection of the "optimum" dual gauge is based on a search only over certain discrete values of the design parameters; the actual dependence of quality factor on each of the design parameters has not been determined, so a continuous multivariable search could not be performed.

Initial and Secondary Experimental Programs

The configurations studied in determining the "optimum" dual gauge are identified and the results of Runs 1 and 2 of the calibration and error program are presented. Finally, the conclusions based on these results are given and an "optimum" dual gauge design is proposed.

Configurations Studied

Initially, data for 23 single-gauge configurations designed to cover the ranges of the three major design parameters were taken. To roughly study the effects of inserting lead energy filters and of increasing source collimation length, and to further study the effects of small changes in source-detector separation, data for five more configurations were taken. These 28 configurations, comprising the initial experimental program, are given in Table A-4 as I-1 through I-28.

Based on the results of the initial experimental program (see Table A-5 and Fig. A-13), a secondary experimental program consisting of 18 configurations was formulated. These configurations are given in Table A-4 as S-1 through S-18. The secondary program was a refinement of the initial program in which small variations in source-detector separation and source collimation length about those values which the initial program indicated were contained in the better dual gauges were studied.

For configurations I-1 through I-28 the source collimator consisted of a $4 \times 4 \times 4$-in. cube with an approximately $\frac{5}{8} \times \frac{5}{8} \times \frac{1}{2}$-in. hole in the center of one side followed by a cylindrical hole of $\frac{3}{16}$-in. diameter and $2\frac{1}{2}$-in. length (Fig. A-14). This allowed for a minimum source collimation length of about $\frac{5}{8}$ in. When a more detailed study of source collimation length was desired, it was necessary to extend the $\frac{5}{8} \times \frac{5}{8}$-in. hole to a total length of 2 in., so that the collimator was as described under "Experimental Apparatus—Prototype Gauge." Thereafter, source collimation length was adjusted in a standard way by use of nuts and washers of known thicknesses. Thus, comparison of source collimation lengths among configurations within the group I-1 through I-28 or within the group S-1 through

TABLE A-5

THE TEN BEST DUAL GAUGES ON THE BASIS OF QUALITY FACTOR, OBTAINED FROM RUN 1 OF THE CALIBRATION AND ERROR PROGRAM

DUAL GAUGE NO.	CONFIGURATION	E_{se} (PCF)	$\sigma_n(\rho)$ (PCF)	V	Q RUN 1	Q RUN 2
1	Co60,4,3,10-Co60,10,4,10	0.23	0.99	0.94	1.03	1.13
2	C137,4,3,10-Co60,10,4,10	0.19	1.05	0.95	0.99	1.18
3	Co60,4,3,18-Co60,10,4,10	1.92	0.89	0.94	0.92	0.48
4	C137,4,1,10-Co60,10,4,10	1.02	1.05	0.95	0.90	1.13
5	Co60,4,3,10-C137,8,4,10	0.20	1.21	0.94	0.85	0.83
6	Co60,4,4,10-Co60,10,4,10	0.11	1.25	0.95	0.85[a,b]	0.96
7	Co60,4,3,10(2)-C137,8,4,10	0.42	1.17	0.94	0.85[a,b]	0.59
8	B133,4,4,10-Co60,10,4,10	0.39	1.19	0.95	0.85	0.88
9	C137,4,3,10-C137,8,4,10	0.32	1.23	0.94	0.83	0.37
10	Co60,4,3,18-C137,8,4,10	2.16	0.99	0.94	0.82	0.72

[a] The Pyrex flush and air-gap responses had to be adjusted as described under "Search Routine for Optimum Dual-Gauge Design" for the first configuration listed.
[b] The response on magnesium had to be adjusted to the corresponding maximum response as described under "Search Routine for Optimum Dual-Gauge Design" for the first configuration listed.

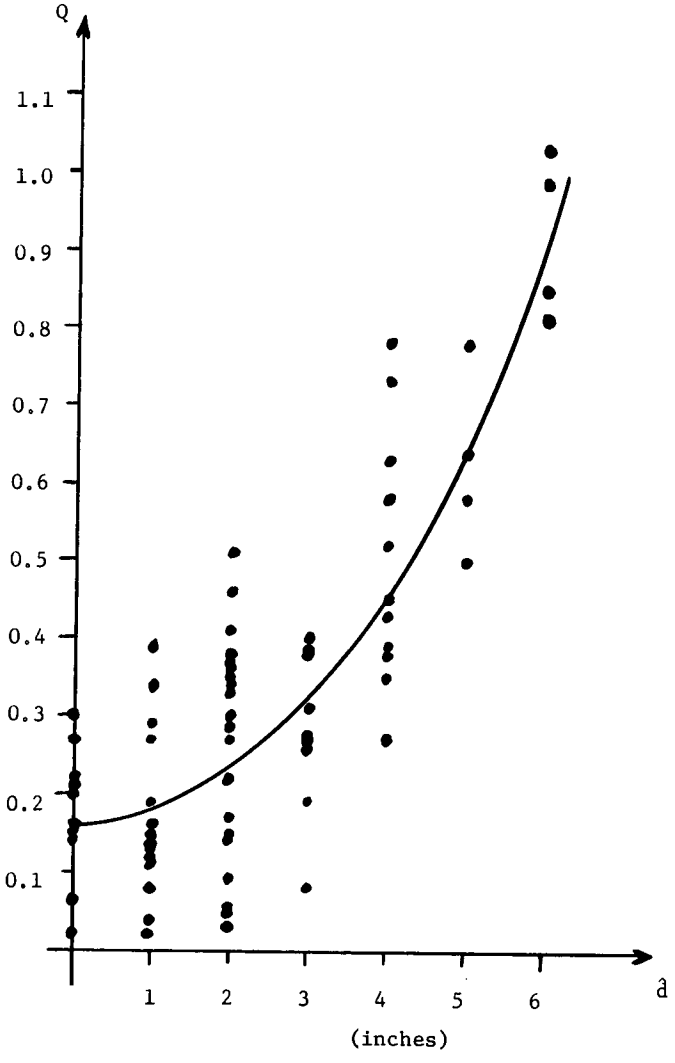

Figure A-13. Plot of quality factor versus source-detector difference for 72 of the dual gauges studied in Run 1 of the calibration and error program.

S-18 could be made with confidence, whereas such comparisons between the two experimental programs were subject to some uncertainty, as the method of determination was not uniform. The amount of uncertainty is expected to be within 1/16 in.

Tabulated Results

The 28 configurations of the initial experimental program can be paired into 378 different dual-gauge combinations. Run 1 of the calibration and error program was used to form and evaluate these dual-gauge combinations, with the following deviations:

1. The flush and 1/16-in. air-gap responses, PYR and PYRP, on Pyrex were obtained by constructing the response-versus-air-gap-height curves by hand instead of using the least-squares fit to a third-degree polynominal.
2. The Fibonacci search for "optimum background," B, was taken over the interval $B_l - 0.5B_l \leq B \leq B_l + 0.5B_l$, in which B_l was a laboratory background obtained as the

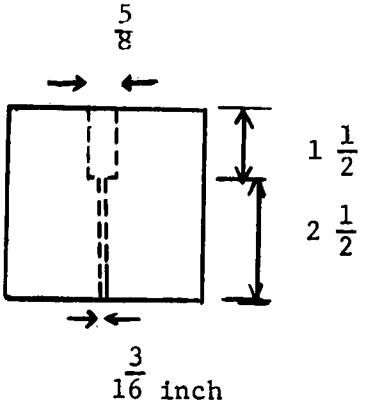

Figure A-14. The source collimator as used in the initial experimental program.

response on lead, a sample of essentially infinite density.

3. The depth data to determine $\hat{x}$, effective sample depth, was taken nonuniformly and was affected by the material below the various thicknesses of Pyrex.

Obviously, these results are lacking and cannot be used as true, accurate indications of gauge performance; however, they were used to give some indication of trends in gauge performance and were the basis for designing the secondary experimental program. For these reasons the ten dual gauges with the largest quality factors as determined in Run 1 of the calibration and error program are listed in Table A-5. Also listed in the table, for comparison, are the corrected quality factors determined in a later run (Run 2) of the calibration and error program. For uniformity, the convention is adopted of listing first the configuration having the smaller source-detector separation.

It is helpful to define a new variable, called source-detector difference, $\hat{d}$, as

$$\hat{d} = d_2 - d_1 \qquad \text{(A-61)}$$

in which d_1 and d_2 are the smaller and larger source-detector separations, respectively, of the two configurations comprising a dual gauge. In Figure A-13, quality factor is plotted versus source-detector difference for 72 of the dual gauges formed in Run 1 of the calibration and error program.

After the secondary experimental program had been completed, data were available for a total of 46 configurations. There was no need to study all of the 1,035 possible dual-gauge combinations, because of the obvious trend for good dual gauges to have a large source-detector difference, $\hat{d}$. Thus, Run 2 of the calibration and error program, as described under "Search Routine for Optimum Dual-Gauge Design," * was run for the 448 dual-gauge combinations of those 32 configurations having source-detector separations less than or equal to 6 in. with those 14 configurations having source-detector separations greater than 6 in. ($32 \times 14 = 448$). Table A-6 lists the 25 best dual gauges, on the basis of quality factor obtained from Run 2 of the calibration and error program.

Table A-7 indicates how varied the results of the initial and secondary experimental programs were and the sensitivity of the quality factor to changes in the various gauge errors.

Tables A-8 and A-9 give the effects of source energy on quality factor. These results were taken from Run 2 of the calibration and error program, as were those of Table A-10, which lists those configurations for which some response(s) had to be adjusted to the corresponding maximum response(s).

Conclusions

The most obvious conclusions to be drawn from the results of Run 1 of the calibration and error program (see Table A-5 and Fig. A-13) is that quality factor in general increases with increasing source-detector difference, $\hat{d}$. Of

* Volume factors were not determined, because suitable depth data were not available. Thus, all volume factors were taken to be 1.00.

TABLE A-6

THE 25 BEST DUAL GAUGES, ON THE BASIS OF QUALITY FACTOR, OBTAINED FROM RUN 2 OF THE CALIBRATION AND ERROR PROGRAM

DUAL GAUGE NO.	CONFIGURATION	$\sigma_c(\rho)$ (PCF)	$\sigma_s(\rho)$ (PCF)	E_{se} (PCF)	$\sigma_n(\rho)$ (PCF)	Q
1	Co60,4.5,3,10-Co60,10,4,10	0.25	0.81	0.04	0.85	1.344
2	Co60,4.75,3,11-Co60,10,4,10	0.05	0.83	0.31	0.83	1.267
3	Co60,4.5,3,8-Co60,10,4,10	0.25	0.75	0.78	0.79	1.261
4	Co60,5,4,10-Co60,10,4,10	0.14	0.79	0.98	0.80	1.236
5	C137,4,3,10-Co60,10,4,10	0.04	0.92	0.20	0.92	1.182
6	C137,4,3,14-Co60,10,4,10	0.13	0.91	0.30	0.92	1.154
7	C137,4,1,10-Co60,10,4,10	0.27	0.55	0.71	0.89	1.131
8	Co60,4,3,10(1)-Co60,10,4,10	0.23	0.84	1.25	0.87	1.128
9	Co60,5,4,10-Co60,10,5,6	0.19	0.83	1.55	0.55	1.088
10	Co60,4.75,3,11-Co60,10,5,6	0.38	0.87	0.81	0.95	1.053
11	Co60,4.75,3,14-Co60,10,5,6	0.36	0.95	0.29	1.02	1.052
12	C137,4,3,10-Co60,10,5,6	0.30	0.97	0.31	1.01	1.051
13	Co60,4.25,3,8-Co60,10,4,10	0.10	1.07	0.11	1.08	1.037
14	Co60,5,4,10-C137,8,4,10	0.35	0.90	1.15	0.97	1.028
15	Co60,5,3,11-Co60,10,4,10	0.22	0.95	1.23	0.98	1.014
16	Co60,4.5,3,8-Co60,10,5,6	0.58	0.78	1.30	0.98	1.011
17	B133,4,4,10-Co60,10,4,10	0.06	1.02	0.55	1.02	1.008
18	C137,4,3,14-Co60,10,5,6	0.49	0.96	0.22	1.08	1.007
19	Co60,4,4,10-Co60,10,5,6	0.30	1.06	0.13	1.11	1.006
20	Co60,4.5,3,10-Co60,10,5,6	0.59	0.85	0.52	1.03	0.999
21	B133,4,4,10-Co60,10,5,6	0.37	1.08	0.05	1.14	0.997
22	C137,4,4,10-Co60,10,5,8	0.46	0.92	1.77	1.03	0.968
23	Co60,4.25,3,11-C137,8,4,10	0.57	0.96	0.27	1.12	0.966
24	C137,4,4,10-Co60,10,5,6	0.51	0.99	0.34	1.11	0.961
25	Co60,4,4,10-Co60,10,4,10	0.50	1.00	0.30	1.12	0.959

TABLE A-7

QUALITY FACTORS FOR SOME ARBITRARILY CHOSEN DUAL GAUGES, FROM RUN 2 OF THE CALIBRATION AND ERROR PROGRAM

DUAL GAUGE NO.	DUAL GAUGE CONFIGURATION	$\sigma_c(\rho)$ (PCF)	$\sigma_s(\rho)$ (PCF)	E_{se} (PCF)	$\sigma_n(\rho)$ (PCF)	Q
1	C137,6,4,10-Co60,7,4,10	15.96	6.84	11.43	17.36	0.06
2	Co60,6,4,10-Co60,7,4,10	2.47	8.37	35.31	8.72	0.06
3	C137,6,3,10-Co60,8,1,10	2.91	6.16	1.66	6.81	0.16
4	Co60,6,3,10-Co60,8,3,10	4.82	3.92	1.97	6.21	0.17
5	Co60,5,3,11-Co60,8,3,10	3.05	2.22	2.70	3.78	0.27
6	B133,6,4,10-Co60,8,4,10	4.25	1.77	0.07	4.60	0.25
7	B133,6,4,10-Co60,10,5,10	3.02	1.18	1.33	3.25	0.32
8	Co60,4,3,18-Co60,8,4,10	1.63	2.22	3.28	2.76	0.36
9	Co60,4.5,3,11-Co60,7,4,10	0.76	2.25	1.62	2.37	0.43
10	C137,4,3,14-Co60,10,5,10	2.02	0.85	0.74	2.19	0.48
11	C137,6,3,10-C137,8,4,10	0.88	1.73	0.29	1.94	0.57
12	Co60,4,1,10-Co60,8,1,10	0.51	1.85	1.06	1.92	0.54
13	Co60,6,1,10-Co60,10,5,6	0.41	1.10	3.36	1.17	0.62
14	C137,4,4,10-Co60,11,5,4	0.48	1.08	2.93	1.18	0.68
15	Co60,4.75,3,11-Co60,10,5,2	0.24	1.02	2.82	1.05	0.73
16	Co60,6,3,10-Co60,10,4,10	0.33	1.25	0.72	1.29	0.79
17	Co60,6,1,10-Co60,10,5,8	0.55	1.01	1.34	1.15	0.87
18	Co60,5,3,11-Co60,10,5,6	0.59	1.01	0.78	1.17	0.87
19	Co60,4.75,3,14-Co60,10,5,4	0.65	0.98	0.18	1.17	0.94
20	Co60,4.5,3,9-C137,8,4,10	0.82	0.93	0.07	1.24	0.91
21	C137,4,1,10-Co60,10,4,10	0.27	0.85	0.71	0.89	1.13
22	Co60,4.5,3,9-Co60,10,4,10	0.25	0.81	0.04	0.85	1.34

TABLE A-8

VARIATION OF QUALITY FACTOR WITH SOURCE ENERGY FOR THOSE DUAL GAUGES INVOLVING ONLY ONE SOURCE ENERGY

DUAL GAUGE	QUALITY FACTOR S=^{60}Co	QUALITY FACTOR S=^{137}C
S,4,1,10-S,8,4,10	0.52	0.77
S,6,1,10-S,8,4,10	0.44	0.66
S,4,4,10-S,8,4,10	0.60	0.86
S,6,4,10-S,8,4,10	0.37	0.37
S,4,3,10-S,8,4,10	0.43	0.88
S,6,3,10-S,8,4,10	0.32	0.57

TABLE A-9

QUALITY FACTOR DEPENDENCE ON THE COMBINATIONS OF SOURCE ENERGIES USED IN THE DUAL GAUGES

DUAL GAUGE	QUALITY FACTORS, FOR (S_1-S_2) Co-Co	Co-Cs	Cs-Co	Cs-Cs
S_1,4,1,10-S_2,8,1,10	0.54	—	0.30	—
S_1,4,1,10-S_2,8,3,10	0.46	—	0.27	—
S_1,4,1,10-S_2,8,4,10	0.52	0.78	0.37	0.77
S_1,4,1,10-S_2,9,4,10	0.63	—	0.83	—
S_1,4,1,10-S_2,10,4,10	0.91	—	1.13	—
S_1,4,3,10-S_2,8,1,10	0.44	—	0.25	—
S_1,4,3,10-S_2,8,3,10	0.39	—	0.35	—
S_1,4,3,10-S_2,8,4,10	0.43	0.83	0.44	0.88
S_1,4,3,10-S_2,9,4,10	0.84	—	0.81	—
S_1,4,3,10-S_2,10,4,10	1.13	—	1.18	—
S_1,4,4,10-S_2,8,1,10	0.33	—	0.21	—
S_1,4,4,10-S_2,8,3,10	0.60	—	0.44	—
S_1,4,4,10-S_2,8,4,10	0.60	0.84	0.55	0.86
S_1,4,4,10-S_2,9,4,10	0.67	—	0.52	—

TABLE A-10

CONFIGURATIONS FOR WHICH SOME RESPONSE HAD TO BE ADJUSTED BECAUSE IT WAS LARGER THAN THE CORRESPONDING MAXIMUM RESPONSE

CONFIGURATION	PYREX FLUSH AND AIR-GAP RESPONSES ADJUSTED	RESPONSES IN ONE OR MORE OF THE CALIBRATION STANDARDS ADJUSTED
Co60,4,4,10	Yes	Yes (magnesium)
Co60,4,3,10,1/16F	No	Yes (limestone)
Co60,5,3,10	No	Yes (magnesium)
Co60,4.5,3,11	Yes	Yes (magnesium)
Co60,4.75,3,14	No	Yes (magnesium)
Co60,4.75,3,17	No	Yes (magnesium)
Co60,4.25,3,8	No	Yes (magnesium)
Co60,4.25,3,10	No	Yes (magnesium)

the design parameters studied and over the ranges considered, source-detector separation has, by far, the strongest effect on quality factor. There are, of course, limitations on the values of source-detector separation that are feasible to use; no values smaller than 4 in. were considered because of background problems and no values larger than 11 in. were considered because extremely long counting times (or source intensities) would have been required to produce large enough gross count responses.

Among the better dual gauges as given in Table A-5,

those requiring the use of two sources (No. 2, 4, 5, 7, 8, and 10) are undesirable because of expense and shielding problems. They would be preferred over the others only if they were substantially better; because they are not, they have been, for the most part, eliminated from further consideration. Of the remaining four dual gauges (No. 1, 3, 6, and 9) three involve use of ^{60}Co, implying that it is the best source. More as regards preferred source energy is considered later in this section.

It is noted that dual gauges No. 1 and 3 in Table A-5 are identical except that the source collimation length of the first configuration in dual gauge No. 3 is larger by ½ in. The surface-effect error for dual gauge No. 3 is larger, indicating, though certainly not proving, that increasing source collimation length causes surface-effect error to increase, as one might expect. However, the combined normal error of dual gauge No. 3 is smaller than that of dual gauge No. 1, indicating that a search on source collimation length is desirable to find an optimum, and such a search was incorporated in the secondary experimental program.

The frequency of occurrence of the configuration Co60, 10,4,10 in Table A-5, the fact that it occurs in each of the four best dual gauges, and the indication that ^{60}Co is the most desirable source, prompted a further study of configurations similar to this. The configurations Co60, 10,5,s, $s = 2,4,6,8,9,10$, and the configuration Co60,11,5,4, were thus included in the secondary experimental program.

Inasmuch as Co60,4,3,10 or Co60,4,3,18 appeared in three of the best five dual gauges, in five of the best ten, and in the best dual gauge, it was decided to include many configurations similar to this in the secondary experimental program. It was noticed, however, that the calibration models of these configurations peak for $\rho = 122$ pcf and that responses on samples having low or medium densities are very near or greater than the maximum responses, a condition that is undesirable because a response greater than the maximum response must be adjusted. Also, background count is very high at 4-in. source-detector separations. Hence, many configurations with source-detector separations greater than, but near, 4 in. were included in the secondary experimental program.

The best results from the combination of the initial and secondary experimental programs are summarized in Table A-6. The quality factors in Table A-7 vary over a large range, indicating that there is indeed an optimum use of the dual-gauge principle. Table A-8 seems to indicate that ^{137}Cs is the preferred source, and in Table A-9 quality factors are consistently larger for those dual gauges for which ^{137}Cs is the source used in the configuration having the larger source-detector separation. An explanation of these results that also supports the argument that ^{60}Co is the over-all preferred source is now proposed. It would seem that the lower-energy gamma rays would carry more useful information about the sample density, because they have interacted more with the sample. At any given source-detector separation (for instance, those studied in Tables A-8 and A-9) for which two source energies are used, the lower source energy should give the best results, because the response due to the higher energy source would be masked by high-energy gamma rays. Hence, ^{137}Cs would appear to be the better source. However, it happens that for source-detector separations larger than 8 in. the ^{137}Cs source does not provide a sufficient response because of the drastic attenuation of its low-energy gamma rays, whereas the ^{60}Co source does provide a significant response for source-detector separations as large as 10 or 11 in. By comparing results using ^{60}Co and source-detector separations of 10 in. with results using ^{137}Cs and source-detector separations of 8 in., the ^{60}Co source becomes the obvious favorite.

Table A-10 gives those configurations that are so sensitive that responses taken on one or more of the laboratory standards had to be adjusted to the corresponding maximum responses, an undesirable characteristic.

The best dual gauge in Table A-6 is seen to be Co60, 4.5,3,10-Co60,10,4,10. However, it is noted that quality factors in this table vary over a small range (see Table A-7), indicating that any of a number of dual-gauge designs are near the optimum and might be suitable for commercial use. Choice of an optimum dual gauge is made difficult by the fact that the eight best dual gauges in the table involve use of G-M tube 4, which was damaged after the initial experimental program and could no longer be used. Hence, the "optimum" dual gauge would have to be one that involves the use of tube 5. The best dual gauge not involving use of tube 4 is seen to be Co60,4.75,3,11-Co60,10,5,6 and this is chosen as the "optimum" dual gauge. The configuration Co60,4.75,3,11, which is in the "optimum" dual gauge, was also part of the second best dual gauge, Co60,4.75,3,11-Co60,10,4,10, lending further support that this configuration should be included in the "optimum" dual-gauge design.

Final Experimental Program

The experimental program designed to study the optimum dual gauge, the results of that program, and conclusions about the optimum dual-gauge design are discussed in the following.

Data Taken

In all, six sets of data were taken for the configuration Co60,4.75,3,11, and four sets for the configuration Co60, 10,5,6. Table A-11 outlines the data taken for the final experimental program. The following should be noted:

1. Data were taken at various counting times to determine the best counting times (or, alternatively, the best source intensities).

2. Data for configurations 3, 5, and 9 are not entirely independent from the data for configurations 2, 4, and 8, respectively, because each response from the former configurations consisted of the corresponding response from the latter configurations plus an additional 4-min response.

3. Data for configurations 2, 3, 4, and 5 were taken consecutively without changing any of the gauge design parameters, and similarly for data for configurations 8 and 9; however, between any other two configurations the gauge was disassembled and reconstructed. Thus, reproducibility among different constructions of the optimum

dual gauge can be studied, as well as reproducibility of one gauge construction tested several times.

4. No air-gap responses were taken for configurations 4 and 5, so the Pyrex air-gap responses from configurations 2 and 3, respectively, were used for these configurations.

5. Air-gap data were taken on chalk, as well as on Pyrex, for configurations 2, 5, and 8.

6. Configurations 2, 3, 4, 5, 8, and 9 are considered the most reliable, because extra supports were used to ensure that the detector was more rigidly held in place, minimizing small changes in source-detector separation as the gauge was moved.

To determine the effective sample depths of each configuration, and thus volume factor for the dual gauge, data were taken at 0-, 1-, 2-, 3-, 4-, 5-, and 6-in. depths of magnesium and aluminum (the lowest and highest density samples, respectively). These data were taken only once. The gauge and the various thicknesses of the samples were suspended on two metal beams approximately 30 ft above the floor, as shown in Figure A-9.

Tabulated Results

For simplicity, the optimum dual gauge is abbreviated C_1-C_2, where C_1 is one of the first six, and C_2 one of the last four configuration numbers listed in Table A-11. Run 3 of the calibration and error program evaluated the 24 dual-gauge combinations of the 10 configurations comprising the final experimental program. Table A-12 gives these results, as well as the results of the two dual gauges that used the air-gap data on chalk to determine surface-effect and counting rate measurement errors. Table A-13 gives the variation of quality factor with counting time (or source intensity). Reproducibility of the system is studied in Tables A-14 and A-15. Table A-16 compares the results determined using the chalk air-gap data with the results determined using the Pyrex air-gap data in the same configurations.

Conclusions

From Table A-13, one is led to deduce that there is an optimum counting time, or source intensity, for each configuration. Fortunately, these counting times appear to be about the same for the two configurations (approximately 9 to 10 min for the source intensity used). One would expect that for too small counting times insufficient back-scattered response would be obtained and for too large counting times electronic instabilities would become appreciable.

Table A-14 is designed to study the reproducibility of the optimum dual gauge—or, really, the sensitivity of the quality factor. However, careful interpretation of the tables shows that in every case the dual gauge $C_1 - 9$ has a smaller quality factor than $C_1 - 8$, which is seemingly due, at least partially, to the fact that the counting times for configurations 8 and 9 are different (by Table A-13 this would seem to be significant). Hence, care should be exercised in comparing quality factors in any column of Table A-14. The counting times for configurations 2 and

TABLE A-11

DATA TAKEN IN THE FINAL EXPERIMENTAL PROGRAM

GAUGE NO.	CONFIGURATION	NOTES
1	Co60,4.75,3,11	a,b,k
2	Co60,4.75,3,11	b
3	Co60,4.75,3,11	c
4	Co60,4.75,3,11	b,h,j
5	Co60,4.75,3,11	c,i,j
6	Co60,4.75,3,11	d
7	Co60,10,5,6	e
8	Co60,10,5,6	f,j
9	Co60,10,5,6	g,j
10	Co60,10,5,6	a,f,l

[a] Data taken from secondary experimental program.
[b] Counting time, 6 min.
[c] Counting time, 10 min. Data taken with preceding configuration; each 6-min count was recorded and counting was resumed for 4 more minutes to obtain a 10-min count.
[d] Counting time, 8 min.
[e] Counting time, 9 min.
[f] Counting time, 7 min.
[g] Counting time, 11 min. Data taken simultaneously with data No. 8; each 7-min count was recorded and counting was resumed for 4 more minutes to obtain an 11-min count.
[h] Only calibration data taken; air-gap data used were for configuration 2.
[i] Only calibration data taken; air-gap data used were for configuration 3.
[j] Additional support was incorporated to keep the detector rigidly located during handling and movement of the gauge.
[k] Configuration same as S-3 in Table A-4.
[l] Configuration same as S-16 in Table A-4.

TABLE A-12

RESULTS OF FINAL EXPERIMENTAL PROGRAM

DUAL-GAUGE COMBINATION [a]	$\sigma_c(\rho)$ (PCF)	$\sigma_s(\rho)$ (PCF)	E_{sc} (PCF)	$\sigma_n(\rho)$ (PCF)	V	Q
1-7	1.00	0.84	0.78	1.31	0.92	0.72
2-7	0.03	0.81	0.88	0.81	0.92	1.13
3-7	0.41	0.73	0.60	0.83	0.92	1.12
4-7	0.03	0.87	1.16	0.87	0.92	1.05
5-7	0.00	0.75	0.79	0.75	0.92	1.23
6-7	0.94	0.80	0.60	1.24	0.92	0.77
1-8	1.57	0.84	2.11	1.78	0.92	0.52
2-8	0.71	0.81	0.64	1.08	0.92	0.87
3-8	1.03	0.74	0.85	1.27	0.92	0.73
4-8	0.73	0.86	0.43	1.12	0.92	0.86
5-8	0.68	0.76	0.70	1.02	0.92	0.92
6-8	1.52	0.80	1.95	1.72	0.92	0.53
1-9	1.77	0.63	1.94	1.88	0.92	0.49
2-9	1.09	0.61	0.75	1.25	0.92	0.76
3-9	1.34	0.55	0.93	1.45	0.92	0.65
4-9	1.11	0.64	0.59	1.28	0.92	0.75
5-9	1.06	0.57	0.80	1.20	0.92	0.78
6-9	1.74	0.60	1.81	1.84	0.92	0.50
1-10	0.38	0.87	0.81	0.95	0.92	0.97
2-10	0.68	0.84	2.62	1.07	0.92	0.70
3-10	0.25	0.73	2.25	0.77	0.92	0.86
4-10	0.70	0.90	2.98	1.14	0.92	0.63
5-10	0.71	0.76	2.48	1.04	0.92	0.73
6-10	0.32	0.82	1.01	0.88	0.92	1.04
2-8 [b]	1.52	0.82	2.98	1.73	0.92	0.50
6-8 [b]	0.71	0.83	0.20	1.10	0.92	0.92

[a] See Table A-11 for numbering of configurations.
[b] Air-gap data taken on chalk and used to determine E_{sc} and $\sigma_s(\rho)$. The calibration and error program was run separately to determine these results.

TABLE A-13

VARIATION OF QUALITY FACTOR WITH COUNTING TIME

CONFIGURATION NO.		QUALITY FACTOR				
$C_1 \downarrow \backslash C_2 \rightarrow$		8	10	7	9	
	COUNTING TIME (MIN)	7	7	9	11	
1	6	0.52	0.97	0.72	0.49	7
2	6	0.87	0.70	1.13	0.76	9
4	6	0.86	0.63	1.05	0.75	9
6	8	0.53	1.04	0.77	0.50	7
3	10	0.73	0.86	1.12	0.65	9
5	10	0.92	0.73	1.23	0.78	9
		10	8	10	10	Preferred counting time (min)

TABLE A-14

REPRODUCIBILITY OF DUAL-GAUGE SYSTEM USING CONFIGURATIONS UNDER THE SAME CONSTRUCTION

CONFIGURATION NO.	QUALITY FACTOR			
$C_2 \downarrow \backslash C_1 \rightarrow$	2	3	4	5
8	0.87	0.73	0.86	0.92
9	0.76	0.65	0.75	0.78

TABLE A-15

REPRODUCIBILITY OF DUAL-GAUGE SYSTEM UNDER SEVERAL CONSTRUCTIONS OF EACH CONFIGURATIONS

CONFIGURATION NO.	QUALITY FACTOR		
$C_2 \downarrow \backslash C_1 \rightarrow$	1	2	6
7	0.72	0.77	1.13
8	0.52	0.53	0.87
10	0.97	1.04	0.70

TABLE A-16

QUALITY FACTORS USING PYREX AND CHALK AIR-GAP DATA

	QUALITY FACTOR	
DUAL GAUGE	PYREX	CHALK
2-8	0.87	0.92
6-8	0.53	0.50

4 were the same, and similarly for configurations 3 and 5. Therefore, the most meaningful comparisons would be dual gauges 2 — 8 (0.87) with 4 — 8 (0.86), 2 — 9 (0.76) with 4 — 9 (0.75), 3 — 8 (0.73) with 5 — 8 (0.92), and 3 — 9 (0.65) with 5 — 9 (0.78). These show reasonable reproducibility, varying by at most 23 percent.

Table A-15 can be interpreted similarly, keeping in mind that the variation in quality factor is partially affected by differences in counting times. This table, as well as the others, serves to demonstrate that performance of the optimum dual gauge is significantly affected by factors other than just the design (for instance, counting time and small variations in construction).

Table A-16 indicates that quality factor is relatively independent of the sample used to determine the surface-effect and counting rate measurement errors. This is significant, because it lends support to the belief that the errors and the quality factors reported are typical of those for most common materials having densities and compositions in the regions of interest.

The results of Table A-12 are used to find average surface-effect and combined normal errors, $\hat{E}_{se}$ and $\hat{\sigma}^n(\rho)$, respectively, from which is obtained an average quality factor, $\hat{Q}$:

$$\hat{E}_{se} = \sum_{i=1}^{26} \frac{E_{se_i}}{26} \qquad \text{(A-62)}$$

$$\hat{\sigma}_n(\rho) = \left[\sum_{i=1}^{26} \frac{\sigma^2{}_{n_i}(\rho)}{25} \right]^{\frac{1}{2}} \qquad \text{(A-63)}$$

$$\hat{E}_c = [(2\ \hat{\sigma}_n(\rho))^2 + (\hat{E}_{se} - \hat{\sigma}_n(\rho)^2]^{\frac{1}{2}} \qquad \text{(A-64)}$$

and

$$\hat{Q} = 2\,V/\hat{E}_c \qquad \text{(A-65)}$$

The values obtained are: $\hat{E}_{se} = 1.29$ pcf, $\hat{\sigma}_n(\rho) = 1.28$ pcf, and $\hat{Q} = 0.78$.

It should be noted that better results would be expected for only one construction of the gauge and for data taken only at the optimum counting time. The reported values reflect all the results obtained in the final experimental program.

SUMMARY AND CONCLUSIONS

Faced with the task of ensuring that, for instance, roadbeds meet compaction requirements, the engineer can propose to use a secondary parameter, in this case density, as a guide or an indicator. Faced then with the problem of determining soil density, he can investigate the plausibility of doing so by measuring the extent of interaction of gamma radiation with the soil. The problem then becomes one of converting a radiation measurement into a density measurement, which is accomplished by constructing a calibration curve—a simple, graphical statement of the relationship between the two quantities. To improve the accuracy of the method—the efficiency of this conversion—an attempt is made to identify the measurement interferences, in this instance variation in composition, surface roughness, and the uncertainties inherent

in counting rate measurements. Having identified these, two methods of minimizing their adverse effects are possible:

1. Measure them by some independent means and construct calibration curves for various combinations of values of the measurement interferences,
2. Work to isolate them in a calibration model and mathematically eliminate them. (This corresponds to using separate, independent measurements, and the knowledge of how the interferences actually interfere, to determine the desired parameter independently of the undesired parameters.)

The latter procedure was employed by Gardner (*6, 7, 8*) and resulted in a dual-gauge principle designed to eliminate the composition variable in this calibration model. Gardner then proposed that a search be made for an optimum use of the dual-gauge principle whereby composition effects are essentially eliminated and the other interferences are minimized. This is a report on the results of such a search.

What has been obtained, the "optimum" dual gauge, is not, probably, an absolute optimum, but rather a relative optimum that is believed to be near the absolute (for this dual-gauge principle) and that is believed to provide significant improvement over existing nuclear density-measuring devices and sufficient accuracy for highway construction purposes. Specifically, the optimum dual-gauge design—represented by the notation Co60,4.75,3,11-Co60, 10,5,6—is characterized by average gauge errors $\hat{E}_{se} = 1.29$ pcf, $\hat{\sigma}_n(\rho) = 1.28$ pcf, and corresponding quality factor, $\hat{Q} = 0.78$.

The optimum system described is somewhat sensitive to small variations in construction. Thus, a gauge built for field use based on this proposed optimum design would likely behave differently than the prototype system. However, based on the reproducibility of "good" results (quality factors greater than 0.7, for example) for various tests of the optimum system and for other systems with designs only slightly different from the optimum system, it is believed that gauges can be manufactured commercially that will be capable of comparable accuracy.

Dual gauge 5 — 7 in Table A-12 represents the best results obtained with the optimum system; surface-effect error is 0.79 pcf, combined normal error is 0.75 pcf, and quality factor is 1.23. This is compared with quality factors of the order of 0.33 for the best use known to the researcher of the dual-gauge principle with commercial gauges.

REFERENCES

1. BALLARD, L. F., and GARDNER, R. P., "Density and Moisture Content Measurements by Nuclear Methods —Interim Report." *NCHRP Report 14* (1965) 32 pp.
2. BELCHER, D. J., CUYKENDALL, T. R., and SACK, H. S., "The Measurement of Soil Moisture and Density by Neutron and Gamma-Ray Scattering." *Tech. Dev. Rep. No. 127,* U.S. Civil Aeronautics Admin. (1950).
3. BELCHER, D. J., CUYKENDALL, T. R., and SACK, H. S., "Nuclear Meters for Measuring Soil Density and Moisture in Thin Surface Layers." *Tech. Dev. Rep. No. 161,* U.S. Civil Aeronautics Admin. (1952).
4. CARLTON, P. F., "Application of Nuclear Soil Meters to Compaction Control for Airfield Pavement Construction." Symposium on Nuclear Methods for Measuring Soil Density and Moisture, *ASTM Spec. Tech. Pub. No. 293* (1961).
5. GARDNER, R. P., and ELY, R. L., *Radioisotope Measurement Applications in Engineering.* Reinhold (1967).
6. GARDNER, R. P., and ROBERTS, K. F., "Density and Moisture Content Measurements by Nuclear Methods —Final Report." *NCHRP Report 43* (1967) 38 pp.
7. GARDNER, R. P., ROBERTS, K. F., HUGHES, C. S., and ANDAY, M. C., "A Calibration Model for Optimizing the Air-Gap Method of Compensating Nuclear Density Gauges for Soil Composition Variations." *Jour. Materials,* Vol. 2, No. 1 (1967), p. 3.
8. GARDNER, R. P., "Minimizing Nuclear Soil Density and Moisture Content Gauge Errors." *Hwy. Res. Record No. 290* (1969) pp. 1-8.
9. HOFFMEYER, C. K., "Control of Compaction by Nuclear Density Meters." Ohio River Division Laboratories, U.S. Army Corps of Engineers (1958).
10. HORONJEFF, R., and GOLDBERG, I., "Field Measurements of Soil Moisture and Density with Radioactive Materials." *Proc. HRB,* Vol. 32 (1953) pp. 500-511.
11. HUGHES, C. S., and ANDAY, M. C., "Correlation and Conference on Portable Nuclear Density and Moisture Systems." *Hwy. Res. Record No. 117* (1967) pp. 239-279.
12. JAFFEY, A. H., "Statistical Tests for Counting," *Nucleonics,* Vol. 18, No. 11 (1960).
13. KUHN, S. H., "The Effects of Type of Material on Nuclear Density Measurements." *Hwy. Res. Record No. 66* (1965) pp. 1-14.
14. PIEPER, G. F., "The Measurement of Moisture Content of Soil by the Slowing of Neutrons." Unpub. thesis, Cornell University (1949).
15. GUNDERMAN, W. G., "Current Status of Nuclear Testing for Moisture and Density of Soils and Related Materials." Presented at Fourth Annual Symposium on Engineering Geology and Soils Engineering, Univ. of Idaho, Moscow, Apr. 19-21, 1966.
16. MCDOUGALL, F. H., DUNN, W. L., and GARDNER, R. P., "Report on Nuclear Soil Gauge Workshop-Symposium." Dept. of Nuclear Eng., North Carolina State Univ. (1969).
17. U.S. ATOMIC ENERGY COMMISSION, *Chart of the Nuclides, Knolls Atomic Power Laboratory, Naval Reactors.* 8th Ed., Allyn and Bacon, Boston (1965).

APPENDIX B

DESIGN STUDIES FOR OPTIMIZATION OF GAMMA-RAY BACKSCATTER DENSITY GAUGES *

By FRANK H. MCDOUGALL

The field of radioisotope applications is rapidly expanding due to new advancements in electronic equipment, improved technology in the use of radioisotopes, and the increasing number of applications being developed. Specifically, gamma-ray backscatter density gauges are evolving in the same manner for the same reasons. This nuclear technique for measuring soil and aggregate densities was conceived because it offered the initial advantage of nondestructive, rapid, and reproducible measurements.

The concept of backscatter density gauges was introduced as early as 1950 (Belcher, et al., 1950); however, the first commercial density gauges did not appear until the late 1950's. Although in current use by some state highway departments and others, gamma-ray backscatter density gauges have not, as yet, found widespread or exclusive appeal, due to discrepancies found in comparing the nuclear measurements with conventional gravimetric measurements. The questionable accuracy of these devices necessitated the formation of a committee on Nuclear Principles and Applications by the Highway Research Board. Project 10-5, and its extension 10-5A, entitled "Density and Moisture Content Measurements by Nuclear Methods," were initiated to resolve the inaccuracies of these gauges. The work reported here was part of the work scheduled under Project 10-5A.

OBJECTIVES

The research covered by this appendix is the last of three phases conducted under Project 10-5A. The first phase was concerned with neutron moisture gauges; the second phase was concerned with optimum design of a dual-gauge system using existing gauge components; this final phase is essentially concerned with the application and optimization of new design concepts, including more sophisticated electronics, to eliminate the surface-effect error while minimizing other gauge errors. The prevailing objective of the over-all project is to reduce backscatter gauge errors to acceptable levels such that these gauges will be preferred for field use over both conventional and nuclear (probe- or depth-type gauges) destructive techniques. The accomplishment of this objective will provide speedy and accurate nuclear methods of density measurement.

Other specific objectives are as follows:

1. Evaluate the extent of the surface-effect or surface roughness error and discover means of eliminating or reducing it to an acceptable level.
2. Evaluate the use of energy discrimination by gamma-ray spectrometry as a means of reducing gauge errors.
3. Determine a means to combine gauge errors or to describe the gauge in terms of all the gauge errors; i.e., assess the quality of the gauge or dual-gauge system.
4. Evaluate new gauge design parameters such as collimation of source and/or detector.
5. Design a prototype gauge that could be extended or modified for practical field use.
6. Suggest new avenues of research for more applications or further improvement of these devices on the basis of results obtained.

The interplay of the primary and other specific objectives is such that all are interdependent and must be approached as such.

The general approach here is to present all pertinent theory and conclusions, however briefly, for the purpose of completeness so that this appendix will represent not only the state of the art but also a review of previous accomplishments.

LITERATURE REVIEW

Previous literature surveys have been extensively reported by Ballard and Gardner (1965), Gunderman (1966), and Csathy (1962). Some of the literature surveyed by Ballard and Gardner (1965) is mentioned briefly here to consistently cover the full range of concepts previously reported; however, this reference provides a more complete survey of earlier, more fundamental literature.

Due to the undesirable chemical composition or soil-type dependence of nuclear density gauges, the most significant problem with these gauges to date has been with their calibration to cover the full range of soils that might be encountered. Gardner, et al. (1967) introduced the dual-gauge principle, which has been the most successful technique yet reported in reducing the composition error and in calibrating gauges to cover the full range of soil types. The principle involves combining two sets of gauge responses from two different gauge design configurations to obtain a solution for density that is independent of soil composition. This concept is discussed in detail herein.

* This appendix comprises the essential portions of a thesis bearing the same title prepared under the NCHRP Project 10-5 contract and submitted to the North Carolina State University (1970) in partial fulfillment of the requirements for the degree of Master of Science.

The calibration model that is used in the dual-gauge principle was developed in fundamental form by Ballard and Gardner (1965) and later refined by Gardner, et al. (1967).

The history of developments in nuclear gauge technology is interesting, yet frustrating, because the nuclear technique was at first believed to be the solution to the problem of accurately measuring soil and aggregate densities. Early testing of a nuclear density gauge, involving a probe- or depth-type device, was reported by Belcher, et al. (1952), who noted that improvements were necessary before these gauges would gain recognition and acceptance. Horonjeff and Goldberg (1953) reported discrepancies between nuclear readings and conventional readings to be as much as 25 percent, although the nuclear readings were reproducible among themselves (Gunderman, 1966). The earliest reported use of a scintillation detection system was by Miles (1952), who studied energy distributions of gamma rays around a depth-probe device.

Gauge inaccuracies have been reduced somewhat through the normal evolution of improved technology (e.g., improved stability of electronic counting systems). However, the chemical composition dependence of these gauges has plagued users and designers since it was recognized by Semmler, et al. (1961) and Kuhn (1963) as a significant error, especially in surface-type gauges. Kuhn (1963) presented a method for reducing composition dependence that involved two readings with the same gauge, one normal flush reading, and another reading at a small air-gap height above the surface of the soil. The ratio of these responses was used in calibrating gauges, but only a small reduction in the error materialized. Ballard and Gardner (1965) observed from the work of Kuhn (1963) that if two gap heights were found yielding the same gauge response, the difference in the heights could be related to the density and only slightly to the composition of the soil. This concept later led to formulation of the dual-gauge principle applied to the air-gap method by Gardner, et al. (1967). The reduction of the composition error by the dual-gauge air-gap technique was shown in laboratory and field tests performed at the North Carolina State University Nuclear Soil Gauge Calibration Workshop-Symposium (McDougall, et al., 1969).

Another surface gauge inaccuracy, which has not received adequate study until recent years, is the surface roughness or surface-effect error which was discussed by Gardner and Roberts (1967). The work of Harland (1966a), who mathematically modeled the depth response of a gauge, also provided an excellent definition for effective sample depth which was applied by Gardner and Roberts (1967) and was used in the study reported herein. These valuable developments cleared the way for evaluation of the magnitude of the surface roughness error.

The research reported herein involved the use of a scintillation detection system which provides the capabilities for studying energy distributions of scattered gamma rays. Miles (1952), Roy and Winterkorn (1959), Preiss (1964), Taylor and Kansara (1966, 1968), Simpson (1968), and Lin, et al. (1969) have based their designs on a single-scatter model of the gamma rays through the soil which was shown inadequate by Ballard and Gardner (1965). The work of Simpson (1968) showed careful use of energy discrimination, and his results of effective sample depth studies are, indeed, useful; however, his gauge design is not very practical for measuring soil density in the field. Simpson's gauge design is similar to the system used by Hine and McCall (1954) in their fundamental study of gamma-ray backscattering. The paper by Hine and McCall (1954), although seemingly unfamiliar to most gauge designers and researchers, provides some very useful information and insight into the observed energy distributions of backscattered gamma rays.

The concept of optimization which employs both the calibration model developed by Ballard and Gardner (1965) and the dual-gauge principle developed by Gardner, et al. (1967) and Gardner and Roberts (1967) is discussed by Gardner (1969). The optimization procedure involves minimizing three gauge errors collectively for the most accurate system. This procedure is necessary because attempting to minimize one error separately may adversely affect the other errors.

An idea of the current performance status of nuclear density gauges may be attained from Table B-1.

THEORY OF GAMMA-RAY BACKSCATTER DENSITY GAUGES *

Interactions of Gamma Rays with Matter

Gamma-ray density gauges employ a radioisotope source such as ^{137}Cs (gamma-ray energy of 0.662 MeV). When sources such as ^{137}Cs and others with gamma-ray energies less than 1.02 MeV are employed, only two interactions of the gamma rays with the sample material are considered: Compton scattering and photoelectric absorption. When radioisotope sources such as ^{60}Co with energies greater than 1.02 MeV are used, a third interaction, pair production, must be considered. Because high-energy sources are rarely used, pair production is not considered here; it is discussed in detail by Evans (1955).

Compton Scattering

A Compton scattering interaction involves a change in direction and energy loss of a gamma-ray photon as it interacts with a "free" electron. Most electrons in any material are "free" electrons because their binding energy is much less than the incident gamma-ray energy. For this reason, when a gamma ray of energy greater than about 0.1 MeV interacts with electrons in a material like soil (most elements found in soil have low atomic numbers), Compton scattering is the predominant interaction.

The energy of a gamma ray after striking the electron depends on the incident energy by

$$E = \frac{0.51 \text{ MeV}}{\frac{0.51 \text{ MeV}}{E_o} + (1 - \cos \phi)} \qquad \text{(B-1)}$$

in which E is the gamma-ray energy after the interaction, 0.51 MeV is the energy equivalent to the rest mass of an

* A background discussion of field applications of backscatter density gauges is available on request to the Program Director, NCHRP.

TABLE B-1

HISTORY OF DENSITY GAUGE ERRORS

ERROR DEFINITION	VIRGINIA CONFERENCE [a]	NCSU WORKSHOP [b]
Average standard error—backscatter gauges	±11.0 [c]	±3.81 [d]
Average standard error—transmission gauges	±7.53 [e]	±2.60 [f]
Average standard deviation—backscatter gauges	2.0 [c]	2.29 [d]
Average standard deviation—transmission gauges	3.1 [e]	3.18 [f]

[a] Definitions of these errors and details appear in Hughes and Anday (1967).
[b] Definitions of these errors and details appear in McDougall, et al. (1969).
[c] 29 gauges were used to determine these results.
[d] 4 gauges were used to determine these results.
[e] 11 gauges were used to determine these results.
[f] 2 gauges were used to determine these results.

electron, E_o is the initial energy of the incident gamma ray, and ϕ is the angle of scatter between incident and exit directions from the point of interaction.

The probability that an incident gamma ray will interact by Compton scattering is described by the Compton cross section. The Klein-Nishina cross-section formula accurately describes the energy dependence of the interaction probability, which decreases with increasing incident gamma-ray energy up to about 1.5 MeV. The Klein-Nishina formula is complicated and is not necessary for the treatment of density measurement used here. Compton scattering interaction probability can be taken as simply proportional to the number and density of electrons in the atoms and sample material respectively, and is given as

$$C = \rho \sum_i \frac{w_i Z_i}{A_i} \qquad \text{(B-2)}$$

in which C is the Compton scattering cross section, ρ is the sample density, w_i is the weight fraction of element i in the sample, Z_i is the atomic number of element i, and A_i is the atomic weight of element i in the sample.

Note that the ratio Z_i/A_i in Eq. B-2 is essentially a constant ~ 0.5, for all elements normally found in soils except hydrogen ($Z/A = 1$). Gardner and Roberts (1967) provide a table that contains Z/A ratios for several elements found in soils. Thus, the Compton scattering interaction probability is essentially dependent only on the density of a normal soil and is very slightly dependent on the chemical composition. For this reason the Compton scattering interaction is associated with useful density information, a fact that will be more evident when considering the photoelectric absorption interaction in the next section. Sometimes it is convenient to use a scattering parameter, C', defined as C/ρ, which is a measure of the composition effect due to Compton scattering. More detailed discussions of Compton scattering appear in Evans (1955) and Kaplan (1962).

Photoelectric Absorption

In a photoelectric absorption interaction a gamma ray is completely absorbed by a tightly bound orbital electron. The electron is ejected from the atom with kinetic energy equal to the incident gamma-ray energy less the atomic binding energy of the electron. Except for low-atomic-number materials, the photoelectric effect is the predominant interaction for gamma-ray energies less than about 0.1 MeV. The photoelectric effect increases rapidly with increasing atomic number of the absorber and decreasing incident gamma-ray energies. For the present purpose, the photoelectric absorption probability is taken as

$$P = \rho \sum_i \frac{w_i Z_i^5}{A_i} \qquad \text{(B-3)}$$

in which P is the photoelectric cross section and w_i, Z_i, and A_i are the weight fraction, atomic number, and atomic weight of element i, respectively. Eq. B-3 shows that the photoelectric absorption probability is proportional to density and is extremely dependent on the chemical composition of a sample material. The power of Z may actually vary from 3, for low gamma-ray energies, to 5, for high-energy gamma rays and high-atomic-number materials. In soils such elements as calcium and iron are the principal photoelectric absorbers with relatively high atomic number.

In terms of density measurement, the strong dependence of the photoelectric cross section on chemical composition is a detriment. For this reason photoelectric absorption represents a measurement interference. However, if the reverse process of evaluating chemical composition is attempted, the photoelectric absorption process is beneficial. This concept is not discussed here, but data are available on request to the Program Director, NCHRP. As in the case with Compton scattering, a composition parameter, P', may be defined as P/ρ. More complete treatments of photoelectric absorption appear in Evans (1955) and Kaplan (1962).

Principles of Density Gauge Operation

Surface-Type Backscatter Gauges

The primary concern of this project is to improve surface-type gamma-ray backscatter density gauges. Figure B-1 shows an example of such a gauge. These gauges have been singled out by the Highway Research Board as having the greatest potential for widespread acceptance, their primary advantages being ease and speed of measurements and nondestructiveness. Other advantages such as safety and convenience in handling are also realized. The present disadvantage of requiring smooth soil surfaces decreases the effectiveness and efficiency of these gauges.

Gauge Components and Parameters

The primary density gauge components are source, detector, and shielding. This section is concerned with how these components are employed to establish the parameters that constitute a gauge configuration. In existing gauges the parameters are source-detector separation, source

energy and intensity, type of detector and efficiency, and air-gap, or response taken at a known height above the sample surface. The design parameters of concern in this project include the degree of source and/or detector collimation, detected energy region, and angles of incidence into the soil for both source and detector collimators.

The purpose of shielding is to remove direct transmission gamma rays from being detected and to eliminate scattering off the gauge housing and immediate surface of the sample to be measured. Source intensity is chosen to provide a sufficient counting rate, usually at least 10,000 counts per minute. A sufficient counting rate is necessary to minimize counting-rate measurement errors. Detector type may be varied to provide either greater or less efficiency for detection, greater efficiency for a particular energy range or for ruggedness, stability, or special spectrometric capabilities. Geiger-Mueller tubes are rugged and stable, thus ideal for field use, but are less efficient in detecting gamma rays than NaI (Tl) scintillation detectors. They may be used to be more efficient in detecting low or high energies. Scintillation detectors such as NaI (Tl) may be used for their spectrometric capabilities and high efficiencies; they suffer somewhat in ruggedness and stability compared to Geiger-Mueller tubes.

Source-detector separation distance may be varied to perform two functions: to adjust the counting rates obtained and to optimize sensitivity to density. According to Ballard and Gardner (1965), increasing source-detector separation increases sensitivity to density when other factors are held constant. By decreasing source-detector separation and holding other factors constant, a decrease in composition sensitivity occurs; thus, an optimum separation distance exists for each gauge (Ballard and Gardner, 1965).

The new design parameters are based on more complex theoretical considerations. Energy discrimination (the exclusion of part of the energy spectrum in favor of another part) was chosen because of its possible use to decrease sensitivity to soil composition and/or surface roughness. It may also be used to optimize the slope of the calibration curve. Source and detector collimation is aimed at both reducing gamma-ray transport at the sample surface and at increasing the effective sample depth of the gamma rays into the soil. These factors should tend to minimize the effect of a finite density difference due to surface roughness. The incident angles of source and detector collimators are varied, hopefully to detect an average path of the gamma rays through the soil.

These parameters are referred to as "new" because to date they have not yet been included in existing commercial gauge designs. Preiss (1964) has analyzed both collimation and energy discrimination with some of the same results reported in this project; however, his results and conclusions were neither complete nor entirely reliable. More detailed discussions of these new parameters in both individual and combined roles appear in later sections.

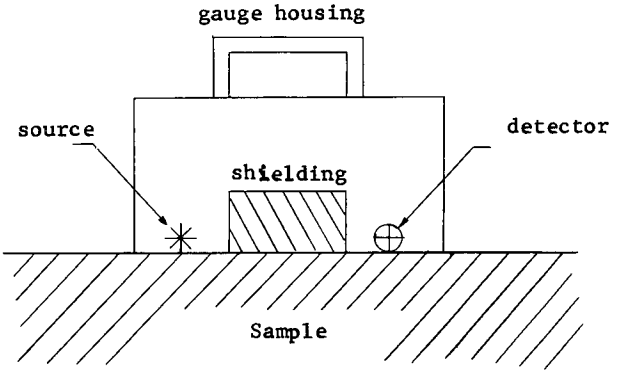

Figure B-1. Typical backscatter gauge.

Gauge Response Models and Sensitivity Analysis

Calibration Model for Single-Gauge Response

Probably the most basic and significant development that led to recent improvements in backscatter density gauges has been the calibration model for single-gauge response developed by Ballard and Gardner (1965) and also discussed in references by Gardner, et al. (1967), Gardner and Roberts (1967), and Gardner (1969). The success of the model is due to the fact that it not only satisfies the boundary conditions of no net response at zero density and low net response at high densities, but it also separates the Compton scattering and photoelectric absorption dependence of the response. The model is given here as defined by Gardner (1969):

$$R = C\ 10^{a+bC+cP} \qquad \text{(B-4)}$$

in which R is the gauge response, which may have units of counts per unit time for either net or gross counts or ratio of counting rate for a measurement to a standard counting rate; C and P are the Compton and photoelectric interaction probabilities as defined in Eqs. B-2 and B-3, respectively; a, b, and c are model constants for a particular gauge configuration determined by a least-squares analysis of data taken on a set of optimum laboratory standards (see "Laboratory Calibration Standards," which follows). For improved sensitivity in the least-squares calculations C and P are scaled down by factors of 10 and 10^6, respectively. Computer programs for determining the model constants are not provided here, but are available to qualified researchers on request to the Program Director, NCHRP. A plot of the calibration model for density is shown in Figure B-2.

Dual-Gauge Principle

One of the significant advantages of the calibration model just discussed is that it isolates the Compton and photoelectric dependence of the gauge response. Because it is shown that the composition effect is a result of photoelectric absorption, it is reasonable to assume that minimization of the term cP to an optimum value in the exponent of Eq. B-4 would reduce the composition effect. Obviously, not enough information is available from the

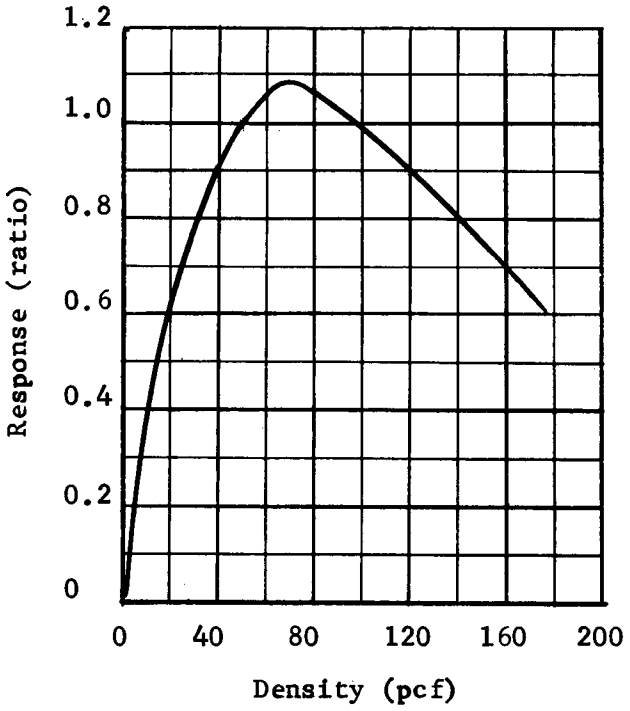

Figure B-2. Calibration model plot for pilot group gauge no. 3, 0-130 KeV discrimination level.

single gauge reading described by Eq. B-4. To accomplish reduction of the term cP to an optimum value another response from another gauge configuration is required, hence the term "dual-gauge" principle (Gardner et al., 1967). The principle was then extended to include any two combinations of gauge parameters, each possessing a specific set of gauge calibration constants in Eq. B-4 (Gardner and Roberts, 1967).

For completeness the essential mathematics of the dual-gauge principle is outlined. Eq. B-4 may be written as

$$R = (\rho/20)\ 10^{a+(\rho/20)+cP} \qquad \text{(B-5)}$$

in which C is replaced by $\rho/20$ because from Eq. B-2 it is noted that $C \approx \rho/2$ for most soil materials, and the previous section indicates that C is scaled down a factor of 10. Using Eq. B-5 for two single-gauge responses, denoting the first gauge response with subscript 1 and the second with subscript 2, taking logarithms and solving for P in each equation yields

$$P = \frac{\log R_1}{c_1} - \frac{\log \rho}{c_1} + \frac{\log 20}{c_1} - \frac{a_1}{c_1} - \frac{b_1\rho}{20c_1} \qquad \text{(B-6}a\text{)}$$

and

$$P = \frac{\log R_2}{c_2} - \frac{\log \rho}{c_2} + \frac{\log 20}{c_2} - \frac{a_2}{c_2} - \frac{b_2\rho}{20c_2} \qquad \text{(B-6}b\text{)}$$

P may be eliminated by subtracting Eq. B-6a from Eq. B-6b, and ρ may be isolated as follows:

$$(0.05)(c_1b_2 - c_2b_1)\ \rho + (c_1 - c_2)\log \rho = (c_1 - c_2)\log 20 + c_2a_1 - c_1a_2 - c_2 \log R_1 + c_1 \log R_2 \qquad \text{(B-7)}$$

Several methods are available for solving Eq. B-7 for density. Most methods for solving nonlinear equations may be applied (Ralston, 1965), but a preferred method, especially for use with a computing machine, is the Newton-Raphson method, due to its rapid convergence. When this method proves troublesome, the method of bisection may be used. Examples of these two particular methods appear in the previously referenced computer programs. The Newton-Raphson method is outlined briefly as follows.

Eq. B-7 may be written in terms of the function $T(\rho)$:

$$T(\rho) = (0.05)(c_1b_2 - c_2b_1)\ \rho + (c_1 - c_2)\log \rho - (c_1 - c_2)\log 20 - c_2a_1 + c_1a_2 + c_2 \log R_1 - c_1 \log R_2 \qquad \text{(B-8)}$$

Taking the derivative yields

$$T'(\rho) = 0.05\ (c_1b_2 - c_2b_1) + \frac{q(c_1 - c_2)}{\rho} \qquad \text{(B-9)}$$

in which $q = \log_{10} e = 0.434294182$. Newton's method provides that for an arbitrary initial value of density, ρ_i, usually taken as the known density of a laboratory standard, a new calculated value is given by

$$\rho_{i+1} = \rho_i - T(\rho_i)/T'(\rho_i) \qquad \text{(B-10)}$$

The process is iterated until a specified accuracy in obtaining the root is obtained.

A more sophisticated method of solution of Eq. B-7, described by Gardner, et al. (1967) and Gardner and Roberts (1967), involves making a series approximation for the cumbersome $\log \rho$ term:

$$\log \rho \approx \log x + 0.86859\left(\frac{\rho - x}{\rho + x}\right) \qquad \text{(B-11)}$$

in which x may be the actual known density of a laboratory standard or may be a typical soil density such as 130 pcf for field use. For $x = 130$ pcf, Eq. B-11 becomes (Gardner, et al., 1967)

$$\log \rho \approx 2.11394 + 0.86859\left(\frac{\rho - 130}{\rho + 130}\right) \qquad \text{(B-12)}$$

When Eq. B-12 is substituted into Eq. B-7 the quadratic solution may be obtained as follows:

$$\rho = \frac{-B - (B^2 - 4AC)^{\frac{1}{2}}}{2A} \qquad \text{(B-13)}$$

in which

$A = 0.05\ (c_2b_1 - c_1b_2)$;

$B = c_1 \log R_2 - c_2 \log R_1 - 1.6815\ (c_1 - c_2) + c_2a_1 - c_1a_2 + 6.5\ (c_2b_1 - c_1b_2)$; and

$C = 130\ c_1 \log R_2 - 130\ c_2 \log R_1 + 7.2384\ (c_1 - c_2) + 130\ (c_2a_1 - c_1a_2)$.

A nomograph solution, which according to Gardner and Roberts (1967) is "simple and surprisingly accurate," may be obtained by assuming that $\log \rho = \log 130 = 2.11394$. Using this assumption in Eq. B-7 yields an equation for density which takes the form

$$\rho = k_1 \log R_1 + k_2 \log R_2 + k_3 \qquad \text{(B-14)}$$

in which the constants k_1, k_2, and k_3 are determined from a least-squares analysis of data (Gardner and Roberts, 1967). The nomograph solution is particularly applicable to field use, as evidenced by the results obtained for the North Carolina State University Workshop-Symposium. A computer program with complete explanation for preparing a nomograph calibration appears in the Final Report of the North Carolina State University Workshop-Symposium (McDougall, 1969).

Sensitivity Analysis for Application to Gauge Response

The technique of optimization in gauge design requires that both density and composition be considered at the same time for determining the sensitivity of a gauge. Eq. B-25 shows that the sensitivity of a gauge is inversely proportional to gauge response. The response is a nonlinear function of both density and composition; for this reason it is not acceptable to consider either density or composition separately with gauge response as others have done (Preiss, 1964). If Eq. B-4 is restated as

$$R = (\hat{C}/b)\ \ 10^{a+\hat{C}+\hat{P}} = (q\hat{C}/b)\ \ e^{a+\hat{C}+\hat{P}} \qquad \text{(B-15)}$$

in which $\hat{C} = bC$, $\hat{P} = cP$, and $q = \log_{10} e \approx 0.4343$, then

$$(\partial R/\partial \hat{P}) = (q\hat{C}/b)\ \ e^{a+\hat{C}+\hat{P}} \qquad \text{(B-16)}$$

and

$$(\partial R/\partial \hat{C}) = \left(\frac{q}{b} + \frac{q\hat{C}}{b}\right) e^{a+\hat{C}+\hat{P}} \qquad \text{(B-17)}$$

and

$$\frac{(\partial R/\partial \hat{P})}{(\partial R/\partial \hat{C})} = \frac{\hat{C}}{\hat{C}+1} \qquad \text{(B-18)}$$

Because $\hat{C}$ for any gauge that behaves according to the calibration model is negative (b is negative, C is positive), the foregoing ratio is always greater than one. However, if the response were expressed as a linear function of $\hat{C}$ and $\hat{P}$

$$R = \hat{C} + \hat{P} \qquad \text{(B-19)}$$

or as in a transmission gauge

$$R = e^{a+\hat{C}+\hat{P}} \qquad \text{(B-20)}$$

then the ratio $(\partial R/\partial \hat{P})/(\partial R/\partial \hat{C})$ would equal to one in each case.

Some useful information may be obtained by including the following relations from Evans (1955):

$$\sigma(E) = NZ\ \sigma_e(E)\ \text{cm}^{-1} \qquad \text{(B-21)}$$

$$\tau(E) = \tau_a(E) N\ \text{cm}^{-1} \qquad \text{(B-22)}$$

in which $\sigma(E)$ is the Compton total linear attenuation coefficient, $\sigma_e(E)$ is the Compton average collision cross section at energy E in cm^2 per electron, N is the number of atoms per cm^3, $\tau(E)$ is the photoelectric linear attenuation coefficient at energy E, and $\tau_a(E)$ is the photoelectric atomic cross section at energy E in cm^2 per atom. Using these equations and Eqs. B-2 and B-3 it can be shown that at a particular energy

$$\hat{C} = bC = x\ \sigma(E) \qquad \text{(B-23)}$$

$$\hat{P} = cP = x\ \tau(E) \qquad \text{(B-24)}$$

in which x is the effective path length of gamma rays through the soil. The ratio bC/cP is equal to the ratio $\sigma(E)/\tau(E)$ which states that when the former ratio is known the effective energy of the gamma rays may be found by finding the energy at which the latter ratio is the same on a plot of linear attenuation coefficient versus gamma-ray energy. As an example, the value of bC/cP for pilot group gauge number three (see "Experimental Procedure and Results"), full energy range, on aluminum is 7.6 times the value of $\tau(E)$ at about 0.11 MeV. This value may be interpreted as the effective energy measured by this gauge. A qualitative look at Figure B-6 shows that the effective energy should lie somewhere within 0.08 and 0.20 MeV and should be closer to the larger peak; so, the value of 0.11 MeV appears a reasonable value.

Results of this sensitivity analysis indicate that one must maintain the perspective that $\hat{C}$ and $\hat{P}$ must be considered in respect to the proper gauge response sensitivity, and not as quantities that are of equivalent significance. More knowledge of the physical situation is obtained by considering $\hat{C}$ and $\hat{P}$ in terms of $\sigma(E)$ and $\tau(E)$, respectively.

THEORY OF GAUGE QUALITY ANALYSIS

Nuclear soil density gauges have not, as yet, lived up to their potential as the most preferred method of measurement, because of the presence of three primary gauge errors. These measurement interferences are due to uncertainties in counting-rate measurement as a result of normal statistical fluctuations and electronic capabilities, variations in soil composition, and rough, irregular soil surfaces. Throughout the course of NCHRP Projects 10-5 and 10-5A these errors have been identified and evaluated. Composition error, discussed in conjunction with the dual-gauge principle in the previous section, was once the primary concern. Recent success with minimization of composition error and subsequent isolation of the surface-effect error has led to the belief that the latter error is currently of prime concern. In the following sections these errors are mathematically defined and discussed in terms of the gauge parameters that may be used to minimize them. The optimization procedure aimed at minimizing all of the errors is discussed with regard to the quality factor of gauge performance. It is recognized that other errors exist, such as electronic gain shift; however, it may be assumed that every precaution was taken to minimize these problems. These steps are further discussed under "Gamma-Ray Spectrometry for Energy Discrimination."

Gauge Errors

Counting-Rate Measurement Error

A gauge response has a well-known inherent statistical fluctuation governed by the random nature of radioactive decay. Electronic components also have a limited capacity to accept and transmit pulses at 100 percent efficiency. These two considerations are jointly termed the counting-rate measurement error. This error may be defined for both single- and dual-gauge systems, the latter being an extension of the former. Figure B-3 shows that this error must necessarily depend on the slope of the specific calibration curve of a gauge; because the relative sensitivity of a gauge to density is given by (Gardner and Roberts, 1967)

$$S_\rho = (1/R)(\partial R/\partial \rho) \qquad \text{(B-25)}$$

in which R is the gauge response, and $\partial R/\partial \rho$ is the slope of the calibration curve. The steeper the slope the more sensitive a gauge is to density measurement; thus, the reverse must be true for the statistical fluctuations in counting-rate measurement. Denoting the uncertainty in measuring density due to uncertainties in the measurement of counting-rate by $\sigma_s(\rho)$ in pounds per cubic foot (pcf), it may be stated that

$$\sigma_s(\rho) = \left[\sum_{i=1}^{n} \sigma^2(R_i)\left(\frac{\partial \rho}{\partial R_i}\right)^2\right]^{\frac{1}{2}} \qquad \text{(B-26)}$$

in which n is one for a single gauge and two for a dual gauge, $\sigma(R_i)$ is the uncertainty in the measurement of the counting-rate itself, and $\partial \rho/\partial R_i$ is the inverse of the slope of the calibration curve. The terms $\partial \rho/\partial R_i$ may be obtained by differentiating Eq. B-13 with respect to the response(s).

To obtain an expression for $\sigma(R)$ a rule-of-thumb approximation is made. It is assumed that a measured counting rate will be within 1 percent of the true mean 68 percent of the time for most counting systems when a total count of 10,000 has been exceeded. This approximation inherently accounts for limitations in electronic counting systems, because, under the ideal systems, $\sigma(R)$ will be the square root of the total count, or better than 1 percent when the total count exceeds 10,000.

Thus,

$$\sigma(R) = 0.01R, \; R \geq 10{,}000 \qquad \text{(B-27)}$$

when R is the total count.

When statistical fluctuation in counting rate is the controlling error, the standard deviation of a ratio response (measured response to reference standard response) is given by

$$\frac{\sigma(R_1/R_s)}{R_1/R_s}\left[\frac{\sigma^2(R_1)}{R_1^2} + \frac{\sigma^2(R_s)}{R_s^2}\right]^{\frac{1}{2}} = (0.01)\sqrt{2} \qquad \text{(B-28)}$$

in which R_1 is the measured total count, and R_s is the standard reference total count, with both $\sigma(R_1)$ and $\sigma(R_s)$ defined by Eq. B-27. The ratio response, however, is taken for the purpose of minimizing the effects of electronic gain shift which becomes the controlling error when R_1 and R_s exceed 10,000 total counts. Thus, when R_1 and R_s are measured within a time span that is small compared to the time span of any electronic gain shift that is present, they do not have normally distributed errors nearly as large as Eq. B-28 would imply. Therefore, their ratio may be treated as a single response and Eq. B-27 can be considered valid for a ratio response as well as for a total count response. The use of Eq. B-27 for ratio responses becomes more reasonable when it is considered that the use of Eq. B-28 would significantly increase counting-rate measurement error, yielding no advantage in the use of a ratio response.

The most obvious way to minimize the counting-rate measurement error is to make the slope of the calibration curve in the density region of interest as steep as possible. This result may be accomplished by subtracting background or by energy discrimination. The former method may be used to eliminate contributions to the response that are not described by the calibration model such as X-rays from lead shielding. This is discussed further in "Results and Conclusions."

Another method of determining the counting-rate measurement error depends on random number sampling. A gauge is first calibrated to determine the model constants in Eq. B-4. The values for C, P, and density of a laboratory standard and the model constants are then substituted into Eq. B-4 to determine a back-calculated response. With this response as the mean value and a standard deviation, σ, equal to $0.01R$, where R is the back-calculated response, a random number is taken from a Gaussian distribution. This random number is then related to a new response, which is, in turn, used to determine a new density.

To calculate the counting-rate measurement error on the basis of the back-calculated densities, the density difference, $\bar{\rho}_i - \rho_{ij}$, is determined, where $\bar{\rho}_i$ is the back-calculated density of sample i and ρ_{ij} is the calculated density of sample i from random number j. The error is then calculated from

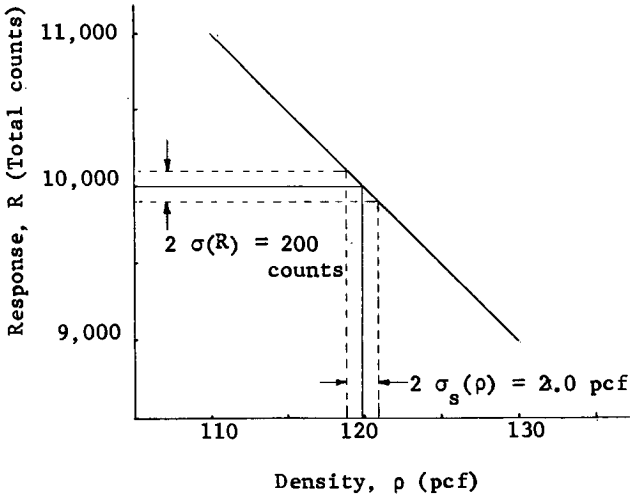

Figure B-3. Dependence on slope of the counting-rate measurement error, shown for a hypothetical case.

$$\sigma_{sR}(\rho) = \left[\frac{\sum_i \sum_j (\hat{\rho}_i - \rho_{ij})}{mn - 1}\right]^{\frac{1}{2}} \quad \text{(B-29)}$$

in which m is the number of samples, and n is the number of random number samplings per sample.

For the sake of continuity and completeness, the remainder of the random number sampling technique is presented. To calculate the composition error on the basis of actual densities from the random number sampling technique, the density difference, $\hat{\rho}_i - \rho_{ij}$, is determined, where $\hat{\rho}_i$ is the actual density of sample i and ρ_{ij} is as defined previously. The composition error is given by

$$\sigma_{cR}(\rho) = \left[\frac{\sum_i \sum_j (\hat{\rho}_i - \rho_{ij})^2}{mn - 1}\right]^{\frac{1}{2}} \quad \text{(B-30)}$$

in which all symbols are as defined previously. From these values calculated on the basis of random number sampling and based on the assumption that only counting-rate measurement error and model fit error constitute the composition error * the model fit error may be defined as

$$\sigma_M(\rho) = [\sigma_{cR}^2(\rho) - \sigma_{sR}^2(\rho)]^{\frac{1}{2}} \quad \text{(B-31)}$$

Composition Error

Composition error is a direct result of the photoelectric absortion that increases with increasing atomic number of elements in the soil. It may be defined on the basis of normal fluctuations about the calibration curve described by Eq. B-4, as follows:

$$\sigma_c(\rho) = \pm\left[\sum_{i=1}^{m} \frac{(\bar{\rho}_i - \rho_i)^2}{m}\right]^{\frac{1}{2}}, \; m \geqq 4 \quad \text{(B-32)}$$

in which $\sigma_c(\rho)$ is the composition error in pcf, m is the number of samples, ρ_i is the density of sample i, and $\bar{\rho}_i$ is the actual density of sample i. When the actual density is not known, the average density of all the samples is used in place of $\bar{\rho}_i$ and the denominator becomes $m - 1$ due to a loss in accuracy. This error may be considered a standard error only when two conditions are met:

1. The laboratory standards chosen should be representative of the density and composition variations found in soil. Thus, an optimum set of laboratory standards (as described later herein) should be used; these standards appear to be statistically representative of compositions and densities encountered in the field.

2. The approximation must be made that density and composition can be considered linear functions of the gauge response.

This approximation results from the use of Eq. B-26. The composition error as defined in Eq. B-32 necessarily includes the error in the model-fit least-squares method and some statistical fluctuations inherent in determining the densities; however, it may be assumed that the counting-rate measurement error may be separately evaluated.

This error may be reduced significantly by the dual-gauge principle (discussed previously). Table B-2 gives the results of the recent North Carolina State University Workshop-Symposium where the air-gap nomograph calibration, an application of the dual-gauge principle, significantly reduced the composition error and thus improved over-all gauge performance. Slight reductions in the composition error were noted for the air-gap ratio technique discussed in detail by Gardner, et al. (1967).

Another method for reducing this error, evaluated in this project, is based on energy discrimination. A plot of cross-section (interaction probability) against photon energy (Preiss, 1964, and Evans, 1955) shows that the photoelectric absorption interaction probability varies strongly with energy decreasing to near zero at 0.2 MeV for most materials. The Compton scattering interaction probability varies only slightly with photon energy and is the predominant interaction for energies between 0.2 and 1 MeV for most materials. With this in mind, it is reasonable to assume that discrimination against lower energy gamma rays would yield a response only slightly affected by photoelectric absorption, thus exhibiting little or no composition effect. Results of this approach are discussed in "Results and Conclusions."

Surface-Effect Error

Soil surfaces are generally rough, warped, or cracked. The soil particles are also usually more loosely packed at the surface, which leads to a small, but finite, density difference. The path that an average gamma ray follows from source to detector includes this density differential in entering and leaving the soil; thus, the response of a detector is usually higher than the true average density of the bulk soil would indicate due to less absorption or scattering, yielding a density measurement lower than the true density. This error in density measurement, known as the surface-effect error, is a significant one and cannot be directly obtained.* It is possible, however, to simulate this error in the laboratory by assuming that the density heterogeneity at the surface is equivalent to an air-gap of thickness h,

* For actual field use the atomic number to atomic mass ratio of the soil varies and must be considered as part of the composition error.

* It is conceivable that the bottom of a gauge housing could be uneven or dented contributing to this effect.

TABLE B-2

RESULTS OF NORTH CAROLINA STATE UNIVERSITY WORKSHOP-SYMPOSIUM

CALIBRATION	AVERAGE GAUGE BIAS [c]	AVERAGE STANDARD ERROR [c]	AVERAGE STANDARD DEVIATION [c]
Backscatter [a]	+1.52	3.81	2.16
Transmission [a]	−0.52	2.60	0.62
Air-gap nomograph [b]	+0.05	0.16	0.57

[a] Results based on manufacturer's calibrations supplied to Symposium; four backscatter gauges were used, while only two transmission gauges were used.
[b] Dual-gauge method outlined herein.
[c] Definitions of these quantities appear in McDougall, et al. (1969).

above a smooth sample. The surface-effect error, E_{se}, in pcf is defined as

$$E_{se} = | \rho - \rho'(h) | \qquad \text{(B-33)}$$

in which ρ is the density of the sample measured with the gauge flush on the sample surface and $\rho'(h)$ is the density measured with the gauge at h air-gap above the surface, where h is arbitrarily taken as 1/16 in. More details concerning the measurement or calculation of this error including the determination of the response at h appear in the section on "Mathematical Modeling of the Surface-Effect Error."

It would appear that if the total path of an average gamma ray through the soil could be made long enough to make the path through the surface heterogeneity negligible by comparison, the surface-effect error would be satisfactorily reduced. This theory may be tested by the use of collimation of source and/or detector. Collimation is used here to mean the elimination of the transmission of gamma rays in all directions by lead shielding save one small opening directed into the soil. Collimation reduces gamma-ray transport near the surface of the sample in an attempt to obtain a response that is more a function of the true density from deeper undisturbed soil. In the prototype gauge shown in Figures B-16 and B-15 the angles of incidence of the source and detector collimators into the soil may be varied in an attempt to obtain a specific average path from source to detector that may be related to variations in surface-effect error. It is recognized, however, that gauge response is not primarily a function of once-scattered gamma rays. The work of Ballard and Gardner (1965) bears this out in more detail.

The possibility of reducing surface-effect error through energy discrimination also exists; unfortunately, this discrimination adversely affects the composition error. Because, on the average, the low-energy gamma rays that are detected have been through more of the sample material, which usually means they have penetrated deeper into the soil, these photons are more representative of the true density. In this case, energy discrimination against the higher energies would emphasize the lower energy response to reduce the surface effect. The use of energy discrimination in improving over-all gauge performance must depend on the extent of the opposing effects on composition and surface-effect errors. Results of the use of energy discrimination to reduce surface-effect error are discussed in "Results and Conclusions."

Quality Factor

The counting-rate measurement error and the composition error as defined previously are normally distributed errors; however, the surface effect error is not normally distributed, and combining these three errors into one representative error to measure over-all gauge performance is difficult. A method has been developed * that uses these three errors and sample volume measured to obtain a quality factor, which is a number whose magnitude describes a gauge's over-all performance. The quality factor appears to be a promising figure of merit for use in the optimization procedure underlying this project.

A combined normal error, $\sigma_n(\rho)$, may be defined as

$$\sigma_n(\rho) \equiv [\sigma_c^2(\rho) + \sigma_s^2(\rho)]^{\frac{1}{2}} \qquad \text{(B-34)}$$

in which the errors, $\sigma_c(\rho)$ and $\sigma_s(\rho)$, are defined by Eqs. B-32 and B-26, respectively. The total error, E_t, is defined as

$$E_t \equiv E_{se} + \sigma_n(\rho) \qquad \text{(B-35)}$$

in which E_{se} is the surface-effect error defined by B-33. If a level, L, is defined as the lowest probable total error and a range, D, as the difference between the lowest and highest probable total errors, then

$$L \equiv E_{se} - \sigma_n(\rho) \qquad \text{(B-36)}$$

$$D \equiv [E_{se} + \sigma_n(\rho)] - [E_{se} - \sigma_n(\rho)] = 2\sigma_n(\rho) \qquad \text{(B-37)}$$

If by some chance two gauges had the same errors or the same level and range, the gauge measuring the greatest sample volume would be the preferred gauge. At any rate some importance should be placed on measurement volume. The relationship of detected response to sample thickness, x, is given by

$$R(x) = R(\infty)(1 - e^{-kx}) \qquad \text{(B-38)}$$

in which $R(x)$, the response on a sample of thickness x, and $R(\infty)$, the response on a sample of effectively infinite thickness, are net responses (Gardner and Roberts, 1967). An effective sample depth, $\bar{x}$, representing the depth to which 68 percent of the gamma rays penetrate and are detected from, is defined by

$$\bar{x} = 1/k \qquad \text{(B-39)}$$

in which k is the constant from Eq. B-38 determined from a least-squares fit for a particular gauge (Gardner and Roberts, 1967, and Harland, 1966a). In a similar manner an effective sample width, $\bar{w}$, may be defined. A volume factor may now be defined by

$$\text{VF} \equiv 0.1\left(\frac{\bar{x}\, w_o\, d}{288}\right) + 0.9 \qquad \text{(B-40)}$$

in which w_o is a sample width taken arbitrarily as 4 in., d is the source-detector separation, and 288 is an arbitrarily chosen maximum sample volume based on an $\bar{x}$ of 6, w_o of 4, and d of 12 in. The factors 0.1 and 0.9 are used to force the volume factor into a small range from 0.9 for zero volume to 1.0 for 288 cu in. The effect of the volume factor will be small due to this range, as shown herein.

The quality factor may now be formulated as

$$\text{QF} = 2\text{VF}\,[D^2 \pm L^2]^{-\frac{1}{2}} \qquad \text{(B-41)}$$

in which VF is the volume factor, D is the range, and L is the level, all defined previously. The positive sign is taken when L is positive; the negative sign, when L is negative. The factor of two is used to normalize the quality factor to 1.0 when VF is 1.0, E_{se} is 1 pcf, and $\sigma_n(\rho)$ is 1 pcf.

* The quality factor was developed in cooperation with W. L. Dunn who had a similar need for measuring gauge performance.

Evaluation of the quality factor defined previously reveals that it is more sensitive to the range than it is to the level. For example, suppose two hypothetical gauges have the following errors: E_{se} of +4 pcf and $\sigma_n(\rho)$ of ±2 pcf for the first, E_{se} of +2 pcf and $\sigma_n(\rho)$ of ±4 pcf for the second. For the second gauge a reading is possible with zero total error; however, because the range is 8 pcf the uncertainty in any measurement is greater than for the first gauge. If both gauges had a volume factor of 0.95 the quality factors would be 0.425 for the first gauge and 0.245 for the second, indicating the range dependence. The range dependence may be justified even more when one considers that greater care of the measurement surface may reduce the surface-effect error, thus lowering the level. The range dependence is shown in Figure B-4.

It should be noted that the quality factor is a figure of merit, not a true combined error, and is used only for rating over-all gauge performance. The definition is somewhat arbitrary and relative and is, therefore, subject to possible refinements.

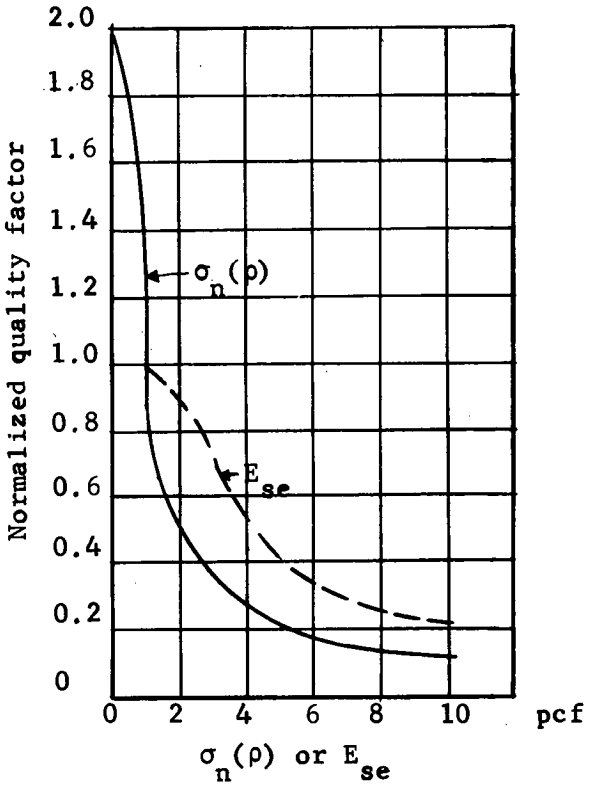

Figure B-4. Quality factor as a function of normal error and surface-effect error.

Gamma-Ray Spectrometry for Energy Discrimination

Calibration Procedure

Due to the use of the sophisticated electronic system shown in Figures B-12 and B-13, including a multichannel analyzer,* stringent calibration procedures were required to obtain accurate responses between energy levels. The emphasis was placed on obtaining reproducible accuracy between spectral calibrations. Several steps were taken to reduce the various electronic instabilities for each set of data taken. The 256-channel pulse-height analyzer was found to drift due to electronic instabilities such as gain shift about one channel every 4 hr; thus, a new calibration spectrum from a ^{137}Cs calibration source was taken at 3- to 4-hr intervals. Each set of data was accompanied by a calibration spectrum, and a computer calibration program was used to determine the calibration and the responses for various energy discrimination levels.

The effects of gain shift and dead-time losses were kept to a minimum. An upper limit of 5 percent dead-time losses was maintained for each measurement. Gain shift was controlled in part by the use of the computer calibration program, limited time of measurement per calibration spectrum, and the use of ratio responses as described previously.** Each calibration was made to provide a 0- to 1-MeV full-scale energy range by setting the 0.662 MeV ^{137}Cs photopeak at channel 170. Carefully controlled and standardized procedures were performed in the taking of all data. Because of its significance, the computer calibration program is described here.

Computer Calibration Program.—For each calibration spectrum a count time of 1,000 sec was deemed sufficient to provide at least 100,000 counts under the 0.662 MeV ^{137}Cs photopeak. This total count was considered adequate to yield an effective Gaussian distribution about the photopeak primary energy. It was then assumed that the 10 channels about the peak channel (11 channels in all) could be represented by a parabola, because the entire photopeak was generally within 36 to 40 channels (the 10 channels about the peak channel were well above the peak's half-maximum). The complete calibration spectrum was read into the computer with paper tape punched by a teletype by signal directly from the multichannel analyzer. The first and last channel numbers of the 10 channels about the peak were also part of the program input. Using each of the 11 channels as the assumed peak channel in turn, a least-squares fit to a parabola was performed using five channels on each side of the assumed peak channel and the sum of the squares of the residuals for each separate fit was determined. A Fibonacci Search Routine (described subsequently) was then used to accurately determine the true peak channel to within at least 1/10 of a channel. This peak channel was considered to be at 0.662 MeV; thus, the calibration in KeV per channel was accomplished. Using the resulting calibration, the pulse-height energies corresponding to the channel numbers to the nearest tenth of a channel were determined for the various energy discrimination levels.

A technique described by Gardner and Whitaker (1967b) was used to determine the counts in a fractional channel. This technique involves linear interpolation of counts in the fractional channel. Suppose one desires the total counts between 50 KeV and the end of the spectrum;

* A description of the multichannel analyzer is available to qualified researchers on request to the Program Director, NCHRP.

** In all cases the responses were normalized to unity for the response on magnesium, since its response was usually the highest.

if channel 12.9 corresponds to 50 KeV, then the total counts obtained from channels 14 to 256 are simply added to nine-tenths of the counts in channel 13. Thus, when fractional channels appear at both ends, the simple formula for obtaining total counts between the limits is

$$(1-f_1)\ C_i + C_{i+1} \ldots + C_{n-1} + f_2\ C_n \quad \text{(B-42)}$$

in which f_1 is the fraction of the total counts in the first channel affected, C_i; C_{i+1} represents the total counts in the second channel of the series; and f_2 is the fraction of the total counts in the last channel affected, C_n. This equation is used to determine each of the energy discrimination responses, which are read out of the program to the nearest count. Because the calibration computer program involves only a simple least-squares fit, use of Eq. B-42, and a Fibonacci search routine, the program is not described further. A FORTRAN IV printout of the program, with an input list and definitions of all input and output symbols is available on request to the Program Director, NCHRP. The Fibonacci search routine, which does not appear to be used commonly, is as follows.

Fibonacci Search Routine.—The Fibonacci routine locates a minimum or maximum value of a function in a given range by successive elimination of subranges where extrema do not exist. The specified range of the search must be chosen so that local minima or maxima do not exist. The function itself must be known explicitly and must be continuous in the specified range. Figure B-5 shows the technique.

For the particular case of the calibration computer program the values of XL and XU are the first and last channels of the 10 channels about the peak channel (channel number is the independent variable) and the function is the sum of the squares of the residuals for the least-squares fits.

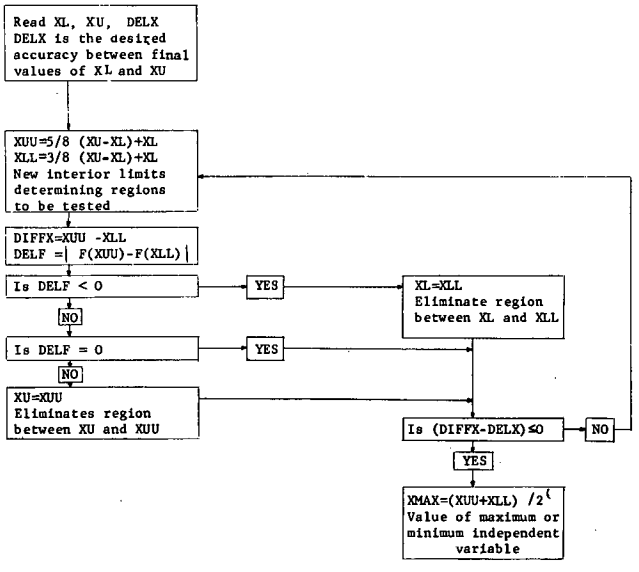

Figure B-5. Fibonacci search routine to find an extreme value of F(X) *between XL and XV, the lower and upper units of the region of interest.*

Energy Discrimination

The energy discrimination regions were selected on the basis of a typical backscattered energy spectrum for a typical gauge configuration using the final prototype gauge design. Some typical backscattered spectra are shown in Figure B-6, where it can be seen that peaks occur near 80 KeV and 200 KeV (background is included for each spectrum). On this basis the following energy regions were selected for initial evaluation: full energy range, 50-1,100, 80-1,100, 90-1,100, 110-1,100, 130-1,100, 150-1,100, 190-1,100, 210-1,100, 230-1,100, 290-1,100, and 350-1,100 KeV. These regions, except for the full energy range, represent the high-energy regions, because in each case low-energy contributions are eliminated. From the responses determined for these regions a new set of responses was obtained which was representative of low-energy regions: 0-50, 0-80, 0-90, 0-110, 0-130, 0-150, 0-190, 0-210, 0-230, 0-290, 0-350 KeV. Finally, two medium-energy regions, 90-290 and 150-290 KeV, were chosen, providing a total of 25 energy regions covering the whole energy spectrum. Owing to the requirement that a minimum of 10,000 net counts be obtained for any gauge response, only those responses meeting this requirement were used for gauge error evaluations.

Figure B-7 shows the background obtained using the stand described in "Experimental Procedure and Results" and the reduced spectrum of Figure B-6d. Some of the background response is attributed to the stand and some is attributed to the gauge housing.

It should be clear that the responses for each energy region were determined by the computer calibration program, thus providing a sound basis for reproducibility. It should be noted, however, that, should there be any error in the computed value of KeV per channel calibration, this error would increase with each channel. This would indicate that the lower values of the variable levels of each energy region would be more accurate. In the case of lower energy discrimination regions this error would be insignificant because as the upper level of the region increases the count totals increase also, thus keeping the error in counts low. However, in the case of high-energy regions the error increases as the lower level increases and the count totals decrease, magnifying the error. This effect is obviated by the fact that no acceptable data were obtained, in general, for regions greater than 210-1,100 KeV for the pilot group results in Tables B-3 through B-7. In general, this "creeping" calibration error does not affect the response determination in the first decimal place of the fractional channels.

Mathematical Modeling of the Surface-Effect Error

The density heterogeneity at the soil surface may be approximated by an effectively equivalent air-gap above a very smooth sample. This air-gap was arbitrarily taken as 1/16 in. in order to compare all gauges on the same basis. Because response as a function of air-gap height may be measured, it is assumed that the surface effect may actually be mathematically modeled. Such a model would eventually lead to a solution for density that would be

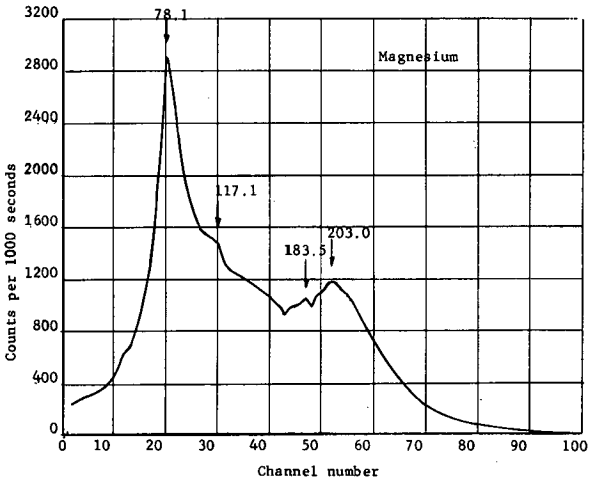

Figure B-6a. Backscattered spectrum from pilot group gauge no. 3 on magnesium.

independent of surface-effect error. The feasibility study that was performed is described as follows.

A gauge configuration including energy region must first be calibrated according to the model of Eq. B-4. Responses at various air-gap heights above each laboratory standard must be taken. A cubic polynomial, determined from a Lagrangian polynomial fit (Ralston, 1965), is calculated for the four air-gap heights of 0, ¼, ½, and 1 in. The model at this point is described by

$$R(C, P, x) = C\ 10^{a+bC+cP}\ (1 + Ax^2 + Bx^2 + Dx^3) \tag{B-43}$$

in which x is the air-gap height in inches; A, B, and D are the constants determined from the Lagrangian polynomial fit; and all other terms are as defined previously.

The constants A, B, and D must necessarily be functions of the variables C and P. A graphical view of these constants as functions of C and P indicated that the following functional relationships should be tested by least-squares analysis:

$$F_1(C, P) = f_{11}\ C + f_{21}\ P + f_{31}\ CP \tag{B-44a}$$

$$F_2(C, P) = f_{12}\ C + f_{22}\ P + f_{32}\ C^2 \tag{B-44b}$$

$$F_3(C, P) = f_{13}\ C + f_{23}\ P + f_{33}\ P^2 \tag{B-44c}$$

in which $F_i(C, P)$ represents any one of the constants A, B, or D as a function of C and P, and the f_{ij} values are least-squares constants. Other functional relationships are possible and should be considered. A regression analysis approach appears to be applicable in this case. Eq. B-43 may be rearranged as follows:

$$x^3 + px^2 + qx + r = 0 \tag{B-45}$$

in which

$$p = B/D;$$
$$q = A/D;$$
$$r = (1 - R')/D; \text{ and}$$
$$R' = R/C\ 10^{a+bC+cP}$$

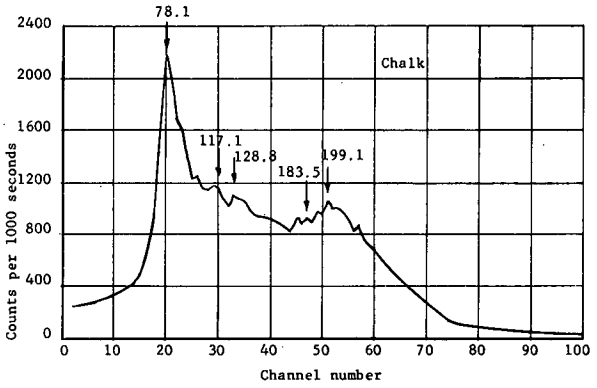

Figure B-6b. Backscattered spectrum from pilot group gauge no. 3 on chalk.

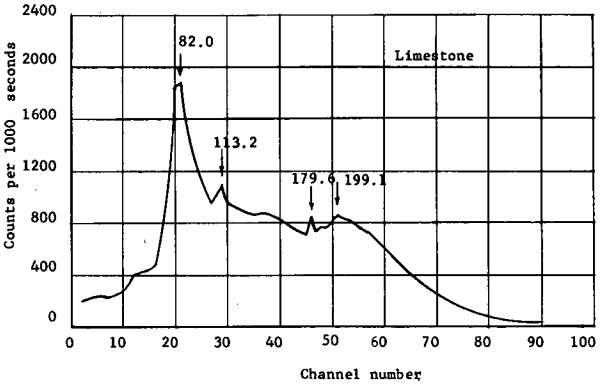

Figure B-6c. Backscattered spectrum from pilot group gauge no. 3 on limestone.

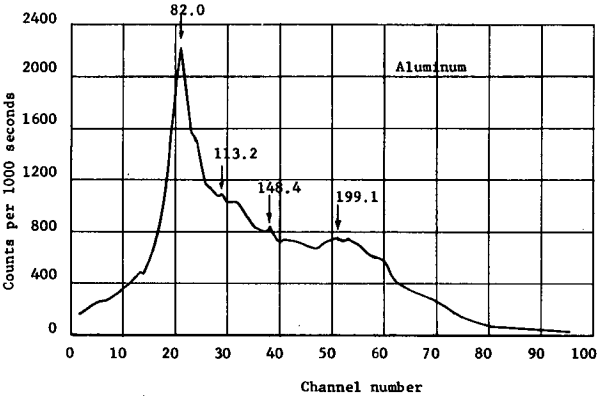

Figure B-6d. Backscattered spectrum from pilot group gauge no. 3 on aluminum.

This equation may be solved according to a technique similar to the quadratic solution outlined in Selby (1965). Three solutions for x are obtained for each gauge model. The procedure from this point has not yet been performed, but the predicted procedure is as follows. Three gauge models are required because three variables exist. The solutions by the cubic method should be compared for

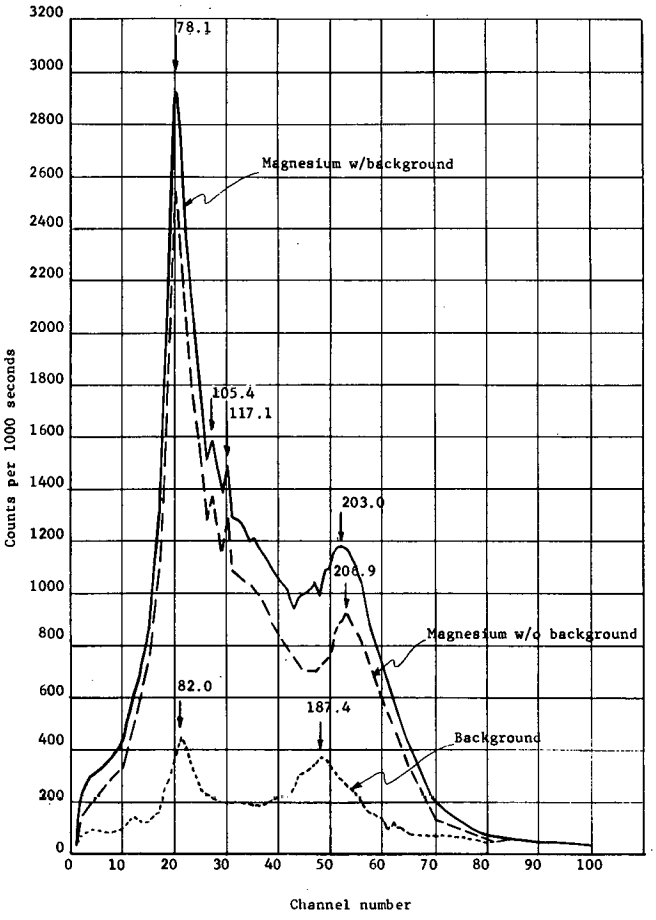

Figure B-7. Backscattered spectra from pilot group gauge no. 3.

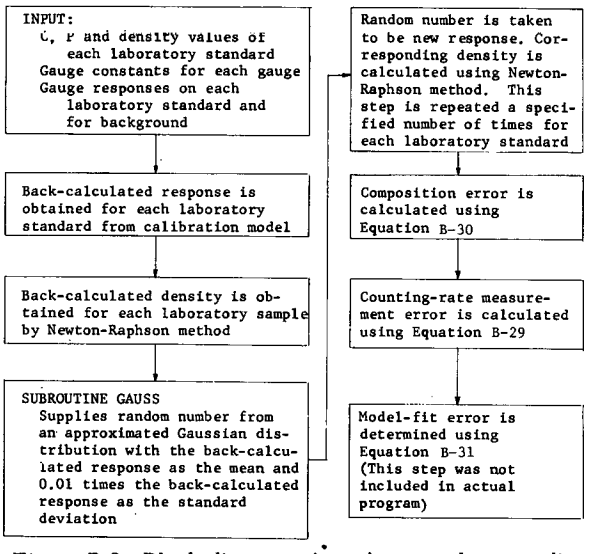

Figure B-8. Block diagram of random number sampling technique for determining composition error complaints for a particular single gauge.

each gauge model. The solutions should match up for each model and those that match from each of the gauges should be equated. Thus, the equations in three unknowns may be used to eliminate x by equating any two equations. A procedure must then be used to solve the two remaining nonlinear equations for C by eliminating P. The resulting solution should be essentially independent of both surface-effect error and composition error, because the variables controlling these errors are mathematically eliminated. This procedure is analagous to the dual-gauge principle discussed previously.

COMPUTER PROGRAMS

Random Number Sampling Technique for Determining Composition Error Components

To reduce the single-gauge composition error into its components, model-fit error, and a variable effect due to counting-rate measurement error, a random number sampling technique was developed. This method is restricted to use with an optimum set of laboratory standards, as discussed previously. With that discussion providing the mathematics and terminology and with a copy of the actual computer program,* with input/output terms defined, it is assumed that the block diagram of the method in Figure B-8 is sufficient to completely describe the technique.

Single-Gauge Calibration and Error Determination

Two computer programs were used to calibrate each single-gauge configuration consisting of the appropriate pilot-group gauge with accompanying energy discrimination region as described in "Experimental Procedure and Results." Two computer programs were necessary because the IBM 1130 computer had limited core storage; this computer was used as a matter of convenience. The first program was used to calibrate each gauge configuration by determining the calibration model constants of Eq. B-4 and to calculate composition error as defined by Eq. B-32 and the counting-rate measurement error ** defined by Eq. B-26. The second program was used to calculate the surface-effect error defined by Eq. B-33, the effective sample depth defined by Eq. B-39, and the quality factor for the single gauge defined by Eq. B-41.

In the second program, the response at 1/16 in. was calculated by interpolation from a Lagrangian polynomial fit to air-gap height data. Some inherent error exists in using a polynomial fit because it is not known how the gauge response varies as a function of air-gap height between 0- and 1/4-in. air gap. It is not reasonable to take data at 1/16-in. air gap because the error in determining this air-gap height is considerable and the gauge bottom may not be even enough to maintain this height over the measurement surface. Thus, the polynomial fit was used over the range from 0 to 3/4 in. in 1/4-in. increments. Another requirement in the evaluation of the surface-effect error is that the calibration model maximum response must be calculated to ensure that a solution for density exists for the response at 1/16 in. In some uses of the

* Available on request to the Program Director, NCHRP.

** This error is referred to in the program as statistical error.

second program the method of bisection was used in place of the Newton-Raphson method for calculating the density for the 1/16-in. response when the latter method exhibited a self-repeating behavior.

Combined use of the theory presented in "Theory of Gauge Quality Analysis" and the previously referenced actual computer programs with the block diagrams shown in Figures B-9 and B-10 should prove sufficient in describing the analytical and numerical methods of analysis as well as the logic.

Optimum Dual-Gauge Program

For the purpose of evaluating quality factors for dual-gauge combinations of the pilot-group single gauges (see "Experimental Procedure and Results") a computer program was written to evaluate dual-gauge errors and effective sample depth. Each error was calculated according to the definitions in "Theory of Gauge Quality Analysis," and both the quadratic solution (Eq. B-13) and the Newton-Raphson method were used to solve for density. The former method was used in calculating the counting-rate measurement error, whereas the latter method was used for calculating composition and surface-effect errors. An alternate method for calculating counting-rate measurement error was provided, mainly for comparison. This method involved differentiating Eq. B-4 with respect to each response separately and calculating the error using Eq. B-26. The volume factor for the dual-gauge is calculated using the average of the individual dimensions for the single gauge. The program is similar in organization to the single-gauge programs discussed previously, thus, the block diagram for this program is not as detailed as the others. The theory presented previously and the referenced actual computer program should complement the block diagram in Figure B-11 to provide an adequate description of the analysis.

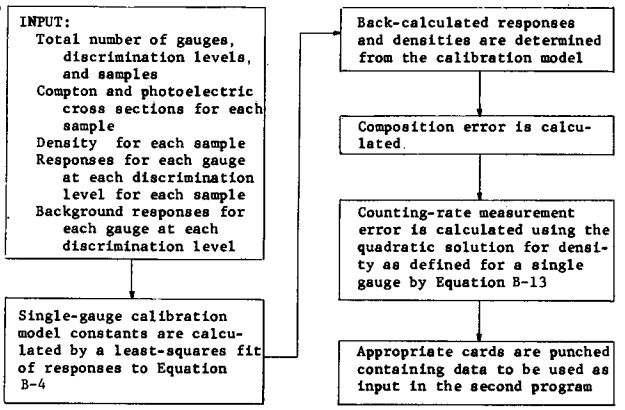

Figure B-9. Block diagram of computer program to calibrate a single gauge and calculate composition and counting-rate measurement errors.

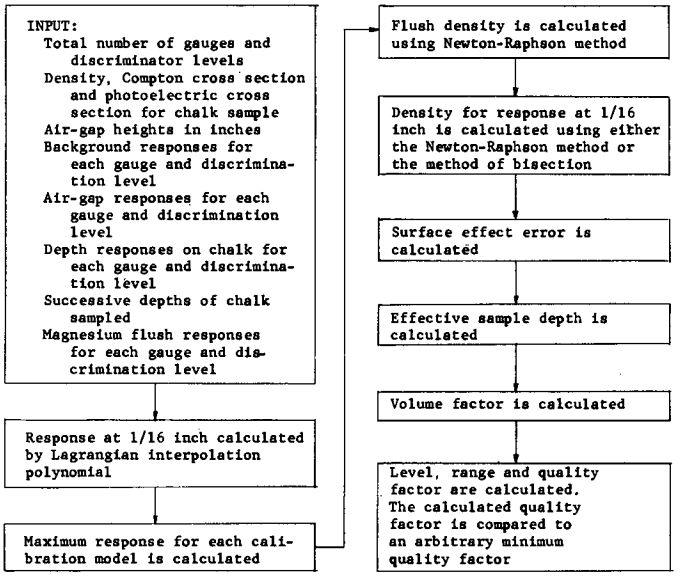

Figure B-10. Block diagram of computer program to calculate surface-effect error, effective sample depth, and quality factor for each single gauge.

EXPERIMENTAL APPARATUS

Electronics

Standard nuclear electronic equipment shown in Figure B-13 was used in the data-taking phases of this project. Several different systems were employed, each depending on the level of sophistication required for the measurements. A complete block diagram of the primary and alternate electronic systems carried from detector to final output is shown in Figure B-12. A third system consisting of detector coupled with photomultiplier, preamplifier, amplifier, and discriminator-scaler was used in preliminary experiments to check out the prototype gauge designs. A complete description of the manufacturer specifications for each item of electronic equipment used is available on request to the Program Director, NCHRP. In this section the performance capabilities and usefulness of each major electronic component are described briefly to demonstrate the versatility of each component.

A 1-in.-diameter by ½-in.-thick NaI (Tl) scintillation detector coupled with a photomultiplier was used in every experimental measurement taken for this project. The scintillation process is described clearly and concisely by Lyon (1964) and in more detail by Price (1964). The description of the scintillation process given here comes mainly from Lyon (1964). When gamma rays coming from the soil sample enter the NaI (Tl) crystal they may produce high-energy electrons from either Compton scattering, photoelectric absorption, or pair production interactions. The electrons resulting from the incoming gamma rays cause luminescence in the crystal which is essentially proportional to the electron energy over a wide energy range. Check-out of the particular detector used in this experiment confirmed linearity over the energy range of primary significance. The photomultiplier essentially converts the light striking a photocathode to a beam of electrons appearing at the anode (collector). A preamplifier is needed to amplify the somewhat "feeble" pulse emanating from the photomultiplier, and should be placed near

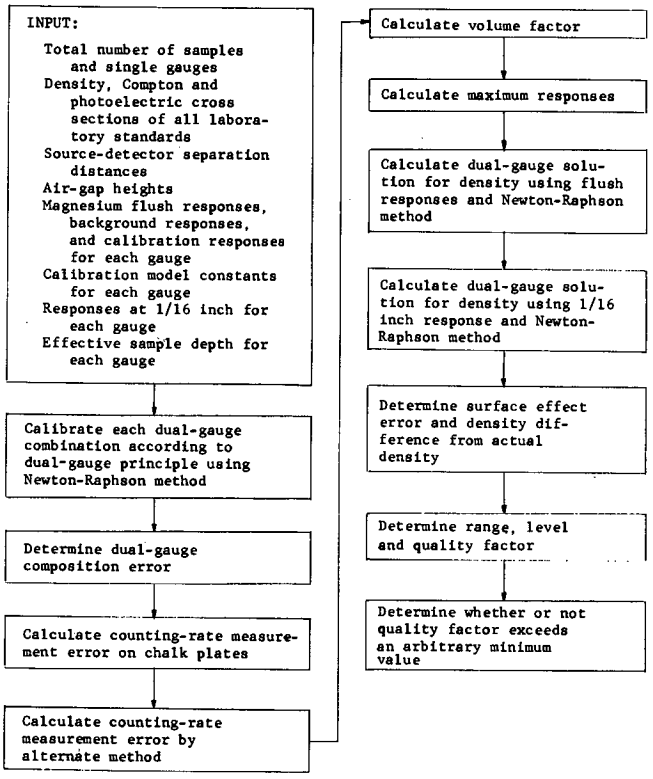

Figure B-11. Block diagram of computer program to analyze dual-gauge combinations for quality factors.

the detector (short cable length) to enable the pulses to pass through the high impedance cable to an amplifier that further amplifies the pulses to make them compatible with the rest of the electronic components. It should be noted that a "bonus" exists over Geiger-Mueller tubes in using scintillation detectors such as NaI (Tl) in radioisotope measurement techniques; they are usually 20 to 40 times as efficient in detecting gamma rays, which means a weaker source may usually be employed in conjunction with scintillation detectors.

The electronic components just described represent the part of the electronic system that is common to each of the three individual systems mentioned previously. It should be emphasized that this integral part of the electronic system is essentially linear with incident gamma-ray energy which was confirmed for the particular components used in this project.

The discriminator-scaler used in the preliminary experiments described in "Experimental Procedure and Results" is a common electronic component in nuclear measurements. It registers all pulses that exceed the voltage setting of the discriminator. If the discriminator is used merely to eliminate electronic noise pulses, then the scaler is essentially measuring the total number of gamma rays that are detected. Similar scaler devices are presently employed in existing commercial nuclear density gauges.

A single-channel analyzer is shown as the main component of the alternate system shown in Figure B-12. As it turned out this device was not employed as often as had been planned; however, it was used in conjunction with the scaler system used for preliminary experiments to analyze the first pilot group of single gauges mentioned in "Experimental Procedure and Results." This device has a "window" and a lower level setting similar to a discriminator. The window width in terms of voltage may be adjusted and the lower level may be set so that any energy region, as narrow or as wide as desired, may be evaluated for total counts. As is the case with any discriminator in general, electronic gain shifts are encountered with the settings of the single-channel analyzer.

The multichannel analyzer is the principal component in the spectrometry system used as the measurement device of this project. It has the capability of taking incoming pulses and sorting them into specified energy ranges. Thus, when 256 channels are used they represent 256 divisions of the full energy range, and the resulting spectrum is a histogram of counts per channel. This device provides rapid and sophisticated data storage that makes energy discrimination and energy spectrum studies practical for the purpose of this project. Although they are

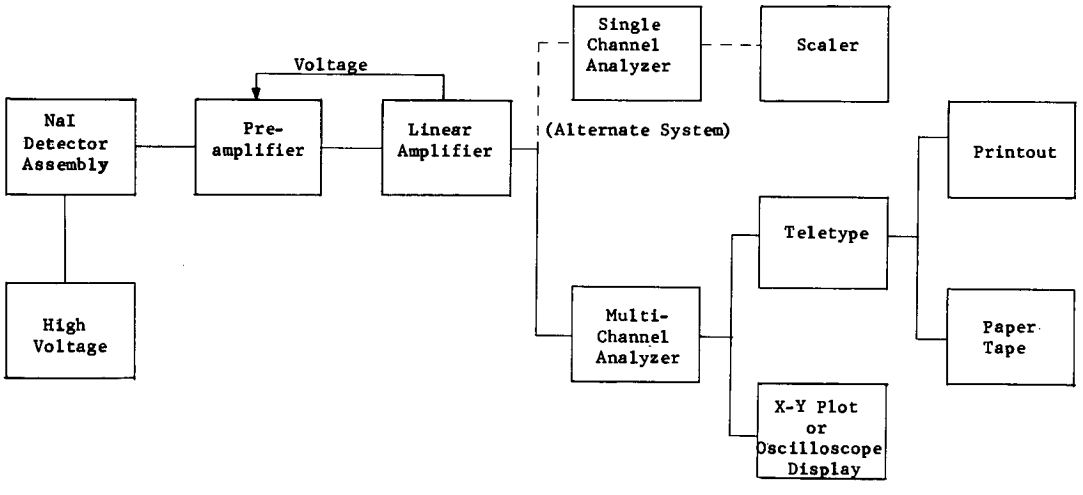

Figure B-12. Electronic block diagram for gamma-ray spectrometry system.

versatile and convenient, some minor problems exist in using multichannel analyzers that may affect results of gauge evaluations. These problems include dead time losses and electronic gain shift. A meter was provided to measure dead time losses. Thus, these losses in effective counts were always kept to less than 10 percent, and usually less than 5 percent; however, permissible counting rates were somewhat controlled by these losses.

A multichannel analyzer is unique in dead time problems due to the use of an analog-to-digital converter which essentially takes pulse heights and converts them to a train of pulses (Lyon, 1964). There is an initial dead time, as in all systems, up to the analyzer, then an additional dead time is attached to each channel in sequence; thus, losses at higher energies generally are greater than those at lower energies. This is not the case with backscattered spectra, as shown in Figure B-5, which indicates that backscattered radiation is concentrated at low energies.

Electronic gain shift, which at worst may result in a loss of part of the spectrum, was kept to a minimum and accounted for by use of a calibration procedure described previously.

Several instruments were employed to obtain the data in output form. An oscilloscope was used in all phases to display the results of the multichannel analyzer. Some spectra were then plotted by an X-Y recorder. A teletype using a paper tape punch was employed to yield a type-out of each spectrum and a paper tape of each spectrum that was eventually read into a computer (IBM 1130) and converted to computer cards for more reliable storage. Thus, all data were easily stored for continued use so that all meaningful information can be eventually extracted from it.

The primary system shown in Figure B-12 was also used in the mathematical modeling experiments described in "Experimental Procedure and Results."

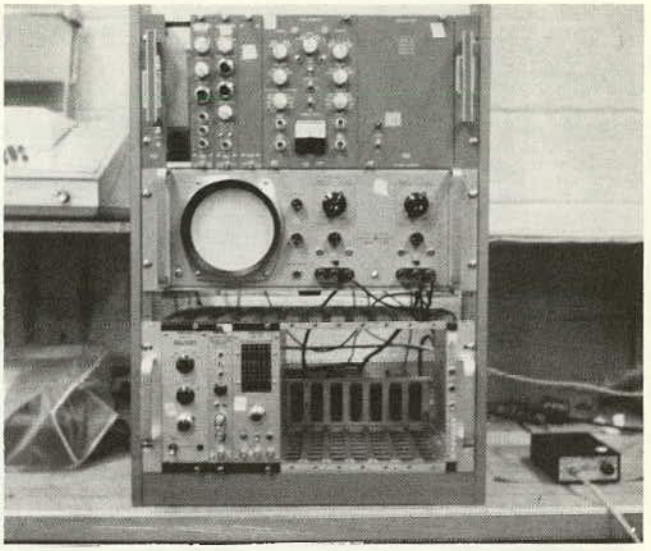

Figure B-13. Panel of electronics used for obtaining data.

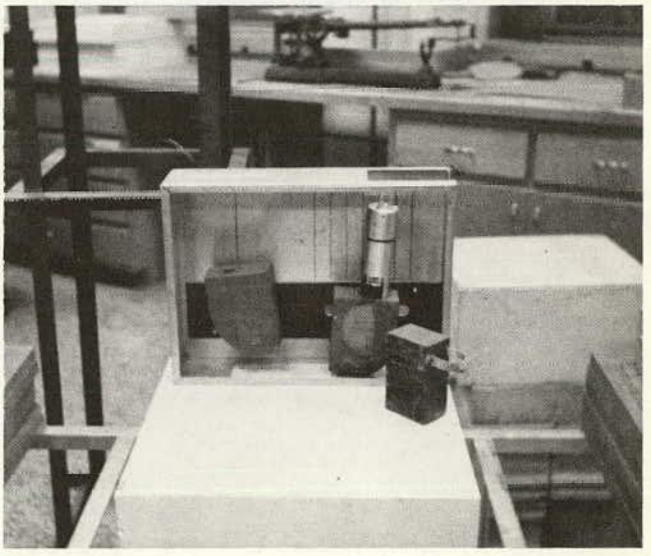

Figure B-14. Original prototype gauge design showing modified detector holder used in modified version.

Design of Prototype Gauges

An initial prototype gauge (Fig. B-14) was designed to allow variable source and detector collimator angles into the soil. One purpose of this design was to attain variable penetration depths of the gamma rays into the soil. Exhaustive testing of this prototype, described in more detail in "Experimental Procedure and Results," indicated that the response versus density relationship was not compatible with the calibration model given by Eq. B-4. It was decided that this problem was due to the stringent collimation which apparently did not allow for detection of a response that was representative of the total gamma-ray transport in the sample. A modification of the initial prototype (Fig. B-13) included a noncollimated detector holder that held the detector flush to the sample surface. Testing of the modified prototype resulted in a response described by the calibration model of Eq. B-4. On the basis of these latter tests, it was decided that the collimators in the initial design were too long, with diameters that were too small. The openings of the collimators were also too far from the sample surface, which led to unacceptable contributions from surface scattering and scattering from the gauge housing. The modified version of the initial prototype was not intended as a separate prototype to be used for subsequent testing; it merely served the purpose of pointing out the faults in the initial design.

On the basis of tests performed by the initial prototype and its modified version, a new prototype gauge was designed. This new prototype is shown in Figures B-15 and B-16. In the new design the detector collimator diameter was increased over the initial design and both source and detector holders were lowered to within less than ½ in. from the sample surface. More lead shielding was added to the sides of both collimators to reduce the background, which was a substantial contribution to the response of the initial prototype design. With the initial

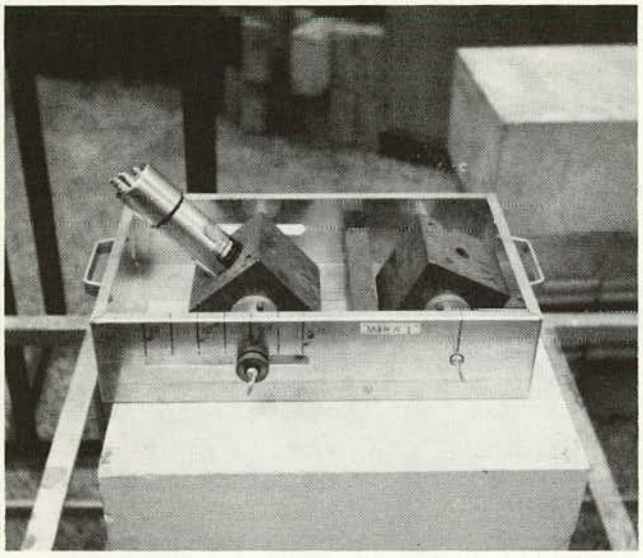

Figure B-15. Final prototype gauge design.

prototype it was found that the response varied strongly with the proximity of the gauge to laboratory items such as concrete walls, and desks; with the new prototype this was not a problem as a result of the added shielding and the addition of a smaller horizontal aluminum chassis as the gauge housing.

It is believed that the dimensions of the initial prototype design are irrelevant; however, the dimensions of the new prototype are available on request to the Program Director, NCHRP. Some relevant features of the new design include the fact that both source and detector collimators pivot about the source point and the detector face, respectively. These two points are on a line parallel to the bottom of the gauge and the sample surface. Another relevant feature of the new protoype is that it has a low center of gravity for better handling and stability.

Preliminary tests of the new prototype confirmed the fact that it was satisfactory as a test gauge to accomplish the project objectives. One major fault with this prototype was revealed: the two collimators could not both be perpendicular to the sample surface (0° angles) at the same time since the response is not described by Eq. B-4. This was not a major problem, because all other combinations of angles proved to yield acceptable results.

The final prototype design has the capability of varying the source-detector separation distance by sliding the detector holder along a slide rail. Sources may also be interchanged in the source holder; ^{133}Ba, ^{60}Co, and ^{137}Cs sources were available for use. The detector holder was designed to hold the particular NaI (Tl) scintillation detector described previously. Further discussion of the final gauge design and its preliminary testing appears in "Experimental Procedures and Results."

Laboratory Calibration Standards

As was first confirmed by Gardner and Roberts (1967) and later by the North Carolina State University Workshop-Symposium (McDougall, 1969), the significance of a proper set of laboratory calibration standards cannot be overemphasized. Some of the properties of optimum laboratory standards are well known (Gardner and Roberts, 1967) but are included here for completeness. An optimum set of laboratory density standards should be:

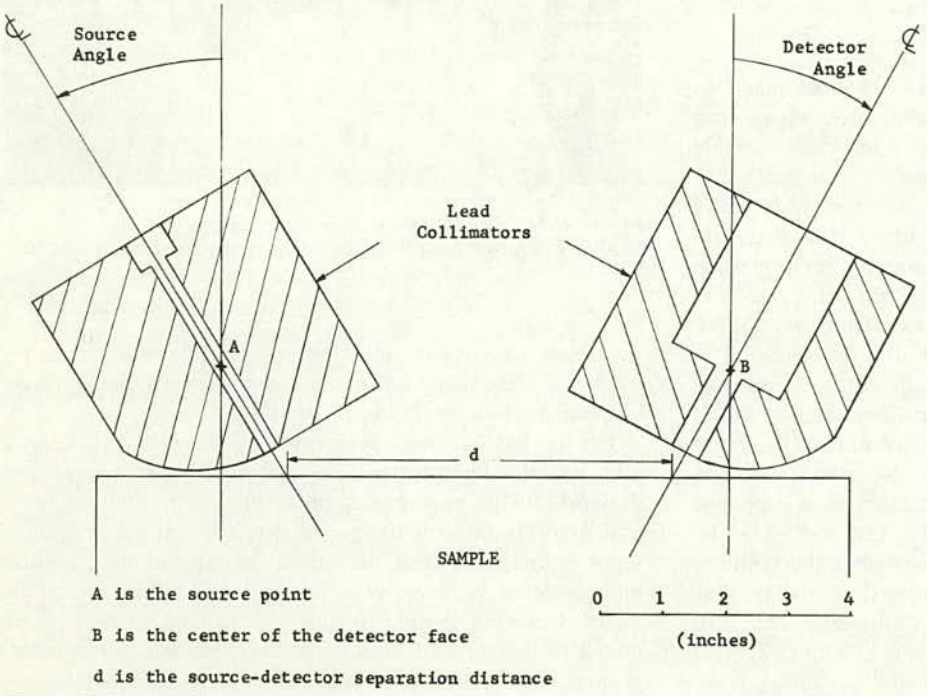

Figure B-16. Final prototype gauge design.

1. Homogeneous.
2. Stable to ambient conditions such as temperature and humidity.
3. Statistically representative of the full range of densities and compositions found in soils.
4. Large enough to provide adequate measurement volume and smooth enough on the surface to minimize the surface roughness effect.
5. Inexpensive, easily obtainable, and/or easy to prepare, and suited to the type of gauge used.

Because density and composition are the soil variables to be considered, two parameters that provide a quantitative indication of the relative amounts of Compton scattering and photoelectric absorption for a given sample are defined as the composition parameter, $P' = P/\rho$ and the scattering parameter, $C' = C/\rho$, where P and C are given by Eqs. B-3 and B-2, respectively. The box concept, described as the minimum number of standards that cover the full range of density and composition parameters encountered, is presented in detail by Gardner and Roberts (1967). Because the scattering parameter is essentially a constant, only the density and composition parameters need to be considered in the choice of optimum standards. Aluminum and magnesium represent extreme high and low density but low P' standards, and limestone and chalk represent high and low density but high P' standards. These standards approximate a "box" when the variables are plotted against each other. These four standards cover a density range from 110 to 168 pcf and a P' range from 1.6×10^4 to 3.3×10^4, or a factor of 2 in absorption capacity. These are all 18 in. $\times$ 18 in. in 1-in.-thick blocks, except for chalk which is a 6-in.-thick block and limestone which is a $17 \times 14 \times 9$-in. block. In general, the dimensions of these standards represent an effective infinite volume; however, in some cases the depth was not quite great enough.

The laboratory in which these standards were used presented some problems to the measurements taken with the gauges. Proximity of the gauges and standards to items such as concrete walls or desks created background problems that adversely affected proper gauge evaluation. The terrazzo floor presented a major problem also. For a gauge 6 ft above the terrazzo floor with nothing between the gauge and the floor the background was a factor of 10 less than that of a similar geometry 2 ft off the floor. Thus, it was necessary to build a 6-ft stand on which depth measurements and background counts would be taken. A similarly structured stand only 2 ft off the floor was constructed as a sample holder because tables and wooden benches proved inadequate as sample holders. The stands used are shown in Figure B-17.*

Six months expired before the extraneous laboratory problems were solved, so the necessity of preliminary measurements and proper location of laboratory standards is apparent.

* Figures B-13, B-14, B-15, and B-17 do not show each apparatus as it was actually used in the project; i.e., the arrangement shown was designated only for photographic purposes.

Figure B-17. Laboratory standards and background stand.

EXPERIMENTAL PROCEDURE AND RESULTS

Preliminary Experiments

Preliminary experiments include measurements taken to check out prototype gauge designs and laboratory equipment for acceptability prior to using them in the primary experiments. These measurements consumed a considerable amount of time due to laboratory changes that were necessitated by background problems. These preliminary experiments included those mentioned in the previous section to check the capabilities of the electronics and prototypes and a preliminary graphical look at energy discrimination using only data accumulated with a variable lower discriminator and scaler.

Check-out of the initial prototype gauge described previously eliminated most design and laboratory problems. Background problems plagued the experiments from the onset, as the initial prototype was not adequately shielded. This discovery led indirectly to some laboratory innovations, which included:

1. Construction of an iron rack (Fig. B-17) to hold the laboratory standards. This rack was designed with as little structural material as possible, to reduce background.
2. Placement of the thicker limestone standard off the rack so that the surface of all standards would be the same distance off the floor, thus minimizing contributions to background from adjacent samples.
3. Construction of a tall iron rack (Fig. B-17) to enable background and less than saturation thickness measurements to be taken. Ideally, a background count should be taken far from any material; however, in the laboratory it was found that taking the background counts 6 ft off the terrazzo floor reduced most background responses to less than 10 percent of the backscattered response, including a small contribution from the iron stand.

These three innovations, in addition to situating the sample

holder away from any walls or other objects, virtually eliminated all background problems.

Response versus density measurements were taken with the initial prototype design with the results discussed previously. On the basis of these tests a new prototype gauge was designed, as described previously. Response versus density measurements were then taken with this new design and a graphical view of energy discrimination effects was accomplished. At the full-energy range, the response versus density plot showed two parallel straight lines of the low-atomic-number and high-atomic-number standards. As the discriminator setting was incrementally varied on the scaler and new responses were obtained, the two individual lines approached each other until, at about 190 KeV, they became one straight line. This trend was noticed in conjunction with a corresponding flattening of the slope of these lines (increasing counting-rate measurement error). Thus, at first glance, energy discrimination appeared to reduce the composition effect, but the counting-rate measurement error was increased. Nothing could be said at this stage about the effect of the energy discrimination on the surface-effect error. This glimpse at the use of energy discrimination as a gauge parameter was sufficient to confirm earlier beliefs that a more detailed investigation was required.

Some additional measurements with the new prototype design were taken, such as air-gap and thickness measurements, background to response ratio, and backscattered spectra. These measurements checked out according to theory. On the basis of these preliminary experiments, the new prototype gauge design and its associated electronics as well as the laboratory environment were considered totally acceptable for use in accomplishing the objectives of the project.

Pilot-Group Experiments for Single Gauges

Because of the unlimited number of gauge parameter settings that is possible with the new prototype gauge design described previously, the pilot-group concept was used to effectively sample the whole range of single gauges exclusive of energy discrimination levels. Two pilot groups were chosen; however, the second pilot group is the only one to be discussed due to equipment incompatibilities encountered with the initial pilot group. The single-gauge parameters chosen are given in Table B-8 for the second pilot group. These particular parameters were chosen on the basis of covering the full range of source-detector separation distances, source and detector angles, counting rates, and slopes of individual calibration curves based on the calibration model given by Eq. B-4.

Each single-gauge combination of parameters was evaluated for each of the major errors described in "Theory of Gauge Quality Analysis," the effective sample depth, the quality factor and for each of 25 separate energy discrimination regions, classified as being either low-, medium-, high-, or full-energy ranges. The methods employed to evaluate these quantities are described in previous sections; the computer programs are available on request to the Program Director, NCHRP. The complete results of the second pilot group evaluation are given in Tables B-3 through B-9.

Only one source, ^{137}Cs, was chosen for the pilot group analysis; this was because maximum calibration possible with the ND-512 multichannel analyzer was only 1.10 MeV full scale without lowering the detector voltage to an unacceptable level, which excluded the use of ^{60}Co (average energy 1.25 MeV). The only other source available was a low-energy ^{133}Ba, which yielded insufficient counting rates. Examination of the backscattered spectra in Figure B-6, made using the new prototype gauge design, shows that all significant data fall well below 1.0 MeV; however, the experiments were run on the basis of having the calibration high enough to contain the primary photopeak of the source to check direct transmission responses through the shielding.

It should be noted that the definitions of the parameter values on the gauge were not precise, but were reproducible because the gauge settings were not changed or moved during testing. Thus, a 45° source angle is not to be construed as being exact, but, instead, as being an approximate angle significantly different from one of 15° or 30°. These criteria apply to all variable parameters, although care was taken to be as precise as possible.

Close examination of the results of the second pilot group indicate large variations with gauge parameter settings, thus verifying the validity of the pilot group sampling technique. It is recognized that a larger number of pilot groups would have been even more representative of true gauge performance; however, sufficient information was obtained to provide conclusive results of variation of errors with gauge parameters.

The data taken for analysis of the second pilot group included normal flush responses of the gauge on each of the four laboratory standards described previously. The counting-rate measurement error for the second pilot-group analysis was determined by Eq. B-26 on the basis of the flush counts on the four laboratory standards. The surface-effect-error evaluation was based on air-gap data taken at ¼, ½, and ¾ in. on chalk plates using a polynomial fit to interpolate for the 1/16-in. response. Chalk was chosen over the other samples on the basis of its composition dependence and rough surface. The surface-effect error was not averaged over all four laboratory standards because of the amount of data necessary to do so. Background and calibration responses accompanied each data set that encompassed 3 to 4 hr of counting time. The counting time of 1,000 sec, live time, for each response of the second pilot group, was chosen on the basis of preliminary experiments that indicated this counting time would yield 10,000 counts for most of the energy discrimination regions. Because of the gain shift problem described previously, this counting time appeared to be the optimum.

Results of the first pilot-group analysis are not reported even though they indicated improvements over existing gauges. These results were obtained under less dependable conditions than those for the second pilot group. Furthermore, the results of the second pilot group provided enough information to establish trends for gauge responses taken under various conditions.

Results for the second pilot group are given in Tables B-1 through B-9. Tables B-1 through B-7 give individual single-gauge results for each configuration of the pilot group. Table B-8 is a summary of the best values obtained for each single gauge under each of the three errors, effective sample depth, quality factor, and energy region for each result. Table B-9 is a summary of results for the random number sampling technique (described previously) to determine the counting rate and model fit components of the composition error.

Dual-Gauge Experiments

The dual-gauge principle was applied to the second pilot group, just described. A sampling process was necessary to reduce the number of dual-gauge combinations to a reasonable number. Each single gauge described by Table B-8 for the second pilot group was used in four energy regions: 0-1,000 KeV or full-energy range, 0-210 KeV or low-energy region, 150-290 KeV or medium-energy region, and 150-1,000 KeV or high-energy region. No particular criterion was used to select the energy region; however, the regions chosen appeared to best represent the gauges in the general regions of low, medium, and high energies. This sampling process yielded 20 single gauges to be combined with each other to yield a total of 190 dual-gauge combinations. For example, the first single gauge of 45° source angle, 45° detector angle, 4-in. separation, and energy region 0-1,000 KeV would be combined with the second single gauge of 30° source angle, 45° detector angle, 4.5-in. separation, and 150-290 KeV energy region and each of the remaining 18 similarly defined single gauges to yield dual-gauge combinations.

The dual-gauge combinations were evaluated using the previously referenced appropriate computer programs and by the theory presented previously in "Dual-Gauge Principle." The purposes of these evaluations were to determine the optimum dual-gauge design of the new prototype gauge design described previously and to determine whether the dual-gauge principle was effective in reducing the surface effect error to acceptable levels.*

The data taken for these dual-gauge experiments were the same as the data taken for the second pilot group described previously. Other than the application of the dual-gauge principle to the calculation of the composition and surface-effect errors, the main difference between the dual-gauge analysis and the single-gauge analysis was in the determination of the counting-rate measurement error, which was calculated only for chalk response in the dual-gauge analysis. The choice of chalk as the only standard was based on conserving computer time and experiment time, which was accomplished because chalk was already being used for surface-effect-error determination. The volume factor for each dual-gauge combination was calculated on the basis of averaging each dimension of the two single gauges and obtaining an average volume factor.

Dual-gauge results are given for the second pilot group, in Tables B-10 through B-13. Table B-10 gives the results of the ten best dual-gauge combinations, based on quality factors; each of the other tables gives the ten best dual gauges under each error; the purpose of this tabulation is to search for trends.

Mathematical Modeling of the Surface-Effect Error

Using the final prototype gauge design and the primary electronic system discussed previously, a full set of data was taken for the purpose of mathematically modeling the surface-effect error. Data included normal flush responses and air-gap responses at 0, ¼, ½, and 1 in. on each laboratory standard. The same calibration procedure and method for obtaining energy discrimination region responses were used as described for the other experiments. Only one gauge configuration was used: 30° source angle, 45° detector angle, 4.5-in. source-detector separation, and a ^{137}Cs source. More gauge configurations should be used to refine the techniques and provide an indication of the sensitivity. Each energy discrimination region response was calibrated for the model constants and for the polynomial fit constants. These latter constants were then fit, in turn, to all of the functions given by Eq. B-44 by least-squares techniques. Unfortunately, this was as far as the project had progressed; the results of the project to this point are discussed in "Results and Conclusions."

RESULTS AND CONCLUSIONS

Pilot Group Experiments for Single Gauges

Results of the second pilot group indicate some significant trends that verify theoretical suppositions. Some unexpected results also appeared but can be explained on the basis of the optimization procedure. Tables B-3 through B-8 give the acceptable results for the five single gauges in the pilot group. Results for energy discrimination levels at the extreme low and high ends are not acceptable. At the low end, such as 0-50 or 0-80 KeV, the X-rays resulting from the lead shielding comprise a significant part of the response; thus, relatively small counting rates due to backscattered gamma rays are detected yielding unreliable results. At the high end, such as 290-1,000 or 350-1,000 KeV, the counting rates are too small and contain large direct transmission contributions. At these extreme discrimination levels the slope of the calibration curve is poorly defined and, in particular, at the high levels, the surface-effect error is too large to be calculated. In general, each gauge has at least 20 discrimination levels with acceptable results, except for the first gauge, Table B-3, which exhibited difficulties for all high-energy discrimination levels.

Examination of the backscattered spectrum and background spectrum in Figure B-7 shows that background is a higher percentage of total response in certain regions (low and high). This fact may have influenced the poor results obtained for very low- and very high-energy discrimination regions. (All gauge responses used to evaluate the errors are net responses, except in the case of evaluating counting-rate measurement error where the gross count ratio is required.)

* W. L. Dunn, one of the researcher's co-workers on the project, has completed his research, which was concerned primarily with gauge optimization using the dual-gauge principle. The objective of the researcher in using the dual-gauge principle was aimed primarily at reducing the surface-effect error.

TABLE B-3

RESULTS FOR PILOT GROUP NO. 2, SINGLE GAUGE NO. 1 (45° SOURCE ANGLE, 45° DETECTOR ANGLE, 4-IN. SOURCE-DETECTOR SEPARATION, ^{137}CS SOURCE)

ENERGY RANGE	COMPOSITION ERROR (PCF)	COUNTING RATE MEASUREMENT ERROR (PCF)	EFFECTIVE SAMPLE DEPTH (IN.)	SURFACE-EFFECT ERROR (PCF)	QUALITY FACTOR
0–80	2.81	3.69	3.37	11.5	0.193
0–90	3.86	6.37	3.38	12.4	0.174
0–100	5.07	—[a]	3.28	14.7	0.143
0–110	6.18	10.13	3.13	15.8	0.128
0–150	4.26	7.78	3.02	16.9	0.131
0–190	3.58	6.92	2.84	19.6	0.114
0–210	3.23	6.30	2.77	20.4	0.109
0–230	2.55	4.86	2.70	19.2	0.115
0–290	1.66	3.36	2.52	17.4	0.124
0–350	2.43	4.09	2.47	25.3	0.086
90–290	1.26	3.02	2.14	22.9	0.092
150–290	0.73	2.30	1.71	17.3	0.120
0–1000	2.87	4.74	2.46	—[b]	—[c]
50–1000	2.90	4.96	2.44	—	—
80–1000	2.79	5.11	2.20	—	—
90–1000	2.64	4.48	2.10	—	—
110–1000	2.30	3.91	1.94	—	—
130–1000	2.51	3.78	1.83	—	—
150–1000	2.39	3.73	1.73	—	—
190–1000	2.59	3.39	1.67	—	—
210–1000	2.80	3.34	1.67	—	—

[a] No value calculated because response at 1σ above response was higher than maximum response on calibration curve.
[b] Errors too high to be calculated using definition in "Gauge Errors."
[c] Quality factors not calculated due to no surface-effect errors available.

TABLE B-4

RESULTS FOR PILOT GROUP NO. 2, SINGLE GAUGE NO. 2 (30° SOURCE ANGLE, 45° DETECTOR ANGLE, 4½-IN. SOURCE-DETECTOR SEPARATION, ^{137}CS SOURCE) [a]

ΔE (KeV)	$\sigma_c(\rho)$ (PCF)	$\sigma_s(\rho)$ (PCF)	$\bar{x}$ (IN.)	E_{se} (PCF)	QF
0–80	2.45	1.61	3.54	6.80	0.306
0–90	2.94	1.85	3.68	7.93	0.260
0–110	2.63	2.10	3.59	8.19	0.262
0–130	2.21	2.11	3.39	8.56	0.258
0–150	2.25	2.12	3.26	9.17	0.242
0–190	2.03	2.08	3.08	9.48	0.236
0–210	1.79	2.01	2.99	9.26	0.241
0–230	1.75	1.90	2.91	9.00	0.248
0–290	1.63	1.75	2.73	9.04	0.247
0–350	1.73	1.90	2.69	9.72	0.230
90–290	1.15	1.74	2.34	9.77	0.224
150–290	1.18	1.46	1.93	8.67	0.255
0–1000	1.80	1.98	2.69	10.70	0.208
50–1000	1.67	1.99	2.68	10.80	0.206
80–1000	1.53	2.10	2.47	13.13	0.167
90–1000	1.32	2.04	2.32	13.02	0.167
110–1000	1.35	1.95	2.14	13.32	0.163
130–1000	1.49	1.92	2.07	13.78	0.158
150–1000	1.35	1.88	1.97	13.67	0.158
190–1000	1.44	1.84	1.86	14.55	0.149
210–1000	1.82	1.92	1.87	18.24	0.119

[a] Symbols used to denote column headings are equivalent to headings in Table B-3.

TABLE B-5

RESULTS FOR PILOT GROUP NO. 2, SINGLE GAUGE NO. 3 (15° SOURCE ANGLE, 15° DETECTOR ANGLE, 4¾-IN. SOURCE-DETECTOR SEPARATION, ^{137}CS SOURCE) [a]

ΔE (KeV)	$\sigma_c(\rho)$ (PCF)	$\sigma_s(\rho)$ (PCF)	$\bar{x}$ (IN.)	E_{se} (PCF)	QF
0–90	1.89	1.45	5.94[b]	2.72	0.516
0–110	1.39	1.53	5.64	2.53	0.664
0–130	1.37	1.58	5.30	2.70	0.655
0–150	1.20	1.56	5.08	3.70	0.577
0–190	1.00	1.45	4.82	3.85	0.574
0–210	0.83	1.37	4.71	3.80	0.588
0–230	1.03	1.36	4.52	4.01	0.552
0–290	1.35	1.47	4.25	4.29	0.501
0–350	1.39	1.50	4.22	4.43	0.485
90–290	1.04	1.50	3.53	5.29	0.423
150–290	1.63	1.35	2.92	5.30	0.408
0–1000	1.45	1.52	4.20	4.41	0.482
50–1000	1.49	1.53	4.14	4.29	0.489
80–1000	1.24	1.60	3.63	5.42	0.412
90–1000	1.16	1.56	3.46	5.56	0.402
110–1000	1.44	1.51	3.17	6.24	0.357
130–1000	1.54	1.45	2.98	6.61	0.337
150–1000	1.85	1.45	2.79	5.82	0.369
190–1000	2.83	1.75	2.34	7.90	0.263

[a] Symbols used to denote column headings are equivalent to headings in Table B-3.
[b] Effective sample depths approaching 6.0 in. are doubtful because the samples are only 6.0 in. deep.

TABLE B-6

RESULTS FOR PILOT GROUP NO. 2, SINGLE GAUGE NO. 4 (30° SOURCE ANGLE, 15° DETECTOR ANGLE, 5½-IN. SOURCE-DETECTOR SEPARATION, ^{137}CS SOURCE) [a]

ΔE (KeV)	$\sigma_c(\rho)$ (PCF)	$\sigma_s(\rho)$ (PCF)	$\bar{x}$ (IN.)	E_{se} (PCF)	QF
0–80	3.18	2.01	5.93	3.69	0.313
0–90	3.39	2.38	5.45	3.93	0.294
0–110	3.61	2.67	5.07	3.31	0.277
0–130	3.54	2.72	4.77	3.70	0.282
0–150	3.29	2.59	4.54	3.98	0.302
0–190	2.15	2.02	4.37	4.17	0.421
0–210	1.89	1.81	4.24	4.02	0.461
0–230	1.93	1.80	4.01	4.13	0.450
0–290	2.13	1.98	3.68	4.44	0.412
0–350	2.15	2.01	3.65	4.52	0.407
90–290	1.66	1.88	2.87	4.84	0.435
150–290	1.16	1.51	2.28	4.79	0.464
0–1000	2.12	2.01	3.64	4.56	0.409
50–1000	1.98	2.04	3.54	4.55	0.423
80–1000	1.71	2.04	2.94	5.20	0.409
90–1000	1.63	1.92	2.82	5.06	0.422
110–1000	1.42	1.77	2.58	5.53	0.401
130–1000	1.24	1.63	2.37	5.25	0.424
150–1000	1.10	1.55	2.18	5.09	0.439
190–1000	1.98	2.01	1.34	6.35	0.339

[a] Symbols used to denote column headings are equivalent to headings in Table B-3.

TABLE B-7

RESULTS FOR PILOT GROUP NO. 2, SINGLE GAUGE NO. 5 (45° SOURCE ANGLE, 45° DETECTOR ANGLE, 6-IN. SOURCE-DETECTOR SEPARATION, ^{137}CS SOURCE) [a]

ΔE (KeV)	$\sigma_c(\rho)$ (PCF)	$\sigma_s(\rho)$ (PCF)	$\bar{x}$ (IN.)	E_{se} (PCF)	QF
0–80	1.39	0.99	4.73	6.14	0.364
0–90	1.61	1.05	4.56	6.30	0.352
0–110	1.37	1.09	4.33	6.57	0.340
0–130	1.50	1.10	4.08	6.80	0.329
0–150	1.32	1.10	3.87	6.84	0.327
0–190	1.11	1.12	3.59	6.88	0.324
0–210	1.05	1.11	3.52	6.85	0.324
0–230	0.99	1.08	3.49	6.73	0.329
0–290	0.83	1.04	3.24	6.60	0.333
0–350	0.88	1.09	2.96	7.09	0.310
90–290	0.47	1.04	2.62	6.85	0.310
150–290	0.22	0.96	2.20	6.21	0.333
0–1000	0.92	1.11	2.87	7.38	0.298
50–1000	1.00	1.13	2.82	7.44	0.297
80–1000	0.71	1.16	2.29	8.21	0.262
90–1000	0.57	1.15	2.13	8.30	0.256
110–1000	0.58	1.14	1.79	8.37	0.254
130–1000	0.33	1.14	1.38	8.50	0.244
150–1000	0.35	1.14	1.51	8.74	0.237
190–1000	0.48	1.11	1.34	8.94	0.235
210–1000	0.53	1.14	1.27	9.86	0.213
230–1000	0.52	1.26	1.93	15.36	0.134

[a] Symbols used to denote column headings are equivalent to headings in Table B-3.

TABLE B-8

SUMMARY OF RESULTS FOR PILOT GROUP NO. 2

GAUGE NO.	SOURCE ANGLE (°)	DETECTOR ANGLE (°)	SOURCE-DETECTOR SEPARATION (IN.)	SOURCE
	(*a*) Gauge configurations			
1	45	45	4	^{137}Cs
2	45	30	4½	^{137}Cs
3	15	15	4¾	^{137}Cs
4	15	30	5½	^{137}Cs
5	45	45	6	^{137}Cs

GAUGE NO.	LOWEST E_{se}/DISC [a]	LOWEST $\sigma_c(\rho)$/DISC	HIGHEST $\bar{x}$/DISC	LOWEST $\sigma_s(\rho)$/DISC	HIGHEST QF/DISC
	(*b*) Best results [b]				
1	11.53	0.73	3.38	2.30	0.193
	0–80	150–290	0–90	150–290	0–80
2	6.79	1.15	3.68	1.46	0.306
	0–80	90–290	0–90	150–290	0–80
3	2.53	0.83	5.94	1.35	0.664
	0–110	0–210	0–90	150–290	0–110
4	3.31	1.10	5.93	1.51	0.464
	0–110	150–1000	0–80	150–290	150–290
5	6.14	0.22	4.73	0.96	0.364
	0–80	150–290	0–80	150–290	0–80

[a] The discriminator settings are given below each value.
[b] Units for each column and discriminator settings same as for Tables B-3 through B-7.

Results of the random number sampling technique for determining the make-up of the composition error are given in Table B-9. These results clearly show that the counting-rate measurement error contributions and the model fit error contribution to the composition error may be accurately extracted. Note in Table B-9 that the values of $\sigma_{sR}(\rho)$ compare very well to the values for $\sigma_s(\rho)$, the mean percentage difference being 4.5 percent. This result was to be expected because these are the same errors based on the rule of thumb given by Eq. B-27 by two different methods. The next comparison is between the values for $\sigma_M(\rho)$ and $\sigma_c(\rho)$. The mean percentage difference between these values is 7.6 percent, also indicating a good correlation. It is also significant that both $\sigma_M(\rho)$ and $\sigma_c(\rho)$ vary in the same manner, having minimum values at the same discriminator level. No correlation should be made between the values of $\sigma_c(\rho)$ and $\sigma_{cR}(\rho)$, because $\sigma_{cR}(\rho)$ is calculated on the basis that the back-calculated density from the calibration model is the mean value.

From these results it may be concluded that for the most part $\sigma_c(\rho)$ is only the error in the model fit, with a slight interference from the counting-rate measurement error. The strongest effect of the counting-rate measurement error appears at discriminator levels 0-190 and 0-210 where the values are so small that the effect may be magnified due to less accuracy in the calculations. It must be noted that this analysis is based on the laboratory standards of known composition, so that in actual field measurements the variation in the ratio of atomic number to atomic mass along with uncertainties in knowing the soil composition contribute to the composition error.

Surface-effect and composition errors * show a wide range of values from low, favorable results to high, unfavorable results. Thus, these errors can be reduced significantly by optimum choice of parameters. The same is not totally true for counting-rate measurement errors, because they do not seem to decrease to acceptably low levels; i.e., less than 1 pcf. Counting-rate measurement errors are high at both low-energy regions and high-energy regions, and are optimum in the medium-energy range. The reason for this appears to be that the slope of the calibration curve is best (steepest) when only true scattered radiation comprises the gauge response. At low-energy regions, the lead X-rays contribute to flattening the calibration curve, and at the high end the direct transmission contributions tend to do the same; thus, when these effects are discriminated the slope is steepest, resulting in the lowest counting-rate measurement errors. This explanation would not be true if net responses were used to determine the counting-rate measurement error; in this case one could only expect that the calibration curve would be steeper at the lower energy region because photoelectric absorption is the predominant interaction. As a specific example, note that in Table B-6 the counting-rate measurement error varies from a high of 2.72 pcf for the region 0-130 KeV to a low of 1.51 pcf for 150-290 KeV, a medium-energy range. Generally, the values for the high-energy regions are lower than those for the low-energy regions, probably because direct transmission contributions have less effect than the lead X-rays, and also due to background effects.

The variation of the surface-effect error should be analyzed in conjunction with variations in effective sample depth to evaluate the effect of collimation. In all cases the surface-effect error decreases as the effective sample depth increases. In Table B-4, note that the surface-effect error at discriminator level 0-100 KeV is 8.2 pcf, with a corresponding effective sample depth of 3.59 in. At 0-190 KeV the surface-effect error has increased to 9.5 pcf, while the effective sample depth has decreased to 3.08 in. Both of these changes were about 15 percent, indicating a proportionality between changes in surface-effect error and effective sample depth.

The magnitudes of both surface-effect error and effective sample depth are significant in that the best values obtained from Tables B-3 through B-7 and summarized in Table B-8 are two or more times better than values reported for commercial gauges. From Table B-5 the lowest surface-effect error is 2.5 pcf, which, when compared to the lowest value obtained for a commercial gauge at the North Carolina State University Workshop of about 6 pcf (McDougall, 1969), is a significant improvement. The corresponding effective sample depth of 5.9 in. from Table B-5 is more than double the best value reported by Gardner and Roberts of 2.3 in. The next step in analyzing these results is to compare magnitudes between the gauges and their amount of collimation.

Table B-5 gives results for a gauge with small angles of incidence for both source and detector collimators. This gauge was designed to provide a response which contains a large contribution of gamma rays that penetrate to larger depths. When the surface-effect errors and effective sample depths from Table B-5 are compared to those of the other tables, for gauges with smaller contributions of gamma rays from large depths, they are generally much better. Thus, it can be concluded that collimation and angle of incidence of source and detector collimators into the soil are parameters that provide a significant improvement in the surface-effect error and in the effective sample depth.

Very encouraging results were obtained for composition error considering that the dual-gauge principle, developed specifically for minimizing composition error, was not used in the single-gauge analysis. Each single-gauge configuration had reasonably low composition errors, as given in Table B-8. However, Tables B-3 through B-7 show that the magnitudes of these errors depend not only on the energy discrimination region, but also on the other gauge parameters such as collimation and source-detector separation, as well as on the slope of the calibration curve. No specific trend is noted with any particular parameter; thus, it is assumed that the optimization procedure can be used to obtain reasonable values for composition error. One notable correlation between counting-rate measurement error and composition error is that, in general, as counting-rate measurement error increases (or decreases) in magnitude from gauge to gauge in the same energy region, the composition error also increases (or decreases), indicating

* The term composition error used in this section includes the model fit error and a relatively minor effect of counting-rate measurement error discussed previously.

that the slope of the calibration curve is a significant factor to optimize.

Regarding energy discrimination as an individual parameter, one significant result can be noted: the best value for each error, effective sample depth, and quality factor, for each gauge, is obtained for an energy region other than the full-energy range. In other words, energy discrimination results in a significant improvement in both the individual criteria, and in the quality factor, or over-all gauge performance. In Table B-5 compare the best value under each column to the value of 0-1,000 KeV, which represents the full-energy range. The lowest composition error of 1.1 pcf at 150-1,000 KeV is about half the value of 2.1 pcf at 0-1,000 KeV. Similarly, a factor of about one-third improvement in surface-effect error and effective sample depth at 0-110 KeV over those at 0-1,000 KeV is noted. Finally, the quality factor of 0.46 at 150-290 KeV is preferred over the value of 0.41 for the full-energy range. Similar generalities can be observed for each of the other gauges except Gauge No. 1, Table B-3, because not enough information is available.

Energy discrimination should prove advantageous in reducing composition and surface-effect errors and in increasing effective sample depth. Unfortunately, different energy regions are required to accomplish improvement in these quantities individually. Tables B-3 through B-7, and in particular Table B-8, show the surface-effect error and effective sample depth to be optimum at low-energy regions as was expected from the concepts presented previously in "Gauge Errors." The composition error is lowest in the high-energy region for only one out of the five gauges, a surprising result. Three of the other four gauges have their lowest composition errors in the medium-energy range and one gauge has the lowest composition error in the low-energy range. These results do not confirm the concept outlined in "Gauge Errors" that the high-energy regions tend to minimize the composition effect. This does not mean, of course, that the theory is not true or well-founded, but only that these results do not confirm the theory. A possible explanation for this result would be that collimation emphasizes the detection of gamma rays that are scattered deeper within the soil, which, in itself, results in more low-energy gamma rays. Discrimination at the higher levels thus tends to adversely affect the slope of the calibration curve by neglecting the strongest component of gauge response, leading to an increase in composition error, or at best only a moderate decrease. This fact is pointed out in "Experimental Procedure and Results." The gauge with the lowest composition error in the high-energy region was Gauge No. 4, Table B-6, which had a large source-detector separation of 5.5 in. and a high counting rate. In this gauge discrimination probably did not remove a high percentage of useful counts at the higher energy levels, judging from the scattered energy spectrum.

The effect of energy discrimination on the counting-rate measurement error is discussed earlier herein; only the quality factor is to be considered. The change in magnitude of the surface-effect error, exhibited in the level of the quality factor, combined with the change in magnitude of the effective sample depth, exhibited in the volume factor, together control the variation in quality factor with energy discrimination. This fact is evident even though changes in composition error run counter to changes in surface-effect error and effective sample depth and even though composition error changes are emphasized in the strong range dependence of the quality factor. The counting-rate measurement error, also a range factor, is a balancing effect between the other opposing effects. The explanation lies in the fact that percentage changes in surface-effect error and effective sample depth from one energy range to another are higher than those for composition error. As a specific example, consider Table B-5, where the quality factor is highest in the low-energy region, 0-110 KeV. The surface-effect error is lowest at the same level and the effective sample depth is highest at 0-90 KeV. This result is obtained despite the fact that composition error is lowest at 0-210 KeV and counting-rate measurement error is lowest for 150-290 KeV. As a result of the strong control of surface-effect error and effective sample depth, the highest quality factor for four out of the five gauges is obtained in a low-energy region.

TABLE B-9

RESULTS OF RANDOM NUMBER SAMPLING TECHNIQUE FOR DETERMINING COMPOSITION AND COUNTING-RATE MEASUREMENT ERROR FOR PILOT GROUP GAUGE NO. 3

DISCRIMINATOR LEVEL (KeV)	$\sigma_c(\rho)$ (PCF)	$\sigma_{cR}(\rho)$[a] (PCF)	$\sigma_s(\rho)$ (PCF)	$\sigma_{sR}(\rho)$[a] (PCF)	$\sigma_M(\rho)$ (PCF)
0–90	1.89	2.19	1.45	1.12	1.88
0–110	1.39	2.16[b]	1.53	1.50[b]	1.55[b]
0–130	1.37	2.02	1.58	1.51	1.34
0–150	1.20	1.89	1.56	1.52	1.13
0–190	1.00	1.66	1.45	1.48	0.76
0–210	0.83	1.58	1.37	1.44	0.65
0–230	1.03	1.57	1.36	1.14	1.08
0–290	1.35	1.84	1.47	1.36	1.24
0–350	1.39	2.15	1.50	1.54	1.50

[a] These values are the average values for two separate runs using ten random numbers per sample.

[b] Separate measurements using 100 random numbers were made to compare with the values at 0-110 KeV, the results were:

$$\sigma_{cR}(\rho) = 1.96$$
$$\sigma_{sR}(\rho) = 1.42$$
$$\sigma_M(\rho) = 1.35$$

Dual-Gauge Experiments

Application of the dual-gauge principle was not a major objective of this phase of Project 10-5A; however, because not much difficulty was involved in applying this principle to the pilot group data, the dual-gauge experiments were run. The primary purpose of these experiments was to check whether the surface-effect error could be reduced with this technique even though there was no sound basis to expect that it would. The best results out of 190 dual-gauge combinations are given in Tables B-10 through B-13. The ten best dual-gauge combinations based on the quality factor are given in Table B-10; the other tables

TABLE B-10

TEN BEST DUAL-GAUGE COMBINATIONS BASED ON PILOT GROUP NO. 2 GAUGES AND QUALITY FACTOR

GAUGE COMBINATION [a]	SURFACE-EFFECT ERROR (PCF)	COUNTING-RATE ERROR [b] (PCF)	COMPOSITION ERROR [b] (PCF)	QUALITY FACTOR [c]
1 L-5 M	4.3	1.3	0.02	0.464
2 F-5 F	0.3	2.2 [d]	0.61	0.451
2 L-5 L	1.5	2.1 [d]	0.05	0.445
1 L-5 F	0.6	2.3	0.26	0.437
3 M-4 M	2.7	2.1 [d]	0.58	0.419
2 F-5 M	4.8	1.5	0.19	0.412
1 L-4 M	3.0	2.0	1.04	0.401
1 L-4 H	3.1	2.1	0.96	0.393
2 L-5 F	4.2	2.1 [d]	0.14	0.392
4 M-5 F	3.6	1.9 [d]	1.26	0.384

[a] Numbers refer to the pilot group gauges described in Tables B-3 through B-8. Letters correspond to the following energy discrimination ranges:

F = 0-1,000 KeV (full-energy range)
L = 0-210 KeV (low-energy range)
M = 150-290 KeV (medium-energy range)
H = 150-1,000 KeV (high-energy range)

[b] Calculated on the basis of the dual-gauge principle.

[c] Include the average volume factor for the two gauges making up the combination.

[d] Two separate techniques for obtaining partial derivatives of density with respect to response were used; these values were calculated using the technique that does not involve eliminating the composition parameter. For each gauge the technique providing the lowest error is provided.

show the ten best dual-gauge combinations under each of three major errors. The purpose of this particular tabulation is to observe any trends that may lead to significant conclusions.

The "Surface-Effect Error" Column in Table B-10 shows that some values of this error are less than 1 pcf. This is a fortunate result, because it shows that applying the dual-gauge principle may indeed reduce this error even below the values obtained for either of the single gauges involved. For example, note that the single-gauge surface-effect errors are 10.7 pcf for Gauge No. 2 in the full-energy range and 7.4 pcf for Gauge No. 5 in the full-energy range, yet their dual-gauge combination yields a surface-effect error of 0.3 pcf (see also Tables B-4 and B-7). No discernible trend of the surface-effect error is noted with decreasing quality factor down the table.

Regarding the column under counting-rate measurement error, note that none of these values is below the ideal 1 pcf level; in general, the values are poor. It should be remembered that these are among the best values out of 190 combinations and most of the other values are considerably worse. Of course, there is no sound basis for the idea that the dual-gauge principle should reduce the counting-rate measurement error. This error appears to be almost constant as the quality factor decreases down the table, thus having a minor influence in determining which of the combinations is the best.

The variation of the composition error down the table shows that it controls the quality factor for these gauges more than any other error. The magnitudes are lower than 1 pcf for most combinations. This result was to be expected because the dual-gauge principle is aimed at reducing this error in particular. The major discernible trend connected with the composition error is that the dual-gauge error appears to be lowest when the dual-gauge combination involves a gauge with poor composition error and one with a very low composition error. For example, the best dual-gauge combination in Table B-10 has a composition error of only 0.02 pcf while single Gauge No. 1 in the range of 0-210 KeV has an error of 3.23 pcf and single Gauge No. 5 in the range 150-290 KeV has the lowest of all single-gauge values at 0.22 pcf (see also Tables B-3 and B-7).

The quality factor values are not very favorable, even though some of the best ones represent values that are half again as good as the commercial gauge evaluations at the North Carolina State University Workshop (McDougall, 1969). One favorable note that is not evident in the table is that many of the 190 dual-gauge combinations had quality factors greater than 0.30, showing potential for possible refinements.

A look at the dual-gauge combinations among the ten best shows that in seven combinations Gauge No. 5 appears, and in all energy ranges except for the high-energy range. The parameter of Gauge No. 5 that is significantly different from the other gauges is the large source-detector separation of 6 in. Most of the other gauges in combination with Gauge No. 5 are the ones with the lower source-detector separations. Thus, this parameter may well be the critical one in optimizing a dual-gauge combination. A look at the worst dual-gauge combinations shows that they are either ones with nearly the same separations or combinations of the same gauge with only different energy discrimination regions.

The best dual-gauge combinations under the individual errors, given in Tables B-12 and B-13, shows some of the same trends just discussed. In Table B-11 Gauge No. 5 is involved in six of the ten combinations; in Tables B-12 and B-13 it is involved in all combinations. No definitive explanation can be given for the unsuspected presence of Gauge No. 5 in so many of the surface-effect-error combinations. The single-gauge surface-effect errors for Gauge No. 5 are intermediate values compared to the other four single gauges; thus, the explanation may be that these intermediate values represent an optimum for combination with other values. At any rate, the values for the surface-effect error are very favorable for the combinations in Table B-11.

The values for the counting-rate measurement error in Table B-12 are not as favorable as those for the other errors, as was previously discussed. The presence of single Gauge No. 5 in the energy range of 150-290 KeV in nine of the ten combinations indicates that large sensitivity difference with at least one very low value is again the criterion for best dual-gauge results. The other single gauges in the combinations have varying results for the counting-rate measurement error. Most of the dual gauge combinations in the set of 190 have very unfavorable counting-rate measurement errors.

Table B-13 gives some very low composition errors; all

TABLE B-11

DUAL-GAUGE COMBINATIONS HAVING TEN LOWEST SURFACE-EFFECT ERRORS [a]

GAUGE COMBINATION	SURFACE-EFFECT ERROR
1 L-1 H	0.000
4 H-5 M	0.000
3 H-5 H	0.000
3 H-4 M	0.030
3 L-3 F	0.051
2 F-5 F	0.343
2 M-5 H	0.472
1 L-5 F	0.584
1 L-2 F	0.860
2 L-5 L	1.517

[a] See Table B-10 for notation and definitions.

TABLE B-12

DUAL-GAUGE COMBINATIONS HAVING TEN LOWEST COUNTING-RATE MEASUREMENT ERRORS [a]

GAUGE COMBINATION	COUNTING-RATE MEASUREMENT ERROR (PCF)
1 L-5 M	1.273
2 L-5 M	1.359
4 L-5 L	1.365
1 F-5 M	1.369
3 L-5 M	1.376
4 F-5 M	1.380
3 F-5 M	1.400
5 L-5 M	1.459
2 F-5 M	1.468
5 F-5 M	1.481

[a] See Table B-10 for notation and definitions.

of these may be considered negligible, especially when compared to the counting-rate measurement error, because both of these errors make up the combined normal error for quality factor determination. These results again point out the strong sensitivity effect of having the single gauge with the lowest composition error in combination with the other single gauges with poor values. Gauge No. 5 appears in all ten combinations again; however, this gauge in the high-energy region, 150-1,000 KeV, appears in six combinations with a single-gauge composition error of only 0.35 pcf. Gauge No. 5, in the energy region 150-290 KeV with composition error of 0.22 pcf, appears in three of the combinations.

In general, the dual-gauge experiments show that each of the errors (except counting-rate measurement error) may be reduced to favorable, even exceptional, levels. In addition, the best results in applying the dual-gauge principle appear when the sensitivities of each of the single gauges in the combination to the errors individually are significantly different and when one of the single gauges has the lowest value for all the gauges of a particular error. In considering the ten best dual-gauge combinations on the basis of quality factor, source-detector separation was a critical parameter, and the best combinations usually contained single gauges with large differences in the source-detector separation.

It is possible that in the somewhat arbitrary choice of the energy regions that were attached to the single gauges in the dual-gauge analysis, the best regions may have been bypassed. This situation is similar to the one with the pilot group gauge configuration selections, because they too represent only a sample of the many possible combinations, but in the dual-gauge analysis both of these arbitrary selections are included. Thus, it is advisable that before any final judgment is made on the possibility of optimizing a gauge for actual use by the dual-gauge principle, a more thorough checkout be made.

TABLE B-13

DUAL-GAUGE COMBINATIONS HAVING TEN LOWEST COMPOSITION ERRORS [a]

GAUGE COMBINATION	COMPOSITION ERROR (PCF)
4 L-5 H	0.009
1 L-5 M	0.023
1 F-5 H	0.037
5 F-5 H	0.048
2 F-5 H	0.053
2 L-5 L	0.053
4 F-5 H	0.058
2 L-5 M	0.063
5 L-5 M	0.064
3 F-5 H	0.065

[a] See Table B-10 for notation and definitions.

Mathematical Modeling of the Surface-Effect Error

The constants for the air-gap polynomial have been tested as functions of C and P, as described previously. Results for the single-gauge configuration described previously show that the constant A, coefficient of x in Eq. B-43, may be described by Eq. B-44a for all energy regions. The constant B of Eq. B-43 may also be described by Eq. B-44a, but in isolated cases Eq. B-44c supplied a better fit. For the constant D in Eq. B-43 at the lower energy regions, less than 210 KeV, Eq. B-44c applies, but at the high-energy regions, greater than 210 KeV, Eq. B-44a applies. For the constant D, the least-squares fits get increasingly worse as the energy region increases. All of these fits were evaluated on the basis of the smallest sum of the squares of the residuals. A regression analysis approach appears to be a more favorable technique for further evaluations. Because these results are so preliminary, they are not tabulated or presented in any more detail.

SUMMARY, CONCLUSIONS, AND SUGGESTIONS FOR FURTHER RESEARCH

Engineers have been made aware of the need for improving existing soil density measurement techniques. The gamma-ray backscatter gauge has the ideal qualities of simplicity, speed, and nondestructivenes in density measurement. However, three primary gauge errors have been identified and defined: counting-rate measurement error, composition error, and surface roughness or suface-effect error. These errors are discussed in terms of design parameters that could be used to reduce each of the errors individually. Because an attempt to reduce one error may tend to increase another, optimization of these design parameters was necessary to improve gauge performance. Gauge performance was rated on the basis of a quality factor which used the gauge errors and soil measurement volume to provide a figure of merit for each gauge design configuration.

Recent concentrated efforts in previous phases of NCHRP Projects 10-5 and 10-5A have resulted in the development of the calibration model for gauge response and the dual-gauge principle of two individual gauge responses. These models have provided the mathematical foundations for a more fundamental analysis of gauge performance, part of which is reported herein.

A final prototype gauge design included the parameters currently in use in conjunction with the new design parameters of collimation of source and detector, variable source and detector collimator angles into the soil and electronic components capable of spectrometry. The sophisticated electronic system included a NaI (Tl) detector and a multichannel analyzer, both used primarily to evaluate energy discrimination as a design feature. The prototype gauge and its associated electronics were used on an optimum set of laboratory standards, effectively covering the full range of soil densities and compositions encountered in the field. Special laboratory precautions were taken to minimize the effects of extraneous interferences and to standardize the experimental procedure.

The experimental program consisted of three main phases, excluding preliminary experiments necessary to assure optimum readiness. The pilot-group method was chosen to effectively sample gauge configurations for performance capabilities. Data acquired for the second pilot group were used in both a single-gauge analysis of new design parameters and an optimum dual-gauge analysis. These evaluations constituted the first two phases of the experimental program; the third phase concentrated on mathematically modeling the surface-effect error to tie down another degree of freedom in the optimization procedure. The results of these evaluations and the specific conclusions drawn from the results are discussed at length. For the purpose of emphasizing the significant results some general conclusions are discussed in the following.

Some of the more fundamental conclusions that may be drawn from the research in this project serve to verify previous theoretical considerations. Not all of the theoretical suppositions were verified, partly due to unsuspected interferences and partly due to the need for more research. Probably the most general conclusion that may be drawn from the entire project is that optimum inclusion of collimation and energy discrimination as design features results in a significant improvement in over-all gauge performance. The combined use of collimation and variable source and detector collimator angles into the soil has led to significant increases in effective sample depth, which, in turn, has led to substantial decreases in surface-effect error. The use of energy discrimination has led to increases in over-all gauge performance in every case evaluated. An optimum energy region exists for each of the individual errors, but discrimination against higher energies appears to provide the best quality factor for most gauge configurations.

Past research shows that the composition error is no longer of prime concern; this fact was also verified in this project. This study shows that the counting-rate measurement error may prove to be the controlling error for new gauge designs. This fact is evident even though, in general, the magnitude of the surface-effect error is still larger; however, some care in the preparation of the measurement surface may accomplish considerable reduction in this error. Refinements in the mathematical modeling of the surface-effect error may be the final step in effectively understanding the performance capabilities of a gauge. The fact that basically all the major gauge errors are now understood and described both physically and mathematically is noteworthy. With these ideas in mind one may now consider the possibility of designing a commercial gauge employing the design features discussed.

The use of sensitive electronic components such as single-channel or multichannel analyzers with NaI (Tl) detectors dictates that more care and expense will be required to maintain a desirable density gauging unit. This consideration should not be considered a disadvantage, although it appears so on the surface. These gauge components would be ideal for use in a continuous density monitor device that would be vehicle-mounted or power driven. With sound engineering design the cost of one such device would be compensated for by its potential to replace many portable devices and to provide rapid, continuous, and more accurate measurements. The advantages and disadvantages of the Lane-Wells Road Logger generally apply to this case. The use of such a device allows the designer more freedom to design for optimum accuracy, because he would have less restrictions on weight, size, and extreme simplicity. In the final analysis, a vehicle-mounted or power-driven density gauge would appear to be a more efficient and reliable instrument, with a capacity for further refinement that does not appear likely with portable devices. This capacity could even include a computerized system to effectively eliminate human evaluations that may lead to deficient results.

Of course, it is difficult to say whether a highly sophisticated system, such as the one just described, would be preferred over a portable system, such as any of the types in current use, with comparable accuracy. Both systems have definite advantages over each other. The most realistic view is not whether one system is preferred over the other, for it may be that both systems could enjoy wide-

spread appeal, but that at least one system be developed to the point of removing all doubts about accuracy and to provide the most efficient means of measuring density. This conclusion leads directly to a consideration of what further work must be done to accomplish the final objectives.

The most practical step to take in further research would be to evaluate gauge configurations that closely parallel the best configurations already considered. Essentially, this research would entail a tapering search on design parameters, one that would lead to optimum conditions by the process of elimination. This search must necessarily be aimed at a practical design that would appeal to the demands of the market. Some specific directions should be taken to achieve this end. The mathematical modeling of the surface effect should be defined and could be used either to tie down another degree of freedom in optimizing gauge performance or to lead to a gauge response that would be essentially independent of surface-effect error in a manner similar to the dual-gauge principle. The latter goal is the objective of current continuing research. The dual-gauge principle should be applied at every opportunity to as many of the design parameters as possible to achieve a more optimum design.

Other considerations for further research may include other applications of the gamma-ray backscatter principle, such as an ore concentration gauge or pavement thickness gauge. The former application would basically be a reverse density gauge, because the composition dependence would be optimized and the effect of density would be minimized. The latter application would take advantage of the depth-sampling sensitivity of gauge designs such as those evaluated in this project.

The current state of the art indicates that the full potential of the gamma-ray backscatter technique of measurement has not yet been attained, whether in measuring density or in other applications. It is hoped that the results of this project have advanced the technology of these measuring devices in the direction of true progress.

REFERENCES

BALLARD, L. F., and GARDNER, R. P., "Density and Moisture Content Measurements by Nuclear Methods—Interim Report. *NCHRP Report 14* (1965) 32 pp.

BELCHER, D. J., CUYKENDALL, T. R., and SACK, H. S., "The Measurement of Soil Moisture and Density by Neutron and Gamma-Ray Scattering. *Tech. Dev. Rep. No. 127,* U.S. Civil Aeronautics Admin. (1950).

BELCHER, D. J., CUYKENDALL, T. R., and SACK, H. S., "Nuclear Meters for Measuring Soil Density and Moisture in Thin Surface Layers." *Tech. Dev. Rep. No. 161,* U.S. Civil Aeronautics Admin. (1952).

BLACKWELL, P. L., BROWN, W. R., and RIZENBERGS, R. L., "Survey of Current Use of Nuclear Gauges in the Highway Field." *Hwy. Res. Circ. No. 85* (1968).

CSATHY, T. I., "Nuclear Methods for Determining Density and Moisture Content—A Review of the Literature." *Rep. No. 30,* Ontario Dept. of Highways, Toronto (1962).

DONHOFFER, D. K., "Determination of Ore Concentration in Exploration Holes by the Gamma-Ray Backscattering Technique." *Proc. Symposium on Nuclear Techniques and Mineral Resources,* International Atomic Energy Agency, Vienna (1968).

EVANS, R. D., *The Atomic Nucleus.* McGraw-Hill (1955).

GARDNER, R. P., "Minimizing Nuclear Soil Density and Moisture Content Gauge Errors." *Hwy. Res. Record No. 290* (1969) pp. 1-8.

GARDNER, R. P., and ELY, R. L., JR., *Radioisotope Measurement Applications in Engineering.* Reinhold (1967).

GARDNER, R. P., and ROBERTS, K. F., "Density and Moisture Content Measurements by Nuclear Methods—Final Report." *NCHRP Report 43* (1967) 38 pp.

GARDNER, R. P., ROBERTS, K. F., HUGHES, C. S., and ANDAY, M. C., "A Calibration Model for Optimizing the Air-Gap Method of Compensating Nuclear Density Gauges for Soil Composition Variations." *Jour. of Materials,* No. 1, Vol. 2 (1967) p. 3.

GARDNER, R. P., and WHITAKER, D. R., "A Study of the Gamma-Ray Scattering Technique for Measuring Atmospheric Density." *Nuclear Applications,* Vol. 3, No. 5 (1967a).

GARDNER, R. P., and WHITAKER, D. R., "Design Studies of a Gamma-Ray Scatter Atmospheric Density Gauge by a Multivariable Search Method." *Nuclear Applications,* Vol. 6, No. 3 (1969).

GARDNER, R. P., and WHITAKER, D. R., "Experimental Verifications of Gamma-Ray Atmospheric Density Sensor Mathematical Model Predictions." *NASA Contractor Report No. 66476* (1967b).

GUNDERMAN, W. G., "Current Status of Nuclear Testing for Moisture and Density of Soils and Related Materials." Presented at Fourth Annual Symposium on Engineering Geology and Soils Engineering, Univ. of Idaho, Moscow, Apr. 19-21, 1966.

HAMPTON, D., and SELIG, E. T., "Fundamental Properties of Compacted Soil." Society of Automotive Engineers, 650692 (1965).

HARLAND, D. G., "Measuring the Density of Thin Asphalt or Concrete Layers with a Gamma-Ray Backscatter Apparatus." *Nuc. Eng. and Design,* Vol. 3 (1966a) pp. 467-475.

HARLAND, D. G., "A Radio-Active Method for Measuring Variations in Density in Concrete Cores, Cubes and Beams." *Mag. of Concrete Research,* Vol. 18, No. 55 (1966b).

HINE, G. J., and MCCALL, R. C., "Gamma-Ray Backscattering." *Nucleonics,* Vol. 12, No. 4 (1954).

HORONJEFF, R., and GOLDBERG, J., "Field Measurements of Soil Moisture and Density with Radioactive Materials." *Proc. HRB,* Vol. 32 (1953) pp. 500-511.

HUGHES, C. S., and ANDAY, M. C., "Correlation and Conference on Portable Nuclear Density and Moisture Systems." *Hwy. Res. Record No. 177* (1967) pp. 239-279.

KAPLAN, I., *Nuclear Physics.* Addison-Wesley (1962).

KUHN, S. H., "The Effect of Type of Material on Nuclear

Density Measurements." *Hwy. Res. Record No. 66* (1965) pp. 1-14.

LIN, K., PIRIE, E., and TAYLOR, D., "A Moving Gamma Source Method of Measuring Soil Densities." *Nuclear Instruments and Methods,* Vol. 72 (1969) pp. 325-328.

LYON, W. S., JR. (ed.), *Guide to Activation Analysis.* Van Nostrand (1964).

MCDOUGALL, F. H., DUNN, W. L., and GARDNER, R. P., "Report on Nuclear Soil Gauge Calibration Workshop-Symposium." Dept. of Nuclear Eng., North Carolina State Univ. (1969).

MILES, E., "Energy Distribution of Gamma Rays Scattered Around a Soil Density Probe." Thesis, Dept. of Eng. Physics, Cornell Univ. (1952).

PRICE, W. J., *Nuclear Radiation Detection.* McGraw-Hill (1964).

PREISS, K., "Analysis and Improved Design of Gamma-Ray Backscattering Density Gauges. *Hwy. Res. Record No. 107* (1966) pp. 1-12.

RALSTON, A., *A First Course in Numerical Analysis.* McGraw-Hill (1965).

ROY, S. E., and WINTERKORN, H. F., "Scintillation Methods for the Determination of Density and Moisture Contents of Soils and Similar Granular Systems." *HRB Bull. 159* (1957) pp. 55-135.

SELBY, S. M. (ed.), *Chemical Rubber Company Standard Mathematical Tables.* Chemical Rubber Co., Cleveland (1965).

SEMMLER, R. A., BRUGGER, J. E., and RIEKE, F. F., "Gamma Scattering Density Meters: Analysis and Design with Applications to Coal and Soil." Univ. of Chicago, Laboratories for Applied Science, LAS-TR-161-35 (1961).

SIMPSON, J. W., "A Non-destructive Method of Measuring Concrete Density Using Backscattered Gamma Radiation." *Building Science,* Vol. 3 (1968) pp. 21-30.

TAYLOR, D., and KANSARA, M., "Measuring Density with the Nuclear Backscatter Method." *Nucleonics,* Vol. 24, No. 6 (1966).

TAYLOR, D., and KANSARA, M., "Improvements in the Method of Measuring the Density of Soil Using Nuclear Back-Scatter." *Nuclear Instruments and Methods,* Vol. 59 (1968) pp. 305-308.

APPENDIX C

MONTE CARLO SIMULATION OF NEUTRON THERMALIZATION IN SOILS *

By WALTER J. LIPPOLD

STATEMENT OF PROBLEM

Since their introduction in 1950, soil moisture neutron gauges have been plagued by calibration problems. That is, although gauge response was certainly a function of the density of hydrogen in soil moisture, it was also a function of soil composition and bulk density, and the hydrogen present in compounds other than water. Thus, a gauge calibrated for response versus bulk density of water, without quantifying the effects of the other "undesirable" parameters on response, could be in considerable error. Recent investigations have produced a number of mathematical models that incorporate the effect of all parameters. Most notable, and currently most widely used, of these models are those used on two- and three-group neutron diffusion theory. Proponents of individual modes claim good accuracy over various moisture content ranges and in many different soil compositions.

To date, there has been no investigation of a Monte Carlo statistical treatment of the calibration problem. Such a treatment is developed in this study and the results are corroborated by physical experiments on some soil mediums of various hydrogen contents.

LITERATURE REVIEW

Ballard and Gardner (1965) conducted a literature survey and evaluation of previous methods, including nuclear, used in measurement of soil moisture content. They summarized some of the nuclear experimental results, primarily the quoted accuracies and conditions of the test, that have been attained since Belcher, et al. (1950) introduced soil moisture gauges. Soil composition was again confirmed as having a secondary effect on nuclear gauge response. It was concluded that soil density had only a slight effect that could be neglected unless densities of

* This appendix comprises the essential portions of a thesis bearing the same title prepared under the NCHRP Project 10-5A contract and submitted to the North Carolina State University (1970) in partial fulfillment of the requirements for the degree of Master of Science.

wide extremes (less than 60 pcf or greater than 150 pcf) were encountered.

Burn (1961) expended considerable effort in researching calibration standards for moisture gauges. His interest was primarily in media other than natural soils; the advantages of using substitute materials are higher stability, better uniformity, and finer control of both bulk density and distribution of hydrogen atoms. Gaseous mixtures, liquids, low-melting-point and laminated solids, solid-liquid suspensions, and Ottawa sand-water mixtures were investigated, to name a few. All had advantages and disadvantages, with none of particular merit over a wide range of moisture contents. However, with a selection of six different standards he could cover the entire moisture density range, 0 to 62 pcf, with good results.

Semmler (1963) investigated the influence of elements other than hydrogen on neutron moisture gauges using a Ra-Be neutron source in a spherical cavity as a model of the gauge. Formulas were given to compute the change in composition using both two-group and age-diffusion theory. Moisture gauge response in coal was found to be significantly affected by the carbon density because of the significant changes in fast neutron transport cross section. Thermal neutron flux equations were given for several geometries. Based on the average composition of the earth's crust, it was concluded that iron was the dominant neutron absorber in soils. Also, the tendency to ignore the influence of nonhydrogen elements on gauge response was not justified in many cases because the scattering as well as the moderating properties of the medium are significant. This meant that changes in the dry medium composition and density can influence gauge response. In addition, although calibration data using laboratory standards with a dry density and various amounts of moisture will give a smooth calibration curve, this may be a misleading indication of gauge accuracy. The media used for calibration should reflect the random changes in density and composition found under field conditions as well as the change in moisture content.

Preiss and Grant (1964) reported that use of a cadmium-covered BF_3 counter made it possible to construct a surface neutron moisture gauge whose response is independent of soil composition and bulk density. Also, there exists an optimum distance between source and detector at which the count time required to reach a given error in water density is a minimum. For their particular design that distance was 7 cm.

Olgaard (1965) reported results of investigations using a three-group diffusion theory model. The geometry was a fast neutron point source in an infinite, homogeneous medium and a line detector with its center at the source. This theory was compared against results from a physical experiment using a large cylindrical drum to hold five different Danish soil samples. The Ra-Be neutron source was located in the center of the system along the axis of the cylinder. The detector probe was lowered into the drum through an aluminum tube along the axis. A new concept was introduced to replace the "sphere of influence" in such calculations. Called "sphere of importance," it is defined as the sphere around the source, situated in a moderating medium, which, if all soil and water outside the sphere are removed, will yield a neutron flux at the source that is 95 percent of the flux obtained if the medium is infinite. It was shown by the numerical calculations that deviations in density, composition, and hydrogen content from those associated with a calibration curve may give significant errors. Agreement between experimental and theoretical results for this subsurface soil probe arrangements was considered excellent. It was therefore concluded that there was little point in attempting to improve the theory, particularly since experimental uncertainty and uncertainty connected with soil composition would remain.

Burn (1966) reported the existence of a very large discrepancy between laboratory and field calibration curves for a scintillation-type neutron meter. Field calibration on a natural deposit of post-glacial clay demonstrated an absorption effect that reduced detected neutron activity at every moisture content by about 11 percent. At first chlorine was suspected, but later experimentation indicated that 7 percent by weight of iron in the soil could reduce gauge response by 9 percent. The other 2 percent was explained as possibly being attributed to small quantities of potassium and chlorine also present in the soil.

Olgaard and Haahr (1967) reported the results of theoretical and experimental investigations of the Danish DM subsurface moisture probe. The three-group diffusion theory model developed by Olgaard (1965) was used in comparative experiments on two Danish soil types. An optimum source-to-detector distance was investigated and found to be dependent on variation in dry soil bulk density and concentration of strong neutron absorbers. It was found that the three-group model theoretical results correlated satisfactorily with experimental data and that it was possible to calculate theoretical calibration curves for soils of known composition and density. The model was suitable for determining the effect of variations in major soil parameters on moisture measurements and was useful in connection with gauge design considerations.

Hughes and Anday (1967) reported the results of the Virginia Correlation and Conference of Portable Nuclear Density and Moisture Systems, July 1965. Calibration curves were obtained for 30 moisture gauges on four different standards—sand, sand and alum, gypsum, and epsom salt. The results produced a predominance of small standard errors, indicating very good accuracy in this part of the analysis. However, because mositure content of the field samples was not determined during compaction and because it rained during the conference, no valid comparison could be made with actual field moisture content.

Zuber and Cameron (1966) summarized the theory and then surveyed the theoretical and practical factors that should be considered in selecting and using neutron soil moisture gauges. The effects of soil parameters, dry bulk density, macroscopic absorption cross section, bound water content, etc., were discussed. The effect of reasonable temperature fluctuations was considered small except possibly at higher moisture contents. An interesting discussion of optimum measurement time versus neutron source strength was also given. The rationale for placing polyethylene around the source to increase count rate came

under some criticism. Although such moderating material allows for a slightly shorter count time, it also increases the influence of soil parameters, and, as the count rate at zero moisture content is higher, it is more difficult to obtain the desired precision. In comparing different moisture gauges, Zuber and Cameron state that the accuracy of neutron moisture measurements is limited mainly by soil parameters and, therefore, in general almost all gauges are equally good as far as ultimate accuracy is concerned.

Gardner and Roberts (1967) discussed a proposed calibration model (two-group diffusion theory), requirements for selection of laboratory standards, results obtained in using the proposed calibration model on the laboratory and field data taken at the Virginia Correlation and Conference (Hughes and Anday, 1967), and the data taken and standards used at the Conference. They concluded that soil density and composition are significant, but only when combined with poor calibration technique. They also suggested that their calibration model and method could be used to calculate a calibration curve for average soil for routine field measurement. If better accuracy is desired, the model could calculate calibration curves for identifiable soil types or individual soils.

Couchat (1967) developed a three-group diffusion theory mathematical model for determining response of a neutron moisture probe. A computer program written in FORTRAN IV was used to fit the model to experimental data on seven media having different chemical compositions—among them sand, limestone, and sandy loam. The dry soil density influence is well represented by this model.

MONTE CARLO NEUTRON TRANSPORT COMPUTER CODE (05R)

General Code Description *

General Features

Oak Ridge Random Research Reactor Routine (05R) was originally developed by R. R. Coveyou in 1958, as a relatively limited reactor physics code for the IBM-704 computer. It has since evolved through a continuing series of expansions and improvements into a versatile instrument applicable to a wide variety of neutron problems. The code is designed as a master control code controlling in excess of 50 subroutines that perform the actual calculations. The version used in this study is all written in FORTRAN IV, with the exception of three assembly language routines, and is compatible with the IBM 360/75 computer.

One of 05R's most distinctive features is its highly detailed representation of neutron cross sections. In this representation the 05R energy range, from 0.070×10^{-3} eV to 77.13 MeV, is first divided into 40 supergroups by energy boundaries a factor of 2 apart. Each supergroup is then divided into n subgroups of equal energy width, where $n = 2^m$ and m is an integer in the range from one to nine. Cross-section data are then forced to be constant across each subgroup. Clearly, the huge volume of cross-section data implied by the foregoing cannot all be held in computer memory. 05R, however, avoids this difficulty by holding in the memory only the cross sections for a single supergroup and using them to process batches of neutrons in parallel. Each neutron is processed as far as possible with the data in memory, then laid aside until all others have been similarly treated. When all have been degraded in energy through a supergroup, more cross sections are read in from tape and the process is repeated.

The general geometry subroutine permits the treatment of very complicated configurations of essentially arbitrary shapes. Surfaces forming material interfaces may be either plane or quadratic, may be oriented in any manner, and may intersect in arbitrary fashion. Because no dimension statements are used in the geometry subroutine, the complexity of the geometry to be considered is limited only by the amount of computer memory available for storage of the geometry input.

XSECT and 05R Program Operation

In the 05R system the user is required to supply point values of microscopic cross sections at arbitrary energy points. A cross-section program, XSECT, which is run separately from and prior to 05R, reads raw cross-section data from cards or tape, performs various manipulations on the point cross sections, and prepares tapes containing macroscopic cross sections in the form required by 05R. Fortunately, the "05R code package" also provides a tape of raw point cross-section information for more than 40 elements.

Figure C-1 shows input, output, and flow of information between XSECT and 05R.

Briefly, the system operates as follows. Cross sections from the master cross-section tape are read into memory by XSECT and manipulated in accordance with card input instructions to produce three data sets: STAPE, PTAPE, and ITAPE. The STAPE data set provides 05R with elastic and total scattering parameters; PTAPE—with anisotropic scattering parameters; and ITAPE—with inelastic scattering parameters. The ITAPE data set, a modification to the 05R package, is discussed subsequently. For the most part, the XSECT PRINTOUT is just a reproduction of card input data. Program 05R is now read into fast core memory and requires all of the 340,000-byte space provided by the IBM 360/75. Information from the aforementioned data sets is read into allocated memory space, a supergroup at a time, and is used to process neutron histories as described previously. Card input, among other things, specifies source neutron parameters and system geometry. The output data set is another modification to the original program and stores pertinent neutron history parameters for later processing (discussed later herein). In addition to providing a reproduction of card input, 05R PRINTOUT includes a display of neutron probability density * as a function of radius interval,

* Much of the discourse in this section is taken from the 05R Code *User's Manual* available from the Radiation Information Shielding Center, Oak Ridge, Tenn.

* Neutron probability density as used here is defined as the weighted number of neutrons (to the nearest whole number) appearing within a given parameter interval or set of parameter intervals; for example, those neutrons appearing at the soil surface within a given radius interval and energy group interval.

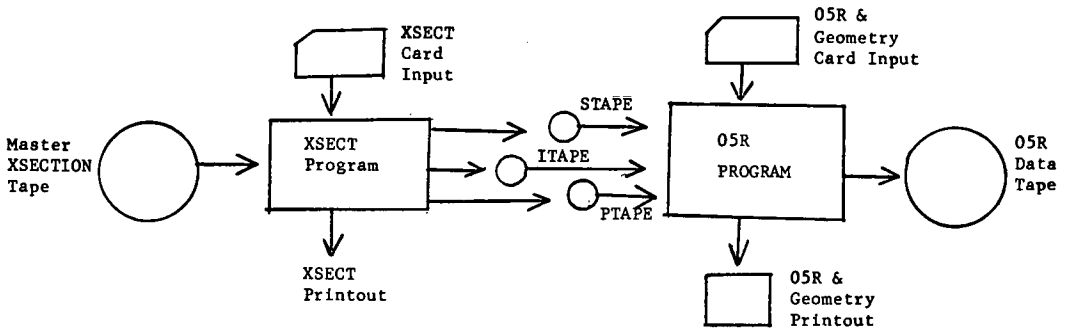

Figure C-1. Input, output, and flow of information between XSECT and 05R.

energy group interval, radius interval versus energy group interval, radius interval versus elevation angle interval, and weight interval versus energy group interval.*

Viewing operation of the system in microcosm, a neutron history is generated as follows:

1. The neutron is assigned a NAME, an integer which thereafter distinguishes it from every other neutron in a batch. Initial speed, direction cosines, and spatial coordinates, X, Y, Z, are assigned.

2. Initial weight is assigned. In 05R absorption is not permitted. Instead, each neutron is originally assigned an initial statistical weight (equal to 1 in this study) which at each collision is multiplied by the probability that the neutron was not absorbed.

3. A geometry routine then determines in which medium the source neutron lies.

The slowing-down process then begins proceeding as follows:

4. The number of Mean Free Flight Times ** the neutron is to travel is chosen from an exponential distribution by random number selection and, from a consideration of the cross sections and the geometry, a tentative position for the next collision is chosen. If the flight path lies entirely within the original medium, the tentative position is adopted as the collision site. If, however, the flight path crosses into another medium, the position of the nearest boundary crossing along the flight path is computed, and the distance to this point is subtracted from the length of the flight path. The boundary crossing point then becomes the starting point for the continuation of the flight in the new medium, the flight path now being the additional distance traveled from the boundary. The process continues until a flight path lying entirely within a single medium is found or until the neutron escapes from the system.

5. A new weight is computed by multiplying the old weight by the survival probability in the medium of the collision point.

6. The nuclide from which the neutron is to scatter is chosen by considering the scattering cross sections of all nuclides of the medium at the collision point. As noted previously, all collisions are treated as scattering collisions.

7. From the mass of the scatter, the neutron velocity in the laboratory system before collision, the type (elastic or inelastic) of scattering, and a selection from the angular distribution associated with the scatterer, a new velocity for the neutron is calculated.

8. The energy corresponding to the new velocity of the neutron is compared to an arbitrary cutoff energy. If the energy is greater than the cutoff, the slowing-down process is continued by returning to step 4. If the neutron energy is less than the cutoff energy, slowing down is concluded and the neutron enters the thermal group. The thermal group is defined as all those neutrons that have slowed down to less than 0.025 eV.

9. The thermal group is given the simple one-velocity group treatment. Therefore, it is assumed that neutrons on the average neither gain nor lose energy in a collision, and all scattering is isotropic in the laboratory system. For each medium the diffusion process is characterized by the mean free path and nonabsorption probability for neutrons in that medium.

General Description of Modifications to 05R

In its original form 05R made no provision for inelastic scattering or multiple-energy neutron sources. To provide for these phenomena and to produce the desired output information, a number of modifications were required. These are described in detail in the next section. Generally, the following additions, deletions, and modifications were made.

A method similar to that for producing the STAPE data set in program XSECT was devised for creating the inelastic scattering cross-section data set ITAPE. In this case, raw inelastic point cross-section information already available from the Master Cross-Section Tape was manipulated by available subroutines to create the necessary number of supergroups, with 32 subgroups per supergroup. As with STAPE, ITAPE cross sections are constant across their respective subgroups. Therefore, each inelastic scattering level for which cross-section information is available is represented on ITAPE in the supergroup/subgroup fashion. When an inelastic collision occurs, a new subroutine, INELAS, in program 05R uses this inelastic scattering cross-section data to calculate a probability of the target nucleus attaining each of its excited levels in a

* Dr. R. P. Gardner, Associate Professor, Department of Nuclear Engineering, North Carolina State University, Raleigh, N.C., has copies of sample 05R printouts.

** Mean Free Flight Time is defined as the number of seconds it takes a neutron of a given energy to traverse a distance of one mean free path in a medium; i.e., $(\Sigma_{TOTAL}\, v)^{-1}$.

given energy subgroup (see next section). Then a random number selection determines at which level the interaction occurs. Finally, the respective Q value serves to determine a new neutron energy and direction cosines. In this study all inelastic collisions are assumed to be isotropic in the Center of Mass system (Goldberg, et al., 1962).

To more closely approximate the physical situation, a neutron source energy spectrum was chosen from those available in the literature (De Paugher, 1958). A new subroutine, SOURCE, forms a cumulative density function from the raw spectrum probability information, and then uses random number selection to determine initial energy for each neutron history.

SPECTM is a new output subroutine that gathers and displays information from PART I geometry and creates the 05R DATA TAPE. Another new subroutine, SDATA, reads 05R DATA TAPE into memory and acts as the neutron source subroutine for PART II geometry. It also produces the output for PART II geometry. The significance of PART I and II geometry is explained in the section on "Monte Carlo Experimental Procedure."

Integration of these new and major modifications to old subroutines into XSECT and 05R required minor changes in many subroutines. In addition, some other unrelated ideas were incorporated as minor changes. All of these innovations are explained in the next section.

Specific Modifications to 05R

The FORTRAN IV statement listings of the new modified 05R code used in this study may be obtained from Dr. R. P. Gardner, North Carolina State University, Raleigh, N.C. New subroutines, modifications to old subroutines, and subroutine deletions are described in the following sections.

Major Modifications to XSECT

CODE 6.—The original version of subroutine CODE 6 generated the STAPE DATA SET, which includes for each subgroup in each medium a value of mean free flight time, nonabsorption probability (Σ_s/Σ_T), and cumulative scattering probabilities $\left(\sum_{j=1}^{n} \Sigma_{sj}/\Sigma_s,\ j = j\text{th element},\ n = 1, 2, \ldots, l,\ \text{and } l = \text{total number of elements in a given medium}\right)$.

The modification to CODE 6 directs generation of the ITAPE DATA SET, consisting of inelastic macroscopic scattering cross sections constructed from raw cross-section data on the master cross-section tape and averaged over each subgroup with a constant 32 subgroups per supergroup. Subroutine CODE 7B does the actual averaging and required some minor modifications to handle inelastic cross sections. Cross sections, at each level, for each element that scatters inelastically in each medium are constructed and stored separately in the data set. A control system similar to that for STAPE allows for retrieval of the proper cross sections when needed by the 05R program.

New Subroutines in 05R

INELAS.—INELAS determines the Q value of an inelastic collision and then calculates the post-collision neutron energy (actually speed squared, SPDSQ) and the magnitudes of the three orthogonal velocity components, U, V, W. Following the procedure step by step, first, the neutron energy subgroup, NINCI, is determined. This allows selection of the proper cross section for each level and its respective Q value. Next, neutron energy is checked against the Q value for each level to ensure that an inelastic collision is in fact possible. If not, control is returned to the previous subroutine and another random selection of target nucleus is made. Assuming inelastic collision is possible, the post-collision velocity can be determined in the manner illustrated as follows. Consider a case with target nuclei cross-section data available for three levels, Σ_1, Σ_2, and Σ_3, with respective Q values, Q_1, Q_2, and Q_3. Thus,

$$\Sigma_T = \Sigma_1 + \Sigma_2 + \Sigma_3 \tag{C-1}$$

and the following probabilities are defined:

$$P_1 = \Sigma_1/\Sigma_T,\ P_2 = \Sigma_2/\Sigma_T,\ P_3 = \Sigma_3/\Sigma_T \tag{C-2}$$

A random number (RAND) selection on the interval [0, 1] determines the excited level; e.g., if $P_1 \leq \text{RAND} < P_1 + P_2$ then the target nucleus is excited to the second level and the neutron loses Q_2 energy in the laboratory system.

A new neutron speed, S, in the laboratory system can be calculated by

$$Q = E_l - E_l' \tag{C-3}$$

in which E_l and E_l' are the neutron energies in the laboratory system before and after collision, respectively. Now

$$kQ = (1/2)\ m\ (v_l^2 - v_l'^2) \tag{C-4}$$

in which k converts Q in MeV to the cgs system, and the target nucleus recoil energy is considered negligible; so,

$$v_l' = \sqrt{v_l^2 - \frac{2k}{m}Q} \tag{C-5}$$

Now, let $X = 2k/m = 1.913220092 \times 10^{18}$ cm^2/sec^2/— MeV; then,

$$v_l' = \sqrt{v_l^2 - XQ} \tag{C-6}$$

By assuming isotropic scattering in the center of mass system for neutrons of less than 10 MeV, subroutine GTISO can be used to randomly select isotropic unit vectors ($U\phi$, $V\phi$, $W\phi$). New orthogonal velocity components are then calculated. For example, determination of a new velocity component in the X direction (U') for a simplified case of $V = W = 0$ would look like Figure C-2.

In Figure C-2:

$\vec{v}_0 = \vec{v}_l \dfrac{m}{m+M} \equiv$ center of mass velocity;

$\vec{v}_l' \equiv$ neutron velocity in center of mass system after collision; and

$\vec{v}_l$ and $\vec{v}_l' \equiv$ neutron velocity in laboratory system before and after collision, respectively.

Because $\vec{v}_c' = \dfrac{M}{m+M}\ \vec{v}_l'$, if $\vec{v}_l'$ (target nuclei post-

collision laboratory velocity) is considered negligible with respect to v_l', then

$$U' = v_0 + \vec{v}_c' \cos\theta \qquad \text{(C-7)}$$

Now, substituting for v_c' and v_0.

$$U' = v_l \frac{m}{m+M} + \frac{M}{m+M} v_l' \cos\theta \qquad \text{(C-8)}$$

SOURCE.—Subroutine SOURCE is capable of forming a cumulative density function (cdf) using up to 100 raw data points from any neutron energy spectrum. It then selects a random number from the interval [0, 1] and compares it with the cdf to determine each neutron's initial source energy. Mathematically, the subroutine operates as in Figure C-3.

Using Figure C-3 as a reference, define

$$\text{SUM} = \sum_{i=1}^{n} (E_i - E_{i-1})\ N_{i-1} \qquad \text{(C-9)}$$

and

$$\text{CDF}_i = \text{SUM}_i/\text{SUM},\ i = 1, 2, 3, \ldots, n \qquad \text{(C-10)}$$

Now, if the random number (RAND) compares as $\text{CDF}_{i-1} \leq \text{RAND} < \text{CDF}_i$, then the initial energy for that source neutron is E_i. Such an operation is performed for each source neutron. The raw data points are inserted into the subroutine by card input. (Changes to *User's Manual* are not reproduced here but are available to qualified researchers on request to the Program Director, NCHRP.)

SPECTM.—Computer memory storage and statistical variance reduction requirements dictated a two-part Monte Carlo treatment of the combined detector-source-soil medium. The rationale is found in the section on "Monte Carlo Experimental Procedure." Subroutine SPECTM is the output routine for PART I geometry which includes the source and soil-plexiglass mediums (see "Physical Experimental Procedure and Apparatus," which follows). The output consists of reproduction of card input, 05R DATA SET (see Fig. C-1), and various displays of neutron frequency distribution as a function of various parameters.

Only the neutrons coming up through the surface of the plexiglass are of interest. Their frequency is noted and logged with respect to radius interval (ΔR) out from the center of the plexiglass surface, energy supergroup (NGROUP), elevation angle above horizontal (ϕ), and weight (WATE) (see Fig. C-4). This frequency distribution is then displayed in matrix form as a function of one or two of these parameters. Because each of these neutrons has a statistical survival probability (WATE) associated with it, this value is actually a measure of the probability that that particular neutron will survive to reach the surface. The sum of these WATE values for each neutron in a parameter interval is then the "true number" of neutrons appearing there. This value is rounded off to the nearest integer value for display.

Seven parameters associated with each neutron coming out of the surface are stored on 05R DATA SET. They are speed squared (SPDSQ), orthogonal velocity components (U, V, W), position vectors (X, Y), and statistical survival probability (WATE).

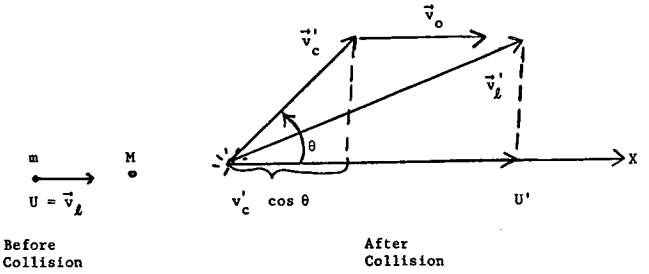

Figure C-2. Vector diagram of post-collision velocity calculation.

SDATA.—As indicated in the previous section, a two-part Monte Carlo treatment is required. Subroutine SDATA serves as the source and output routine for Part II geometry which includes only the detector medium. SDATA reads 05R DATA SET into computer memory. This information about each neutron then serves as the initial source condition for its respective neutron in the PART II geometry. These neutrons are laid out along a single horizontal ray emanating from the center of the system ($Z = 0$). The particular location of each neutron along this ray is determined by its X, Y coordinates. This "line source" is then the source for PART II. An infinite number of these line sources can be arranged as "spokes" of a wheel about the system center. The number of rays and angle between adjacent rays is determined by card input. The number of rays is limited only by the economics of computer run time. The explanation for this unusual procedure is found in the section on "Monte Carlo Experimental Procedure."

Two methods are available in SDATA for logging the number of neutrons "detected" by the detector medium.

1. Straight Monte Carlo. If and when a neutron is determined to have a collision in the detector medium, control is passed to SDATA by way of the ADDNTS entry point. Here the probability that the neutron has survived to this point (WATE) is calculated and multiplied by the absorption probability. Then a random number selection (RAND) on [0,1] is compared with this survival-then-absorption probability (QT). If RAND $\leq$ QT, the neutron is tallied, then killed. If RAND $>$ QT, control is

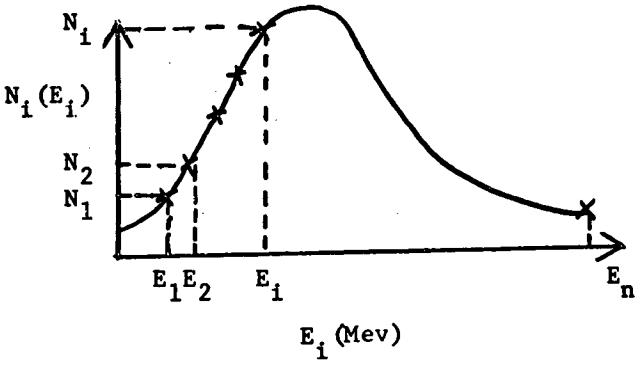

Figure C-3. Subroutine SOURCE sample energy spectrum.

passed back to the previous routine and the history is continued.

2. Summation of Probabilities. If and when it is determined that a neutron will cross a detector medium boundary, control is passed to SDATA via the CTNUTS entry point. The following calculations are made:

a. The total straight-line distance an uncollided neutron would travel in the medium (D).
b. Medium macroscopic absorption cross section (Σ_a).
c. Survival probability at that point (WATE).

Clearly then, the first collision absorption probability in the medium (PROB) is

$$\text{PROB} \equiv [1 - \exp(-\Sigma_a D)]\ (\text{WATE}) \quad \text{(C-11)}$$

This value is tallied and added to previous neutron absorption probabilities, and the neutron is killed. No account is taken of second- and higher-order scattering using this method. However, detector medium macroscopic scattering cross section is so small ($\sim 10^{-6}$ cm^{-1}) in this study that second- and higher-order scatters in the medium are extremely remote. At the end of the run, SDATA is called again and it prints out the number of neutrons detected and a standard deviation.

Major Modifications to 05R

05R.—Subroutine 05R is the control routine for program 05R. It has been modified to:

1. Allow use of the original 05R program output subroutine and sample program output subroutine in the same program by proper card input selection of an index for NTESTX.*

2. Call ADDNTS, entry point into SDATA, with proper selection of index for NTESTX, NCTYPE, and MEDX.* MEDX is the medium in which tabulation of neutrons will take place. The particular subroutine called to do this tabulation depends on the values of NTESTX and NCTYPE.

3. Tabulate and print out for each run:

a. The total number of elastic collisions [UNUSED (6)].
b. The total number of inelastic collisions [UNUSED (7)].
c. The number of times INELAS is called but neutron energy is below lowest Q value of collided target nucleus [UNUSED (8)].
d. The number of neutrons that escape from the system without being killed in MEDX.

INPUT.—Subroutine INPUT reads all card input for 05R (except that required by the geometry package) and reads the first records from STAPE and PTAPE (see Fig. C-1). These records contain the control information for their respective data sets. It has been modified to:

1. Read the first record from 05R DATA TAPE. This record is the number of neutrons that have parameters on the tape.

2. Read the logical number of ITAPE from card input, then read ITAPE's first record.

3. Use the mass of a neutron based on the C^{12} scale rather than the 0^{16} scale.

4. Read Q values from card input for those elements experiencing inelastic collisions.

5. Read from card input the raw neutron energy spectrum data.

6. Read from card input MEDX, NTESTX, NGPCUT, XOFF, ZOFF, PANGLE, RCUT, THECUT, CTYPE, and HISTN—all of which are control parameters in various subroutines (an explanation of each is available on request to the Program Director, NCHRP).

Minor Modifications to XSECT Subroutines

1. CODE 1, 1A, and 2. The original versions of these subroutines were designed to read a Master Cross-Section Tape whose raw cross-section data were stored on the tape in binary form. In this study unknown computer incompatibilities prevented the Triangle Universities Computation Center (Research Triangle Park, N.C.) IBM 360/75 from reading a binary tape produced by Oak Ridge National Laboratories (Oak Ridge, Tenn.) IBM 360/75. Therefore, a Master Cross-Section Tape written in card image was used. Modifications to CODE 1, 1A, and 2 reflect this change.

2. CODE 7B. Subroutine CODE 7B averages neutron cross sections across each subgroup, including now, inelastic scattering cross-section subgroups. The addition of this requirement by CODE 6 (described previously) forced some modifications to CODE 7B.

Minor Modifications to 05R Subroutines

1. GETNC. Instead of just calling EXIT when a subgroup is out of its supergroup range, subroutine GETNC prints out some information that may be helpful in diagnosing the problem.

2. MSOUR. Subroutine MSOUR has been modified to pass control to either SDATA or SOURCE, depending on the value of the control variable NTESTX and parameter ESOUR (see "New Subroutines in 05R"). It also allows for biasing of all PART I source neutron velocity vectors in either the positive or negative Z direction, depending on the value of the control variable YOFF.

3. NXTCOL. Subroutine NXTCOL has been modified to allow the values of control parameters MEDX, NTESTX, and NCTYPE to determine when and if subroutine SPECTM and entry point CTNUTS will be called.

4. READR and RWCON. Modifications to subroutines READR and RWCON reflect the addition of an ITAPE DATA SET read and rewind requirement.

5. SCATR. Subroutine SCATR modifications do the actual indexing of UNUSED (6) and UNUSED (7) (see "Major Modifications to 05R").

6. Labelled common statements MEDIA and MDELEM have been modified wherever they appear in a subroutine. In order to increase the number of elements allowed per medium without changing over-all computer memory stor-

* Available on request to the Program Director, NCHRP.

age requirements, the limiting values of 8 elements per each of a maximum of 16 mediums were changed to 16 elements in each of 8 mediums.

Subroutine Deletions

Unused subroutines were deleted from XSECT and 05R to conserve computer storage.

1. The following subroutines were deleted from the original program XSECT:

BNL325	LOGLOG	TENS
BTENS	LETTER	RS
BXTENS	POINT	YS
DATE	CURVE	MBE
LINEAR	ADVANC	EXPON
SEMLOG	XTENS	CODE 9 *

2. The following subroutines were deleted from the original 05R program:

BANKR *	FSOUR *
DATE	FSTRT *
FBANK *	KINNY
FPROB *	OUTPT (sample problem) *

Computer Utility Programs

FORTRAN IV statement listings and required card input information for the utility programs are not reproduced here but are available on request to the Program Director, NCHRP.

Program EDIT

Program EDIT can be used to perform a number of functions.

1. It will sequentially store, on permanent disc or tape storage, output data sets from PART I geometry, adding new data sets to those already there if necessary.
2. It will prepare the input data set for PART II geometry from data in permanent disc or tape storage.
3. By proper selection of card input data, EDIT will "edit" permanent storage data before placing it in PART II geometry's input data set. Card input values for EGPCUT, RCUT, THECUT, and WTCUT are the "edit parameters." If the neutron energy, position radius, or elevation angle is greater than EGPCUT, RCUT, or THECUT, respectively, or its weight less than WTCUT, the neutron will not be added to the input data set. In this study this tool was used to delete those neutrons from consideration in PART II that would contribute little or nothing to detector count rate, yet take up precious computer time and space. However, such a technique could have more general application in further research, particularly with relation to EGPCUT and WTCUT.

Program TRANSF

In the interest of conserving computer time, the STAPE, PTAPE, and ITAPE output data sets from program XSECT could be generated once for a given set of input data and placed in permanent disc storage. Then they could be called up time and again for use by 05R. This was a valuable technique for use in debugging program 05R. The technique was also used in Monte Carlo experimental data generation, because PART II geometry and medium (detector) were invarient in this study. Hence, the XSECT output data sets could be generated for this configuration once and then stored.

A peculiarity of the local IBM 360/75 system made it more economical if these data sets were transferred to temporary storage in the computer in the job step prior to running the 05R program. Copies of the data sets were still retained in permanent storage. Program TRANSF performs this transfer function. Because only STAPE is needed in PART II geometry, the program is also written so that proper card input will cause its transfer only.

Program TRANSX

Program TRANSX is another outgrowth of the computer incompatibility problem and of the peculiarity mentioned in the previous paragraphs. The cross sections on the Master Cross-Section Tape have already been manipulated by subroutine CODE 1 and are ready for immediate use by subroutine CODE 6 (CODE 1 and CODE 6 being subroutines in program XSECT). Like program TRANSF, TRANSX transfers data from permanent storage (in this case Master Cross-Section Tape) to temporary storage just prior to the job step that runs program XSECT. Card input dictates the actual procedure. Note that in this program the Master Cross-Section Tape is unit 10 and temporary storage is unit 9.

Program DISPLAY

Program DISPLAY exhibits information gleaned from 05R DATA SET (described previously). This particular program will read information from 05R DATA SET into computer memory, edit out those neutrons and neutron parameters not required as indicated by card input, and then display results in a tabular and/or graphic format (available on request to the Program Director, NCHRP).

1. The tabular display lists the cumulative weighted number of neutrons appearing at the surface versus their radius from the source in increasing value of radius (R).
2. The graphic format displays the cumulative weighted neutron yield as a function of radius from the source.

MONTE CARLO EXPERIMENTAL PROCEDURE

General Procedure and Rationale

Early in the study it became clear that yield from a straightforward Monte Carlo experiment would not be significantly high enough to give reasonable statistical variance; that is, the detector-to-source yield inherent in the physical experiment would be on the order of 10^{-3} even for the best "soil medium," pure water. Therefore, about 1,000 histories would have to be laboriously followed to produce but one count in the detector. Following 100,000

* The respective SUBROUTINE, RETURN, and END statements are left in for these subroutines, because other subroutines call them in the normal course of a run.

histories to get even a 10 percent relative standard deviation would require too much computer time.

With the following variance reduction technique, relative standard deviations of 4 to 5 percent could be obtained on pure water in a reasonable computer run time. The technique is based on the theory that the frequency distribution of neutrons coming back out of the surface of the soil is independent of the azimuthal angle (θ) about the center of the system (see Fig. C-4). This should be true if the neutron source is an isotropic emitter and if the soil medium is homogeneous.

Therefore, a relatively small number (~ 500) of neutrons leaving the soil surface at various angles θ could be placed on a ray emanating from the system center (neutrons maintaining their relative radial position) and still be said to accurately represent the number of neutrons that would appear along that radius in an experiment with strong neutron sources (10^4 neutrons/sec). This is providing, of course, that the neutron sample leaving the surface is within statistically precise limits. That is, the representation would increase in accuracy as the size of the sample is increased. If the representation is accurate, this same neutron aggregation can be placed on any number of rays around the system center, equally spaced in θ through 360°, and accurately describe the total neutron population coming out of the soil.

This technique was applied to the problem in the following manner. A series of 1,000 history runs were made using the modified 05R code, and the parameters associated with each neutron leaving the soil surface were tabulated and stored. This was labelled PART I of the procedure and is described more fully in the following section. PART II of the procedure consisted of placing the neutrons from PART I on rays (normally 40 rays, 9° apart) about the center of the system using subroutine SDATA (described previously), and then following their histories until they were either "detected" or left the system. A more detailed description of PART II follows. On the average, 500 neutrons came out of the soil surface. This number times 40 yielded a healthy 20,000 source neutrons for PART II. Because most of PART II geometry consists of void space, the computer run time per history is about one quarter of that for a PART I history.

Another variance reduction technique used in Part I was to "emit" all source neutrons in the negative z direction (i.e., into the soil). Therefore, although 2,000 neutrons were emitted isotropically, only 1,000 neutrons passed into the soil medium, and their histories followed. A single run, that followed 1,000 neutrons with positive z velocity vectors, was made to determine their contribution to detector counts. This contribution would be the same for all soil mediums.

The same modified 05R program described previously can be used to run both PART I and PART II. In this study the modified 05R program designated as 05RA was again slightly modified by deleting subroutine SPECTM and calling the resultant program 05RC. 05RC was then used to process PART II geometry histories. This was done to conserve computer memory, making more of it available for storage of neutron parameters.

Geometry Description PART I

The package of subroutines included in program 05R which accomplish the tracing and tallying of neutron paths through a system is called GEOM. The initial step in the description of a system for GEOM is to enclose the entire system in a rectangular parallelepiped whose faces are parallel with the xy, yz, and xz coordinate planes. This parallelepiped is then divided into several smaller parallelepipeds, called zones, by planes parallel to the coordinate planes and extending entirely across the system. The zones in turn are then divided into smaller parallelepipeds, called blocks, by planes again parallel to the coordinate axes but extending only across individual zones. Quadric surfaces

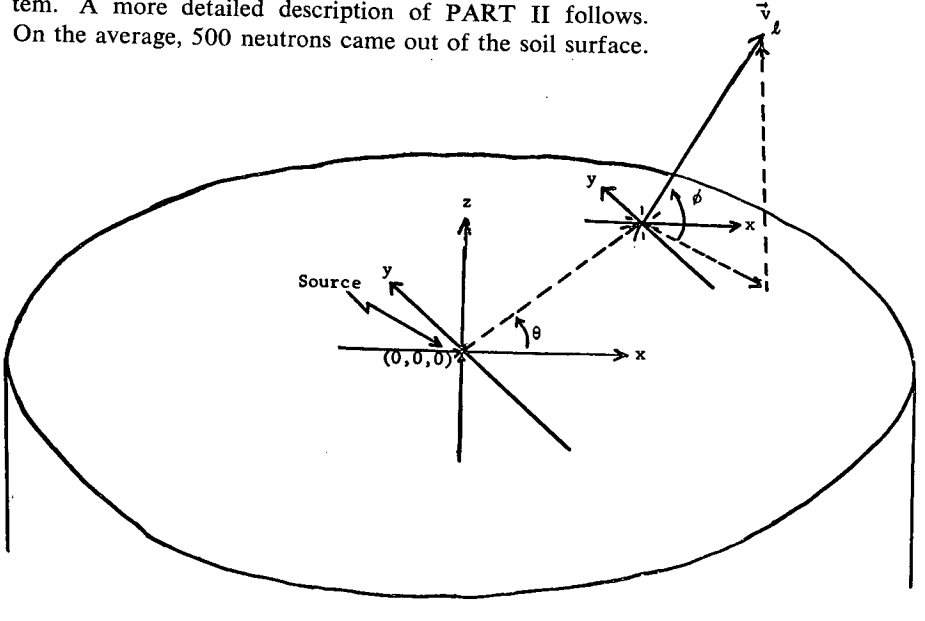

Figure C-4. Experimental theoretical geometry.

can then be inserted into individual blocks. A quadric surface is defined by the zeros of a quadratic function, and divides all space into two sectors. There may be only one medium per sector. Most of the foregoing discussion is taken from 05R Code *User's Manual.*

The geometry of the system used in this study (see "Experimental Procedure," which follows) is divided into two parts for simulation by the Monte Carlo Code. PART I consists of the plexiglass, soil, and neutron source. It is represented by Figure C-5 in the form required by GEOM. Some, but not all, of the dimensions are included for reference. The printout of the geometry description read into GEOM is available on request to the Program Director, NCHRP. All space not bounded by the parallelepiped is "Exterior Void," and neutrons finding themselves in an Exterior Void are killed by the program. That volume inside the parallelepiped, but outside the two cylinders, designated by MED = 0, is also Exterior Void. The rectangular-shaped volume sitting on top of the plexiglass medium is considered "Interior Void" and designated MED = 1,000. It is in this medium that the tallying for PART I takes place as soon as a neutron crosses the boundary between plexiglass and Interior Void. Note also that the neutron source is simulated by a point source just below the surface of the plexiglass. This approximation is reasonable, because the source volume is comparatively small. MED = 1 and 2 are the plexiglass and soil mediums, respectively. Their composition is defined by the STAPE, PTAPE, and ITAPE data sets, described previously. A neutron history is followed throughout this system until it escapes from it or passes into either medium 0 or medium 1,000.

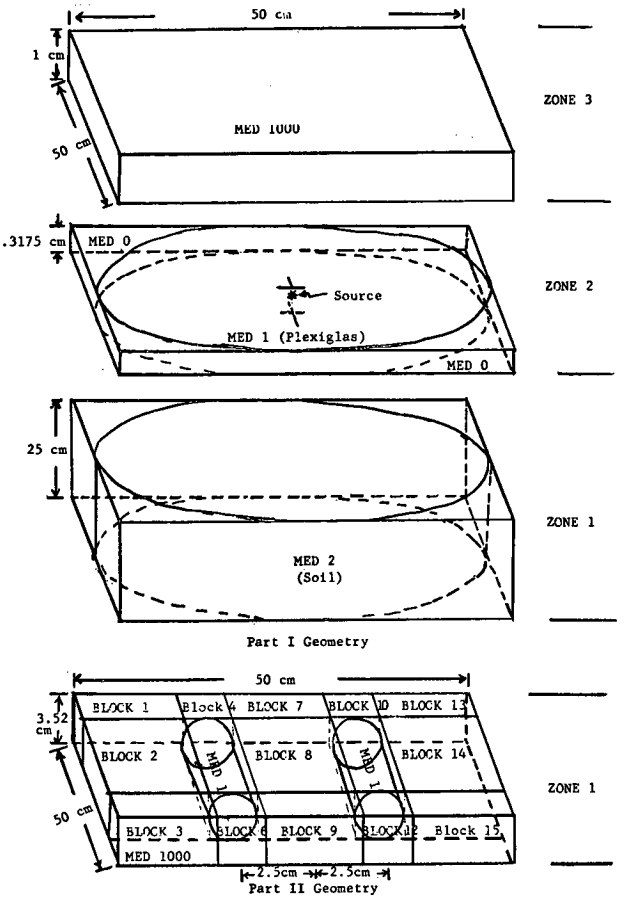

Figure C-5. Monte Carlo code stylized PART I and PART II geometry.

Geometry Description PART II

In PART II geometry, the parallelepiped encompasses a system consisting only of two cylindrical thermal neutron detectors and imaginary line neutron sources on rays located in the horizontal plane and emanating from the center of the system. The stylized geometry required by GEOM is shown in Figure C-5. (For a brief discussion of geometry construction used in GEOM refer to the previous paragraphs.) MED 1 in the BF_3 gas medium defined by a STAPE data set generated by program XSECT. PTAPE and ITAPE data sets are not required to define this medium. An approximation is made that any scattering or absorption due to the brass containment cylinders of the detectors is negligible. Therefore, it does not appear in the PART II simulated geometry. That part of the system outside the cylinders but inside the parallelepiped is Interior Void, MED = 1,000. Here the neutrons travel unattenuated until they leave the system or enter the detector mediums. Counting is done in the detector mediums. This is a different role from that played by mediums 1 and 1,000 in PART II geometry.

Monte Carlo Source Yield

If the source emits 2,000 neutrons in a perfectly isotropic manner, 1,000 of them will start down into the soil. If of that 1,000, 500 come back out of the soil surface (more exactly, the plexiglass surface) and are placed on 40 equally spaced rays, then their number is now effectively 20,000. If those 20,000 are allowed to leave the plexiglass surface in their predestined directions to ultimately cause 40 counts to register in the detectors, then the Monte Carlo source yield (Ym) is simply:

$$\mathrm{Ym} = \underbrace{\frac{500}{2{,}000}}_{\text{PART I}} \times \underbrace{\frac{40}{(500)(40)}}_{\text{PART II}} = 5 \times 10^{-4}$$

The Probability Addition method was used to determine detector counts. This technique then raised the question of how to attach a statistical error to the detector counts, since variance reduction techniques made a calculation based on a simple Poisson distribution suspect. Because no agreeable, straightforward method was evident, a relative standard deviation was calculated for a variety of soil mediums using the general statistical estimator for each 1,000 history run,

$$\sigma(n) = \left[\frac{1}{N-1}\sum_{i=1}^{N} (n-n)^2\right]^{\frac{1}{2}}$$

in which

N = number of 1,000 history runs (9);
n_i = number of detector counts registered in run i;

$\bar{n}$ = average number of detector counts per 1,000 histories; and
$\sigma(n)$ = standard deviation of the number of detector counts of any 1,000 history run.

Then the relative standard deviation for all runs was obtained from

$$\frac{\sigma(\bar{n})}{n} = \frac{\sigma(n)}{\bar{n}\sqrt{N}}$$

in which $\sigma(n)$ is the standard deviation of the best estimate of n from all runs.

The Monte Carlo method was used in an investigation to ensure that the Probability Addition method was not biased. The results of this investigation and of the aforementioned standard deviation calculations appear in the section on "Experimental Results and Correlation."

Sample Run

The sample run is demonstrated on the 32 w/o CH_2 + 68 w/o SiO_2 soil medium. The physical experimental data required by the Monte Carlo code comes from the results of the "Sample Calculations" which follow and are reproduced in Tables C-8 and C-9.

A Monte Carlo run in this study requires data cards for programs TRANSX, XSECTA, and 05RA (including GEOM) and subsequently for programs TRANSF, EDIT, and 05RC (including GEOM).* Program XSECTA is the new modified version of XSECT. The procedure is as follows:

1. Prepare input cards for program TRANSX designating which element's cross sections will be made available from the Caster Cross-Section Tape for use by XSECTA.

2. Prepare input cards for program XSECTA, specifically for CODE 6 and CODE 8. (The list of input cards is available on request to the Program Director, NCHRP. Note that the atom densities are punched on the CARD D's for each medium.) Plexiglass atom densities were previously determined and are invariant in this study.

3. Prepare input cards for program 05RA. This will include GEOM input cards describing PART I geometry. (The list of input cards is available on request to the Program Director, NCHRP.) SLOTH and SLOPS are punched on the CARD F's for each medium. Now run programs TRANSX, XSECTA, and 05RA sequentially to produce ultimately nine separate data sets from runs of 1,000 histories each. In this case the data sets are stored on disc for eventual permanent storage on tape.

4. Prepare input cards for program TRANSF. This will transfer the previously generated detector medium's STAPE data set from permanent to temporary storage in readiness for the PART II run.

5. Prepare input cards for program EDIT. Neutrons with radii in excess of 16 cm and elevation angles greater than 45° can never intersect the detectors no matter what the value of θ. So, RCUT = 16. and THECUT = 45. will delete these neutrons from contention. However, it is not desired to delete a neutron based on its energy or weight. Therefore, EGPCUT = 10^9 eV and WTCUT = 0. With INDEX = 3 and L = LL = 1, only the first data set will be read into memory, manipulated by the "Cutoff Parameters" and stored as the PART II input data set.

6. Prepare input cards for program 05RC. (The list of input cards is available on request to the Program Director, NCHRP.) This includes those for GEOM. SLOTH and SLOPS for the detector mediums were previously determined and are punched on CARD F.

7. Run programs TRANSF, EDIT, and 05RC sequentially to calculate detector counts. Counting is done using the Probability Addition method and yields 183.595.

8. Calculate Monte Carlo yield (Ym):

$$\mathrm{Ym} = \frac{1}{18{,}000} \times \frac{183.595}{40} = 2.5499 \times 10^{-4}$$

PHYSICAL EXPERIMENTAL PROCEDURE AND APPARATUS

Apparatus

Sample Mixer and Scales

The ingredients for all samples were weighted out on a Fairbanks-Morse Company (Yonkers, N.Y.) Tel-A-Dial scales, Model No. B35. Weight could be read to the nearest 0.1 lb. Homogeneous mixing of the sample constituents was performed by a small Sears, Roebuck Company (Greensboro, N.C.) utility cement mixer, which could easily hold a 120-lb batch. The mixing drum was driven at 60 cpm by a ¼-hp AC motor.

Variable Speed Shaker

A variable speed shaker, manufactured by All American Tool and Manufacturing Co. (Skokie, Ill.), was used to uniformly pack all soil samples. It was driven by a variable-speed ½- to 1-hp AC motor and produced a vibration frequency range of 15 to 60 cps. The vibrating plate could be adjusted to give lateral back and forth motion with a maximum off-center displacement of 0.125 in. (see Fig. C-6).

Source

The source was a 1.1 millicurie ^{226}Ra-Be neutron source doubly incapsulated in 304 stainless steel. The container was a cylinder with outside dimensions of 0.356 in. in diameter by 0.572 in. in length. The active material was located on a horizontal disc approximately 3 mm above the base of the container. Atomic Energy of Canada, Ltd. (Ottawa, Canada) specified the neutron emission rate to be 1.77×10^4 neutrons per second at time of production in 1957. This figure is in good agreement with the Radium Millicurie value (Anderson, 1948; Marion and Fowler, 1960).

* Utility program statements and card input descriptions for programs EDIT, TRANSF, TRANSX, and DISPLAY are available on request to the Program Director, NCHRP.

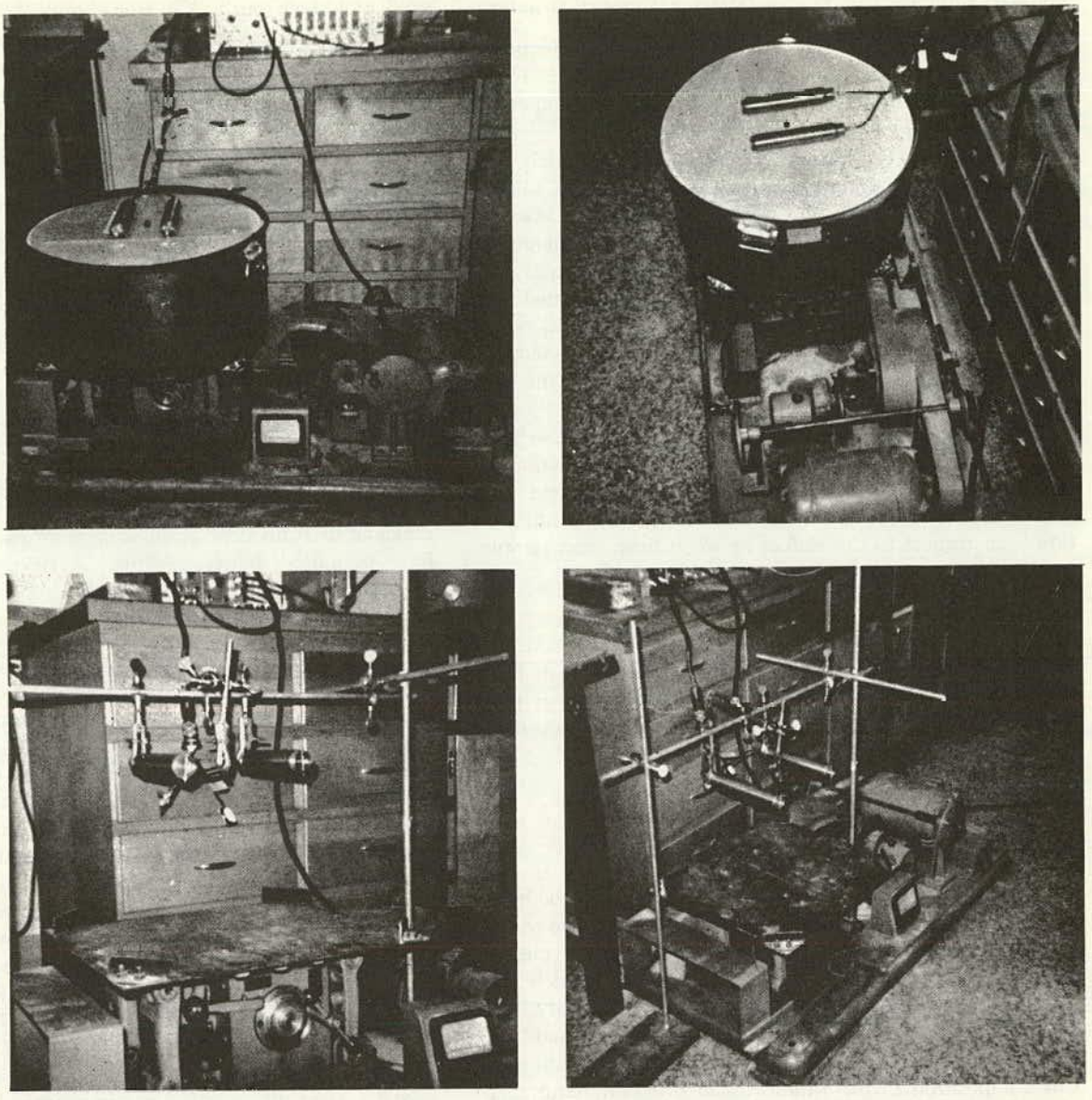

Figure C-6. Physical experiment apparatus.

This source was calibrated against a 3-mc Ra-Be source manufactured by AECL in 1965. The 3-mc source served as a calibration standard for Troxler Electronics, Inc. (Raleigh, N.C.). As a result of this calibration, the neutron emission rate of the source used in this study was recalculated to be 3.295×10^4 neutrons per second. This was the emission rate value used throughout this study.

Counting Equipment

A portable scaler and preamplifier from a commercial combination density/moisture gauge, Model 1602, built by Troxler Electronics, Inc., was used for all sample measurements. The two BF_3 proportional counters manufactured for Troxler by Nancy Wood Laboratories have the following pertinent physical characteristics:

Gas medium	BF_3, 96 percent enriched B^{10}
Pressure	25 cm Hg abs.
Casing	Brass
Sensitive volume:	
Inside diameter	3.49 cm
Length	16.91 cm

The detectors plateaued for thermal neutrons at 1,150 volts and had a plateau length of about 300 volts, and a recommended operating voltage of 1,300 volts. The scaler had a built-in timer designed only for 1-min count intervals. This device was checked frequently against an ORTEC Motor Driven X-ray Time Switch, Model 42, Oak Ridge, Tenn. The scaler's batteries were recharged after each counting session by a simple attachment to a 115 VAC receptacle. The manufacturer recommended making all measurements without this attachment.

Sample Container and Source-Detector Support Structure

Sawed-off steel 55-gal drum bottoms, 23 in. in diameter and 12 in. high, held the soil samples (Fig. C-6). Their volume was accurately determined and used in conjunction with sample weight to calculate medium density.

A plexiglass (ROHM-HAAS) disc approximately 56 cm in diameter and 0.3175 cm thick served as a source and detector holder. It was perforated with No. 3 screw holes strategically placed to allow repeatable alignment of the detectors at various distances from its center. A larger hole in the center of the disc accommodated the cylindrical source. The bottom of this hole was taped over so that when the disc rested flat on the soil medium the tape was between the base of the source and the soil surface.

Stands, supports, and clamps shown in Figure C-6 performed for background measurement the same function as the disc did for soil measurement. That is, detector and source were maintained in the same repeatable configuration with respect to the shaker as when drum and sample were present.

Sizing Equipment

A NUMINCO shaker was used in conjunction with U.S. Standard Sieves (Pittsburgh, Pa.) from 841- down to 125-micron size for sizing determinations on sand, polyethylene, and iron.

Experimental Procedure

Selection of Components for Soil Samples

Components for the soil medium were selected on the basis of their economical availability, frequent occurrence in the earth's crust, stability, nuclear characteristics, and chemical purity. Some pertinent characteristics of each are given in Table C-1. Economical availability, stability, and frequent occurrence in the earth's crust made sand an obvious choice. The necessity for accurate simulation of soil composition in the Monte Carlo program required a sand of known purity. A silica sand (SiO_2) was readily available, and activation analysis of representative samples indicated that impurities constituted no more than 1 to 2 ppm. A high-purity iron was chosen for its relatively high neutron absorption cross section over a wide energy spectrum and its frequent occurrence in soils. Polyethylene (CH_2) provided the "moisture" constituent. As an alternative to water, it proved superior in almost every respect. Past attempts at preparing stable soil standards with variable moisture contents were complicated by evaporation of water located close to the surface and its settling to the bottom at the higher moisture ratios. It would also act to oxidize metals, again complicating Monte Carlo simulation. On the other hand, using polyethylene avoided these problems and provided a more attractive hydrogen-to-carbon weight ratio than that of hydrogen to oxygen. A drawback was the decrease in sample specific density with an increase in the weight percentage of polyethylene. Although an effort was made to obtain sand, iron, and polyethylene of equivalent grain size, more careful sizing may have permitted denser packing. A sieve analysis of the constituents is given in Table C-2.

Preparation of Samples

Each constituent of a given soil sample was carefully weighed out to the nearest 0.1 lb, and combined with the other components, and the mixture was homogeneously blended in the cement mixer for 30 to 35 min. Normally, two and sometimes three batches of each soil sample were prepared in this manner. All of the batches were then combined in a drum and packed by the shaker for 15 to 20 min. Shaker settings were 17 cps with 0.05-in. lateral movement off center. The plexiglass disc was placed on the surface of the sample and light pressure was applied during the shaking operation to prevent the top ¼ to ½ in. of sample from vibrating its way over the lip of the drum. There was some slight evidence of constituent separation and inhomogeneous mixing in this top layer after shaking. However, the rest of the sample remained uniformly mixed. After all counting measurements had been taken on a particular soil medium, its volume was determined from a bench mark around the inside of the drum and the sample was weighed. Bulk density was calculated. Table C-3 gives a breakdown of percent by weight (w/o) of every constituent in each of the ten samples.

TABLE C-1

SOIL CONSTITUENT CHARACTERISTICS

MATERIAL	CHARACTERISTICS	SOURCE
Silica sand (SiO_2)	Crushed quartz with 1 to 2 ppm metallic impurities	Cast-A-Stone, Inc. (Raleigh, N.C.). Quarried near Sandhills, N.C.
Polyethylene (CH_2)	Texite Polyethylene low-density formula, apparent density 0.923 gm/cm³	Plastics Division Eastman Chemical Products, Inc. (Kingsport, Tenn.).
Iron (Fe)	I-60, Iron Powder (Electrolytic-Pure) 99+percent pure	Fisher Scientific Co. (Fair Lawn, N.J.)

TABLE C-2

CONSTITUENT COMPARATIVE SIEVE ANALYSIS

W/O LESS THAN (MICRONS)	CONSTITUENTS		
	SiO_2	CH_2	Fe
841	99.8	100.0	100.0
595	94.0	100.0	100.0
250	40.0	56.1	100.0
177	18.1	24.1	99.7
125	6.7	4.3	94.7

Source-Detector-Soil Medium Geometry

The simplest possible physical geometry was devised in order to ease the Monte Carlo simulation of that geometry. Figure C-6 shows the relative location of detectors, plexiglass disc, and soil medium. The plexiglass disc rests evenly and solidly on the smooth surface of the soil medium. The neutron source capsule fits tightly into its hole in the center of the disc, with the base of the source flush with the bottom of the disc. The two detectors lie flat on the disc and are affixed to it. They straddle and are equally spaced from the source with their axes parallel to each other. The soil medium is a cylinder approximately 57 cm in diameter and 26 cm deep contained in the open drum.

This apparatus rests in the drum bracket of the variable speed shaker, and all soil measurements are taken with equipment in this repeatable geometry. The stands, supports, and clamps arrayed around and above the shaker are used to hold the two detectors and neutron source in repeatable geometry for measurement of background radiation. In this case the drum and soil medium are absent, but source and detectors are maintained in the same relative positions with respect to the shaker.

Counting Procedure

Once the geometry was established for each soil sample, the Troxler counting equipment was used to take a series of 1-min counts. Sufficient 1-min counts were taken to ensure a relative standard deviation in count rate of less than 3 percent. A less-than-1-percent relative standard deviation was obtained at the higher moisture contents. Such mundane considerations as laboratory space and equipment availability, unshielded source criteria, and experimenter fatique precluded longer counting sessions (20 hr versus 2 hr). A breakdown of a typical counting session, in chronological order, is as follows:

NO. OF 1-MIN COUNTS	MEDIUM	PERP. DIST. BETWEEN DETECTOR AXES (CM)
20	Background	5
20	Soil sample	5
10	Soil sample	12
10	Soil sample	20
10	Background	5
10	Background	12
10	Background	20

Calculation of Source Neutron Yield

Neutron source calibration yielded a neutron emission rate of 3.295×10^4 neutrons per second. Experimental source yield (Ye) is then simply determined by

TABLE C-3

CONSTITUENT WEIGHT PERCENT BREAKDOWN AND SAMPLE DENSITY

SAMPLE NO.	CONSTITUENT (W/O) SiO_2	CH_2	Fe	H_2O	SAMPLE DENSITY (GM/CM^3)
1	92	8	—	—	1.3350
2	84	16	—	—	1.0779
3	76	24	—	—	0.9123
4	68	32	—	—	0.8239
5	53	32	15	—	0.86317
6	61	24	15	—	0.98743
7	69	16	15	—	1.2057
8	77	8	15	—	1.4657
9	—	—	—	100	0.99883
10	100	—	—	—	1.58999

$$Ye = \frac{R \pm \sigma}{N} \qquad \text{(C-14)}$$

in which R ≡ soil medium net count rate = gross count rate − background count rate (cpm).
Also,

$$\sigma = \sqrt{\frac{R}{T} + \frac{R_b}{T_b}} \qquad \text{(C-15)}$$

in which

$N \equiv$ neutron source emission rate (dpm);
$R_p \equiv$ background count rate (cpm);
$T \equiv$ count interval on soil medium (min);
$T_b \equiv$ background count interval (min); and
$\sigma \equiv$ standard deviation (cpm).

Sample Calculations

Atom Density Calculation

To correlate the experimental source yield with the yield from the Monte Carlo program, the atom density of each element in a soil sample had to be accurately calculated from the physical experiment data. The procedure used to mix a sample and subsequently calculate those densities is demonstrated here using raw data from Sample No. 4 (see Table C-3).

In the interest of conserving some rather expensive soil materials, each new sample was constructed using a portion of the previous sample. In this case some CH_2 would have to be added to the 76 w/o SiO_2 + 24 w/o CH_2 sample to create a 68 w/o SiO_2 + 32 w/o CH_2 sample. By knowing the weight of the previous sample ($W = 125.3$ lb), the following calculation could be made to determine the required addition of CH_2(C′).
Because

$$W_{SiO2} + W_{CH2} = W \qquad \text{(C-16)}$$

* Weight and volume of sample could be measured to only four significant digits. More digits were carried in subsequent calculations as a hedge against round-off error and as a convenience. Thermal neutron cross-section data used in all calculations is the latest appearing in *BNL-325*, 2d ed. (1958), plus supplements 1 and 2, 1960, 1964, and 1966.

i.e.,

$$0.76W + 0.24W = W \qquad \text{(C-17)}$$

Also,

$$0.68W' + 0.32W' = W' \qquad \text{(C-18)}$$

in which

$W' \equiv$ new total weight of 68 w/o SiO_2 + 32 w/o CH_2; and

$$W' = W + C' \qquad \text{(C-19)}$$

and because no SiO_2 was being added or subtracted in this process,

$$0.76W = 0.68W' \qquad \text{(C-20)}$$

Substituting Eq. C-20 in Eq. C-19 yields

$$C' = (0.76/0.68 - 1)W \qquad \text{(C-21)}$$

and substituting for W yields $C' = 14.74118$

The contents of each cement mixer batch are given in Table C-4.

Weight (W') of the sample after packing by the shaker into the known volume ($V = 2.3428421$ ft^3) of the drum was 120.5 lb. Note that not all of the mixed sample could be accommodated in the drum. However, what there was homogeneously mixed in the desired proportions of SiO_2 and CH_2; i.e.,

Sample Bulk Density (ρ_{comp}) $\equiv W'/V = 0.82388156$ gm/cm^3

Weight percentage of elements in the SiO_2 and CH_2 compounds are given in Table C-5.

The weight fraction of each element in the sample was then determined and is given in Table C-6. For example, w/f of Si $= (0.68)(0.4674393) = 0.317858724$.

From the foregoing data, atom density of each element in the soil medium was calculated from

$$N = \frac{\text{w/f}\,\rho_{comp}\,N_a}{A} \qquad \text{(C-22)}$$

in which $N_a \equiv$ Avogadro's Number, and e.g.,

$$N_{Si} = \frac{\text{w/f}_{Si}\,\rho_{comp}\,N_a}{A_{Si}} \qquad \text{(C-23)}$$

and

$$N_{Si} = \frac{(0.317858724)(0.82388156)(0.6024 \times 10^{24})}{28.086}$$

$$= 0.005616865 \times 10^{24} \text{ atoms/cm}^3$$

Table C-7 gives the atom densities for each element.

Calculation of Thermal Mean Free Path and Scattering Probability

Soil medium thermal mean free path (mfp) and thermal neutron scattering probability (P_S) were other input parameters required by the Monte Carlo program. Their calculation follows for Sample No. 4.

Thermal mean free path:

$$\Sigma_T = N_C\bar{\sigma}_C + N_O\bar{\sigma}_O + N_{Si}\bar{\sigma}_{Si} + N_H\bar{\sigma}_H \qquad \text{(C-24)}$$

where $\bar{\sigma}$'s are mean thermal total cross sections; e.g.,

$$\Sigma_T = (0.01132223)(4.8034) + (0.01123373)(4.2) + (0.005616865)(1.86) + (0.0226373)(38.332)$$
$$= 0.979747 \text{ cm}^{-1}$$

i.e., $\text{mfp} = \dfrac{1}{\Sigma_T} = 1.02067$ cm.

Scattering probability:

$$\Sigma_S = (0.01132223)(4.8) + (0.01123373)(4.2) + (0.005616865)(1.7) + (0.0226373)(38)$$
$$= 0.971294436,$$

$$P_S = \frac{\Sigma_S}{\Sigma_T} = 0.99137271$$

EXPERIMENTAL RESULTS AND CORRELATION *

Physical Experiment Results

Monte Carlo Code Input Parameters

Mathematical simulation of the physical system by the Monte Carlo code required some input parameters computed in the physical experiment. Those parameters for each soil sample are given in Tables C-8 and C-9.

Because the same detectors and plexiglass disc were used in experiments on all soil sample mediums, their atom densities and thermal parameters were invariant. Those parameters were calculated in the manner described previously in "Sample Calculations" and are given in Table C-10. The chemical composition of the plexiglass (methyl

* The yields, mean free paths, and nonabsorption probabilities listed throughout this section are accurate to only three significant figures. More figures are included here as a convenience.

TABLE C-4

SAMPLE NO. 4 CEMENT MIXER BATCH CONTENTS

BATCH	WEIGHT (LB) SiO_2+24 w/o CH_2	CH_2
1	41.77	4.91
2	41.77	4.91
3	41.77	4.91

TABLE C-5

WEIGHT FRACTION OF ELEMENTS IN SiO_2 AND CH_2

COMPOUND	ELEMENT (W/F) Si	O	C	H
SiO_2	0.4674393	0.5325606	—	—
CH_2	—	—	0.856282	0.143718

TABLE C-6

WEIGHT FRACTION AND ATOMIC WEIGHT OF ELEMENTS IN SAMPLE NO. 4

ELEMENT	WEIGHT FRACTION (W/F)	ATOMIC WEIGHT (A)
Si	0.317585724	28.086
O	0.362141208	15.9994
H	0.045975	12.01115
C	0.2740102	1.00797

TABLE C-7

ATOM DENSITIES OF ELEMENTS IN SAMPLE NO. 4

ELEMENT	ATOM DENSITY ($\times 10^{24}$)
C	0.01132223
O	0.01123373
Si	0.005616865
H	0.0226373

TABLE C-8

MONTE CARLO SOIL MEDIUM ATOM DENSITIES

SAMPLE NO.	ATOM DENSITY ($\times 10^{24}$ ATOMS/CM^3)				
	HYDROGEN	CARBON	OXYGEN	SILICON	IRON
1	0.009173	0.004587	0.02463	0.012314	—
2	0.014808	0.007406	0.01816	0.009078	—
3	0.018800	0.009403	0.01390	0.006951	—
4	0.02264	0.011322	0.01123	0.005617	—
5	0.02372	0.01186	0.009173	0.004586	0.001397
6	0.02035	0.01018	0.01208	0.006039	0.001598
7	0.01656	0.008285	0.01668	0.008341	0.001951
8	0.010068	0.005036	0.02263	0.01131	0.002371
9	0.066797	—	0.033398	—	—
10	—	—	0.03188199	0.015941	—

TABLE C-9

MONTE CARLO SOIL MEDIUM THERMAL MEAN FREE PATHS AND SCATTERING PROBABILITIES

SAMPLE NO.	THERMAL MEAN FREE PATH (CM)	SCATTERING PROBABILITY PER TOTAL INTERACTION PROB. (Σ_S/Σ_T)
1	2.0001	0.9899
2	1.4361	0.9908
3	1.1945	0.9912
4	1.0207	0.9914
5	0.9690	0.9882
6	1.0959	0.9870
7	1.2713	0.9852
8	1.7914	0.9800
9	0.3703	0.9918
10	6.1142	0.9844

TABLE C-10

DETECTOR AND PLEXIGLASS DISC MEDIUMS, MONTE CARLO CODE INPUT PARAMETERS

PARAMETER	DETECTOR	PLEXIGLASS DISC
(*a*) Atom Density ($\times 10^{24}$ atoms/cm^3)		
Boron-10	7.8826×10^{-6}	—
Boron-11	3.2844×10^{-7}	—
Fluorine	2.46331×10^{-5}	—
Carbon	—	0.0355392
Oxygen	—	0.01421588
Hydrogen	—	0.0568688
(*b*) Thermal		
Mean free path (cm)	32.922	0.4149
Scattering probability	0.0042	0.9921

methacrylate) is eight hydrogen atoms, two oxygen atoms, and five carbon atoms per mole with a nominal density of 1.18133 gm/cm^3.

Physical Experiment Yields

The term experimental yield (Ye) as used here refers to the ratio of count rate (cpm) registered by the detector equipment on a soil sample to neutron source disintegration rate (dpm). A yield was calculated for each of three detector configurations on each soil sample. The configurations were determined by the position of the detectors off the center line, either 2.5, 6, or 10 cm. So in each case the detectors were symmetrically positioned about and equidistant from the source at 5, 12, or 20 cm between detector axes. The yields are given in Table C-11 along with the hydrogen density of each soil sample.

TABLE C-11

PHYSICAL EXPERIMENT YIELDS AND HYDROGEN DENSITIES

SAMPLE NO.	HYDROGEN DENSITY (GM/CC)	YIELDS ($\times 10^{-4}$) (YE) FOR SOURCE-DETECTOR DISTANCES 2.5 CM	6 CM	10 CM
1	0.01535	0.8298 ± 0.0207	0.7754 ± 0.0229	0.6166 ± 0.0201
2	0.02479	1.7648 ± 0.0244	1.5650 ± 0.0302	1.2849 ± 0.0280
3	0.03147	2.2844 ± 0.0267	1.9954 ± 0.0338	1.5721 ± 0.0298
4	0.03789	2.9034 ± 0.0293	2.3986 ± 0.0366	1.9428 ± 0.0328
5	0.03970	2.6199 ± 0.0282	2.2347 ± 0.0354	1.8670 ± 0.0323
6	0.03406	2.2329 ± 0.0268	1.9256 ± 0.0331	1.7193 ± 0.0308
7	0.02773	1.7008 ± 0.0243	1.5154 ± 0.0300	1.1578 ± 0.0263
8	0.01685	0.7924 ± 0.0188	0.6501 ± 0.0220	0.6115 ± 0.0200
9	0.11177	9.482 ± 0.0505	6.008 ± 0.0562	3.020 ± 0.0401
10	0.0	0.581 ± 1.26×10^{-2}	2.782 ± 1.14×10^{-2}	0.759 ± 0.956×10^{-2}

Monte Carlo Code Results

Monte Carlo Experiment Yields

A Monte Carlo source yield (explained previously) was calculated for each soil sample for the 2.5-cm source-detector distance. A total of 9,000 initial neutron histories were followed into the simulated soil medium. This gave a "source" strength of 18,000 neutrons, assuming isotropic emission. The contribution of detector counts from the 9,000 initial histories in the positive Z direction was between one and two counts per 3,000 initial histories. This was considered negligible even for low-yield soil mediums. At any rate this contribution was effectively subtracted out of the physical experiment yields because it appeared as a portion of the background count rate. Therefore, to be consistent, it was not considered in the Monte Carlo yield calculation. The Monte Carlo yield for each soil sample appears in Table C-12. From Table C-13 the mean count is $\bar{n} = \frac{1}{N}\sum_{i=1}^{N}$, $\bar{n} = 18.333$ and the standard deviation (σ) using the general statistical estimator formula is

$$\sigma(n) = \left[\frac{1}{N-1}\sum_{i=1}^{N} 1(\bar{n} - n_i)^2\right]^{\frac{1}{2}} = 3.141$$

Comparing both methods:

Monte Carlo counts (MC) = 18.333

Probability Addition counts (PA) = 20.570

$$\text{Percent difference} = \left|\frac{\text{MC} - \text{PA}}{\text{MC}}\right| \times 100 = 12.2 \text{ percent}$$

and

Monte Carlo relative standard deviation (σ/MC) = 17.13 percent

The significance of the standard deviation is that the range $\bar{n} \pm \sigma$ represents the precision with which the detector counts of another 1,000 history run can be predicted. Specifically, there is a 68.2 percent probability that the next count will fall within $\bar{n} \pm \sigma$; a 95.4 percent probability it will fall within $\bar{n} \pm 2\sigma$; and a 99.7 percent probability it will fall within $\bar{n} \pm 3\sigma$.

Data Display and Additional Experimental Runs

PART I data (i.e., 05R DATA SET) were generated for nine additional soil samples (Sample Nos. 11 through 19).

TABLE C-12

MONTE CARLO EXPERIMENT YIELD [a]

SAMPLE NO.	COUNTS	YIELD ($\times 10^{-4}$) (YM)
1	48.507	0.6737
2	105.653	1.4670
3	146.430	2.0337
4	183.595	2.5499
5	169.936	2.3602
6	145.997	2.0277
7	115.986	1.6109
8	60.480	0.8399
9	713.062	9.9036
10	1.23	0.0170

[a] Based on 9,000 initial neutron histories with initial directions into the soil medium.

TABLE C-13

CALCULATION OF MEAN COUNT AND STANDARD DEVIATION FOR MONTE CARLO METHOD [a]

MONTE CARLO RUN NO. (i)	COUNTS (n_i)	$(\bar{n}-n_i)^2$
1	13	28.441
2	18	0.111
3	17	1.777
4	22	13.447
5	20	2.779
6	20	2.779
Total	110	49.334
Average	($\bar{n}$=18.333)	

[a] Based on 1,000 initial neutron histories directed into the 32 w/o CH_2 + 15 w/o Fe + 53 w/o SiO_2 (Sample No. 5) soil medium.

Each of the Sample Nos. 11 through 18 was identical to the Sample Nos. 1 through 8, respectively, given in Tables C-3 and C-11 except that water replaced the polyethylene in each case and all eight samples had a bulk density of 130 lb/ft^3 (2.0823998 gm/cc). The hydrogen density remained the same for each respective case. This manipulation changed other soil parameters of course, such as weight percentage of water in each of the eight new samples. Table C-14 gives pertinent characteristics of each sample.

The ninth additional sample (No. 19) was identical to Sample No. 5 in every respect except that oxygen in the form of water replaced carbon in the form of polyethylene. A Monte Carlo source yield was calculated for this run (2.5334×10^{-4}) and plotted in Figure C-7 along with source yields for Samples No. 1 through 8.

Tables of radii versus cumulative weighted number of neutrons and graphs of cumulative Monte Carlo source yields as a function of radii were constructed for all 19 soil samples using program DISPLAY (discussed previously).* A representative table and graph produced from soil Sample No. 4 data are available on request to the Program Director, NCHRP. Monte Carlo yields were also determined for Sample Nos. 11 through 18; they are given in Table C-14 and plotted in Figure C-8.

Monte Carlo Source Yield Variance Calculation **

The general statistical estimator is used to calculate the relative standard deviation of the average detector counts ($\bar{n}$) registered on a representative range of soil mediums. The relative standard deviation [$R(\bar{n})$] of the average detector counts is defined as

$$R(\bar{n}) = \frac{\sigma(n)}{\bar{n}\sqrt{N}} \qquad \text{(C-25)}$$

in which

$$\bar{n} = \frac{1}{N}\sum_{i=1}^{N} = n_i \qquad \text{(C-26)}$$

* Copies of these tables and graphs may be obtained from Dr. R. P. Gardner, North Carolina State University, Raleigh, N.C.

** Variance is another term by which statistical error can be represented and is equal to σ^2.

and $\sigma(n)$, n_i, and N are as defined previously in "Monte Carlo Source Yield."

Although the standard deviation of the Monte Carlo source yield is not equal to the standard deviation of the average detector counts, their respective relative standard deviations are equal. Therefore, the calculation of the relative standard deviation of the average count rate associated with a soil medium is representative of the precision with which the yield is known.

The soil mediums H_2O, 32 w/o CH_2 + 15 w/o Fe + SiO_2, and 8 w/o CH_2 + SiO_2 were selected because they cover the range of yields from all soil samples. The average count rates and relative standard deviations given in Table C-15 are based on nine independent runs of 1,000 initial source neutron histories each. Therefore, it can be said that the neutron yield calculated for the H_2O medium is known with a precision of ± 5.63 percent, and that the precision with which all the other soil medium yields are known is between 6 percent and 10 percent. The pure silica sand (SiO_2) medium is an exception.

Correlation of Monte Carlo and Physical Experiment Results

The physical neutron source yield (Ye) and the Monte Carlo neutron source yield (Ym) as measured at the BF_3 detectors are presented and compared in Table C-16 and Figure C-7 for Sample Nos. 1 through 10. Percent difference as used here is defined as

$$\text{Percent difference} = \left|\frac{\text{Ye} - \text{Ym}}{\text{Ye}}\right| \times 100 \qquad \text{(C-27)}$$

Sample No. 9 (H_2O) yield is not shown in Figure C-7.

SUMMARY AND CONCLUSIONS

As a result of this investigation (1) neutron thermalization in a soil medium was successfully simulated by a Monte Carlo statistical computer code; (2) a number of permanent soil/moisture calibration standards were prepared and tested; (3) a group of computer utility programs was developed for use in conjunction with the Monte Carlo Code for the purpose of generating data useful in design

TABLE C-14

COMPOSITION AND YIELDS OF SAMPLES NO. 11 THROUGH NO. 19

SAMPLE NO.	COMPOSITION (W/O)			HYDROGEN DENSITY (GM/CC)	MONTE CARLO YIELD (YM) $\times 10^{-4}$
	SiO_2	H_2O	Fe		
11	93.413	6.587	—	0.01535	1.1672
12	90.108	9.892	—	0.02479	2.2676
13	86.493	13.507	—	0.03147	2.9895
14	83.742	16.258	—	0.03788	3.6568
15	67.965	17.035	15.0	0.03969	2.9846
16	70.383	14.617	15.0	0.03406	2.5140
17	73.103	11.897	15.0	0.02772	1.8020
18	77.765	7.235	15.0	0.01686	0.8204
19	43.915	41.085	15.0	0.03968	2.5334

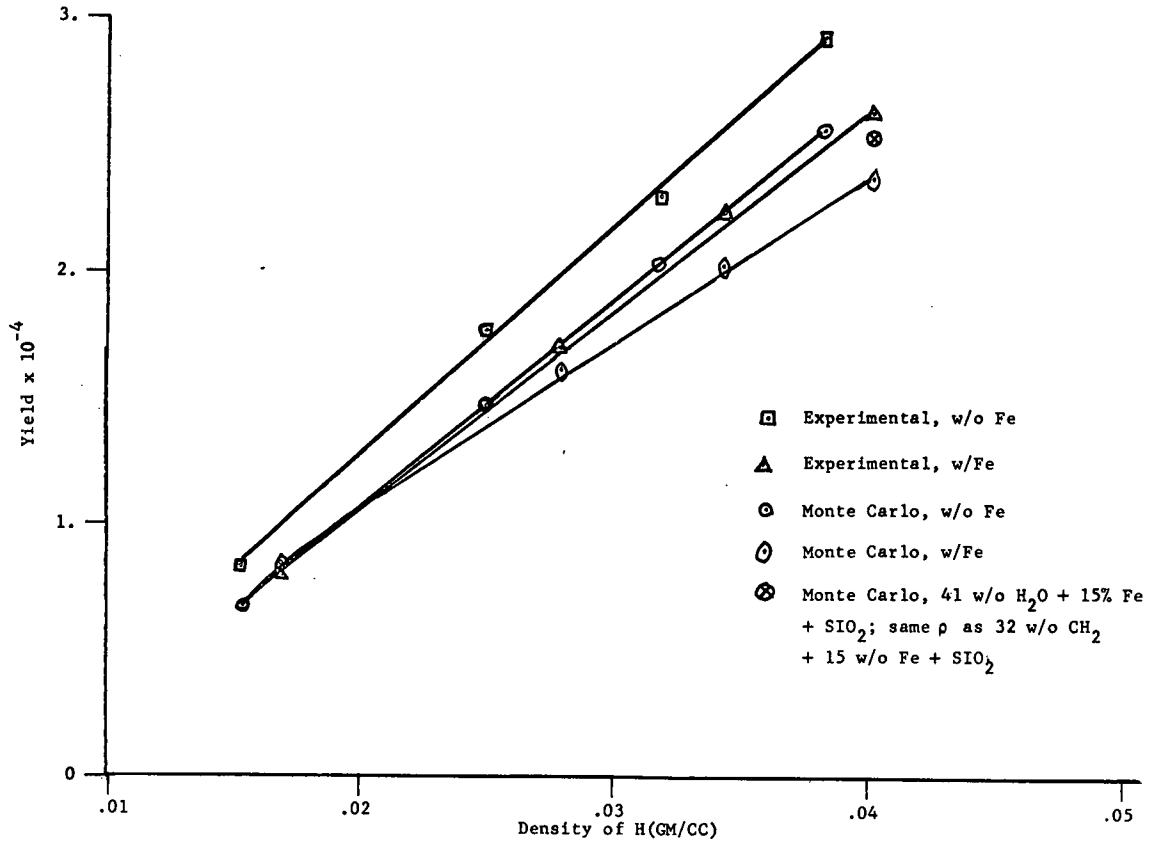

Figure C-7. Monte Carlo and physical experimental yield versus hydrogen density (gm/cc).18.

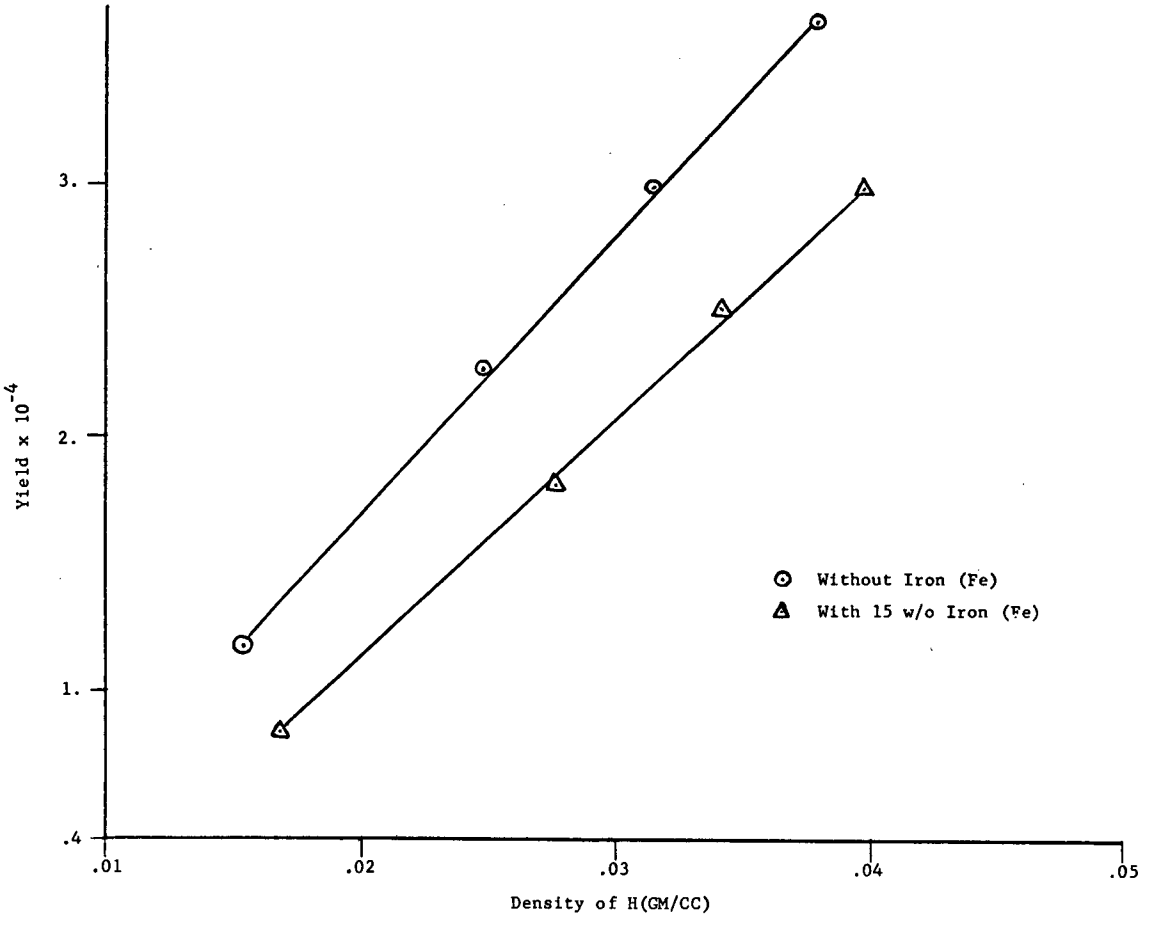

Figure C-8. Monte Carlo yields versus hydrogen density (gm/cc) for Sample Nos. 11 through

and calibration of gauges; and (4) some potentially useful design data were generated.

A correlation of physical and Monte Carlo experimental results on soil mediums of various combinations of polyethylene, iron, and silica sand produced an average relative difference of about 8 percent. The Monte Carlo experiment yields were consistently less than their respective physical experiment yields. A comparison of the yields from a pure silica sand sample was made, but statistical error in the precision of both measurements, physical and Monte Carlo, was too great to attach any significance to the results. It should be noted also that the physical experiment neutron source was calibrated against a standard source whose neutron emission rate was specified by the manufacturer as $4.4 \times 10^4 \pm 7$ percent neutrons/sec.

Hydrogen in the form of polyethylene was uniformly mixed into a silica sand or silica sand/iron soil medium to make four stable calibration standards, equivalent to a water/soil medium in every respect except that the hydrogen atoms are paired with a carbon atom instead of an oxygen atom. A Monte Carlo yield was calculated for a water, silica sand, and iron soil medium equivalent in bulk density, hydrogen density, and weight percent of iron to a polyethylene, silica sand, and iron medium in order to provide an indication of the relative effects of carbon and oxygen in the "moisture" component upon detector response. Yield was slightly higher for the former soil medium, possibly justified by the lower thermal absorption cross section of oxygen. However, the difference (about 10 percent) was not sufficiently out of the range of statistical error to be significant.

Four relatively short computer utility programs were written in the course of this study to facilitate transfer, manipulation, and display of data generated by the Monte Carlo Code. Input parameter selection in program EDIT, for instance, allows the investigator to determine exactly which energy group, radius interval group, and/or elevation angle group of neutrons to follow from the soil surface into a detector medium. Program DISPLAY will tabulate the cumulative weighted number of neutrons coming out of the soil surface versus increasing radius from the center of the soil surface and graph cumulative neutron yield as a function of the same radius using the CALCOMP plotter. The raw data associated with each neutron history (energy, soil surface position vectors, statistical weight, and velocity components) generated and stored by the Monte Carlo Code are available for manipulation by any program suited to the needs of the researcher.

A tabular and graphic display, mentioned in the preceding paragraph, was made of the thermal and the epithermal neutron groups for each of the 19 soil mediums simulated in this study by the Monte Carlo technique. Hopefully, this information will be useful in any future study which might include the following: (1) construction of a simplified calibration model that can be easily checked against these Monte Carlo results; and (2) investigation of a method for predicting the neutron flux (thermal or otherwise) at the surface as a function of soil medium composition.

TABLE C-15

RELATIVE STANDARD DEVIATIONS OF REPRESENTATIVE MONTE CARLO YIELDS

SOIL MEDIUM	AVERAGE COUNTS ($\bar{n}$)	$R(\bar{n})$ (%)
H_2O	79.23	5.63
32 w/o CH_2+15 w/o Fe+SiO_2	18.89	6.0
8 w/o CH_2+SiO_2	5.39	9.95

TABLE C-16

CORRELATION OF PHYSICAL AND MONTE CARLO NEUTRON SOURCE YIELDS

	YIELD ($\times 10^{-4}$)		
SAMPLE NO.	PHYSICAL (Ye)	MONTE CARLO (Ym)	DIFFERENCE (%)
1	0.8298	0.6737	−18.81
2	1.7648	1.4670	−16.87
3	2.2844	2.0337	−10.97
4	2.9034	2.5499	−12.17
5	2.6199	2.3602	−9.91
6	2.2329	2.0277	−9.19
7	1.7008	1.6109	−5.29
8	0.7924	0.8399	+5.99
9	9.482	9.9036	+4.45
10 [a]	0.00581	0.017	+192.0

[a] The statistical error in the measurement precision of both Monte Carlo and physical yields was too great to attach any significance to the results. However, their values are included here for completeness.

REFERENCES

ANDERSON, H. L., Neutrons from Alpha Emitters. *Report No. 3,* Committee on Nuclear Science, NAS-NRC (1948).

BALLARD, L. F., and GARDNER, R. P., "Density and Moisture Content Measurements by Nuclear Methods—Interim Report." *NCHRP Report 14* (1965) 32 pp.

BELCHER, D. J., CUYKENDALL, T. R., and SACK, H. S., "The Measurement of Soil Moisture and Density of Neuton and Gamma-Ray Scattering." *Tech. Dev. Rep. No. 127,* U.S. Civil Aeronautics Admin. (1950).

BURN, K. N., "Design and Calibration of a Neutron Moisture Meter." *ASTM Spec. Tech. Pub. No. 293 (NRC 6131)*, Symposium on Nuclear Methods of Soil Density and Moisture, Ottawa, Ontario, Canada (1961) pp. 14-26.

BURN, K. N., "Effect of Iron on the Determination of Moisture Content by Neutron Method." *Canadian J. Earth Sci.,* Vol. 3 (1966).

COUCHAT, P. J., "La Methode Neutronique de Mesure de l'Humidité des Sols." *Rapport CEA-R3298,* Centre d'Etudes Nucléaires de Cadarache (1967).

DE PAUGHER, J., "Double Moderation Neutron Dosimeter." USAEC HW-57293 (July 1958).

GARDNER, R. P., and ROBERTS, K. F., "Density and Moisture Content Measurements by Nuclear Methods—Final Report." *NCHRP Report 43* (1967) 38 pp.

GOLDBERG, M. D., MAY, V. M., and STEHN, J. R., "Angular Distributions in Neutron Induced Reactions." *BNL-400,* 2d ed., U.S. Brookhaven National Laboratory (1962).

HUGHES, C. S., and ANDAY, M. C., "Correlation and Conference on Portable Nuclear Density and Moisture Systems." *Hwy. Res. Record No. 177* (1967) pp. 239-279.

MARION, J. B., and FOWLER, J. L., *Fast Neutron Physics, Part I.* Interscience, N.Y. (1960).

OLGAARD, P. L., "On the Theory of the Neutronic Method for Measuring the Water Content in Soil." *Risø Report No. 97,* Danish Atomic Energy Comm., Research Establishment Risø, Denmark (1965).

OLGAARD, P. L., and HAAHR, V., "Comparative Experimental and Theoretical Investigations of the DM Neutron Moisture Probe." *Nuc. Eng. and Design,* Vol. 5 (1967) p. 311.

PREISS, K., and GRANT, P. J., "The Optimization of a Neutron Scattering Water Content Gauge for Soils or Concretes." *J. Sci. Instrum.,* Vol. 41 (1964) p. 548.

SEMMLER, R. A., "Neutron-Moderation Moisture Meters: Analysis of Application to Coal and Soil." Final report from Laboratories for Applied Sciences, Univ. of Chicago Div. of Isotopes Development, USAEC, C00-712-73 (1963).

ZUBER, A., and CAMERON, J. F., "Neutron Soil Moisture Gauges." *Atomic Energy Rev.,* Vol. 4, No. 4 (1966) p. 143.

Published reports of the

NATIONAL COOPERATIVE HIGHWAY RESEARCH PROGRAM

are available from:

Highway Research Board
National Academy of Sciences
2101 Constitution Avenue
Washington, D.C. 20418

Rep. No. *Title*

—* A Critical Review of Literature Treating Methods of Identifying Aggregates Subject to Destructive Volume Change When Frozen in Concrete and a Proposed Program of Research—Intermediate Report (Proj. 4-3(2)), 81 p., $1.80

1 Evaluation of Methods of Replacement of Deteriorated Concrete in Structures (Proj. 6-8), 56 p., $2.80

2 An Introduction to Guidelines for Satellite Studies of Pavement Performance (Proj. 1-1), 19 p., $1.80

2A Guidelines for Satellite Studies of Pavement Performance, 85 p.+9 figs., 26 tables, 4 app., $3.00

3 Improved Criteria for Traffic Signals at Individual Intersections—Interim Report (Proj. 3-5), 36 p., $1.60

4 Non-Chemical Methods of Snow and Ice Control on Highway Structures (Proj. 6-2), 74 p., $3.20

5 Effects of Different Methods of Stockpiling Aggregates—Interim Report (Proj. 10-3), 48 p., $2.00

6 Means of Locating and Communicating with Disabled Vehicles—Interim Report (Proj. 3-4), 56 p. $3.20

7 Comparison of Different Methods of Measuring Pavement Condition—Interim Report (Proj. 1-2), 29 p., $1.80

8 Synthetic Aggregates for Highway Construction (Proj. 4-4), 13 p., $1.00

9 Traffic Surveillance and Means of Communicating with Drivers—Interim Report (Proj. 3-2), 28 p., $1.60

10 Theoretical Analysis of Structural Behavior of Road Test Flexible Pavements (Proj. 1-4), 31 p., $2.80

11 Effect of Control Devices on Traffic Operations—Interim Report (Proj. 3-6), 107 p., $5.80

12 Identification of Aggregates Causing Poor Concrete Performance When Frozen—Interim Report (Proj. 4-3(1)), 47 p., $3.00

13 Running Cost of Motor Vehicles as Affected by Highway Design—Interim Report (Proj. 2-5), 43 p., $2.80

14 Density and Moisture Content Measurements by Nuclear Methods—Interim Report (Proj. 10-5), 32 p., $3.00

15 Identification of Concrete Aggregates Exhibiting Frost Susceptibility—Interim Report (Proj. 4-3(2)), 66 p., $4.00

16 Protective Coatings to Prevent Deterioration of Concrete by Deicing Chemicals (Proj. 6-3), 21 p., $1.60

17 Development of Guidelines for Practical and Realistic Construction Specifications (Proj. 10-1), 109 p., $6.00

18 Community Consequences of Highway Improvement (Proj. 2-2), 37 p., $2.80

19 Economical and Effective Deicing Agents for Use on Highway Structures (Proj. 6-1), 19 p., $1.20

20 Economic Study of Roadway Lighting (Proj. 5-4), 77 p., $3.20

21 Detecting Variations in Load-Carrying Capacity of Flexible Pavements (Proj. 1-5), 30 p., $1.40

22 Factors Influencing Flexible Pavement Performance (Proj. 1-3(2)), 69 p., $2.60

23 Methods for Reducing Corrosion of Reinforcing Steel (Proj. 6-4), 22 p., $1.40

24 Urban Travel Patterns for Airports, Shopping Centers, and Industrial Plants (Proj. 7-1), 116 p., $5.20

25 Potential Uses of Sonic and Ultrasonic Devices in Highway Construction (Proj. 10-7), 48 p., $2.00

26 Development of Uniform Procedures for Establishing Construction Equipment Rental Rates (Proj. 13-1), 33 p., $1.60

27 Physical Factors Influencing Resistance of Concrete to Deicing Agents (Proj. 6-5), 41 p., $2.00

28 Surveillance Methods and Ways and Means of Communicating with Drivers (Proj. 3-2), 66 p., $2.60

29 Digital-Computer-Controlled Traffic Signal System for a Small City (Proj. 3-2), 82 p., $4.00

30 Extension of AASHO Road Test Performance Concepts (Proj. 1-4(2)), 33 p., $1.60

31 A Review of Transportation Aspects of Land-Use Control (Proj. 8-5), 41 p., $2.00

32 Improved Criteria for Traffic Signals at Individual Intersections (Proj. 3-5), 134 p., $5.00

33 Values of Time Savings of Commercial Vehicles (Proj. 2-4), 74 p., $3.60

34 Evaluation of Construction Control Procedures—Interim Report (Proj. 10-2), 117 p., $5.00

35 Prediction of Flexible Pavement Deflections from Laboratory Repeated-Load Tests (Proj. 1-3(3)), 117 p., $5.00

36 Highway Guardrails—A Review of Current Practice (Proj. 15-1), 33 p., $1.60

37 Tentative Skid-Resistance Requirements for Main Rural Highways (Proj. 1-7), 80 p., $3.60

38 Evaluation of Pavement Joint and Crack Sealing Materials and Practices (Proj. 9-3), 40 p., $2.00

39 Factors Involved in the Design of Asphaltic Pavement Surfaces (Proj. 1-8), 112 p., $5.00

40 Means of Locating Disabled or Stopped Vehicles (Proj. 3-4(1)), 40 p., $2.00

41 Effect of Control Devices on Traffic Operations (Proj. 3-6), 83 p., $3.60

42 Interstate Highway Maintenance Requirements and Unit Maintenance Expenditure Index (Proj. 14-1), 144 p., $5.60

43 Density and Moisture Content Measurements by Nuclear Methods (Proj. 10-5), 38 p., $2.00

44 Traffic Attraction of Rural Outdoor Recreational Areas (Proj. 7-2), 28 p., $1.40

45 Development of Improved Pavement Marking Materials—Laboratory Phase (Proj. 5-5), 24 p., $1.40

46 Effects of Different Methods of Stockpiling and Handling Aggregates (Proj. 10-3), 102 p., $4.60

47 Accident Rates as Related to Design Elements of Rural Highways (Proj. 2-3), 173 p., $6.40

48 Factors and Trends in Trip Lengths (Proj. 7-4), 70 p., $3.20

49 National Survey of Transportation Attitudes and Behavior—Phase I Summary Report (Proj. 20-4), 71 p., $3.20

* Highway Research Board Special Report 80.

Rep. No. *Title*

50 Factors Influencing Safety at Highway-Rail Grade Crossings (Proj. 3-8), 113 p., $5.20

51 Sensing and Communication Between Vehicles (Proj. 3-3), 105 p., $5.00

52 Measurement of Pavement Thickness by Rapid and Nondestructive Methods (Proj. 10-6), 82 p., $3.80

53 Multiple Use of Lands Within Highway Rights-of-Way (Proj. 7-6), 68 p., $3.20

54 Location, Selection, and Maintenance of Highway Guardrails and Median Barriers (Proj. 15-1(2)), 63 p., $2.60

55 Research Needs in Highway Transportation (Proj. 20-2), 66 p., $2.80

56 Scenic Easements—Legal, Administrative, and Valuation Problems and Procedures (Proj. 11-3), 174 p., $6.40

57 Factors Influencing Modal Trip Assignment (Proj. 8-2), 78 p., $3.20

58 Comparative Analysis of Traffic Assignment Techniques with Actual Highway Use (Proj. 7-5), 85 p., $3.60

59 Standard Measurements for Satellite Road Test Program (Proj. 1-6), 78 p., $3.20

60 Effects of Illumination on Operating Characteristics of Freeways (Proj. 5-2) 148 p., $6.00

61 Evaluation of Studded Tires—Performance Data and Pavement Wear Measurement (Proj. 1-9), 66 p., $3.00

62 Urban Travel Patterns for Hospitals, Universities, Office Buildings, and Capitols (Proj. 7-1), 144 p., $5.60

63 Economics of Design Standards for Low-Volume Rural Roads (Proj. 2-6), 93 p., $4.00

64 Motorists' Needs and Services on Interstate Highways (Proj. 7-7), 88 p., $3.60

65 One-Cycle Slow-Freeze Test for Evaluating Aggregate Performance in Frozen Concrete (Proj. 4-3(1)), 21 p., $1.40

66 Identification of Frost-Susceptible Particles in Concrete Aggregates (Proj. 4-3(2)), 62 p., $2.80

67 Relation of Asphalt Rheological Properties to Pavement Durability (Proj. 9-1), 45 p., $2.20

68 Application of Vehicle Operating Characteristics to Geometric Design and Traffic Operations (Proj. 3-10), 38 p., $2.00

69 Evaluation of Construction Control Procedures—Aggregate Gradation Variations and Effects (Proj. 10-2A), 58 p., $2.80

70 Social and Economic Factors Affecting Intercity Travel (Proj. 8-1), 68 p., $3.00

71 Analytical Study of Weighing Methods for Highway Vehicles in Motion (Proj. 7-3), 63 p., $2.80

72 Theory and Practice in Inverse Condemnation for Five Representative States (Proj. 11-2), 44 p., $2.20

73 Improved Criteria for Traffic Signal Systems on Urban Arterials (Proj. 3-5/1), 55 p., $2.80

74 Protective Coatings for Highway Structural Steel (Proj. 4-6), 64 p., $2.80

74A Protective Coatings for Highway Structural Steel—Literature Survey (Proj. 4-6), 275 p., $8.00

74B Protective Coatings for Highway Structural Steel—Current Highway Practices (Proj. 4-6), 102 p., $4.00

75 Effect of Highway Landscape Development on Nearby Property (Proj. 2-9), 82 p., $3.60

Rep. No. *Title*

76 Detecting Seasonal Changes in Load-Carrying Capabilities of Flexible Pavements (Proj. 1-5(2)), 37 p., $2.00

77 Development of Design Criteria for Safer Luminaire Supports (Proj. 15-6), 82 p., $3.80

78 Highway Noise—Measurement, Simulation, and Mixed Reactions (Proj. 3-7), 78 p., $3.20

79 Development of Improved Methods for Reduction of Traffic Accidents (Proj. 17-1), 163 p., $6.40

80 Oversize-Overweight Permit Operation on State Highways (Proj. 2-10), 120 p., $5.20

81 Moving Behavior and Residential Choice—A National Survey (Proj. 8-6), 129 p., $5.60

82 National Survey of Transportation Attitudes and Behavior—Phase II Analysis Report (Proj. 20-4), 89 p., $4.00

83 Distribution of Wheel Loads on Highway Bridges (Proj. 12-2), 56 p., $2.80

84 Analysis and Projection of Research on Traffic Surveillance, Communication, and Control (Proj. 3-9), 48 p., $2.40

85 Development of Formed-in-Place Wet Reflective Markers (Proj. 5-5), 28 p., $1.80

86 Tentative Service Requirements for Bridge Rail Systems (Proj. 12-8), 62 p., $3.20

87 Rules of Discovery and Disclosure in Highway Condemnation Proceedings (Proj. 11-1(5)), 28 p., $2.00

88 Recognition of Benefits to Remainder Property in Highway Valuation Cases (Proj. 11-1(2)), 24 p., $2.00

89 Factors, Trends, and Guidelines Related to Trip Length (Proj. 7-4), 59 p., $3.20

90 Protection of Steel in Prestressed Concrete Bridges (Proj. 12-5), 86 p., $4.00

91 Effects of Deicing Salts on Water Quality and Biota—Literature Review and Recommended Research (Proj. 16-1), 70 p., $3.20

92 Valuation and Condemnation of Special Purpose Properties (Proj. 11-1(6)), 47 p., $2.60

93 Guidelines for Medial and Marginal Access Control on Major Roadways (Proj. 3-13), 147 p., $6.20

94 Valuation and Condemnation Problems Involving Trade Fixtures (Proj. 11-1(9)), 22 p., $1.80

95 Highway Fog (Proj. 5-6), 48 p., $2.40

96 Strategies for the Evaluation of Alternative Transportation Plans (Proj. 8-4), 111 p., $5.40

97 Analysis of Structural Behavior of AASHO Road Test Rigid Pavements (Proj. 1-4(1)A), 35 p., $2.60

98 Tests for Evaluating Degradation of Base Course Aggregates (Proj. 4-2), 98 p. $5.00

99 Visual Requirements in Night Driving (Proj. 5-3), 38 p., $2.60

100 Research Needs Relating to Performance of Aggregates in Highway Construction (Proj. 4-8), 68 p., $3.40

101 Effect of Stress on Freeze-Thaw Durability of Concrete Bridge Decks (Proj. 6-9), 70 p., $3.60

102 Effect of Weldments on the Fatigue Strength of Steel Beams (Proj. 12-7), 114 p., $5.40

103 Rapid Test Methods for Field Control of Highway Construction (Proj. 10-4), 89 p., $5.00

104 Rules of Compensability and Valuation Evidence for Highway Land Acquisition (Proj. 11-1), 77 p., $4.40

Rep. No. *Title*

105 Dynamic Pavement Loads of Heavy Highway Vehicles (Proj. 15-5), 94 p., $5.00

106 Revibration of Retarded Concrete for Continuous Bridge Decks (Proj. 18-1), 67 p., $3.40

107 New Approaches to Compensation for Residential Takings (Proj. 11-1(10)), 27 p., $2.40

108 Tentative Design Procedure for Riprap-Lined Channels (Proj. 15-2), 75 p., $4.00

109 Elastomeric Bearing Research (Proj. 12-9), 53 p., $3.00

110 Optimizing Street Operations Through Traffic Regulations and Control (Proj. 3-11), 100 p., $4.40

111 Running Costs of Motor Vehicles as Affected by Road Design and Traffic (Proj. 2-5A and 2-7), 97 p., $5.20

112 Junkyard Valuation—Salvage Industry Appraisal Principles Applicable to Highway Beautification (Proj. 11-3(2)), 41 p., $2.60

113 Optimizing Flow on Existing Street Networks (Proj. 3-14), 414 p., $15.60

114 Effects of Proposed Highway Improvements on Property Values (Proj. 11-1(1)), 42 p., $2.60

115 Guardrail Performance and Design (Proj. 15-1(2)), 70 p., $3.60

116 Structural Analysis and Design of Pipe Culverts (Proj. 15-3), 155 p., $6.40

117 Highway Noise—A Design Guide for Highway Engineers (Proj. 3-7), 79 p., $4.60

118 Location, Selection, and Maintenance of Highway Traffic Barriers (Proj. 15-1(2)), 96 p., $5.20

119 Control of Highway Advertising Signs—Some Legal Problems (Proj. 11-3(1)), 72 p., $3.60

120 Data Requirements for Metropolitan Transportation Planning (Proj. 8-7), 90 p., $4.80

121 Protection of Highway Utility (Proj. 8-5), 115 p., $5.60

122 Summary and Evaluation of Economic Consequences of Highway Improvements (Proj. 2-11), 324 p., $13.60

123 Development of Information Requirements and Transmission Techniques for Highway Users (Proj. 3-12) 239 p., $9.60

124 Improved Criteria for Traffic Signal Systems in Urban Networks (Proj. 3-5) 86 p., $4.80

125 Optimization of Density and Moisture Content Measurements by Nuclear Methods (Proj. 10-5A), 86 p., $4.40

Synthesis of Highway Practice

No. *Title*

1 Traffic Control for Freeway Maintenance (Proj. 20-5, Topic 1), 47 p., $2.20

2 Bridge Approach Design and Construction Practices (Proj. 20-5, Topic 2), 30 p., $2.00

3 Traffic-Safe and Hydraulically Efficient Drainage Practice (Proj. 20-5, Topic 4), 38 p., $2.20

4 Concrete Bridge Deck Durability (Proj. 20-5, Topic 3), 28 p., $2.20

5 Scour at Bridge Waterways (Proj. 20-5, Topic 5), 37 p., $2.40

6 Principles of Project Scheduling and Monitoring (Proj. 20-5, Topic 6), 43 p., $2.40

7 Motorist Aid Systems (Proj. 20-5, Topic 3-01), 28 p., $2.40

8 Construction of Embankments (Proj. 20-5, Topic 9), 38 p., $2.40

THE NATIONAL ACADEMY OF SCIENCES is a private, honorary organization of more than 700 scientists and engineers elected on the basis of outstanding contributions to knowledge. Established by a Congressional Act of Incorporation signed by President Abraham Lincoln on March 3, 1863, and supported by private and public funds, the Academy works to further science and its use for the general welfare by bringing together the most qualified individuals to deal with scientific and technological problems of broad significance.

Under the terms of its Congressional charter, the Academy is also called upon to act as an official—yet independent—adviser to the Federal Government in any matter of science and technology. This provision accounts for the close ties that have always existed between the Academy and the Government, although the Academy is not a governmental agency and its activities are not limited to those on behalf of the Government.

THE NATIONAL ACADEMY OF ENGINEERING was established on December 5, 1964. On that date the Council of the National Academy of Sciences, under the authority of its Act of Incorporation, adopted Articles of Organization bringing the National Academy of Engineering into being, independent and autonomous in its organization and the election of its members, and closely coordinated with the National Academy of Sciences in its advisory activities. The two Academies join in the furtherance of science and engineering and share the responsibility of advising the Federal Government, upon request, on any subject of science or technology.

THE NATIONAL RESEARCH COUNCIL was organized as an agency of the National Academy of Sciences in 1916, at the request of President Wilson, to enable the broad community of U. S. scientists and engineers to associate their efforts with the limited membership of the Academy in service to science and the nation. Its members, who receive their appointments from the President of the National Academy of Sciences, are drawn from academic, industrial and government organizations throughout the country. The National Research Council serves both Academies in the discharge of their responsibilities.

Supported by private and public contributions, grants, and contracts, and voluntary contributions of time and effort by several thousand of the nation's leading scientists and engineers, the Academies and their Research Council thus work to serve the national interest, to foster the sound development of science and engineering, and to promote their effective application for the benefit of society.

THE DIVISION OF ENGINEERING is one of the eight major Divisions into which the National Research Council is organized for the conduct of its work. Its membership includes representatives of the nation's leading technical societies as well as a number of members-at-large. Its Chairman is appointed by the Council of the Academy of Sciences upon nomination by the Council of the Academy of Engineering.

THE HIGHWAY RESEARCH BOARD, organized November 11, 1920, as an agency of the Division of Engineering, is a cooperative organization of the highway technologists of America operating under the auspices of the National Research Council and with the support of the several highway departments, the Federal Highway Administration, and many other organizations interested in the development of transportation. The purpose of the Board is to advance knowledge concerning the nature and performance of transportation systems, through the stimulation of research and dissemination of information derived therefrom.

HIGHWAY RESEARCH BOARD
NATIONAL ACADEMY OF SCIENCES—NATIONAL RESEARCH COUNCIL
2101 Constitution Avenue Washington, D. C. 20418

ADDRESS CORRECTION REQUESTED